DYNAMIC DATA DRIVEN INVESTIGATION OF PETROPHYSICAL AND GEOMECHANICAL PROPERTIES FOR RESERVOIR FORMATION EVALUATION

By

©David Ojonugwa Onalo

A thesis submitted to the School of Graduate Studies

In partial fulfillment of the requirements for the degree of

Doctor of Philosophy

Faculty of Engineering and Applied Science

Memorial University of Newfoundland

January 2019

St. John's Newfoundland, Canada

Dedication

This work is dedicated to the Almighty God for His divine favor and mercy in along the way. To my parents, Colonel (RTD) C. D. Onalo and Mrs. A. A. Onalo. To my siblings Stacy, Joan, Daniel and Michael Onalo. And finally, to the pastor (Pst. Innocent Owasi) and members of the Deeper life bible church, St John's, Newfoundland.

ABSTRACT

Petrophysical and geomechanical properties of the formation such as Young's modulus, bulk modulus, shear modulus, Poisson's ratio, and porosity provide characteristic description of the hydrocarbon reservoir. It is well-established that static geomechanical properties are good representatives of reservoir formations; however, they are non-continuous along the wellbore, expensive and determining these properties may lead to formation damage. Dynamic geomechanical formation properties from acoustic measurements offer a continuous and non-destructive means to provide a characteristic description of the reservoir formation. In the absence of reliable acoustic measurements of the formation, such as sonic logs, the estimation of the dynamic geomechanical properties becomes challenging. Several techniques like empirical, analytical and intelligent systems have been used to approximate the property estimates. These techniques can also be used to approximate acoustic measurements thus enable dynamic estimation of geomechanical properties. This study intends to explore methodologies and models to dynamically estimate geomechanical properties in the absence of some or all acoustic measurements of the formation. The present work focused on developing empirical and intelligent systems like artificial neural networks (ANN), Gaussian processes (GP), and recurrent neural networks (RNN) to determine the dynamic geomechanical properties. The developed models serve as a cost-effective, reliable, efficient, and robust methods, offering dyanmic geomechanical analysis of the formation. This thesis has five main contributions: (a) a new data-driven empirical model of estimating static Young's modulus from dynamic Young's modulus, (b) a new data-driven ANN model for sonic well log prediction, (c) a new data-driven GP model for shear wave

transit time prediction, (d) a new dynamic data-driven RNN model for sonic well log reproduction, and (e) an assessment on the ANN as a reliable sonic logging tool.

Keywords: Sonic transit time, Well logs, Artificial neural networks, Rock formation properties, Recurrent neural networks and Gaussian processes

ACKNOWLEDGMENTS

I sincerely wish to express my profound gratitude to my supervisors, Dr. James Lesley, Dr. Stephen Butt and Dr. Faisal Khan for their love, patience and guidance during my doctoral degree program at the Memorial University of Newfoundland. It is a great privilege and a rare opportunity to have worked under their supervision. I have undoubtedly benefitted from their expertise in the field of enhanced oil recovery, geomechanics and data-driven problem-solving techniques in engineering respectively. I would like to acknowledge my co-authors, Dr. Sunday Adedigba Adeshina, Olalere Oloruntobi and Cleverson Esene for their assistance in intelligent systems, petrophysical concepts and reservoir simulations respectively.

I would like to extend my deepest appreciation to my lovely parents, Colonel (RTD) and Mrs. Onalo for their emotional support and words of encouragement during the program. They have been a source of great inspiration and motivation. My family always believed in me and that I had what it took to accomplish my degree even when the light at the end of the tunnel seemed dim.

To Pastor and Mrs. Innocent Owasi, my brothers and sisters of the Deeper Life Bible Church, St. John's and all those who had me in their prayers, I indebted to you, I appreciate all your prayers and support. I am grateful to all my colleagues at the Hibernia Enhanced Oil Recovery Laboratory and the Drilling Technology Laboratory groups at Memorial University.

TABLE OF CONTENTS

ABSTRACT iii

ACKNOWLEDGMENTS v

TABLE OF CONTENTS vi

LIST OF TABLES xvi

LIST OF FIGURES xix

Chapter 1 Introduction 1

1.1 Background 1

1.2 Research Questions 4

1.3 Motivation 4

1.4 Objectives of the Research 5

1.5 Novelty and contributions 5

1.6 Organization of thesis 6

References 9

Chapter 2 Novelty and contribution 15

Chapter 3 Literature review 19

Co-authorship statement 19

Abstract 20

3.1 Introduction 21

3.1.1 Types of acoustic waves 21
3.1.2 Background 22
3.1.3 Compressional Wave Velocity 22
3.1.4 Shear Wave Velocity 25
3.1.5 Compression to Shear Wave Ratio 30
3.2 Rock Formation Properties 34
3.2.1 Porosity 34
3.2.2 Permeability and Fluid Flow 35
3.2.3 Rock strength 39
3.2.4 Sonic wave velocities 39
3.2.5 Formation Density 41
3.3 Well Logs 45
3.3.1 Gamma-ray log (API) 45
3.3.2 Bulk density log (RHOB) 45
3.3.3 Deep resistivity log (RESD) 46
3.3.4 Neutron log (NPHI) 46
3.3.5 Shale Volume (Vsh) 47
3.3.6 Total porosity (PHIT) 47
3.3.7 Effective porosity (PHIE) 47

3.3.8 Compressional wave sonic transit time log (DTCO) 47

3.3.9 Shear wave sonic transit time log (DTSM) 48

3.4 Conclusions 49

References 51

Chapter 4 Static young's modulus model prediction for formation evaluation 65

Preface 65

4.1 Introduction 67

4.2 Methodology 75

4.3 Results and discussion 82

4.4 Sensitivity and Uncertainty Analysis 87

4.5 Conclusion 89

Acknowledgments 90

Nomenclature 91

References 92

Chapter 5 Data-driven model for sonic well log prediction 97

Preface 97

5.1 Introduction 99

5.2 Artificial Neural Network (ANN) 107

5.2.1 Multi-layer perceptron artificial neural network 107

5.3 Methodology to develop the ANN model 109
5.3.1 Data collection and determination for ANN 110
5.3.2 Quality assurance and quality checks (QAQC) 110
5.3.3 ANN model and architecture 110
5.3.4 Learning and training of the ANN 111
5.3.5 Generalization of the ANN 114
5.4 Case Study 114
5.4.1 Input parameters 116
5.4.2 Output parameters 116
5.4.3 Selection of Models 116
5.4.4 Estimated Formation Mechanical Properties 118
5.5 Results and discussion 121
5.5.1 Sonic transit time log estimation 121
5.5.2 Formation Mechanical Property Prediction 125
5.6 Conclusions 134
Acknowledgment 136
Nomenclature 137
References 138
Appendix 5A 150

Disclaimer 151

Chapter 6 Data Driven Model for Shear wave Transit Time Prediction 152

Preface 152

Abstract 153

6.1 Introduction 154

6.2 Gaussian Process (GP) 159

6.2.1 Gaussian process theory 160

6.2.2 Covariance and kernel Function 161

6.3 Model Development Methodology 163

6.3.1 Data collection and preparation 163

6.3.2 Quality assurance and quality checks (QAQC) 164

6.3.3 Gaussian process model development 164

6.3.4 Gaussian process selection 166

6.3.5 Generalization of the GP 169

6.4 Application of the developed Model 170

6.5 Results and discussion 172

6.5.1 Shear Sonic transit time log estimation 172

6.6 Predicting Dynamic Geomechanical properties 175

6.6.1 Dynamic Young's Modulus 175

6.6.2 Poisson's Ratio (PR) 176

6.7 Conclusions 178

Acknowledgment 180

Nomenclature 181

References 182

Appendices 189

Disclaimer 194

Chapter 7 Dynamic Data Driven Sonic Well Log Model for Formation Evaluation 196

Preface 196

Abstract 197

7.1 Introduction 198

7.2 Recurrent Neural Network (RNN) 203

7.2.1 Nonlinear auto-regressive with exogenous inputs (NARX) 204

7.3 Methodology to develop the NARX model 206

7.3.1 Collection and determination of data for NARX 207

7.3.2 Quality assurance and quality control (QAQC) 207

7.3.3 Development of NARX model architecture 207

7.3.4 Learning and training of the NARX 209

7.3.5 Generalization of the NARX 210

7.4 Results and discussion 211
7.4.1 Model development and calibration 211
7.4.2 Model parameter selection 213
7.4.3 Model testing and validation 215
7.5 Case study 217
7.5.1 First Case study - Well 1A. 217
7.5.2 Second Case study -Well 1B 221
7.5.3 Third Case study – Well OK 226
7.6 Conclusions 233
Acknowledgment 234
Nomenclature 235
Appendix: Supplementary data and information 236
Sample MATLAB generated code for modeling sonic well logs 237
References 239
Chapter 8 Are ANN model reliable Well Log Tools? 248
Preface 248
Abstract 249
8.1 Introduction 250
8.2 Case Study 255

8.2.1 Development of ANN model 257
8.3 Challenges and limitations of ANN model development 259
8.3.1 Input data 259
8.3.2 Target data 261
8.3.3 Data quality 262
8.3.1 Data size 263
8.3.2 Generalization of the ANN 264
8.3.1 Model Architecture 267
8.3.2 Training of ANN models 270
8.3.3 Repeatability 273
8.3.4 Uncertainty 274
8.4 Conclusions 276
Acknowledgments 278
Nomenclature 279
References 280
Chapter 9 Summary, Conclusions and Recommendations 291
9.1 Summary 291
9.2 Conclusions 291
9.2.1 A new static Young's modulus prediction model for formation evaluation 291

9.2.2 A new data-driven sonic well log prediction model for sanding potential evaluation 292

9.2.3 A new data-driven model shear transit time prediction model for field development 293

9.2.4 A new dynamic data-driven model for sonic well log prediction for formation evaluation 293

9.2.5 An assessment of ANN as a reliable sonic well logging tool. 294

9.3 Recommendations 295

Appendixes 297

A.1 Modeling Investigation of Low Salinity Water Injection in Sandstones and Carbonates: Effect of Na^+ and SO_4^{2-} 298

Preface 298

Abstract 299

A.1.1. Introduction 300

A.1.2. Theoretical analysis: ion exchange in lswi 305

A.1.3. Model development 311

A.1.3.1. Fluid Behavior Modeling 311

A.1.3.2. Reservoir Modeling 318

A.1.4. Results and discussion 325

A.1.4.1. Effect of LSWI on Oil Recovery in Sandstone and Carbonate. 325

A.1.4.2. Effect of LSWI on Mineral Dissolution and Precipitation. 333

A.1.5.Conclusions 337

Nomenclatures 339

References 343

A.2 A New Shear Wave Velocity Prediction Technique for Clastic Rocks 347

Preface 347

Abstract 348

A.2.1.Introduction 349

A.2.2.Model Development 356

A.2.3.Field Examples 359

A.2.4.Discussion 366

A.2.5.Conclusion 372

Acknowledgments 373

Nomenclature 374

Reference 375

LIST OF TABLES

Table 4.1. A list of existing static Young's Modulus equations found in the literature 72

Table 4.2. Sources of data used for the study 75

Table 4.3. Summary of statistical comparative analysis 85

Table 4.4. Dynamic Young's Modulus Monte Carlo simulation 87

Table 4.5. Density Monte Carlo simulation 87

Table 4.6. Combined Monte Carlo simulation 88

Table 5.1. The differences between the current work and the following intelligent system articles 104

Table 5.2. Main features of the proposed ANN model 111

Table 5.3. Interval Travel times of some formations and fluids (after (Asquith and Gibson, 2004)) 119

Table 5.4. Summary of statistical analysis 122

Table 5.5. Sample measured sonic well log and ANN derived values 123

Table 5.6. Sample measured well log and ANN derived mechanical rock properties 126

Table 5.7. Formation classification table 127

Table 6.1. Summary of the results of the GP regression model selection 168

Table 6.2. Main features of the proposed GP regression model 168

Table 6.3. 50 feet of available well log data for the study 189

Table 6.4. Sensitivity analysis data (Dynamic Young's Modulus and Poisson's Ratio) 191

Table 7.1: Examples of intelligent systems used in the petroleum industry 199

Table 7.2. Main features of the proposed NARX model 209

Table 7.3. Available Well Data Summary 211
Table 7.4. Model Development and calibration 212
Table 7.5. Testing of the model on external data 215
Table 7.6. Statistical analysis of Well 1A formation evaluation properties 221
Table 7.7. Statistical analysis of Well 1B formation evaluation properties 226
Table 7.8. Statistical analysis of Well OK formation evaluation properties 231
Table 7.9. Actual and predicted sonic evaluation properties of 10 feet of well 1A 236
Table 8.1 Statistical representation of the well log data 255
Table 8.2. The features of the base model 257
Table 8.3. Summary the model performance based on the selected input data 259
Table 8.4. Model performance summary based on data size 263
Table 8.5 Summary of model performance based on the number of neurons 268
Table 8.6 Summary of model performance based on the number of layers 269
Table 8.7. Summary of model performance based on the optimization algorithm 271
Table 8.8 Summary of model performance based on model repetition 273
Table 8.9. A list of the challenges and limitations discussed 276

Table A1. 1 Black oil composition [46] 313
Table A1. 2. Laboratory heavy fraction analysis for C7 – C30+ [46] 313
Table A1. 3. Experimental and modeled fluid properties 317
Table A1. 4 Model properties [46] 320
Table A1. 5. Laboratory end-point relative permeability data [46] 320
Table A1. 6. Initial laboratory formation water compositions/mineral volume fractions [46] 322

Table A2. 1. Other empirical relationships 353

Table A2. 2. Type and source of the data used for calibration. 357

Table A2. 3. The well data summary 362

Table A2. 4. Comparison of RMSE and maximum deviation for different models. 368

LIST OF FIGURES

Figure 2.1 Outline of research contribution and novelty 15

Figure 2.2 Tasks Integration and Scientific Contribution 18

Figure 4.1. Plot of static and dynamic Young's modulus 77

Figure 4.2. Density versus static and dynamic Young's modulus 80

Figure 4.3 Validation of the measured and predicted static modulus 81

Figure 4.4. Measured and predicted static correlations from dynamic Young's modulus 83

Figure 4.5. Cross plot of static modulus predicted from correlation the measured static modulus 84

Figure 5.1. Proposed ANN model methodology flowchart 109

Figure 5.2. Schematic of the proposed ANN architecture 113

Figure 5.3. Well Log Data 115

Figure 5.4. Schematic diagram of ANN architecture for sonic interval travel time 117

Figure 5.5. Depth vs Interval Travel Time 124

Figure 5.6. Comparison of measured and predicted compressional wave travel time 124

Figure 5.7. Comparison of measured and predicted shear wave travel time 125

Figure 5.8. Comparison of measured and predicted Young's modulus 128

Figure 5.9. Comparison of measured and predicted bulk modulus 129

Figure 5.10. Comparison of measured and predicted shear modulus 130

Figure 5.11. Comparison of measured and predicted sonic porosity 131

Figure 5.12 Comparison of measured and predicted sanding potential 132

Figure 6.1. Framework for the proposed model development 163

Figure 6.2. Actual target response 165
Figure 6.3. The response of the tested GP model 166
Figure 6.4 Cross-plot of the tested GP models 167
Figure 6.5. Errors of the tested GP models 167
Figure 6.6. Available well log data 171
Figure 6.7. Shear wave transit time versus depth 173
Figure 6.8. Predicted shear wave transit time versus measured shear wave transit time 174
Figure 6.9. Cross-validation plot of predicted and measured dynamic Young's Modulus 176
Figure 6.10. Cross-validation plot of predicted and measured Poisson's Ratio 177
Figure 7.1: Parallel NARX architecture 204
Figure 7.2: Series-parallel NARX architecture 205
Figure 7.3: Proposed NARX model methodology flowchart 206
Figure 7.4: Proposed NARX network model 207
Figure 7.5. LM and BR model performance 212
Figure 7.6. Model parameter selection based on the number of hidden layer neurons 214
Figure 7.7. Model parameter selection based on the number of time delays 215
Figure 7.8. Well 1A log data 218
Figure 7.9. Measured and predicted sonic well logs versus depth 219
Figure 7.10. Well 1A formation evaluation properties 220
Figure 7.11. Well 1B well log data 223
Figure 7.12. Measured and predicted sonic well logs versus depth 224
Figure 7.13. Well 1B formation evaluation properties 225
Figure 7.14. Well OK well log data 228

Figure 7.15. Well OK measured and predicted sonic well logs versus depth 229

Figure 7.16. Well OK formation evaluation properties 230

Figure 8.1. Well log data from Well 15/9-F-1A, Volve Field, Norway (Equinor, 2018)..... 256

Figure 8.2. Cross-validation of All-model 258

Figure 8.3. Cross-validation of models based on data size generalization 266

Figure A1. 1. Schematic representation of clay mineral, ionic bridge, oil and typical ions to describe the important interaction mechanisms in LSWI (Modified after Lager et al. [32]..... 306

Figure A1. 2 A control volume/element of a 3-D flow in directions x, y, and z 309

Figure A1. 3 Flowchart to prepare the EOS fluid model 312

Figure A1. 4. Pressure-temperature (P-T) diagram of the modeled reservoir fluid. 315

Figure A1. 5. Comparison of measured gas oil ratio (GOR), initial GOR (before tuning), and final GOR (after tuning) 315

Figure A1. 6. Comparison of measured relative oil volume (ROV), initial ROV (before tuning) and final ROV (after tuning) 316

Figure A1. 7. Comparison of measured Psat, initial Psat (before tuning) and final Psat (after tuning) 317

Figure A1. 8. A simple approach to develop GEM reservoir compositional model for LSWI .. 318

Figure A1. 9. Schematic of the 1-D model structure 319

Figure A1. 10. Relative Permeability curve 321

Figure A1. 11. Design of simulation runs to understand the impact of Na^+ and SO_4^{2-} in the LSWI process 322

Figure A1. 12. Experimental high and low Salinity relative permeability curves [46]. 324

Figure A1. 13. Oil recovery versus injected pore volume and Na+ concentration..... 325

Figure A1. 14. Final oil recovery for different Na+ concentration in the sandstone case..... 326

Figure A1. 15. Oil recovery factor by altering S042- concentration 327

Figure A1. 16. Ultimate oil recovery versus the magnitude of SO42- concentration 328

Figure A1. 17. 3D representation of pH change in sandstone for A(3.5 kppm), B(15 kppm), and C (62.52 kppm).. 329

Figure A1. 18. pH change in sandstone versus Na+ concentration 331

Figure A1. 19. 3D representation of pH change in carbonate for A (0.1 kppm), B (0.08 kppm), and C (0.065 kppm) 332

Figure A1. 20. pH change in carbonates in terms of SO42-..... 333

Figure A1. 21. Effect of LSWI on mineral (calcite) precipitation in carbonates..... 334

Figure A1. 22. Influence of LSWI on mineral (dolomite) dissolution in carbonates 335

Figure A2. 1 Comparison of predicted and measured shear wave velocities. 358

Figure A2. 2. Location map for well A, B and C..... 361

Figure A2. 3. Measured petrophysical data for well A..... 363

Figure A2. 4. Measured petrophysical data for well B..... 364

Figure A2. 5. Measured petrophysical data for well C..... 365

Figure A2. 6. Comparison of predicted and measured (log) shear wave velocities profile..... 367

Figure A2. 7Comparison of predicted and measured (log) shear wave velocities for well A.... 369

Figure A2. 8. Comparison of predicted and measured (log) shear wave velocities for well B .. 370

Figure A2. 9. Comparison of predicted and measured (log) shear wave velocities for well C .. 371

Chapter 1 Introduction

1.1 Background

Energy deposits can be found in the earth's crust as several energy sources (Buffett, 2016; Majorowicz et al., 2013; McMahonSean et al., 2016; Miller et al., 2016). These sources of energy range from thermal energy, geothermal energy, coal and nuclear, to hydrocarbons and other fossil fuel energy (Sagan, 1972; Stringer, 2008; Viswanathan, 2016; Vivoda, 2009). Natural gas and petroleum production are expected to grow more than 35% in the next 20 years (IEA International Energy Agency, 2016). Reservoir formations containing oil and gas are often located deep underground within the earth under high overburden pressure and temperatures (Santarelli et al., 1989; Song et al., 2013). Investments and management in the exploration and production of resources from these formations require forward prediction of the formation properties and their alteration under naturally or artificially induced operations (den Brok et al., 1997). The flow of fluids through porous media formations such as oil and gas reservoirs alter the rock properties of the formation (Hernandez-Uribe et al., 2017; Holt et al., 2000; Nouri et al., 2005; Song et al., 2013; Younessi et al., 2013). Conducting investigations directly on reservoir formations may not always be feasible due to their accessibility deep within the earth. For this reason, samples of the reservoir formation are cored, extracted and transported to laboratories to subject them to the desired investigations. Unconsolidated sandstones are very fragile and crumble easily during coring (Mese and Tutuncu, 1997). Even so, during the coring, extraction, and transportation of the formation cores, the cores are exposed to severe damage (Holt et al., 2000). The results of these tests such as triaxial compressional and cyclic loading test to determine geomechanical deformation properties are very dependent on the pressures under which the tests are conducted (Ma et al., 2013).

Laboratory tests for formation properties obtained from the stress-strain relationship are referred to as static formation properties. To determine the stress-strain relationship of the formation, the formation must be subjected to deformation that exceeds the elastic region of the formation (Fjær, 2009; Harouaka et al., 1995; King and Jing, 2001; Ravazzoli et al., 2003). Such procedures are destructive and therefore costly; countless samples are destroyed and lost in the process.

An alternative to the destructive static derived deformation properties is dynamically estimated geomechanical deformation properties. Dynamic formation properties are properties estimated from the sonic velocity or transit time measurements of the formation (Fjær, 2009). Static and dynamic estimations of geomechanical formation properties do not present the same values for a particular property in the same formation (Fjær, 2009; Holt et al., 2012; Mockovčiaková and Pandula, 2003; Svitek and Republic, 2014). The difference has been reported to be due to microcracks, porosity, void spaces and saturating fluid amongst others (Onalo et al., 2018b). Therefore, differences in static and dynamic derived formation properties are higher in unconsolidated and weaker formations.

Dynamic tests are less expensive and non-destructive in comparison to static tests. They do not require the specimen to be destroyed during each test, therefore a new specimen is not always required. Fewer formation samples can be used to carry out several formation evaluation investigations. Dynamic formation geomechanical properties require accurate and reliable acoustic measurements for the precise evaluation of the formation, however, acoustic measurements are not available in all reservoir formation during exploration and development to perform these formation evaluations (Mullen et al., 2007; Schön, 2015). For example, in reservoir formations where sonic logging tools have obtained false acoustic measurements. This may be due to irregularities in the borehole like washout (Onalo et al., 2018a). In scenarios where the logging

tool is stuck or damaged in-hole, it becomes costly to pull out and re-run the logging tool due to the large depth range; thus, acoustic measurements may not be available throughout the entire well sections (Ramcharitar and Hosein, 2016). Moreover, in older offset wells which have been logged with older generation logging tools, not all array of acoustic measurements is obtainable (Paillet, 1985; Pickett, 1963; Tixier et al., 1975). Typical borehole compensated logging tools measure the compressional wave transit time, but do not measure the shear wave transit time (Akhundi et al., 2014; Nourafkan and Kadkhodaie-Ilkhchi, 2015). This limits the quality of elastic formation properties that can be estimated from the dataset, hence, a limitation in the formation evaluation quality. The critical question remains, how then can accurate and reliable data required to make these dynamic geomechanical properties for formation evaluation assessment be obtained?

Intelligent systems have been used in many engineering industries to solve highly complex non-linear problems due to their high precision and accuracy (Rajabi et al., 2010). Intelligent systems have succeeded where other empirical and analytical techniques have not been so successful (Ibrahim and Potter, 2004; Rajabi and Tingay, 2013; Rezaee et al., 2007; Sbiga and Potter, 2017; Zendehboudi et al., 2012).

In this research study, we investigate and evaluate suitable techniques to provide reliable data for the estimation of the geomechanical dynamic properties for formation evaluation during field exploration and development. The aim of the research is to provide safe, efficient and reliable techniques for providing tools for proper field management and strategic planning from readily available field data, instantaneously.

1.2 Research Questions

The most reliable method of determining formation properties is through experimental analysis of samples acquired from reservoir formations. This method is expensive, discrete and static. Alternatively, dynamic estimation provides a safe, non-destructive means of continuous determination of the formation properties. This work is focused on dynamic estimation, attempting the following questions:

- Can static petrophysical properties be estimated from dynamic petrophysical properties for a better description of the reservoir formation?
- In the absence of compressional and shear acoustic measurements, how can geomechanical properties like sanding potential be estimated?
- In offset wells where compressional acoustic measurements are available, what technique can be suggested to estimate the shear wave acoustic transit time to determine the formation petrophysical properties?
- What other techniques can be recommended to reproduce and validate sonic well logs where real well logs are questionable?
- Is ANN a reliable tool for sonic log prediction?

1.3 Motivation

Lack of static, laboratory derived formation properties should not be a limiting factor in the determination of the properties of the formation. Though this challenge is often surmounted by using acoustic measurements to estimate the dynamic formation properties, the absence of actual measured acoustic data should also not be an impediment. The research aims to investigate

techniques of acquiring and validating sonic logs and their dynamically estimated formation properties through the use of empirically derived correlations and intelligent systems

1.4 Objectives of the Research

Six research questions mentioned in section 1.2 led to formulate key objectives:

- To establish that a static formation property (Young's Modulus) can be estimated from its dynamic counterpart by developing a model to predict the static property from the dynamic property.
- To develop a model to estimate compressional and shear wave transit time to determine sanding potential of a reservoir formation.
- To develop a model to estimate shear wave transit time with available compressional wave time logs.
- To improve predictability and reproduction of previous sonic log determination models.
- To assess the suitability of these dynamic data driven techniques for industry use.

1.5 Novelty and contributions

The novelty and the contributions are presented in chapter 2 and are summarized as follows:

- A new data-driven model to estimate the static Young's modulus of a formation from its dynamic Young's modulus and a lithology dependent parameter.
- A new data-driven methodology for determining the sanding potential of a formation using artificial neural network as an intelligent system.

- A new data-driven model to determine shear wave transit time in offset wells using a Gaussian process distribution system.

- A new data-driven model to estimate the sequential sonic well log data in reservoir formations using a recurrent neural network as an improved intelligent system.

- An assessment to determine the suitability of ANN as a reliable sonic logging tool.

1.6 Organization of thesis

A manuscript style format has been adopted in preparing this thesis. The outline of the thesis and each chapter is presented as follows:

Chapter 2 presents the concepts, contributions and innovations of the thesis for the determination of dynamic petrophysical and geomechanical properties for reservoir evaluation.

Chapter 3 presents a review of relevant literature which has not been presented in the subsequent chapters.

Chapter 4 presents an empirically derived model for estimating static Young's modulus from dynamic Young's modulus from laboratory data. This paper improves on previously established models by including a lithology dependent variable. This chapter has been published in the JOURNAL OF PETROLEUM SCIENCE AND ENGINEERING 171 (2018): 394-402. HTTPS://DOI.ORG/10.1016/J.PETROL.2018.07.020

Chapter 5 presents a model to determine the likelihood of a formation to sanding in the absence of compressional and shear wave transit time. The technique used is a back propagation artificial neural network. This chapter has been published in the JOURNAL OF PETROLEUM SCIENCE AND ENGINEERING 2018. HTTPS://DOI.ORG/10.1016/J.PETROL.2018.06.072

Chapter 6 presents a model estimating the formation shear wave transit time when compressional transit time and other well logs are available for the estimation of mechanical formation properties. The technique used is a Gaussian process regression. This chapter has been reviewed by the supervisory committee and has been submitted to the JOURNAL OF PETROLEUM EXPLORATION AND PRODUCTION TECHNOLOGY.

Chapter 7 presents a dynamic model for estimating and reproducing sonic well logs. Actual well logs are presented in the study from the Norwegian continental shelf and the Niger Delta. This chapter has been published in the JOURNAL OF PETROLEUM SCIENCE AND ENGINEERING 2019.

Chapter 8 presents an assesment of artificial neural network models as a reliable technique to provide sonic well logs where acoustic measurement data are missing or have been damaged. This chapter has been reviewed by the supervisory committee and has been submitted to the JOURNAL OF PETROLEUM SCIENCE.

Chapter 9 presents the summary, conclusions and recommendations of this thesis.

The appendixes present other outputs during the research period in collaboration with other students that have resulted in publications

Appendix 1 presents a reservoir model to investigate Effect of Na^+ and SO_4^2 on sandstone and carbonates during low water salinity injection. This appendix has been published in FUEL JOURNAL 2018. FUEL 232, 362–373. HTTPS://DOI.ORG/10.1016/J.FUEL.2018.05.161"

Appendix 2 presents a new empirical model for the estimation of shear wave velocity in siliciclastic rocks which can be applied to any geological region. This appendix has been submitted to the JOURNAL OF PETROLEUM SCIENCE AND ENGINEERING 2018.

References

Akhundi, H., Ghafoori, M., Lashkaripour, G.-R., 2014. Prediction of Shear Wave Velocity Using Artificial Neural Network Technique, Multiple Regression and Petrophysical Data: A Case Study in Asmari Reservoir (SW Iran). Open J. Geol. 04, 303–313. https://doi.org/10.4236/ojg.2014.47023

Buffett, B., 2016. Earth science: Another energy source for the geodynamo. Nature. https://doi.org/10.1038/529288a

den Brok, S.W.J., David, C., Bernabé, Y., 1997. Preparation of synthetic sandstones with variable cementation for studying the physical properties of granular rocks. Comptes Rendus l'Académie des Sci. - Ser. IIA - Earth Planet. Sci. 325, 487–492. https://doi.org/10.1016/S1251-8050(97)89866-7

Fjær, E., 2009. Static and dynamic moduli of a weak sandstone. GEOPHYSICS 74, WA103-WA112. https://doi.org/10.1190/1.3052113

Harouaka, A., Mtawaa, B., Abdulraheem, A., Klimentos, T., 1995. Multistage triaxial testing of actual reservoir cores under simulated reservoir. SCA Conf. 1–10.

Hernandez-Uribe, L.A., Aman, M., Espinoza, D.N., 2017. Assessment of Mudrock Brittleness with Micro-scratch Testing. Rock Mech. Rock Eng. 50, 2849–2860. https://doi.org/10.1007/s00603-017-1279-y

Holt, R.. M., Brignoli, M., Kenter, C.. J., 2000. Core quality: Quantification of coring-induced rock alteration. Int. J. Rock Mech. Min. Sci. 37, 889–907. https://doi.org/10.1016/S1365-1609(00)00009-5

Holt, R.M., Nes, O.-M., Stenebraten, J.F., Fjaer, E., 2012. Static Vs. Dynamic Behavior of Shale. 46th U.S. Rock Mech. Symp.

Ibrahim, M.A., Potter, D.K., 2004. Prediction of Residual Water Saturation Using Genetically Focused Neural Nets. SPE Asia Pacific Oil Gas Conf. Exhib. https://doi.org/10.2118/88457-MS

IEA International Energy Agency, 2016. Annual Energy Outlook 2016 Early Release: Annotated Summary of Two Cases. Annu. Energy Outlook 2016 1–61.

King, M.S., Jing, X.D., 2001. Petrophysical Studies of Sandstones Under True-Triaxial Stress Conditions. Int. Symp. Soc. Core Anal. 1–11.

Ma, L., Liu, X., Wang, M., Xu, H., Hua, R., Fan, P., Jiang, S., Wang, G., Yi, Q., 2013. Experimental investigation of the mechanical properties of rock salt under triaxial cyclic loading. Int. J. Rock Mech. Min. Sci. 34–41.

Majorowicz, J., Unsworth, M., Chacko, T., Gray, A., Heaman, L., Potter, D.K., Schmitt, D.R., Babadagli, T., 2013. Geothermal energy as a source of heat for oil sands processing in northern Alberta, Canada.

McMahonSean, ParnellJohn, J.F., B., 2016. Evidence for Seismogenic Hydrogen Gas, a Potential Microbial Energy Source on Earth and Mars. https://home.liebertpub.com/ast. https://doi.org/10.1089/AST.2015.1405

Mese, A.I., Tutuncu, A.N., 1997. An investigation of mechanical, acoustic and failure properties in unconsolidated sands. Int. J. Rock Mech. Min. Sci. 34, 314.e1-314.e9. https://doi.org/10.1016/S1365-1609(97)00244-X

Miller, D.H., Van Mieghem, J., Hales, A.L., 2016. Energy at the Surface of the Earth : an Introduction to the Energetics of Ecosystems. Elsevier Science.

Mockovčiaková, A., Pandula, B., 2003. Study of the relation between the static and dynamic moduli of rocks. Metalurgija 42, 37–39.

Mullen, M.J., Roundtree, R., Turk, G.A., 2007. A Composite Determination of Mechanical Rock Properties for Stimulation Design (What to Do When You Don't Have a Sonic Log). Rocky Mt. Oil Gas Technol. Symp. https://doi.org/10.2118/108139-MS

Nourafkan, A., Kadkhodaie-Ilkhchi, A., 2015. Shear wave velocity estimation from conventional well log data by using a hybrid ant colony-fuzzy inference system: A case study from Cheshmeh-Khosh oilfield. J. Pet. Sci. Eng. 127, 459–468. https://doi.org/10.1016/j.petrol.2015.02.001

Nouri, A., Vaziri, H., Belhaj, H., Shomakhi, N., Butt, S., Donald, A., Islam, R., 2005. Experimental study of sand production from a supported wellbore in weakly consolidated sandstone. Geotech. Test. J. 28, 413–422.

Onalo, D., Adedigba, S., Khan, F., James, L.A., Butt, S.D., 2018a. Data Driven Model for Sonic Well Log Prediction. J. Pet. Sci. Eng. https://doi.org/10.1016/j.petrol.2018.06.072

Onalo, D., Oloruntobi, O., Adedigba, S., Khan, F., James, L., Butt, S., 2018b. Static Young's modulus model for drilling operation planning. J. Pet. Sci. Eng.

Paillet, F.L., 1985. Applications Of Borehole-Acoustic Methods In Rock Mechanics. 26th U.S. Symp. Rock Mech.

Pickett, G.R., 1963. Acoustic Character Logs and Their Applications in Formation Evaluation. J.

Pet. Technol. 15, 659–667. https://doi.org/10.2118/452-PA

Rajabi, M., Bohloli, B., Gholampour Ahangar, E., 2010. Intelligent approaches for prediction of compressional, shear and Stoneley wave velocities from conventional well log data: A case study from the Sarvak carbonate reservoir in the Abadan Plain (Southwestern Iran). Comput. Geosci. 36, 647–664. https://doi.org/10.1016/J.CAGEO.2009.09.008

Rajabi, M., Tingay, M., 2013. Applications of Intelligent Systems in Petroleum Geomechanics-Prediction of Geomechanical Properties in Different Types of Sedimentary Rocks, in: International EAGE Workshop on Geomechanics and Energy.

Ramcharitar, K., Hosein, R., 2016. Rock Mechanical Properties of Shallow Unconsolidated Sandstone. SPE Trinidad Tobago Sect. Energy Resour. Conf. https://doi.org/10.2118/180803-MS

Ravazzoli, C.L., Santos, J.E., Carcione, J.M., 2003. Acoustic and mechanical response of reservoir rocks under variable saturation and effective pressure. J. Acoust. Soc. Am. 113, 1801–1811. https://doi.org/10.1121/1.1554696

Rezaee, M.R., Kadkhodaie Ilkhchi, A., Barabadi, A., 2007. Prediction of shear wave velocity from petrophysical data utilizing intelligent systems: An example from a sandstone reservoir of Carnarvon Basin, Australia. J. Pet. Sci. Eng. 55, 201–212. https://doi.org/10.1016/J.PETROL.2006.08.008

Sagan, L.A., 1972. Human costs of nuclear power. Science 177, 487–93. https://doi.org/10.1126/science.177.4048.487

Santarelli, F.J., Detienne, J.L., Zundel, J.P., 1989. Determination of the Mechanical Properties of

Deep Reservoir Sandstones to Assess the Likelyhood of Sand Production. ISRM Int. Symp.

Sbiga, H.M., Potter, D.K., 2017. Prediction of Resistivity Index by Use of Neural Networks With Different Combinations of Wireline Logs and Minimal Core Data (see associated supplementary discussion). SPE Reserv. Eval. Eng. 20, 240–250. https://doi.org/10.2118/181751-PA

Schön, J., 2015. Basic Well Logging and Formation Evaluation Basic Well Logging and Formation Evaluation 4 Contents, 1st ed.

Song, R., Yue-ming, B., Jing-Peng, Z., De-yi, J., Chun-he, Y., 2013. Experimental investigation of the fatigue properties of salt rock. Int. J. Rock Mech. Min. Sci. 64, 68–72. https://doi.org/10.1016/j.ijrmms.2013.08.023

Stringer, K.D., 2008. Energy Security: Applying a Portfolio Approach. Balt. Secur. Def. Rev. 10, 121–142.

Svitek, T., Republic, C., 2014. Laboratory approach to the study of rock dynamic and static elastic anisotropy under high hydrostatic pressure 1–6.

Tixier, M.P., Loveless, G.W., Anderson, R.A., 1975. Estimation of Formation Strength From the Mechanical-Properties Log (incudes associated paper 6400). J. Pet. Technol. 27, 283–293.

Viswanathan, B., 2016. Energy Sources. Elsevier Science.

Vivoda, V., 2009. Diversification of oil import sources and energy security: A key strategy or an elusive objective? Energy Policy 37, 4615–4623. https://doi.org/10.1016/J.ENPOL.2009.06.007

Younessi, A., Rasouli, V., Wu, B., 2013. Sand production simulation under true-triaxial stress conditions. Int. J. Rock Mech. Min. Sci. 61, 130–140. https://doi.org/10.1016/j.ijrmms.2013.03.001

Zendehboudi, S., Ahmadi, M.A., James, L., Chatzis, I., 2012. Prediction of condensate-to-gas ratio for retrograde gas condensate reservoirs using artificial neural network with particle swarm optimization. Energy and Fuels 26, 3432–3447. https://doi.org/10.1021/ef300443j

Chapter 2 Novelty and contribution

The novelty and contribution of this research are in the area of safe, inexpensive and reliable dynamic formation evaluation for the exploration and development of reservoir formations. The highlights of these novelties and contributions are presented in Figure 2.1 and summarized below:

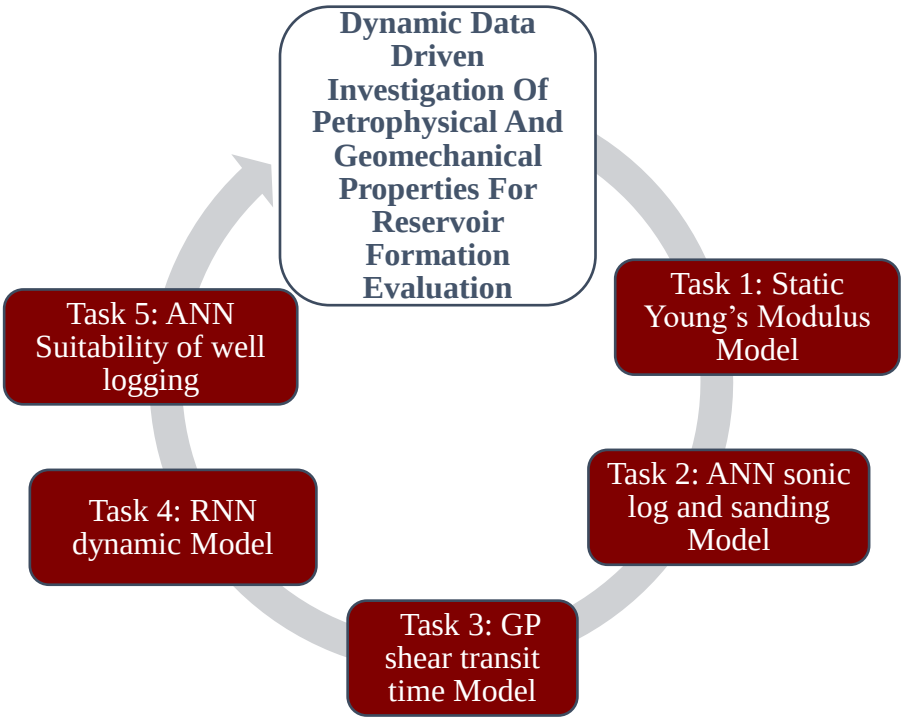

Figure 2.1 Outline of research contribution and novelty

- A novel and innovative model to estimate static Young's modulus. The model is novel and outperforms previously established empirical models. The major step forward is the inclusion of a lithology-porosity dependent parameter which constrains the estimations of the novel model to improve the accuracy of the model. The significance of such a novel model is that it presents the industry with a model to describe a more reliable static formation property (static Young's modulus). This allows for better characteristic

description of the formation for formation evaluation. This contribution is presented in chapter 4.

- An innovative intelligent system sanding prediction model. The model is based on the dynamic determination of compressional and shear sonic transit time in the absence of reliable acoustic measurements. The model is data-driven by real well logs from the Niger Delta of West Africa. The novel model intelligent system is an artificial neural network which is the first model to combine gamma-ray, formation bulk density and shale volume predictively to determine the sonic logs. This contribution and significance of this model are that it provides real-time ability for engineers to make on the spot decision of the likelihood of the formation to sand thereby enabling the engineers to make quick, efficient and effective formation evaluation for field development. This contribution is presented in chapter 5.

- An innovative shear sonic wave transit time model. The model is based on Gaussian process and is data driven by real well logs from a sandstone formation located in the Niger Delta. The significance of model is that in many offset wells which have not been logged by logging tools capable of acquiring shear wave transit time, the data can be completed to provide dynamic descriptions of the formation characteristic properties for formation evaluation. This contribution is presented in chapter 6.

- An innovative dynamic sonic logging model. The model is based on an intelligent system known as Non-linear autoregressive with exogenous input recurrent neural network. The model is data driven by sequential log data from the Norwegian continental shelf and the Niger Delta. The model provides a means of validating and producing existing sonic logs

with the knowledge of either gamma-ray or neutron logs from the same formation. This contribution is presented in chapter 7.

- In chapter 8, an innovative assessment of the reliability of artificial neural networks (ANN) as a reliable tool for providing sonic well logs where well log data is missing or damaged. The assessment provides a critical look into the limitations, pitfalls and shortcoming of ANN as a technique especially in its growing use in the oil and gas industry. The assessment also resents some challenges often encountered in the development of the ANN models.

Figure 2.2 demonstrates how each of the scientific contribution and task are integrated and developed to form a wholistic and a significant body of knowledge during this research.

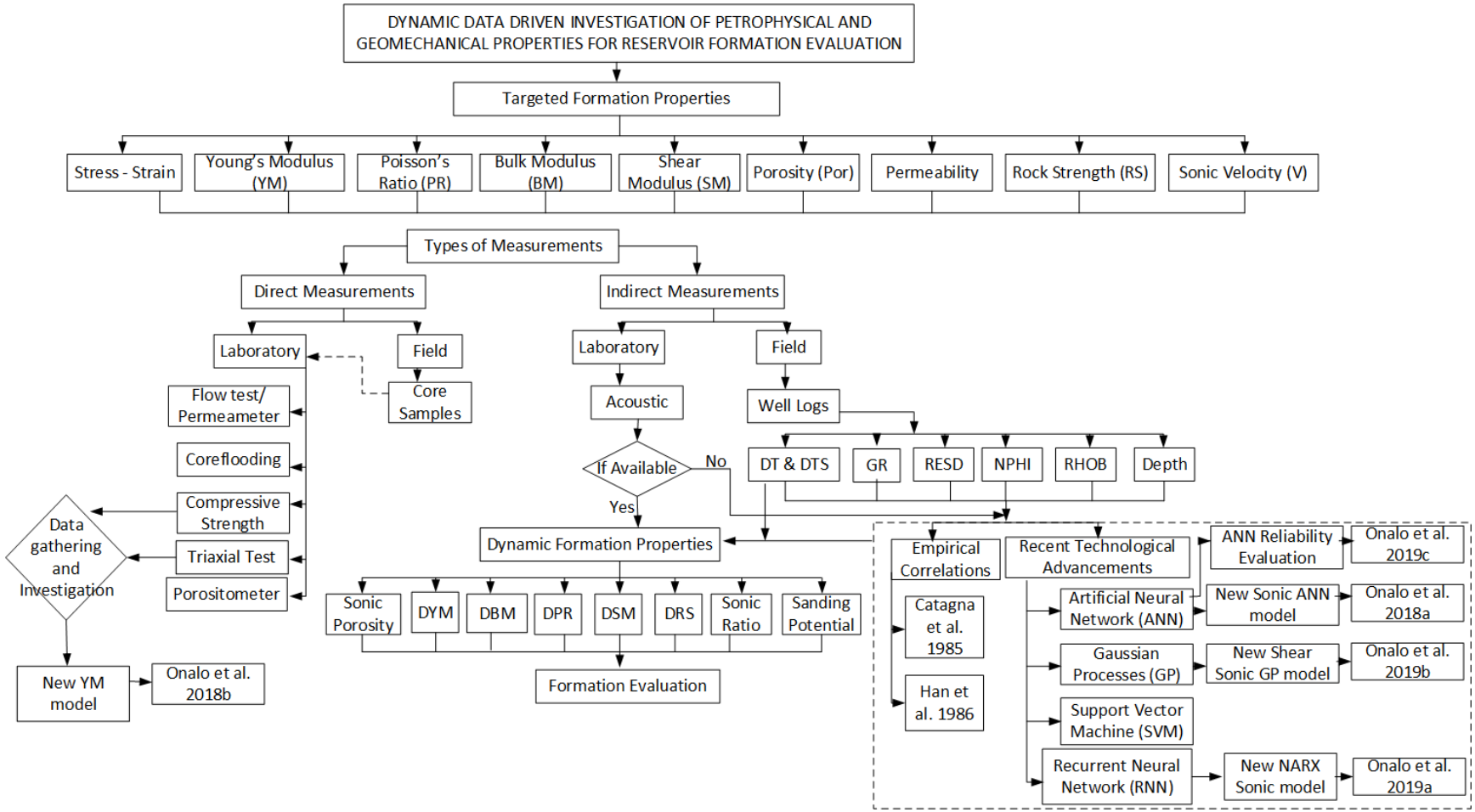

Figure 2.2 Tasks Integration and Scientific Contribution

Chapter 3 Literature review

Co-authorship statement

A version of this manuscript has been submitted to the supervisory committee. The lead author, David Onalo, performed the literature review, gathered the data for the development of the models, developed the models, analyzed the results and drafted the manuscript. Co-author Dr. Lesley James, Dr. Faisal Khan and Dr. Stephen Butt supervised the collection of literature, data collection, data analysis and literature review. The co-authors reviewed and provided feedback on the manuscript. I revised the manuscript based on the feedback from the Co-authors and throughout the peer review process.

Abstract

In the absence of static geomechanical formation properties or readily available cores to perform these destructive and expensive static tests, dynamic geomechanical estimations provide a reliable and inexpensive alternative. A review of properties, compressional and shear sonic velocities, is presented to evaluate how they are acquired, how their estimations can be improved and what alternatives exist peradventure the sonic data or tool is corrupted The relationship between the geomechanical formation properties and acoustic wave energy traveling through the earth has been used by scientists to explore and determine reservoir formation properties like formation lithology, fluid saturation, formation strength, porosity, and clay content. It is not always possible to acquire direct estimations from every area of the prospective formation; therefore, empirical estimations like those developed by Tosaya, Castagna, and Ebert-Phillip have been used to estimate the values of the ratio of the velocities. This chapter reviews the evolution of the estimations of compressional velocity, shear velocity, and their ratio in different formations. It is observed that although the compressional and shear wave velocity are functions of porosity, their ratio is not a function according to previous equations. This may not be the case according to field data analyzed. The main aim of this chapter is to investigate previously established means of calculating compressional and shear wave velocity to provide a characteristic description of reservoir formations. In addition, brief descriptions of typical rock properties of interest in the oil and gas industry and well logs are presented to aid the reader understand the material in the subsequent chapters.

3.1 Introduction

Acoustic wave energy propagating through rock formations in the earth have proven to be very strong, and reliable methods for defining, and characterizing formation properties. Some of the properties which acoustic waves energy propagating through the formations have been used to identify include: lithology, density, fluid saturation, and dynamic elastic constants like bulk modulus and modulus of rigidity (Zoback, 2010). The characteristic properties of the wave energy that are used to estimate the formation rock properties tend to be one or more of the following: velocity, frequency, slowness, amplitude, attenuation, and quality factor (Khazanehdari and Mccann, 2005). This review lays emphasis on the acoustic wave energy velocities because this is the most commonly observed characteristic property used in such investigations.

3.1.1 Types of acoustic waves

There are four main types of acoustic waves, two body waves namely: compressional and shear waves, surface waves, namely: Rayleigh and Stoneley waves (Pickett, 1963). In this article, we shall focus on body waves.

Compressional waves (P-waves) are also known as primary or pressure waves. They travel along the body in the direction of the body's particle motion. P-waves have the fastest arrival times from an acoustic energy source. In rock formations that are saturated with fluids, P-waves travels through both the solid and the liquid (Hamada, 2004).

Shear waves (S-waves) are also known as secondary. They travel across the body in a direction that is perpendicular to the body's particle of motion; therefore, S-waves are transverse in nature. S-waves are the second fastest waves; however, they do not travel through fluids in a saturated porous media (rock formation). They only travel in the solid because fluids do not shear.

Compressional waves and shear waves are of particular interest in the oil and gas industry for formation evaluation. Sonic tools which contain source pulse transmitters and signal receivers can be found in logging tool assemblies for wireline and "logging while drilling" (LWD) operations. The information from these logging tools can be interpreted at the surface real time to identify the porosity, lithology, density, overpressure, fluid saturation, and other formation rock properties (Mavko et al., 2003). The values of the acoustic wave energy response vary not only with the lithology, and fluid saturation/content but also with depth. This is to say that, within a homogenous rock formation, the acoustic wave energy transmitted is uniform. Changes in the pore geometry, mineralogy, confining pressure, porosity, clay content, pore pressure, consolidation, temperature, and cementation alter the response of the acoustic wave energy transmitted through a formation (Han et al., 1986).

3.1.2 **Background**

Researchers over the years have proposed several empirical, and analytical equations/solutions to estimate, and predict the relationship between acoustic wave energy and other rock properties. Compressional wave attributes like the velocity are the most commonly used attribute of the wave energy transmitted through the formations because they flow through the solid matrix and formation fluid. Over time, researchers observed that the shear waves also responded considerably to changes in the formation (Castagna et al., 1985). This proved to be very useful to well log analysis in oil and gas exploration (Hamada et al., 2004).

3.1.3 **Compressional Wave Velocity**

The velocity of the waves traveling parallel to the direction of particle motion in the formation is probably the most studied attribute of acoustic wave energy and was originally the only attribute of interest in the formation evaluation (Picket 1963). One of the earliest investigations of

compressional wave velocity is seen in the work by Wyllie in 1956. Sonic pulse measuring velocity technique (transmitter) was used to investigate the changes in compressional wave velocity due to changes in the formation fluid (brine, oil, gas), salinity, saturation, and temperature (Wyllie et al., 1956). Wyllie was able to relate wave velocity with porosity through equation (3.1) and included the density in equation (3.2).

$$\frac{1}{v} = \frac{\varphi}{v_{ma}} + \frac{1-\varphi}{v_{fl}} \tag{3.1}$$

$$\frac{1+G}{v^2} = \left[\frac{\varphi}{{v_{ma}}^2 \rho_{ma}} + \frac{(1+G)(1-\varphi)}{{v_{fl}}^2 \rho_{fl}}\right] * (\varphi\rho_{ma} + (1-\varphi)\rho_{fl} \tag{3.2}$$

φ=porosity, v= velocity, G=shear modulus and ρ= density, while the subscripts ma and fl indicate attributes of the matrix and fluid respectively

Wyllie's investigations show that velocity increases as the porosity reduced with increasing depth. Velocity reduces in porous media as the saturation of the fluid reduces except in cases where the effluent is replaced with a denser fluid. Biot (1941) and Gassmann (1951) theory suggests that the elastic constants, particularly the Biot's coefficient, bulk modulus and shear modulus also vary with fluids in the interconnected pores (effective porosity) (Biot, 1941; Gassmann, 1951). Birch in 1960 furthers the research by transmitting wave energy at pressures up to 12 Kilobars in metamorphic and igneous rocks. His research shows that velocity increases with increasing pressure, but he does not consider sedimentary rocks or the effects of porosity (Birch, 1960). Birch later demonstrated that at low pressures, velocity is a function of porosity, composition, and anisotropy, but at higher pressures, it is more of a function of density and atomic weight. In homogenous or isotropic formations with the same atomic weight, velocity has a linear relationship

with porosity (Birch, 1961). Most elastic constants can be estimated if at least two of the elastic constast of the formation are known. Birch suggested that these estimations were only valid if the formations test were performed at the same pressure and temperature. However, above 10 kilobars and 600^0C, the effects of temperature and pressure can be neglected. Porosity across formations while drilling is not constant; Raymer, Hunt, & Gardner (1980) described this change by the "lack of compaction factor" (Cp) which is related to the apparent porosity term used in Wyllie's equation by equation (3.3):

$$\varphi_c = \frac{\varphi}{Cp} \tag{3.3}$$

Raymer, Hunt, & Gardner (1980) proposed different equations to characterize different ranges of porosity as follows:

Less than 37% porosity

$$v_p = (1-\varphi)^2 v_{ma} + \varphi v_{fl} \tag{3.4}$$

$$\Delta t_{p<37} = 10^6/v_p \tag{3.5}$$

Between 37% - 47% porosity

$$\Delta t_{p37-47} = \frac{0.47-\varphi}{0.1}\Delta t_{p<37} + \frac{\varphi - 0.37}{0.1}\Delta t_{p>47} \tag{3.6}$$

Greater than 47% porosity

$$\Delta t_{p>47} = \sqrt{\frac{\varphi\rho{\Delta t_{fl}}^2}{\rho_{fl}} + \frac{(1-\varphi)\rho{\Delta t_{ma}}^2}{\rho_{ma}}} \tag{3.7}$$

Δt= travel time

In 1982, Tosaya investigated the dependence of compressional waves on clay content. Clay content is observed to have a lower effect on the compressional velocity than porosity (Tosaya and Nur, 1982). Tosaya (1982) proposes the following equation:

$$v_p = -2.4C - 8.6\varphi + 5.8 \quad (3.8)$$

C= clay content

Equation (3.8) illustrates a linear relationship between compressional velocity and clay content in consolidated formations, but the compressional-velocity of unconsolidated sandstone formation deviates from this trend and are lower than predicted. Beside the porosity of the formation, the clay microporosity increases the void fillable by formation fluids to further reduce the velocity (Kowallis et al., 1984). Kowallis, Jones and Wang (1984) proposed equation (3.9) for Dry West Delta Sandstone:

$$v_p = -5.7C - 9.2\varphi + 5.6 \quad (3.9)$$

3.1.4 **Shear Wave Velocity**

In 1943, Birch (1960) refers to earlier research he performed on S-waves at elevated temperatures to buttress the fact that secondary waves velocity has been around for a long time. Pickett's work with shear waves may very well be one of the cornerstone discoveries in the use of shear waves in formation evaluation. Pickett observed that previous research only focused on the first arrival time of the wave energy, but they neglected they secondary and following wave arrivals. He believed that these could be categorized in such a way that a trend could be established. This led to the famous porosity estimation from sonic well logs based on the compressional waves and the ability to identify possible lithological intervals along a well. They were also able to observe that fractures

in the formations affected the travel time of the wave energy. This resulted in a reduction in the velocity and signal amplitude which was greater in the shear-wave than in the compressional-waves, again proving that the potential of shear waves. Though he did not provide an empirical correlation, the graphs, and charts from his laboratory experiments were utilized as benchmarks for slope and trends in clean sandstone, dolomite, limestone and limy sandstone (Pickett, 1963). The fluid considered in Pickett 1963 is the borehole fluid; he did not consider the formation fluid content or saturation. Nur and Simmons 1969 also validated Birch's work in their investigations, which showed that the velocities are higher at higher pressures. Laboratory investigation of seismic velocity under ambient conditions; therefore, underestimate the velocities found in reservoir formations. In saturated formations, the reduction in the primary velocity is less and assumed to be negligible in shear-velocity. Pickett's work proves otherwise; the effect of saturating the pores with fluid can be observed more closely in the amplitude of the arrival wave. A formation can have matrix pore porosity and porosity of the cracks or fractures. It was observed that the velocity of saturated granite was higher in cores with cracks than those with pores (Nur and Simmons, 1969). It would be logical to conclude that the matrix porosity is part of the grain structure of the formation, thus, their bulk modulus is much higher than the formation. A similar observation should be observed when confining pressure is increased. The elastic constants are observed to be similar in dry formation and saturated formations and can be expressed as functions of the velocities (Nur and Simmons, 1969).

$$K = (v_p{}^2 - \frac{4}{3} v_s{}^2)\rho \tag{3.10}$$

$$G = v_s{}^2 \rho \tag{3.11}$$

K= bulk modulus, G= shear modulus, v_p= compressional velocity and v_s=shear velocity

In 1976, Toksoz, Cheng, and Timur narrowed the effects of pore shape and sizes in the formation in sandstone and limestone for brine, water, oil, kerosene, gas and air; their results validate Nur and Simmons conclusions. In addition. They observed that gas velocities were lower than brine velocities round the pores; however, the amplitude or frequency of the response was not considered. At temperatures before freezing point, the velocities increased significantly to close the pores (Toksöz et al., 1976). Wang's investigation demonstrates the reverse; increase in temperature reduces the velocity (Wang and Nur, 1986). The compression reflection coefficient was found to be:

$$R = \frac{v_{pfl}\rho_{fl} - v_{pma}\rho_{ma}}{v_{pfl}\rho_{fl} + v_{pma}\rho_{ma}} \tag{3.12}$$

According to Gregory (1977), the Faust equation can be used to estimate velocity as a function of the age of the rock formation:

$$v = J\sqrt[6]{(zT)} \tag{3.13}$$

J= 125.3, z= depth (m) and T = age (years)

Gregory (1977) expresses Geertsma (1961) compressional-velocity as a function of velocity at a frequency of zero and infinity in equations (3.14) and (3.15):

$$v_p = \left\{\frac{1}{\rho_b}\left[\left(\frac{\beta}{c_s} + \frac{4}{3}G_b\right) + \frac{(1-\beta)^2}{(1-\varphi-\beta)c_s + \varphi c_f}\right]\right\}^{0.5} \tag{3.14}$$

$$v_p = \left\{\left(\frac{\beta}{c_s} + \frac{4}{3}G_b\right) + \left[\frac{\varphi\rho_b/K\rho_f + (1-\beta)(1-\beta-\frac{2\varphi}{k})}{(1-\varphi-\beta)c_s + \varphi c_f}\right] * \frac{1}{\rho_b(1-\frac{\rho_f}{\rho_b}\frac{\varphi}{k})}\right\}^{0.5} \tag{3.15}$$

c_s, c_b, c_f= matrix, bulk, fluid compressibility, $\beta = \frac{c_s}{c_b}$ and G_b=dry shear modulus

Similar to porosity, clay content in a formation affects the velocity, it reduces the velocity in seismic waves (Minear, 1982). Minear (1982) observed that the reduction in velocity occurred more in laminated and structural clay, but the reduction was negligible in dispersed clay. Perhaps, this is due to the mobility of the dispersed clay in the formation. It is likely that the dispersed clay is randomly oriented (on average) and opposed to laminated clay that is strongly oriented. The orientation results in an expression of the anisotropy of the clay minerals. The dispersed clay does not adhere to the pore surface and are free to flow is the pore fluid. Tosaya (1982) updated equation (3.8), and includes shear velocity (Tosaya, 1982) in equation (3.16) and (3.17):

$$v_p = -2.4C - 8.6\varphi + 5.8 \tag{3.16}$$

$$v_s = -2.1C - 6.3\varphi + 3.7 \tag{3.17}$$

Domenico modifies equation (3.1) to include two new constants; A and B:

$$\frac{1}{v} = A + B\varphi \tag{3.18}$$

$$A = \frac{1}{v_{ma}} \tag{3.19}$$

$$B = \frac{1}{v_{fl}} - \frac{1}{v_{ma}} \tag{3.20}$$

A is the inverse of the matrix velocity, while B is the change of the velocity with porosity. His work notes that the rate of change with porosity is greater in shear wave velocity (Domenico, 1984). Similar to the Tosaya, Castagna (1985) proposed equation (3.21) and (3.22) based laboratory investigation on sandstones (Castagna et al., 1985):

$$v_p = -2.21C - 9.4\varphi + 5.81 \tag{3.21}$$

$$v_s = -2.04C - 7.07\varphi + 3.89 \tag{3.22}$$

Han, Nur, & Morgan (1986) conducted their investigation at 40 Mpa, and 1 Mpa pore pressure, and proposed equation for shaley sandstones:

$$v_p = -2.18C - 6.93\varphi + 5.59 \tag{3.23}$$

$$v_s = -1.89C - 4.91\varphi + 3.52 \tag{3.24}$$

In geomechanics, effective pressure(P_e) is the difference between the pore pressure and the total overburden pressure when the Biot coefficient is assumed to be unity (Zoback, 2010). Velocity increases as the effective pressure is increases. Eberhart-Phillips, Han, & Zoback (1989) described this relationship in equation (3.25) and (3.26):

$$v_p = -1.73\sqrt{C} - 6.94\varphi + 5.77 + 0.446(P_e - e^{-16.7P_e}) \quad (3.25)$$

$$v_s = -1.57\sqrt{C} - 4.94\varphi + 3.70 + 0.361(P_e - e^{-16.7P_e}) \quad (3.26)$$

More recently, Ramcharitar & Hosein (2016) proposed the following empirical model which included the density of the formation:

$$\Delta t_p = 19C - 0.0066\varphi + 139Z - 18\rho + 153 \quad (3.27)$$

$$\Delta t_s = 33C - 0.0052\varphi + 159Z + 205\rho + 2.89\Delta t_p \quad (3.28)$$

3.1.5 **Compression to Shear Wave Ratio**

The ratio of the velocities can be an effective tool in determining changes in the reservoir formations. The ratio of compressional: shear-velocity is less than 2 in consolidated sands but greater in some unconsolidated sands. During the production of reservoir fluids, the reservoir pressure shifts below the bubble point over time; velocity ratio is observed to reduce, indicating a liberation of gas into the formation (gas saturation is increased) (Gregory, 1977). Tatham (1982) suggest that this ratio is constant in isotropic formations; therefore, any variation would indicate a change in lithology. Furthermore, cracks in the formation are observed to cause deviations in these values, indicating that the ratio can be used to indicates the presence of faults, and cracks in a formation.

$$\left(\frac{v_p}{v_s}\right)^2 = \frac{2(1-\vartheta)}{1-2\vartheta} = \frac{k}{\vartheta} + \frac{4}{3} \quad (3.29)$$

ϑ= Poisson's ratio

Velocity ratios in some formations as observed include Limestone – 1.9, Dolomite – 1.8, and Sandstones – 1.6 – 1.75. The equation (3.29) results in a ratio of 1.732 when ϑ is 0.25 for a typical sandstone specimen (Tatham, 1982). Similarly, Poisson's ratio in these formations include: Limestone – 0.29-0.33, Dolomite – 0.27-0.29, and Sandstone – 0.17- 0.26 (Domenico, 1984). Investigations by Castagna (1985) show that this ratio decreases with increasing compressional-velocity. The relationship between compressional and shear velocity in mudrocks follows a linear trend, which is given by equation (3.30)

$$v_p = 1.16v_s + 1.36 \tag{3.30}$$

But for clean sandstone equation (3.31) was proposed, while for a sandstone containing clay, equation (3.32) was proposed:

$$\frac{v_p}{v_s} = 1.33 + \frac{0.63}{3.89 - 7.07\varphi} \tag{3.31}$$

$$\frac{v_p}{v_s} = 1.08 + \frac{1.63}{3.89 - 2.04C} \tag{3.32}$$

We observe that the porosity term is ignored in equation (3.32); this is because Castagna assumed that shaley sandstones had no porosity. It was also observed that the ratio reduced with saturation (Castagna et al., 1985). Han, Nur, & Morgan (1986) suggested that the relationship could be represented by equation (3.33) in dry formations.

$$\frac{v_p}{v_s} = 0.43C + 0.56\varphi + 1.55 \tag{3.33}$$

$$v_p = 1.26v_s + 1.07 \tag{3.34}$$

Nonetheless, this did not explain the effect of saturating the formation with fluids; therefore, Han proposed a new function 'D' that represented the difference between saturated and dry sample formations. The new function is expressed as a function of porosity and clay content:

$$D = \left(\frac{v_p}{v_s}\right)_s - \left(\frac{v_p}{v_s}\right)_d = 0.47C + 0.36\varphi + 0.018 \tag{3.35}$$

Fluid saturation type can lead to a deviation in the equation, thus, It is assumed that brine was the saturated fluid (Han et al., 1986). Saturation fluid type (brine, light hydrocarbon, heavy hydrocarbon, paraffin and wax) is a very important factor in formations where the temperature and pressure vary especially with production, injection or enhanced oil recovery (EOR) operations. Velocity reduces by up to 50% in heavy hydrocarbons with an increase in temperature; in contrast, this reduction is negligible in gas-saturated formations (Wang and Nur, 1986). It can be observed by equation (3.25) and (3.26) that as the effective pressure is increased, the ratio is reduced. This indicates a greater effect on shear wave energy by the effective pressure in comparison to compressional wave energy. Miller and Stewart (1991) proposed that in the absence of density logs, sonic velocity in sandstones and limestone can be estimated through empirical correlations as seen in the proposed equation for sandstones:

$$v_p = 1.25v_s + 1076 \tag{3.36}$$

Khazanehdari & Mccann (2005) investigates low shale sandstones in the North Sea with pressures up to 40 Mpa in several fluids. They described the ratio in brine for one of the wells by the following equation:

$$v_p = 1.598v_s + 69.35 \tag{3.37}$$

Similar models were developed by William (1990), Vernik et al. (2002), Xu and white (1995); however, the porosity was found to not be a function of the velocity ratio (Mavko et al., 2003).

The ratio of the squares of the velocities is seen to have a linear slope which may be even more sensitive than the velocity ratio to formation lithology and saturating fluid. Krief, Garat, Stellingwerf, & Ventre (1990) describes the relationship as follows:

$$\frac{{v_p}^2 - {v_{pfl}}^2}{{v_s}^2} = \frac{{v_{pma}}^2 - {v_{pfl}}^2}{{v_{sma}}^2} \tag{3.38}$$

3.2 Rock Formation Properties

3.2.1 Porosity

Porosity is a critical parameter to be considered when evaluating reservoir formations with pore volume to store the reservoir fluids and more so, conduct reservoir representative investigations (Ahmed, 2006; Fjaer, 2008). The most common method of estimating the porosity of a specimen in the laboratory is derived from its definition; the ratio of pore volume to the bulk volume of the sample (Ahmed et al., 2013; Civan, 2015; Davis et al., 2002; Johansen, 2008). For regular and even shaped samples, the bulk volume can be estimated using standard volumetric relationships; however, for irregular and uneven samples, Archimedes principle can be adopted (Huerta et al., 2005; Loverude et al., 2003). This is achieved by immersing the sample in a fluid of known density and volume; the volume of the fluid displaced after the immersion of the sample is equivalent to the volume of the sample (Heron et al., 2003; Loverude et al., 2003). The use of sophisticated equipment like mercury porosimeter has been utilized in the estimation of the void spaces and pore distribution of a sample; however, the size of the part of the investigated sample is limited (Chatzis and Dullien, 1981; Moscou and Lub, 1981; Turturro et al., 2017). The result of the mercury porosimeter can be applied to the rest of the sample in cases where the sample is homogeneous (Kuila et al., 2014). However, in samples where the formation is largely heterogeneous, other techniques are applied (Okolo et al., 2015). A common method of estimating the pore volume in the laboratory is by using Archimedes theory; the dry mass of a porous sample can be eliminated from the wet mass of the sample saturated in a fluid of known density (Heron et al., 2003; Huerta et al., 2005). The relationship between density and mass is then applied to estimate the volume of the connected pores in the formation. The methodology used for estimating density and porosity in the laboratory is presented below.

$$\rho_{unsat} = \frac{M_{unsat-air}}{M_{unsat-air} - M_{unsat-water}} \tag{3.39}$$

$$\rho_{sat} = \frac{M_{sat-air}}{M_{sat-air} - M_{sat-water}} \tag{3.40}$$

$$M_p = M_{sat-air} - M_{unsat-air} \tag{3.41}$$

$$V_p = \frac{M_p}{\rho_w} \tag{3.42}$$

$$M_B = M_{sat-air} - M_{unsat-water} \tag{3.43}$$

$$V_B = \frac{M_B}{\rho_w} \tag{3.44}$$

$$\varphi = \frac{V_p}{V_B} \tag{3.45}$$

Porosity can also be estimated from grain size distribution and the packing arrangement of the grains in the sample (Dick et al., 2017). Dynamic porosity can be estimated from sonic logs, gamma-ray logs and neutron density logs for larger samples such as wells during exploration; nonetheless, along with neutron magnetic resonance, they can be used in the laboratory when appropriately sized (Goldberg and Gurevich, 1998; Gruber et al., 2011; Hernández et al., 2000; Ouchiyama and Tanaka, 1984; Ouchlyama and Tanaka, 1986; Ramamoorthy et al., 1997).

3.2.2 **Permeability and Fluid Flow**

The pores in reservoir formations and specimen serve as storehouses for fluids such as water and hydrocarbon in petroleum reservoirs (Dake, 2008, 1996). In a petroleum reservoir, apart from the total amount of recoverable oil, the quality of the field is often described in terms of the permeability and flow rate (Tiab and Donaldson, 2015). The pressure in petroleum reservoirs

decreases as the reservoir is being produced due to the pressure difference between the reservoir and the surface, thereby forcing the Fluid flow to the surface (Rivière, 2008). Investigation of the in-situ response of the fluid in reservoir formations can be observed from the permeability of the formation (Jackson et al., 1989). Permeability is dependent on the amount of stress applied to the specimen, the higher the applied stress, the lower the permeability value. This is due to the closure of the pores and fractures to reduce the overall accessible flow path (Han and Dusseault, 2003). The effective porosity of specimen determines the flow path and channels; this can be different depending on the flow conditions simulated in the laboratory (Tiab and Donaldson, 2015). Idealistic assumptions of linear and radial flow are the most commonly simulated scenarios in the laboratory; yet, this is not obtainable realistically due to the irregularity of the flow regimes and boundaries (Economides and Boney, 2000). The most popular method for describing fluid flow in porous media formation is by Darcy's law (Ahmed, 2006; Dake, 2008). For a specimen with a fluid flowing parallel in a single direction across a constant cross-sectional area, Darcy's linear flow equation is as follows (Ahmed and McKinney, 2005):

$$k = -\frac{Q * \mu * L}{A * \Delta P} \tag{3.46}$$

For a specimen with fluid flowing into the center in a circular pattern, Darcy's radial flow is as follows (Ahmed and McKinney, 2005):

$$k = \frac{Q * \mu * \ln({}^{r_e}/_{r_w})}{2\pi h * \Delta P} \tag{3.47}$$

Darcy's law is only valid for steady state, the laminar viscous flow of incompressible fluids in homogenous specimen because if any of the above listed conditions are not valid, then the results tend to be erroneous (Ahmed, 2006; Ahmed and McKinney, 2005). For turbulent flow regimes

and multiphase fluids modifications to Darcy's equation, more so, for complex flow systems, Navier-stokes equations are applied (Andrade et al., 1997). Although these complex flow systems exist in nature, they are challenging to simulate under laboratory conditions; thus, they are simulated with computerized flow models to solve the complex coupled flow equations (BuKhamseen and Ertekin, 2017; Chin et al., 2002). The models do not account for fractures in the specimen; fracture as little as 0.02 μm can drastically alter the flow path, porosity, and permeability of the reservoir specimen. In such cases, the cubic law is applied (Witherspoon et al., 1980).

$$Q/\Delta h = C(2b)^3 \tag{3.48}$$

C is a constant that depends on the geometry and fluid properties. The permeability of gas in the reservoir tends to be higher than the permeability of liquids in the reservoir by a factor close to 2 due to the Klingenberg effect (Wang et al., 2017). This is should be taken into consideration for investigations of gas flow in the reservoir samples. Although the relationship between permeability and porosity is not very clear, it is understood that porosity and permeability are directly proportional (Ramandi et al., 2016). Kozeny correlation describes this relationship in a reservoir by combining Poiseuille's equation (3.49) with Darcy's equation (3.46) as follows:

$$Q = (\frac{n\pi r^4}{8\mu})\frac{\Delta P}{L} \tag{3.49}$$

$$k = (\frac{n\pi r^4}{8A}) \tag{3.50}$$

$$k = \frac{\varphi r^2}{8} \tag{3.51}$$

The flow pathways are often straight and parallel as assumed in many models; a parameter known as tortuosity accounts helps minimize the effect of the irregular flow paths (Ozgumus et al., 2014). Tortuosity is the ratio of actual flow pathway length to the ideal flow pathway length assuming the specimen was absent. Tortuosity can be estimated from the Kozeny equation as follows:

$$\tau = \frac{\varphi {d_t}^2}{32k} \tag{3.52}$$

d_t - channel diameter, k – permeability, τ- tortuosity

Carman modifies this equation by introducing the Kozeny constant which takes into account the effects of the tortuosity to produce to Kozeny-Carman permeability equation (3.53) (Ozgumus et al., 2014).

$$k = \frac{\varphi {d_h}^2}{16k_k} \tag{3.53}$$

$$d_h = \frac{4\varphi}{A_0(1-\varphi)} \tag{3.54}$$

d_h - pore hydraulic diameter, A_0 - fluid-solid interfacial area to the solid volume ratio, k_k - Kozeny constant.

For investigations of samples of equal porosity of about 36%, the permeability was different by factors of up to 1000 due to the presence of clay (Ozgumus et al., 2014). Other factors that affect the permeability of the reservoir specimen exist and should be noted or made constant to ensure the quality of the laboratory investigations is not compromised.

3.2.3 **Rock strength**

The force applied per unit area of a specimen is referred to as the stress applied to the specimen; the stress value at which the specimen fails is referred to as the strength of the specimen (Fjaer, 2008). The specimen can fail in compression or tension. When a force or load is applied to a specimen, the specimen will deform elastically before the peak failure stress is reached (Zoback, 2010). Any deformation within this region is largely reversible with the exception of any region beyond the yield point (Bjorlykke, 2010). Unconfined compressive strength (UCS) direct test, confined compressive strength (CCS) direct test and Brazilian indirect tests are the most common laboratory test performed to determine the resistance of a specimen to deformation. Coates (1964) classifies the unconfined compressive strength of rocks less than 35 MPa as weak rocks, rocks between 35 MPa and 170 MPa as strong rocks and rocks grater than 170 MPa as very strong rocks (Coates, 1964). In North America, Rocks with less than 50 MPa strength can be considered as low strength rocks, and less than 25 MPa as low-low strength rocks (Deere and Miller, 1966). The shape of the sample largely affects the strength of the material during testing (Thuro et al., 2001). For this reason, a lack of consistency can be observed when conducting strength tests of the same specimen (Hawkins, 1998); therefore, it is recommended as per the American Society for Testing and Materials (ASTM) standard that the length should be at least two times more than the diameter for compressive test whereas the ratio of 1:1 is acceptable for Brazilian test (ASTM, 2010, 2008; ASTM C39, 2016; Astm D3148-02, 2002).

3.2.4 **Sonic wave velocities**

Sonic wave velocities of the specimen are used to obtain dynamic rock mechanical properties of the specimen such as elastic modulus, shear modulus, density, porosity, and strength (Ding et al., 2014; Fjær, 2009a; Geyer and Myung, 1970; Horsrud, 2001; I. Myung and P. Helander, 1972;

Lacy, 1997; Takahashi and Tanaka, 2010; Vasconcelos et al., 2008). In contrast to other rock tests such as UCS for strength and mercury porosimeter for porosity, sonic wave velocity measurements are non-destructive; hence, tests are carried out without destroying the specimen (Najibi et al., 2015; Yale and Swami, 2017). In the field, sonic well logs are generated using monopole and dipole sonic logs with multiple transmitters and receivers to measure the transit time of one feet interval into the formation; Whereas in the laboratory, this is achieved by laboratory transmitters which send out sonic pulses through the specimen (Fjær, 2009a; Morcote et al., 2010; Pickett, 1963; Vasconcelos et al., 2008); It is relatively simple and economical (Vasconcelos et al., 2008). Compressional (primary) wave velocity and shear (secondary) wave velocity are the most frequently measured sonic wave velocities; most dynamic rock mechanical estimations employ one or both of the velocities in their correlations (Ba, 2015; Chang et al., 2006; Eberhart-Phillips et al., 1989; Fabricius et al., 2007; Ramcharitar and Hosein, 2016; Wang et al., 2001; Zoback, 2010). For example, some empirical estimations of UCS for sandstone and shale in the Gulf of Mexico (GOM) is presented as follows (Chang et al., 2006; Zoback, 2010):

$$GOM\ Sandstone: UCS = 3.87\exp(1.14 * 10^{-10}\rho {v_p}^2) \tag{3.55}$$

$$North\ Sea\ Shale: UCS = 7.97E^{0.91} \tag{3.56}$$

$$Shale: UCS = 7.22E^{0.712} \tag{3.57}$$

The elastic constants are estimated from the acoustic wave velocity and matrix bulk density (Tixier et al., 1975).

$$E = \frac{{v_s}^2\rho(3{v_p}^2 - 4{v_s}^2)}{({v_p}^2 - {v_s}^2)} \tag{3.58}$$

$$G = {v_s}^2 \rho \tag{3.59}$$

$$\vartheta = \frac{({v_p}^2 - 2{v_s}^2)}{2({v_p}^2 - {v_s}^2)} \tag{3.60}$$

$$\lambda = \rho({v_p}^2 - 2{v_s}^2) \tag{3.61}$$

$$K = \frac{\rho(3{v_p}^2 - 4{v_s}^2)}{3} \tag{3.62}$$

For sandstone and shale, compressional velocity less than 3000 m/s is a considered a weak poorly consolidated sand (Fjær, 2009b; Tronvoll et al., 1997). Local calibration of empirical estimations of rock strength from sonic wave velocities is recommended due to the insufficiency of the empirical relations to accurately predict all formation from different locations (Wang et al., 2001). The general trend of for compressional velocity to increase with an increase in strength and a reduction in porosity; however, the relationship with permeability is unclear. In addition, the presence of cracks, faults, and fluid saturation affect the measured values of the sonic wave velocity; therefore, experiments should be designed to be consistent in order to achieve accurate values (ASTM, 2005; Vasconcelos et al., 2008).

3.2.5 **Formation Density**

Formation bulk density is very essential in determining the mechanical rock properties of a formation. In the laboratory, with small sized cores, bulk density may be estimated by a simple mass to volume ratio calculation of the core sample. However, in the field during hydrocarbon exploration, this is not feasible. Several logs are measured while drilling; a typical set of logs while drilling includes formation density logs, neutron-porosity log, sonic logs, gamma-ray log and resistivity log. Formation density log estimates the formation bulk density and is perhaps the most

essential log measured while drilling because it can be used to estimate the formation total porosity, identify fluid content and identify different lithologies. In shale-free formation, the formation density can be used to estimate the total formation porosity if the matrix grain-grain density and saturating fluid density are known. Fluid content can be determined by combining the density and resistivity log in a density vs resistivity plot to determine the water-bearing formations

Birch (1961) was one of the first to establish a relationship between bulk density and compressional sonic velocity from laboratory experimental data by plotting the compressional velocity against the density of ultramafic rocks and serpentine rocks (Birch, 1961, 1960). The plot suggests that density is a function of compressional velocity. Higher bulk density resulted in a higher compressional velocity, and the relationship was observed to be exponential in ultramafic rocks, but linear in rock consisting mainly of plagioclase feldspar. Faust (1953) confirmed that compressional velocity and bulk density both increase with the degree of compaction, effective stress and burial depth; but did not capture the trend with shear velocity (Faust, 1953). Density was also found to be a function of shear velocity (Bailey, 2012; Brocher, 2005; Dey & Stewart, 1997; Mavko et al., 2003; Miller & Stewart, 1991; Miller & Stewart, 1990; Takahashi, Mukerji, & Mavko, 2000; Tatham, 1982; Vernik, Fisher, & Bahret, 2002). Some works by Stewart Miller suggest that shear velocity is more closely related to density than compressional velocity (Dey and Stewart, 1997; Quijada and Stewart, 2007). Since density, compressional and shear wave velocities increase with depth, it is analogous to say that density is a function of compressional velocity and shear velocity.

Previous empirical estimation of bulk density from sonic logs attempted to express density as a function of compressional velocity by fitting formation density log data to a polynomial or linear regression. Ludwig et al. (1970) plotted the Nafe-Drake curve density versus compressional

velocity but did not establish a relationship between density and compressional wave (Ludwig, 1970). Brocher (2005) derived a polynomial regression to fit the Nafe-Drake Curve by Ludwig (1970). The polynomial regression in equation (3.63) can be used to estimate density from compressional velocity and is valid for compressional velocity from 1.5 km/s to 8.5 km/s (Brocher, 2005).

$$\rho = AV_p - BV_p^2 + CV_p^3 - DV_p^4 + EV_p^5 \tag{3.63}$$

Where A=1.6612, B=0.421, C=0.0671, D=0.0043 and E=0.000106

Gardiner et al (1974) established a range of relationships between rock mechanical properties, their composition and the environment from laboratory and field experiments. They found that in sedimentary rocks density was a power function of compressional velocity according to equation (3.64).

$$\rho = AV_p^B \tag{3.64}$$

Where A= 0.31 in km/s and 0.23 in ft/s, and B= 0.25. Brocher (2005) reports A to be 1.74 for his dataset which is valid in continental and tectonic active plates.

Gardiner's equation is valid for brine saturated clastic rocks from 1.5 km/s to 6.1 Km/s compressional velocity. Perhaps, one of the most applied estimations of bulk density from sonic well logs in the petroleum industry is the Gardiner equation (3.64). Barton (1986) investigated density prediction from compressional velocity.

Miller and Stewart (1991) proposed the following equations for sandstones:

$$\rho = 0.019{V_p}^{0.58} \quad \textit{(3.65)}$$

$$\rho = 0.049{V_s}^{0.5} \quad \textit{(3.66)}$$

$$\rho = b{V_p}^{a}(c + dV_s) \quad (3.67)$$

Where a, b, c, and d are constants which are dependent on the formation.

Lindseth (1979) derived a linear relationship between density and impedance from which density can be estimated as follows.

$$\rho = \frac{V_p - d}{cV_p} \quad (3.68)$$

Where c and d are constants (0.308 and 3460 respectively) with velocity in m/s.

Christensen and Mooney (1995) suggest that the relationship between density and compressional velocity is linear in equation (3.69). Their equation is valid for compressional velocity from 5.5 km/s to 7.5 km/s (Christensen and Mooney, 1995).

$$\rho = AV_p + B \quad (3.69)$$

Where A= 0.3601 and B= 0.541

Godfrey et al. (1997) also suggest that the relationship between density and compressional velocity is linear in equation (3.70). Their equation is valid for compressional velocity from 5.9 km/s to 7.1 km/s (Godfrey et al., 1997).

$$\rho = AV_p + B \quad (3.70)$$

Where A= 0.70761 and B= 2.4372

3.3 Well Logs

3.3.1 Gamma-ray log (API)

Gamma-ray logs measure the level of natural radioactive minerals in the formation. Minerals emit natural radioactive gamma rays. A gamma ray log measures these emissions, and therefore, the gamma-ray log can be used to identify different lithologies along the well. It is measured in g.API. Shales typically have high radioactivity due to the presence of clay minerals like thorium, potassium and uranium, while sands have low radioactivity values. The gamma-ray log in combination with the resistivity log can be used to identify potential hydrocarbon reservoir formations along the well (Rolon et al., 2009).

3.3.2 Bulk density log (RHOB)

The formation bulk density log measures the scatter gamma ray from the loss of energy due to the interaction of the emitted gamma ray and the formation (Asquith and Gibson, 2004). This is achieved by deploying a gamma-ray source like cesium-137 or cobalt-60 into the formation. The electron density of the formation is given by the high energy Compton scattering. The lower energy photoelectric effect aids in providing better reasoning for lithology indication. The tool has a shallow depth of investigation. Bulk density is measured in g/cc. The bulk density is a function of the formation lithology, formation fluid (saltwater = 1.1 g/cc, freshwater = 1 g/cc, oil = 0.8 g/cc and gas = 0.7 g/cc), and porosity. A formation density log is a porosity log; hence, it can be used to calculate the density derived porosity (Rolon et al., 2009).

$$\phi_{den} = \frac{\rho_{ma} - \rho_b}{\rho_{ma} - \rho_{fl}} \tag{3.71}$$

Density logs are used to identify evaporites, gas bearing formations and lithology and to determine the density of the hydrocarbon (Khandelwal and Singh, 2010). In combination with the neutron-

density log, it can be used to identify gas bearing formations as well. Shale formations emit radiations which can lead to errors in the reading of the formation density tool; therefore, in shaley formations, the density-sonic log plot is used to determine shale porosity.

3.3.3 **Deep resistivity log (RESD)**

Resistivity logs measure the level of electric conductivity of the formation fluids. More specifically, the resistivity log measures the resistance of the formation fluids to the flow of electric currents through the formation. It is measured in ohm.m. Water tends to have a low resistance to electric currents, but hydrocarbons have a high resistance to electric current; therefore, the resistivity log is used to differentiate oil-bearing formations from water-bearing formations. Together with the gamma-ray log, potential hydrocarbon bearing reservoirs can be identified. The mud during drilling can affect the reading of the resistivity due to the invasion of the mud fluid. To correct for this, shallow, medium and deep resistivity logs are measured during logging operations by adjusting the length of the tool's electrode (magnetic deeper) (Asquith and Gibson, 2004; Bhatt, 2002; Rolon et al., 2009; Schön, 2015).

3.3.4 **Neutron log (NPHI)**

The hydrogen ion concentration in a formation is measured by the neutron log to give an indication of the porosity in clean, shale-free water or hydrocarbon bearing formations; this porosity is known as the neutron porosity. The tool measures the amount of energy loss from the collision of the neutrons with hydrogen ions (protons). The neutron porosity log in combination with the gamma-ray and resistivity log is used to identify gas bearing formations. Similarly, identification of the gas zones along the well can help prevent blowout and kick in the well. This is because neuron porosity measures the hydrogen ions in water and oil which are much higher than the hydrogen density of gas in the formation. Hence, the neutron log is lower in gas-bearing formations and is

known as the gas effect (Khandelwal and Singh, 2010). This is a porosity log, and as such, the neutron porosity can be estimated as follows (Schön, 2015).

$$\phi_N = \phi * \phi_{N,fl} + (1 - \phi) * ((1 - V_{sh}) * \phi_{N,ma} + V_{sh} * \phi_{N,sh}) \quad (3.72)$$

3.3.5 Shale Volume (Vsh)

This is the measure of the volume of shale in the formation and can be estimated from the gamma-ray log.

$$V_{sh} = \frac{GR - GR_{min}}{GR_{max} - GR_{min}} \quad (3.73)$$

3.3.6 Total porosity (PHIT)

The total porosity is the volume of the all the pore spaces saturated by water, hydrocarbon, and gas in the formation, both mobile and immobile. It includes interconnected pore and non-connected pores trapped with the formation. Secondary porosity and fracture porosity are also included in the total porosity estimation.

3.3.7 Effective porosity (PHIE)

This is the measure of the total pore spaces with the exception of the water attached to the clay; therefore, the volume of clay is subtracted from the total porosity to derive the effective porosity.

$$PHIE = PHIT - V_{sh} \quad (3.74)$$

3.3.8 Compressional wave sonic transit time log (DTCO)

The compressional wave sonic transit log measures the time it takes for a compressional sonic wave to travel through a foot of the formation along the axis of the borehole (Tixier et al., 1975). It is also known as the slowness of the compressional travel wave and is measured in μsec/ft

(inverse of velocity). The compressional wave sonic travel time can be measured with a borehole compensated (BHC) sonic tool or dipole sonic tool consisting of one or more ultrasonic transmitters and two or more receivers.

3.3.9 **Shear wave sonic transit time log (DTSM)**

The shear wave sonic transit time log measures the time it takes for a shear sonic wave to travel through a foot of the formation. It is also known as the slowness of the shear travel wave and is measured in μsec/ft. The shear wave sonic travel time cannot be measured with a borehole compensated sonic tool; it is measured with the dipole or array sonic tool, consisting of transmitters and receivers. Less than 1% of wells in most fields acquire their sonic logs with a dipole sonic tool; hence, many offset wells lack shear wave travel time logs (Mullen et al., 2007).

3.4 Conclusions

Compressional and shear wave velocity are found to be functions of lithology and fluid saturation. These can be observed by lithology and fluid dependent properties like density and porosity. The velocities increase as the porosity reduces. The trend is thought to be a linear function by researchers, but this may not be the case. The velocity ratio is assumed to not be a function of porosity according to most empirical correlations, but this review suggests otherwise; it reduces with the increase of porosity.

Compressional and shear wave velocity is observed to be a function of clay content in sandstone, but a less critical dependency in comparison to porosity and density. In addition, the microporosity of clays increases the reduction in the velocities. A specific trend was not observed for velocity ratio with clay content.

Compressional wave velocities are observed to be a function of effective pressure. As the effective pressure increases, the velocities increase. A similar relationship is observed for formation density and overburden pressure. The velocity ratio is observed to reduce with increasing effective pressure, which signifies that there is a greater change in shear-velocity with effective pressure.

Compressional and shear waves can be very effective tools in the lithological identification of formations and determination saturation fluid. Gas saturated formations are observed to have lower velocities in comparison to liquid saturated formations.

The velocity ratio is observed to be a more sensitive value to the formation lithology and saturating fluid type. More so, the ratio of the square of the velocities has not been critically investigated in literature, but may prove to be more sensitive, and an effective tool for formation property identification.

The inclusion of all parameters and factors that affect the velocities and their ratio may not be feasible; nevertheless, the inclusion of critical properties in empirical correlations will reduce the margin of error in empirical estimations.

The use of well logs indicative of these lithology and fluid dependent properties bridge the gap of hard to reach reservoir formations where cores may not be readily available. The well logs provide a means of having continuous data along the formation for formation evaluation.

As technology evolves, other methods of improving the empirical and analytical techniques for estimating sonic velocities, well logs and formation properties should be investigated.

The objective of this research will be to investigate techniques of improving current empirical and analytical geomechanical formation properties through dynamic methods. Intelligent systems like artificial neural networks, support vector machines, Gaussian processes and recurrent neural networks will be evaluated for use in this research.

References

Ahmed, T., 2006. Reservoir Engineering Handbook, Chemical, Petrochemical & Process.

Ahmed, T., McKinney, P.D., 2005. Advanced Reservoir Engineering, Advanced Reservoir Engineering. https://doi.org/10.1016/B978-0-7506-7733-2.X5000-X

Ahmed, T., Mohammed, M., M-, M., Foster, A., Environment, W., August, U., Rose, W., Stimulation, R., Economides, M.J., Abou-sayed, A.S., International, A., Economides, M.J., Mcleod, H.O., Norman, W.D., Dowell, S., Robert, J. a, Crowe, C.W., Dowell, S., Fredd, C.N., Dowell, S., Hill, a D., Schechter, R.S., Economides, M.J., Hill, D.G., Liétard, O.M., y Piot, B.M., Thomas, R.L., Morgenthaler, L.N., Poe, B.D., Halleck, P.M., Economides, M.J., Elbel, J., Britt, L., Economides, M.J., Constien, V.G., Hawkins, G.W., Prud'homme, P.K., Navarrete, R., Gulbis, J., Hodge, R., Fjær, E., Holt, R.M., Horsrud, P., Raaen, A.M., Risnes, R., Economides, M.J., Smith, M., Shlyapobersky, J., Desroches, J., Bratton, T., Thiercelin, M.C., Dowell, S., Ehlig-Economides, C. a., Economides, M.J., Boney, C., Nolte, K., Boney, C., Nolte, K., Avenue, S., Calgary, S.W., Place, F.T.D., St, W.S., Centre, F.T.D., Halifax, B., Statement, S.I., Report, S.D., Plan, D., Summary, D.A., Exxonmobil Canada Properties, The, I.N., Area, L.O., Rose, W., Otiotio, D., Haynes, S., McDonough, M., Gruschwitz, K., Johnson, T., Stacey, E., Eor, A., Hungarian, H., Gujarat, N., Field, O., Tpexozephoe, R., Field, T., Field, W.W., Field, W.W., Pool, D.L.A., Field, E., Field, D.O., Sheng, J.J., Akintunji, F., Austad, T., Brown, L., Chang, H.L., Dindoruk, B., Govreau, B., Johns, R.T., Kam, S.I., Lee, S., Marcotte, B., Putnam, J.M., Sheehy, A., Shen, C., Sheng, J.J., Tapper, S., Town, K., Tremblay, B., Turta, A., Wang, D., Zahner, B., Sheng, J.J., Tremblay, B., Govreau, B., Marcotte, B., Sheehy, A., Town, K., Zahner, B., Tapper, S., Akintunji, F., Brown, L., Lee, S., Kam, S.I., Sheng, J.J., Turta, A., Shen, C., Sheng, J.J., Putnam, J.M., Sheng, J.J., Chang,

H.L., Johns, R.T., Dindoruk, B., Austad, T., Oort, E. Van, Hoxha, B.B., Hale, A., Aldin, M., Patterson, R., Yang, H., Ye, H., Zhai, S., Wang, G., Mo, S.L., Summary, I., Jain, S., Gadiyar, B., Stamm, B., Abad, C., Parlar, M., Shah, S., Toonder, J. den, Osode, P.I., Bataweel, M.A., Alkhaldi, M.H., Vollmer, D.P., Alleman, D.J., Stability, P., Scheuennan, R.F., Rdf, W., Sea, N., Sea, N., Nabzar, L., Chauveteau, G., Roque, C., Formation, C., Problems, D., Formations, P., Clay, M., Capacity, C.E., Swelling, S., Science, P., Engineering, A.R., Galvanic, G., Gamma, G., Gap, G., Civan, F., Vii, P., Civan, F., Wells, I., Civan, F., Testing, P., 2013. Reservoir Stimulation. Enhanc. Oil Recover. F. Case Stud. 53, 1–28. https://doi.org/10.1017/CBO9781107415324.004

Andrade, J.S., Almeida, M.P., Mendes, J., Havlin, S., Suki, B., Stanley, H.E., 1997. Fluid flow through porous media: The role of stagnant zones. Phys. Rev. Lett. 79, 3901–3904. https://doi.org/10.1103/PhysRevLett.79.3901

Asquith, G., Gibson, C., 2004. Basic well log analysis for geologists, American Association of Petroleum Geologists Methods in Exploration. https://doi.org/82-73052

ASTM, 2010. Standard test method for compressive strength and elastic moduli of intact rock core specimens under varying states of stress and temperatures. D7012-10 1–8. https://doi.org/10.1520/D7012-13.1

ASTM, 2008. Standard Test Method for Standard Penetration Test (SPT) and Split-Barrel Sampling of Soils. ASTM Stand. Test Method D1586–08a, 1–9. https://doi.org/10.1520/D1586-11.2

ASTM C39, 2016. Standard Test Method for Compressive Strength of Cylindrical Concrete Specimens. Am. Soc. Test. Mater. 1–7. https://doi.org/10.1520/C0039

Astm D3148-02, 2002. Standard Test Method for Elastic Moduli of Intact Rock Core Specimens in Uniaxial Compression. Astm 04, 1–6. https://doi.org/10.1520/D7012-10.1

ASTM, S.D.-05, 2005. Standard Test Method for Laboratory Determination of Pulse Velocities and Ultrasonic Elastic Constants of Rock. Astm i, 5–11. https://doi.org/10.1520/D2845-08.2

Ba, J., 2015. Seismic exploration of hydrocarbons in heterogeneous reservoirs : new theories, methods and applications.

Bailey, T., 2012. An empirical Vp/Vs shale trend for the Kimmeridge Clay of the Central North Sea, in: 74th EAGE Conference & Exhibition Incorporating SPE EUROPEC 2012. Copenhagen, Denmark, pp. 4–7.

Bhatt, A., 2002. Reservoir properties from well logs using neural networks.

Biot, M.A., 1941. General theory of three-dimensional consolidation. J. Appl. Phys. 12, 155–164. https://doi.org/10.1063/1.1712886

Birch, F., 1961. The velocity of compressional waves in rocks to 10 kilobars: 2. J. Geophys. Res. 66, 2199–2224. https://doi.org/10.1029/JZ066i007p02199

Birch, F., 1960. The velocity of compressional waves in rocks to 10 kilobars: 1. J. Geophys. Res. 65, 1083–1102. https://doi.org/10.1029/JZ065i004p01083

Bjorlykke, K., 2010. Petroleum Geoscience from Sedimentary Environments to Rock Physics, Petroleum Geoscience. https://doi.org/10.1007/978-3-642-02332-3

Brocher, T.M., 2005. Empirical Relations between Elastic Wavespeeds and Density in the Earth's Crust. Bull. Seismol. Soc. Am. 95, 2081–2092. https://doi.org/10.1785/0120050077

BuKhamseen, N.Y., Ertekin, T., 2017. Validating Hydraulic Fracturing Properties in Reservoir

Simulation Using Artificial Neural Networks. SPE Kingdom Saudi Arab. Annu. Tech. Symp. Exhib. https://doi.org/10.2118/188093-MS

Castagna, J.P., Batzle, M.L., Eastwood, R.L., 1985. Relationships between compressional-wave and shear-wave velocities in clastic silicate rocks. Geophysics 50, 571–581. https://doi.org/10.1190/1.1441933

Chang, C., Zoback, M.D., Khaksar, A., 2006. Empirical relations between rock strength and physical properties in sedimentary rocks. J. Pet. Sci. Eng. 51, 223–237. https://doi.org/10.1016/j.petrol.2006.01.003

Chatzis, I., Dullien, F.A.L., 1981. Mercury porosimetry curves of sandstones. Mechanisms of mercury penetration and withdrawal. Powder Technol. 29, 117–125. https://doi.org/10.1016/0032-5910(81)85010-3

Chin, L.Y., Thomas, L.K., Sylte, J.E., Pierson, R.G., 2002. Iterative Coupled Analysis of Geomechanics and Fluid Flow for Rock Compaction in Reservoir Simulation. Oil Gas Sci. Technol. – Rev. IFP 57, 485–497.

Christensen, N.I., Mooney, W.D., 1995. Seismic velocity structure and composition of the continental crust: A global view. J. Geophys. Res. Solid Earth 100, 9761–9788. https://doi.org/10.1029/95JB00259

Civan, F., 2015. Reservoir Formation Damage: Fundamentals, Modeling, Assessment, and Mitigation, Reservoir Formation Damage: Fundamentals, Modeling, Assessment, and Mitigation: Third Edition. https://doi.org/10.1017/CBO9781107415324.004

Coates, D.F., 1964. Classification of rocks for rock mechanics. Int. J. Rock Mech. Min. Sci.

Geomech. Abstr. 1, 421–429. https://doi.org/10.1016/0148-9062(64)90008-7

Dake, L.P., 2008. Fundamentals of Reservoir Engineering. Environ. Sci. Technol. https://doi.org/http://dx.doi.org/10.1016/S0376-7361(08)70005-0

Dake, L.P., 1996. The practice of reservoir engineering. J. Pet. Sci. Eng. 14, 263. https://doi.org/10.1016/0920-4105(95)00060-7

Davis, B.H., Sing, K.S.W., Schüth, F., Levitz, P.E., Neimark, A. V, Tesche, B., Ramsay, J.D.F., Pikunic, J., Lastoskie, C.M., Gubbins, K.E., 2002. Handbook of porous solids.

Deere, D.U., Miller, R.., 1966. Engineering classification and index properties for intact rock. Tech. Report, Air Force Weapons Lab. 1, 65–116.

Dey, A.K., Stewart, R.R., 1997. Predicting density using V s and Gardner ' s relationship. CREWES Res. Rep. 9, 1–9.

Dick, M.J., Green, D., Kenney, T., Veselinovic, D., Tallarita, J., Smith, M.A., 2017. Quick and Simple Porosity Measurement at the Well Site 1–10.

Ding, P., Di, B., Wang, D., Wei, J., Li, X., 2014. P and S wave anisotropy in fractured media: Experimental research using synthetic samples. J. Appl. Geophys. 109, 1–6. https://doi.org/10.1016/J.JAPPGEO.2014.07.005

Domenico, S.N., 1984. Rock lithology and porosity determination from shear and compressional wave velocity. Geophysics 49, 1188–1195. https://doi.org/10.1190/1.1441748

Eberhart-Phillips, D., Han, D.-H., Zoback, M., 1989. Empirical relationships among seismic velocity, effective pressure, porosity, and clay content in sandstone. Geophysics 54, 82–89. https://doi.org/10.1190/1.1442580

Economides, M.J., Boney, C., 2000. Formation Characterization : Well and Reservoir Testing, in: Reservoir Stimulation.

Fabricius, I.L., Baechle, G., Eberli, G.P., Weger, R., 2007. Estimating permeability of carbonate rocks from porosity and vp ⁄ vs. Geophysics 72, E185–E191. https://doi.org/10.1190/1.2756081

Faust, L.Y., 1953. A velocity function including lithologic variation. Geophysics 18, 271–288. https://doi.org/10.1190/1.1437869

Fjaer, E., 2008. Petroleum related rock mechanics. Elsevier.

Fjær, E., 2009a. Static and dynamic moduli of a weak sandstone. Geophysics 74, WA103-WA112. https://doi.org/10.1190/1.3052113

Fjær, E., 2009b. Static and dynamic moduli of a weak sandstone. Geophysics 74, WA103. https://doi.org/10.1190/1.3052113

Gardner, M.W., Dorling, S.R., 1998. Artificial neural networks (the multilayer perceptron) - a review of applications in the atmospheric sciences. Atmos. Environ. 32, 2627–2636. https://doi.org/10.1016/S1352-2310(97)00447-0

Gassmann, F., 1951. Elastic waves through a packing of spheres. Geophysics 16, 673–685. https://doi.org/10.1190/1.1437718

Geyer, R.L., Myung, J.I., 1970. The 3-D Velocity Log; A Tool For In-Situ Determination Of The Elastic Moduli Of Rocks. 12th U.S. Symp. Rock Mech.

Godfrey, N.J., Beaudoin, B.C., Klemperer, S.L., 1997. Ophiolitic basement to the Great Valley forearc basin, California, from seismic and gravity data: Implications for crustal growth at the

North American continental margin. Geol. Soc. Am. Bull. 109, 1536–1562. https://doi.org/10.1130/0016-7606(1997)109<1536:OBTTGV>2.3.CO;2

Goldberg, I., Gurevich, B., 1998. Porosity estimation from P and S sonic log data using a semi-empirical velocity-porosity-clay model, in: Transactions of the SPWLA Annual Logging Symposium (Society of Professional Well Log Analysts). pp. QQ1-QQ10.

Gregory, A.R., 1977. Aspects of Rock Physics From Laboratory and Log Data that are Important to Seismic Interpretation: Section 1. Fundamentals of Stratigraphic Interpretation of Seismic Data 165, 15–46.

Gruber, F.K., Venkataramanan, L., Freed, D.E., Habashy, T.M., 2011. A new approach for the estimation of the porosity in NMR, in: ICASSP, IEEE International Conference on Acoustics, Speech and Signal Processing - Proceedings. pp. 1797–1800. https://doi.org/10.1109/ICASSP.2011.5946852

Hamada, G.M., 2004. Reservoir Fluids Identification Using Vp /Vs Ratio. Oil Gas Sci. Technol. – Rev. IFP 59, 649–654.

Han, D., Nur, A., Morgan, D., 1986. Effects of porosity and clay content on wave velocities in sandstones. Geophysics 51, 2093–2107. https://doi.org/10.1190/1.1442062

Han, G., Dusseault, M.B., 2003. Description of fluid flow around a wellbore with stress-dependent porosity and permeability. J. Pet. Sci. Eng. 40, 1–16. https://doi.org/10.1016/S0920-4105(03)00047-0

Hawkins, A.B., 1998. Aspects of rock strength. Bull. Eng. Geol. Environ. 57, 17–30. https://doi.org/10.1007/s100640050017

Hernández, M.G., Izquierdo, M.A.G., Ibáñez, A., Anaya, J.J., Ullate, L.G., 2000. Porosity estimation of concrete by ultrasonic NDE. Ultrasonics 38, 531–533. https://doi.org/10.1016/S0041-624X(99)00095-5

Heron, P.R.L., Loverude, M.E., Shaffer, P.S., McDermott, L.C., 2003. Helping students develop an understanding of Archimedes' principle. II. Development of research-based instructional materials. Am. J. Phys. 71, 1188–1195.

Horsrud, P., 2001. Estimating Mechanical Properties of Shale From Empirical Correlations. https://doi.org/10.2118/56017-PA

Huerta, D.A., Sosa, V., Vargas, M.C., Ruiz-Suárez, J.C., 2005. Archimedes' principle in fluidized granular systems. Phys. Rev. E 72, 31307.

I. Myung, J., P. Helander, D., 1972. Correlation of elastic moduli dynamically measured by in-situ and laboratory techniques, Log Analyst.

Jackson, P.D., Lovell, M.A., Waring, J.M., Hassett, S.P., 1989. Laboratory studies of the electrical and fluid flow properties of porous media. Mar. Pet. Geol. 6, 379. https://doi.org/10.1016/0264-8172(89)90047-0

Johansen, T.E., 2008. Principles of reservoir engineering.

Khandelwal, M., Singh, T.N., 2010. Artificial neural networks as a valuable tool for well log interpretation. Pet. Sci. Technol. 28, 1381–1393. https://doi.org/10.1080/10916460903030482

Khazanehdari, J., Mccann, C., 2005. Acoustic and petrophysical relationships in low-shale sandstone reservoir rocks. Geophys. Prospect. 53(4), 447–461.

Kowallis, B.J., Jones, L.E.A., Wang, H.F., 1984. Velocity-porosity-clay content systematics of poorly consolidated sandstones. J. Geophys. Res. Solid Earth 89, 10355–10364. https://doi.org/10.1029/JB089iB12p10355

Krief, M., Garat, J., Stellingwerf, J., Ventre, J., 1990. A Petrophysical Interpretation Using The Velocities Of P And S Waves (full-waveform Sonic). Log Anal. 31, 355–369.

Kuila, U., McCarty, D.K., Derkowski, A., Fischer, T.B., Prasad, M., 2014. Total porosity measurement in gas shales by the water immersion porosimetry (WIP) method. Fuel 117, 1115–1129.

Lacy, L.L., 1997. Dynamic Rock Mechanics Testing for Optimized Fracture Designs. SPE Annu. Tech. Conf. Exhib. https://doi.org/10.2118/38716-MS

Lindseth, R.O., 1979. Synthetic sonic logs—a process for stratigraphic interpretation. Geophysics 44, 3. https://doi.org/10.1190/1.1440922

Loverude, M.E., Kautz, C.H., Heron, P.R.L., 2003. Helping students develop an understanding of Archimedes' principle. I. Research on student understanding. Am. J. Phys. 71, 1178–1187. https://doi.org/10.1119/1.1607335

Ludwig, W.J., 1970. Seismic refraction. sea 4 53–84.

Mavko, G., Mukerji, T., Dvorkin, J., 2003. The Rock Physics Handbook: Tools for Seismic Analysis of Porous Media.

Miller, S., Stewart, R., 1990. Effects of lithology, porosity and shaliness on the P and S-wave velocities from sonic logs. J. Can. Soc. Expl. Geophys. 26, 94–103.

Miller, S.L.M., Stewart, R.R., 1991. The relationship between elastic-wave velocities and density

in sedimentary rocks: A proposal. Crewes Res. Rep. 260–273.

Minear, J.W., 1982. Clay Models and Acoustic Velocities, in: SPE Annual Technical Conference and Exhibition. Society of Petroleum Engineers. https://doi.org/10.2118/11031-MS

Morcote, A., Mavko, G., Prasad, M., 2010. Dynamic elastic properties of coal. Geophysics 75, E227–E234. https://doi.org/10.1190/1.3508874

Moscou, L., Lub, S., 1981. Practical use of mercury porosimetry in the study of porous solids. Powder Technol. 29, 45–52. https://doi.org/10.1016/0032-5910(81)85003-6

Mullen, M.J., Roundtree, R., Turk, G.A., 2007. A Composite Determination of Mechanical Rock Properties for Stimulation Design (What to Do When You Don't Have a Sonic Log). Rocky Mt. Oil Gas Technol. Symp. https://doi.org/10.2118/108139-MS

Najibi, A.R., Ghafoori, M., Lashkaripour, G.R., Asef, M.R., 2015. Empirical relations between strength and static and dynamic elastic properties of Asmari and Sarvak limestones, two main oil reservoirs in Iran. J. Pet. Sci. Eng. 126, 78–82. https://doi.org/10.1016/J.PETROL.2014.12.010

Nur, A., Simmons, G., 1969. The effect of saturation on velocity in low porosity rocks. Earth Planet. Sci. Lett. 7, 183–193. https://doi.org/10.1016/0012-821X(69)90035-1

Okolo, G.N., Everson, R.C., Neomagus, H.W.J.P., Roberts, M.J., Sakurovs, R., 2015. Comparing the porosity and surface areas of coal as measured by gas adsorption, mercury intrusion and SAXS techniques. Fuel 141, 293–304.

Ouchiyama, N., Tanaka, T., 1984. Porosity Estimation for Random Packings of Spherical Particles. Ind. Eng. Chem. Fundam. 23, 490–493. https://doi.org/10.1021/i100016a019

Ouchlyama, N., Tanaka, T., 1986. Porosity estimation from particle size distribution. Ind. Eng. Chem. Fundam. 25, 125–129. https://doi.org/10.1021/i100021a019

Ozgumus, T., Mobedi, M., Ozkol, U., 2014. Determination of kozeny constant based on porosity and pore to throat size ratio in porous medium with rectangular rods. Eng. Appl. Comput. Fluid Mech. 8, 308–318. https://doi.org/10.1080/19942060.2014.11015516

Pickett, G.R., 1963. Acoustic Character Logs and Their Applications in Formation Evaluation. J. Pet. Technol. 15, 659–667. https://doi.org/10.2118/452-PA

Quijada, M.F., Stewart, R.R., 2007. Density estimation using density-velocity relations and seismic inversion. CREWES Res. Rep. 19, 1–20.

Ramamoorthy, R., Johnson, D.L., Murphy, W.F., 1997. Porosity estimation method in carbonate rock.

Ramandi, H.L., Mostaghimi, P., Armstrong, R.T., Saadatfar, M., Pinczewski, W.V., 2016. Porosity and permeability characterization of coal: a micro-computed tomography study. Int. J. Coal Geol. 154, 57–68.

Ramcharitar, K., Hosein, R., 2016. Rock Mechanical Properties of Shallow Unconsolidated Sandstone. SPE Trinidad Tobago Sect. Energy Resour. Conf. https://doi.org/10.2118/180803-MS

Raymer, L.L.L., Hunt, E.R.R., Gardner, J.S., 1980. An Improved Sonic Transit Time to Porosity-to-Porosity transform. 21st SPWLA Logging Symp. Trans. 1–13.

Rivière, B., 2008. Discontinuous Galerkin Methods for Solving Elliptic and Parabolic Equations. Society for Industrial and Applied Mathematics. https://doi.org/10.1137/1.9780898717440

Rolon, L., Mohaghegh, S.D., Ameri, S., Gaskari, R., McDaniel, B., 2009. Using artificial neural networks to generate synthetic well logs. J. Nat. Gas Sci. Eng. 1, 118–133. https://doi.org/10.1016/J.JNGSE.2009.08.003

Schön, J., 2015. Basic Well Logging and Formation Evaluation Basic Well Logging and Formation Evaluation 4 Contents, 1st ed.

Takahashi, I., Mukerji, T., Mavko, G., 2000. Vp - Vs relations of sandstones and carbonates:Implications about the pore structure, in: SEG Technical Program Expanded Abstracts 2000. Society of Exploration Geophysicists, pp. 1838–1841. https://doi.org/10.1190/1.1815786

Takahashi, T., Tanaka, S., 2010. Rock Physics Model For Interpreting Dynamic And Static Young's Moduli Of Soft Sedimentary Rocks. ISRM Int. Symp. - 6th Asian Rock Mech. Symp.

Tatham, R.H., 1982. Vp/Vs and lithology. Geophysics 47, 336–344. https://doi.org/10.1190/1.1441339

Thuro, K., Plinninger, R.J., Zäh, S., Schütz, S., 2001. Scale effects in rock strength properties. Part 1: Unconfined compressive test and Brazilian test. ISRM Reg. Symp. 3-7 June 169–174.

Tiab, D., Donaldson, E.C., 2015. Petrophysics: Theory and Practice of Measuring Reservoir Rock and Fluid Transport Properties: Fourth Edition, Petrophysics: Theory and Practice of Measuring Reservoir Rock and Fluid Transport Properties: Fourth Edition. https://doi.org/10.1016/C2014-0-03707-0

Tixier, M.P., Loveless, G.W., Anderson, R.A., 1975. Estimation of Formation Strength From the

Mechanical-Properties Log. SPE J. Pet. Technol. 27, 283–293. https://doi.org/10.2118/4532-pa

Toksöz, M.N., Cheng, C.H., Timur, A., 1976. VELOCITIES OF SEISMIC WAVES IN POROUS ROCKS. Geophysics 41, 621–645. https://doi.org/10.1190/1.1440639

Tosaya, C., Nur, A., 1982. Effects of diagenesis and clays on compressional velocities in rocks. Geophys. Res. Lett. 9, 5–8. https://doi.org/10.1029/GL009i001p00005

Tosaya, C.A., 1982. Acoustical properties of clay-bearing rock. Stanford University.

Tronvoll, J., Skj┤rstein, A., Papamichos, E., 1997. Sand production: Mechanical failure or hydrodynamic erosion? Int. J. Rock Mech. Min. Sci. 34, 291.e1-291.e17. https://doi.org/10.1016/S1365-1609(97)00195-0

Turturro, A.C., Caputo, M.C., Gerke, H.H., 2017. Mercury porosimetry for comparing piece-wise hydraulic properties with full range pore characteristics of soil aggregates and porous rocks, in: EGU General Assembly Conference Abstracts. p. 18729.

Vasconcelos, G., Lourenço, P.B., Alves, C.A.S., Pamplona, J., 2008. Ultrasonic evaluation of the physical and mechanical properties of granites. Ultrasonics 48, 453–466. https://doi.org/10.1016/j.ultras.2008.03.008

Vernik, L., Fisher, D., Bahret, S., 2002. Estimation of net-to-gross from P and S impedance in deep-water turbidites. Lead. Edge 21, 380–387. https://doi.org/10.1190/1.1471602

Wang, S., Shi, J., Wang, K., Sun, Z., Zhao, Z., 2017. New coupled apparent permeability models for gas transport in inorganic nanopores of shale reservoirs considering multiple effects. Energy & Fuels 31, 13545–13557.

Wang, Z. (Zee), Wang, H., Cates, M.E., 2001. Effective elastic properties of solid clays. Geophysics 66, 428. https://doi.org/10.1190/1.1444934

Wang, Z., Nur, A., 1986. Effect of Temperature on Wave Velocities in Sands and Sandstones with Heavy Hydrocarbons. J. Geophys. Res 90, 6793–6800.

Witherspoon, P.A., Wang, J.S.Y., Iwai, K., Gale, J.E., 1980. Validity of Cubic Law for fluid flow in a deformable rock fracture. Water Resour. Res. 16, 1016–1024. https://doi.org/10.1029/WR016i006p01016

Wyllie, M.R.J., Gregory, A.R., Gardner, L.W., 1956. Elastic wave velocities in heterogeneous and porous media. Geophysics 21, 41–70. https://doi.org/10.1190/1.1438217

Yale, D.P., Swami, V., 2017. Conversion of dynamic mechanical property calculations to static values for geomechanical modeling. Am. Rock Mech. Assoc. 17-0644.

Zoback, M.D., 2010. Reservoir Geomechanics. Cambridge University Press.

Chapter 4 Static Young's modulus model prediction for formation evaluation

Preface

A version of this chapter has been published in the ***Journal of Petroleum Science and Engineering 171 (2018): 394-402.*** *I am the primary author. Co-author Olalere Oloruntobi was the originator of the concept. Dr. Sunday Adedigba provided technical assistance for data analysis and review of the first draft. Co-author Dr. Faisal Khan reviewed and provided valuable insights on how to improve the concept in the paper to a journal level publication. Co-author Dr. Lesley James provided technical assistance, review and financial support to carry out the research. Co-author Dr. Stephen Butt provided technical assistance, review and financial support during the research, as well as developing the knowledge gap. I carried out most of the data collection and analysis. The first draft of the manuscript was prepared by me, and I subsequently revised the manuscript, based on the feedback from the co-authors and a peer review process. The co-authors assisted in the development of the concept and testing the model, reviewed and corrected the model and results. They also contributed to the review and revision of the manuscript.*

Abstract

Accurate estimation of rock mechanical properties such as static Young's modulus is very critical to reducing the risks associated with exploration and production activities. Ideally, the determination of the rock static Young's modulus will require experimental studies to be conducted on core data taken from the formations of interest. Where core data are not available (possibly due to economic reasons), the static Young's modulus is often estimated from the dynamic Young's modulus using empirical relationships since dynamic Young's modulus can easily be obtained from the petrophysical data. The higher the formation porosity, the greater the difference between the static and dynamic Young's modulus. The existing empirical relationships are lithology specific and they are suitable over the porosity range to which they have been derived. Therefore, the generalization of these relationships may produce erroneous results. To be applicable to various lithologies and porosity range, a new relationship between static and dynamic Young's modulus is being proposed. The new model incorporates a lithology-porosity dependent parameter. The model is purely empirical based on the analysis of extensive laboratory data obtained from the literature. Comparisons are then made with the existing relations using statistical analysis. The results show that the newly proposed model outperformed all previously established models.

Keywords**:** Young's modulus, geomechanics, reservoir, drilling, formation characterization.

4.1 Introduction

Theoretical and experimental investigations of mechanical properties of rocks have suggested that static Young's Modulus (E) is the most critical parameter for carrying out geomechanical analysis on rocks (Al-Shayea, 2004; Elkatatny et al., 2018; King, 1983; Najibi et al., 2015; Yale and Swami, 2017). Al-Shayea (2004); Lacy (1997); Pan et al. (2010); Yale and Swami (2017) (Kılıç and Teymen, 2008; Zhou et al., 2015). Accurate prediction of static Young's Modulus is very essential for reducing the risk associated with exploration and production operations. Young's modulus has been used to estimate formation properties to determine sweet spots and hydrocarbon reservoir locations (Zong et al., 2013). Young's modulus has been used in forward prediction of formation properties to determine potential wellbore failure (Ohen, 2003; Rahimi and Nygaard, 2014). In difficult to produce reservoirs like unconventional gas fields, Young's modulus has been used to determine the elasticity of the reservoir and its potential for enhanced oil recovery (Goodway et al., 2010). Static Young's modulus has also found applications in hydrofracturing jobs where the fracture size and aperture are important to the quality of the design for hydrofracturing treatments (Yale and Jamieson, 1994). The quality of well-logging data during exploration can also be investigated with the estimates of Young's modulus (Balarabe and Isehunwa, 2017; McCann and Entwisle, 1992; Mullen et al., 2007; Onalo et al., 2018; Tixier et al., 1975) Young's modulus has been used in the characterization of rocks for disposal of hazardous and waste materials (Appendino et al., 2004; King, 1983). Young's modulus has been used to characterize underground mines to ensure the mines do not collapse under the miners-workers during mineral excavations (Ghasemi et al., 2018; Hahn et al., 2017; McCann and McCann, 1977). Static Young's modulus (E_s) is usually estimated from uniaxial and triaxial tests under drained conditions. This allows the

rock mechanical properties to be characterized without the influence of the pore fluids (Lacy, 1997; Yale and Jamieson, 1994).

Ideally, core samples from the actual formations of interest must be acquired to determine the Static Young's Modulus in the laboratory. These laboratory tests are expensive and destructive. However, it is not always possible to acquire core samples at every point in the well; therefore, the information is often not continuous along the wellbore (Onalo et al., 2018). In hole sections where core data are not available, static Young's modulus is usually estimated from the dynamic Young's modulus (E_d) using empirical relationships since dynamic Young's modulus can easily be obtained from the petrophysical data. Estimation of static Young's modulus from dynamic Young's modulus provides a cheaper, non destructive and continuous log of data along the well path (Fjaer et al., 1989; Yale and Jamieson, 1994; Jaeger et al., 2007; Fjaer, 2008; Mavko et al., 2009; Holt et al., 2012; Al-Ameri and Al-Kattan, 2012; Najibi et al., 2015b; Yale and Swami, 2017). Dynamic Young's Modulus can be estimated from a complex relationship of the compressional and shear wave velocity. (Yale and Jamieson, 1994). The dynamic modulus often overpredicts the static Young's Modulus (Eissa and Kazi, 1988; King, 1983). King (1983) attributes this to the presence of microcracks because the extent of the strain is a function of these microcracks. The values of dynamic modulus differ with magnitudes of up to 70% from the static modulus (Yale and Jamieson, 1994). If a material is perfectly elastic, the drained dynamic modulus should be close or approximately equal to the drained static moduli (Ledbetter, 1993).

The major reasons for this discrepancy in the measurement of static and dynamic Young's moduli can be summarized into the following groups (Yale and Swami, 2017):

1 – The degree of compaction is determined by several factors including the presence of cracks, porosity, density, cementation and consolidation. As the pore spaces in the formation increase, the porosity increases and so the potential extent of strain increases; this suggests that Young's modulus is inversely proportional to the porosity. This is similar to the presence of cracks, microcracks and fracture; they all indicate an increase or decrease in the total porosity of the formation. In contrast to porosity, the density, cementation and consolidation are directly proportional to the elastic moduli. Yale and Jamieson (1994) observed that the cementing material between the matrix grain controls the lithological table that they established during their investigations. This implies that with more cementing of the material, the stiffer and denser the material becomes; hence higher the elastic moduli of the formation. For example, dolomite cement is stiffer than calcite cement, thus it has a higher elastic modulus.

2- Rocks under in-situ condition are under some form of in-situ stress prior to any stress induced by human activities (Zoback, 2010). The confining pressure and overburden stress determine the extent of consolidation and are grouped together because they determine the stiffness of the material. The deeper the formation, the higher the overburden stress and confining pressure are. Most reservoir formations and truly confined formations may be found at depths of more than 6000 feet (Ramcharitar and Hosein, 2016); which in turn signifies higher values of Young's modulus.

3 - Fluid saturation has been observed to decrease the static Young's modulus; however, an increase is observed in the dynamic Young's modulus (Yale and Jamieson, 1994). This supports the notion that the disparity in both moduli increases with fluid saturation.

4 – The discrepancy has been attributed to the amplitude and frequency of the strain. Static moduli are measured at high strains to a hundredth value (10^{-2}) while dynamic moduli are measured at lower strains of a millionth value (10^{-5}) (Al-Shayea, 2004).

5- In addition, the method and equipment used to conduct the experiments do not always provide the same results, even after calibration (Yale and Swami, 2017). A typical example is seen in the work of Al-Shayea (2004) where the static modulus estimated by the secant and tangent method varies. The discrepancy is less than 20%, but nonetheless, this presents inconsistency in estimations and model development attempts. Apart from the method and equipment variation, the measured static values of different loading and unloading cycles are not equal (Al-Shayea, 2004; Fiona and Cook, 1995). This may be due to the fact that during each loading and unloading, microcracks are closed and opened, leading to permanent deformation, even though the formation has not been loaded to failure. Therefore, it would be expected that the relationship should be a function of these parameters. It may not be possible to measure all these parameters simultaneously in an economic and efficient manner. However, the degree of disparity in the correlations can be reduced by including parameters that represent one or more of these factors.

Estimating static Young's Modulus from dynamic Young's Modulus has been attempted by many but it is very challenging (Mavko et al., 2009). There have been several correlations developed to capture the relationship indicating linear, power, logarithmic and polynomial relationships between static and dynamic moduli.

King (1983) conducted static investigations on 174 dry and saturated samples of metamorphic and igneous rocks from the Canadian Shield Association (CSA) with low porosity (1 – 8 %), and

developed a linear relationship between the static and dynamic moduli of these measurements as follows:

$$E_s = 1.26E_d - 29.5 \quad (4.1)$$

Eissa and Kazi (1988) conducted investigations on a wider set of 342 specimens and suggested the following linear relationship:

$$E_s = 0.74E_d - 0.82 \quad (4.2)$$

Equation (4.2) was found to be inadequate for weak formations with poorly consolidated grains (Morales and Marcinew, 1993).

Heerden (1987) on the contrary, states that the relationship is exponential. Heerden (1987) performed tests on 18 specimens and developed a power relationship from 14 of these cores.

$$E_s = aE_d^b \quad (4.3)$$

where the constant a range from 0.097-0.152 and b ranges from 1.29059-1.22688 depending on the amount of stress applied.

Najibi et al. (2015) conducted experiments on 45 limestone specimens from two fields in Iran and also proposed a power model to represent the relationship between the local static and dynamic Young's modulus. The power model is presented as follows:

$$E_s = 0.014E_d^{1.96} \quad (4.4)$$

Some researchers have also described the relationship using polynomial models. Lacy (1997) proposed different equations for sandstones and shale for estimating Young's modulus to enable

the successful design of fracture jobs. The following equation was suggested to be suitable for all formations:

$$E_s = 0.278{E_d}^2 + 0.422E_d \quad (4.5)$$

More recently, Yale and Swami (2017) fitted a polynomial regression analysis to over 50 data sets to develop the following equation.

$$E_s = 0.001447{E_d}^2 + 6.928E_d - 1.177 \quad (4.6)$$

Other researchers have investigated the relationship between the logarithms of the static and dynamic Young's modulus. Savich (1984) indicated that the relationship between the logarithms of the moduli varies with the formation. The formation can be grouped into four categories: 1 - sedimentary carbonate rocks, 2 - igneous rocks, 3 - gneiss and metamorphic schists and 4 - clastic, silts, sandstones, siltstones and tuff. The general equation is presented in equation (4.7):

$$log\ Es = Ao + A1\ log\ Ed \quad (4.7)$$

where Ao and A1 are constants that are dependent on the type of lithology. Eissa and Kazi (1988) also proposed a relationship between the logarithms of the moduli and went a step further to include the density term in equation (4.8):

$$logE_s = 0.77log\rho E_d + 0.02 \quad (4.8)$$

A list of previously established estimations of static Young's Modulus from dynamic Young's Modulus found in the literature is presented in Table 4.1.

Table 4.1. A list of existing static Young's Modulus equations found in the literature

SN	Author	Equation	Lithology
1	Candy (2010)	$E_s = \frac{\ln(E_d + 1) * (E_d - 1)}{4.5}$	Soft & hard rocks
2	Wang (2000)	$E_s = E_d - 15.2$	Sandstone
3	King (1983)	$E_s = 1.263E_d - 29.5$	Igneous
4	Belikov (1970)	$E_s = 1.137E_d - 9.685$	Granite
5	McCan (1992)	$E_s = 0.69E_d - 6.4$	Granite
6	Eissa (1988)	$E_s = 0.74E_d - 0.82$	Sandstone
7	Eissa-Den (1988)	$logE_s = 0.77log\rho E_d + 0.02$	Sandstone
8	Lacy (1997)	$E_s = 0.278{E_d}^2 + 0.422E_d$	Sandstone, shale, limestone, dolomite & silt
9	Nor & Wang (1999)	$E_s = 1.153E_d - 15.2$	Hard rock
10	Van Herdeen (1987)	$E_s = 0.139{E_d}^{1.411}$	Sandstone, quartzites, norites & magnetite

11	Yale (2017)	$E_s = 0.001447{E_d}^2 + 6.928E_d - 1.177$	Variety
12	Ameen et al. (2009)	$E_s = 0.54E_d - 12.852$	Limestone
13	Morales & Marcinew (2009)	$E_s = 0.956E_d - 0.69$	Sandstone
14	Ohen (2003)	$E_s = 0.015{E_d}^{2.739}\ (psi)$	Sands
15	Fei et al. (2016)	$E_s = 0.564E_d - 3.4941$	Sandstone

The major downfall of previous models is mainly that they can not be applied extensively to a rock column. This is because they are lithology specific and can only be applied to a particular porosity range under certain confining pressure regimes. This makes the application of the existing empirical relations limited in terms of estimating the static Young's Modulus over any existing rock column. The negative consequences of such estimations can lead to poor determination and analysis of mechanical rock properties; therefore, they should not be used of rock formations with varying lithology, porosity and effective pressure regimes.

The main objective of this study is to develop a data-driven model that can be used to estimate static Young's moduli that is simple, inexpensive and non-destructive, irrespective of the formation type, lithology and porosity range thereby making the model universal.

4.2 **Methodology**

The approach used in this paper is largely empirical. Laboratory measurements of core data from different regions of the world and lithologies are used to derive the new empirical relationship between the static and dynamic Young's modulus. The dataset covers a wide range of regions (the Gulf of Mexico, USA, Canada, Iran, Saudi Arabia, Venezuela, the former Soviet Union, South Africa, and the North Sea), formations (sandstones, shales and carbonates), porosity range and confining pressures. This will make the model to be applicable universally. Table 4.2 summarizes the sources of the data used in this paper.

Table 4.2. Sources of data used for the study

Sn	Source	Region	Lithology
1	Najibi et al. (2015)	Iran	Limestone
2	Yale and Jamieson (1994)	Kansas	Dolomite, Dolostone, Limestone, Mudstone, silt w/dolomite, Siltstone
3	Elkatatny et al. (2018)		Dolomite, Dolomitized grain stone, Calcite, Lime Mudstone & Sandstone
4	Price et al. (1994)	Nevada	Tuff
5	Heerden (1987)	South Africa	Norite, Sandstone, Quartzite & Magnetite

6	Deere and Miller (1966)	Washington, Oregon, New York, Virginia, Pennsylvania, Minnesota, Missouri, Idaho, Vermont, Colorado, Bavaria, Georgia, Wisconsin, Ohio, Tennessee, Arizona, New Jersey and Nevada	Basalt, Diabase, Dolomite, Gnesis, Granite, Limestone, Marble, Quartzite, Sandstone, Schist &Tuff
7	Lacy (1997)	USA	Sandstone, Dolomites, Siltstones, Limestone & Shale
8	Al-Tahini et al. (2004)	Saudi Arabia	Sandstone
9	Mockovčiaková and Pandula (2003)	Slovakia and Czech Republic	Andesite, Amphibolite, Dolomite, Granite, Limestone, Siderite, Sandstone, Marble, Magnesite, Norite, Diabase & Slate
10	Morales and Marcinew (1993)	Venezuela, Canada, Alaska, and the North Sea	Sandstones Synthetic Sandstones: Sinclair, Berea & Brown
11	Al-Shayea, (2004)	Iran, Saudi Arabia, Canada and USA	Limestone

The dataset is plotted to depict the relationship between the static and dynamic Young's Modulus in Figure 4.1. To generalize the data, the initial approach was to perform linear, exponential and quadratic regression on all the available data. irrespective of the region, lithology, porosity and confining pressure. The equations generated from the exponential, linear and polynomial equations are presented in equation (4.9), (4.10) and (4.11) respectively.

$$E_s = 8.1357e^{0.0253E_d} \tag{4.9}$$

$$E_s = 0.7134E_d + 1.9584 \tag{4.10}$$

$$E_s = 0.0031{E_d}^2 + 0.3831E_d + 7.9818 \tag{4.11}$$

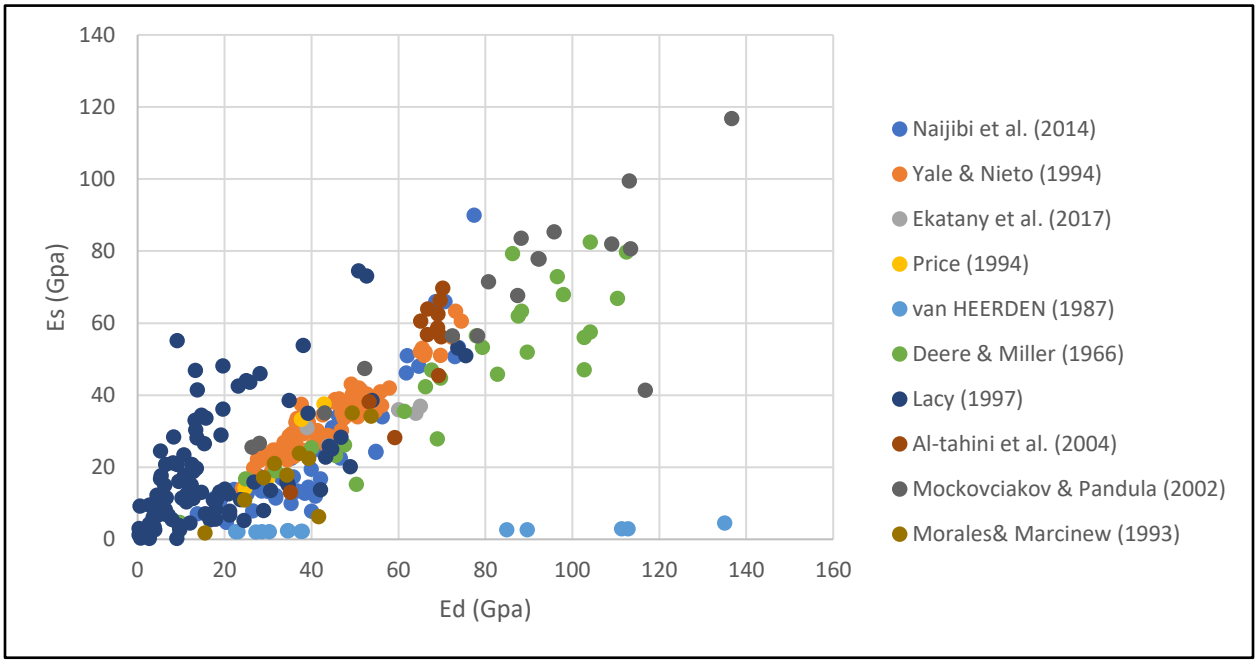

Figure 4.1. Plot of static and dynamic Young's modulus

The exponential regression model had a coefficient of determination of 0.56 as illustrated in Figure 4.1 a and the linear regression model had a coefficient of determination of 0.74 as illustrated in Figure 4.1 b. The polynomial has been limited to a two-order polynomial regression model to produce a quadratic regression model. The quadratic regression model result provided the best fit to the data points with a coefficient of determination of 0.76, as illustrated in Figure 4.1 c.

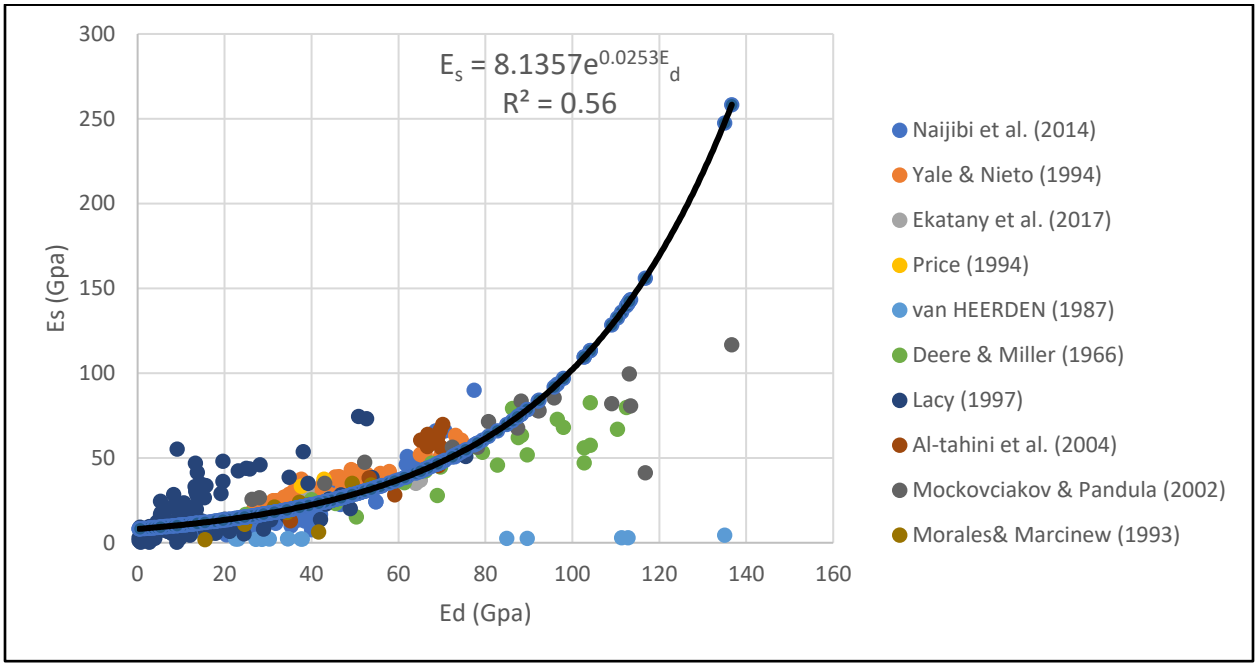

Figure 4.1 a. Exponential regression of the dataset

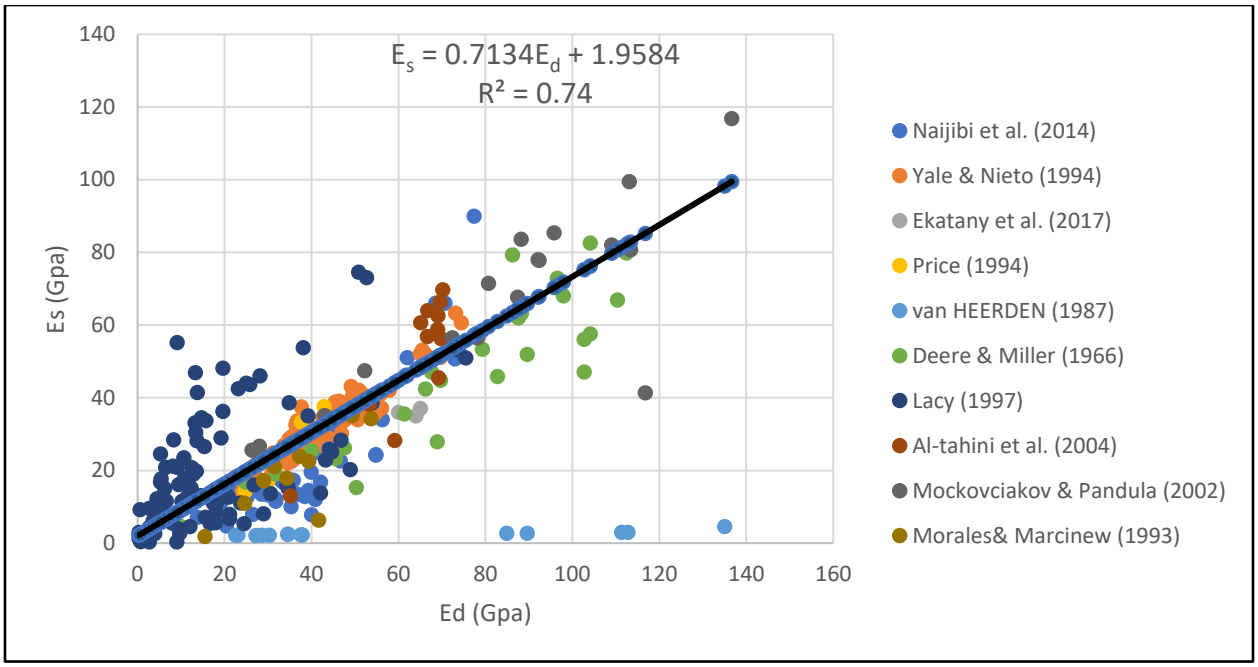

Figure 4.1 b. Linear regression of the dataset

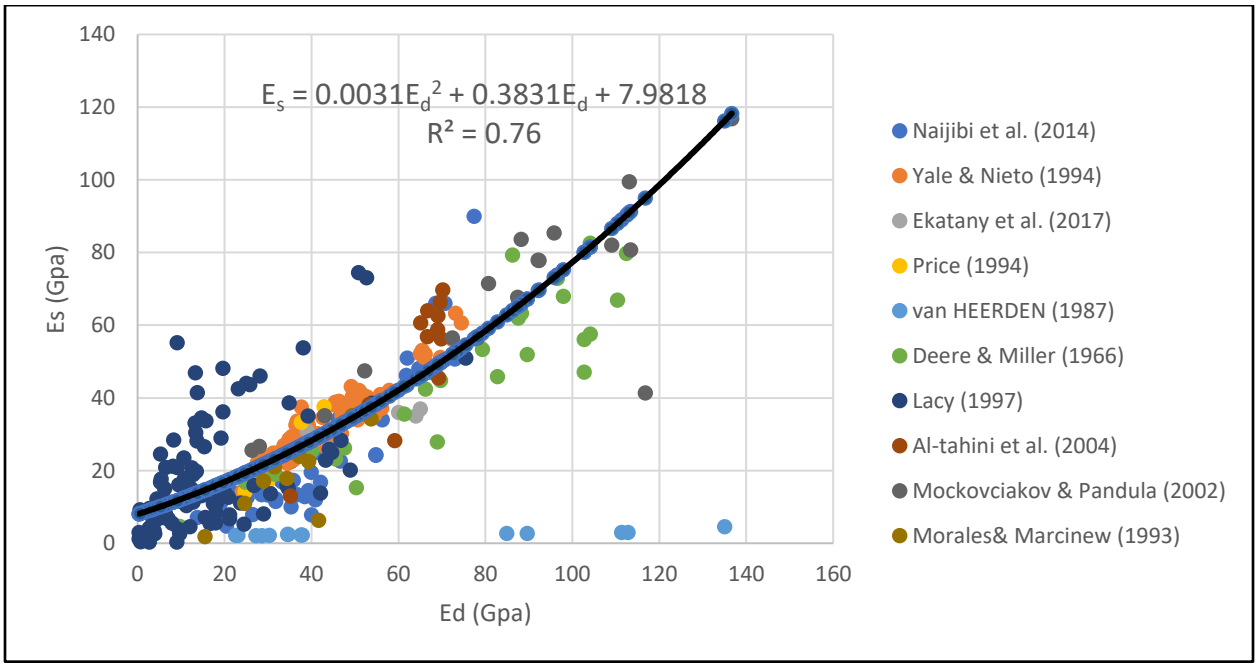

Figure 4.1 c. Quadratic regression of the dataset

From the plots, the coefficients of determination are observed to be generally low; therefore, there will be a need to develop an equation that would provide better coefficients of determination which would indicate better estimation capability. To develop a universal equation, the need to include a

new parameter that accounts for the lithology, porosity and confining pressure becomes evident. Elkatatny et al. (2018); Lacy (1997); Yale and Swami (2017) suggested that static and dynamic Young's moduli are functions of density. Density is also affected by lithology, porosity and confining pressure changes. To prove this assumption, a plot of all datasets with corresponding density values were plotted in Figure 4.2. Figure 4.2 illustrates that Young's modulus increases as the density increases; however, the relationship is non-linear. As a quality check to ensure that the 150 data points used were representative of the entire 350 data points, a polynomial regression analysis was performed on the dataset. The polynomial regression model remained unchanged, indicating that the more than 150 data points were representative of the total data set.

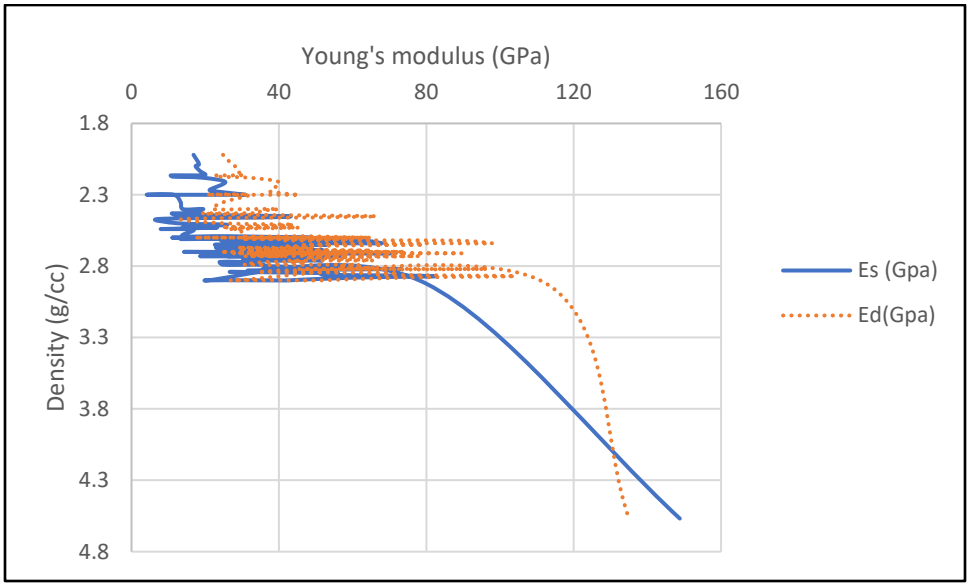

Figure 4.2. Density versus static and dynamic Young's modulus

Since most of the empirical relations are lithology specific over certain porosity range, the objective in this paper is to incorporate an additional parameter which is a lithology-porosity dependent variable to the static Young's Modulus expression. This allows the new model to be applicable to various porosity and lithology range. The parameter chosen is the formation bulk

density because it accounts for formation porosity and lithology. This means that any model that does not take porosity, lithology and confining pressure into consideration is not accurate. The newly proposed model is proposed equation based on the analysis of laboratory data, and is presented as follows:

$$E_s = 0.3361 E_d \rho^{0.8} - 2.4603 \quad (4.12)$$

The proposed model was applied to the dataset and the results are shown in a cross-validation plot in Figure 4.3.

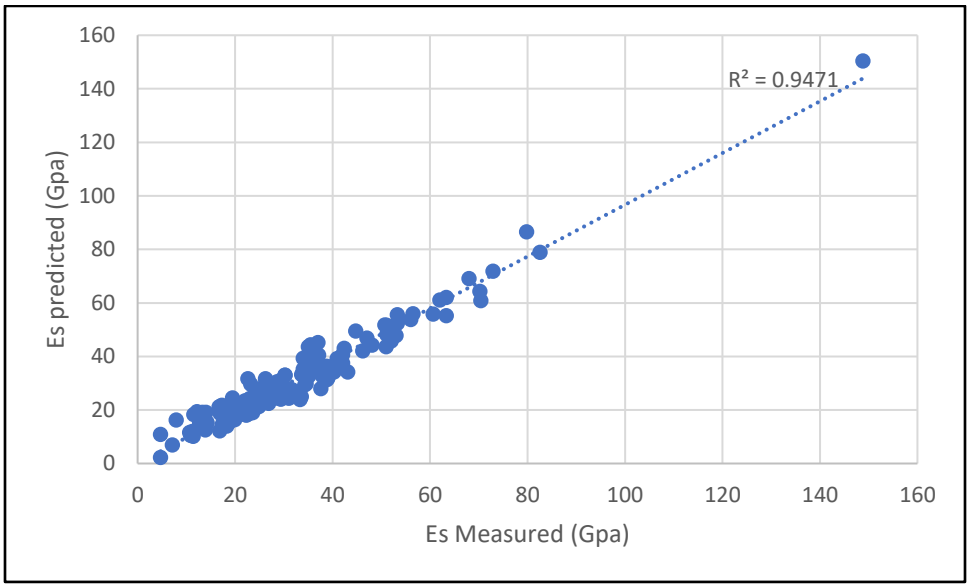

Figure 4.3 Validation of the measured and predicted static modulus

Figure 4.3 shows a good agreement between the values estimated from the proposed model, with a coefficient of determination of approximately 0.95. The root mean square error (RSME) was calculated to be 4.14 and the absolute average error was calculated to be 3.38 with an average error percentage (AEP) of 13%.

4.3 Results and discussion

To test the performance of the newly proposed model a comparative study of the proposed model and other previously established models was conducted. In Figure 4.4, the measured static Young's modulus is plotted against the dynamic Young's modulus. In addition, the static Young's modulus estimated from the dynamic static modulus of several previous correlations is also plotted Figure 4.4. It also emphasizes whether the static Young's modulus from any of the previous correlations adequately represents the trend observed between the measured static and dynamic moduli. Figure 4.4 suggests that the relationship between the static and dynamic moduli is not likely to be a power relationship nor an exponential function of the dynamic modulus, as had been suggested by Ohen (2003). Linear relationships and trendlines could be observed from the plot in Figure 4.4, but the linear trendline was not consistent throughout the data points. At lower values of Young's modulus, less than 35 GPa, a linear relationship could be established; however, this linear relationship could not accurately represent data points above 35 GPa. Therefore, a quadratic fit was chosen to better represent the dataset. This was validated by the coefficient of determination obtained from the power, linear and quadratic fit regressions; the quadratic regression had the highest determination coefficient of approximately 0.75. The quadratic regression trendline is represented by the solid black line that passes through the data points in Figure 4.4. Most of the tested models stray from the fitting line substantially. Models by Heerden (1987), Lacy (1997), Yale and Swami (2017) and Eissa and Kazi (1988) seemed to be the closest fit to the quadratic trendline and thus provided a better representation of the data moduli relationship. The proposed new model outperformed all the previous models including the quadratic regression model with a coefficient of determination of approximately 0.95.

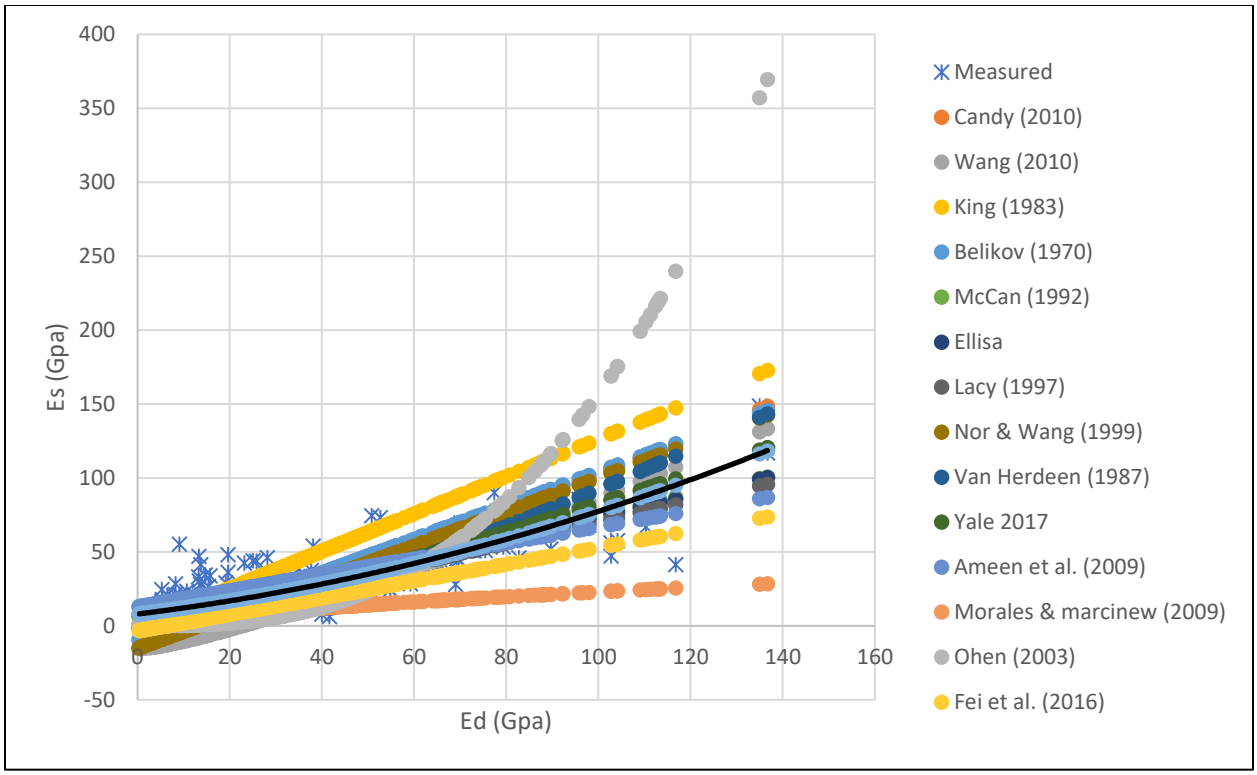

Figure 4.4. Measured and predicted static correlations from dynamic Young's modulus

In Figure 4.5 the static Young's modulus from the various correlations is plotted against the measured static Young's modulus. This is to check whether the predictions from these models were accurate, and hence, sufficient to adequately estimate the static Young's modulus from the dynamic Young's modulus. A perfect trendline of a unit slope i.e. slope =1, which represents a perfect model, is also plotted in Figure 4.5 to emphasize what pattern a perfect model would follow.

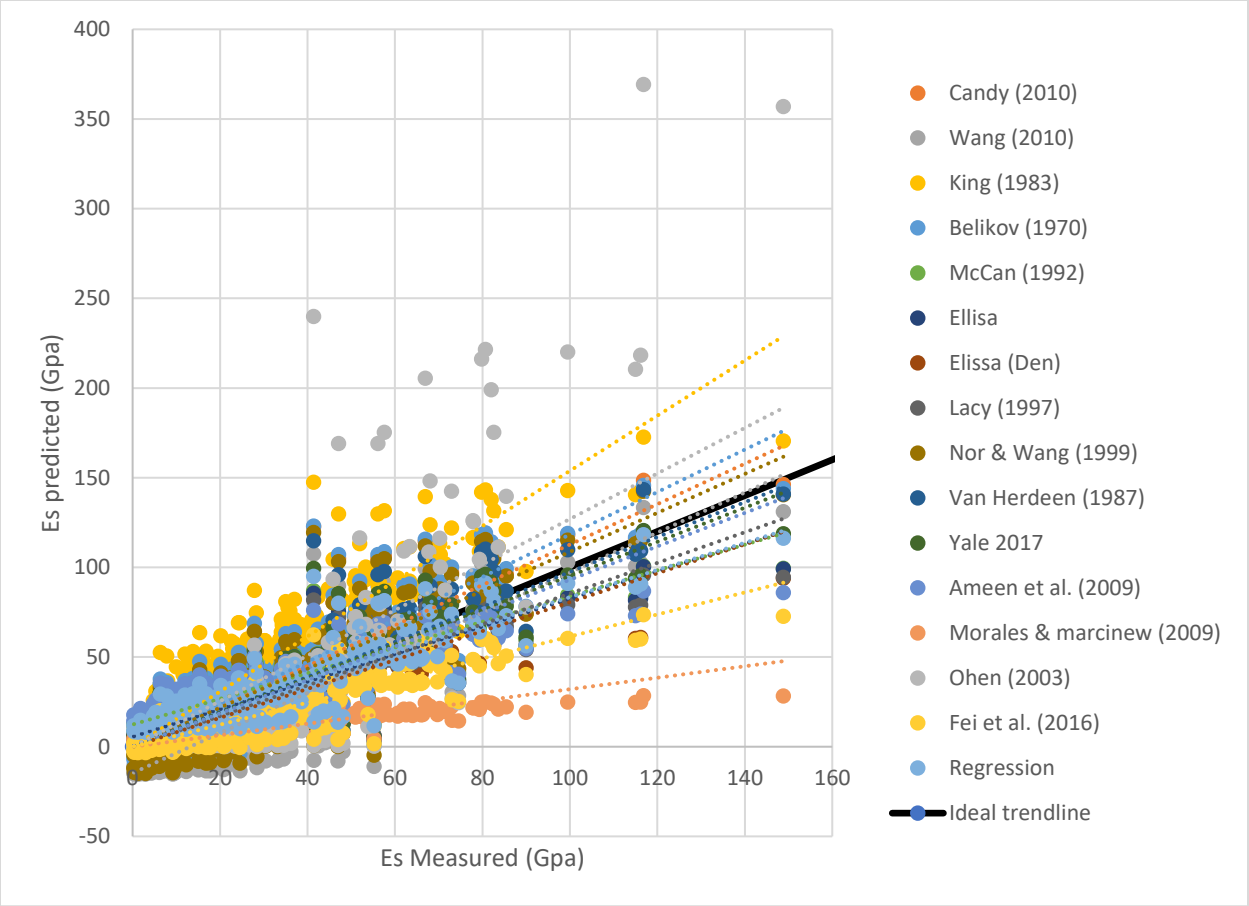

Figure 4.5. Cross plot of static modulus predicted from correlating the measured static modulus

The cross plot reveals that most models do not accurately predict the static modulus from the dynamic modulus. The coefficient of determination of each model is estimated. The best coefficient of determination was obtained from the research of Heerden (1987), Candy (2010) and Wang (2010) which portrayed determination coefficients of approximately 0.76. However, the root mean square implied that Yale and Swami (2017), Eissa and Kazi (1988), Heerden (1987) and Lacy (1997) had better error values of 5.62, 6.12, 6.37 and 6.44 respectively. A closer look at the absolute average error showed that the models of Eissa and Kazi (1988), Yale and Swami (2017), Lacy (1997), Heerden (1987) were more accurate with lower errors of 4.06, 4.17, 4.21 and 4.75 respectively. The absolute percentage error reported by Heerden (1987), Lacy (1997) and Eissa

and Kazi (1988) was 16%, 17% and 17% respectively. The proposed new model presents a coefficient of determination of 0.95, an RMSE of 4.14, an AAE of 3.38 and an AEP of 13%. The proposed model outperformed all the previous models, including the quadratic regression model, on all statistical measures quantifying the predictions efficiency.

A summary of the determination of coefficient, root mean square error, average absolute error and average percentage error of all the models are presented in Table 4.3.

Table 4.3. Summary of statistical comparative analysis

Sn	Source of Equation	R^2	RMSE	AAE	AEP
1	Candy (2010)	0.76	9.93	7.25	0.25
2	Wang (2010)	0.76	11.14	10.03	0.42
3	King (1983)	0.70	27.14	25.30	0.92
4	Belikov (1970)	0.74	12.69	10.20	0.35
5	McCan (1992)	0.74	8.57	6.65	0.32
6	Elissa (1988)	0.74	6.12	4.06	0.17
7	Elissa Den (1988)	0.40	10.63	9.66	0.43
8	Lacy (1997)	0.71	6.44	4.21	0.17
9	Nor & Wang (1999)	0.73	9.56	6.99	0.23
10	Van Herdeen (1987)	0.76	6.37	4.75	0.16
11	Yale (2017)	0.75	5.62	4.17	0.19

12	Ameen et al. (2009)	0.26	9.85	7.46	0.38
13	Morales & Marcinew (2009)	0.40	24.07	19.44	0.55
14	Ohen (2003)	0.56	27.39	16.69	0.52
15	Fei et al. (2016)	0.74	12.95	10.30	0.31
16	Quadratic regression	0.76	5.68	4.33	0.20
17	New Model	0.95	4.14	3.38	0.13

4.4 Sensitivity and Uncertainty Analysis

To test the sensitivity of the proposed model to uncertainties that can be generated during the process of acquiring the input data, Monte Carlo simulations have been performed on the data set. The sensitivity of dynamic Young's Modulus and density are considered and finally, a combined simulation is run to investigate the combined effect of the uncertainties of both dynamic Young's Modulus and density in the estimation of the static Young's Modulus.

Firstly, to test the sensitivity of the proposed model to the dynamic Young's Modulus, an uncertainty of -/+ 10% is simulated in the input data while other input parameters are kept constant. A total of 1001 Monte Carlo simulations are run on the data, after which, the root mean square error, average absolute error and average percentage errors are recalculated. The results of the dynamic Young's Modulus Monte Carlo simulation are presented in Table 4.4.

Table 4.4. Dynamic Young's Modulus from Monte Carlo simulation

	RMSE	AAE	AEP (%)
Average	4.69	3.75	14.34
Min	4.04	3.29	12.81
Max	5.39	4.23	15.95

Similarly, a Monte Carlo simulation of 1001 runs is performed on the proposed model by varying the density input data. The uncertainty of the density is simulated to be -/+ 10%. Based on the results of the 1001 simulation, the RMSE, AAR and AEP are calculated. The minimum and maximum values are also presented in Table 4.5.

Table 4.5. Density from Monte Carlo simulation

	RMSE	AAE	AEP (%)
Average	4.51	3.63	14.02
Min	4.04	3.23	12.65
Max	5.05	4.05	15.45

Finally, a combined Monte Carlo simulation is performed on the data by randomly varying the density and the dynamic Young's modulus. The results of the simulation are presented in Table 4.6.

Table 4.6. Combined from Monte Carlo simulation

	RMSE	AAE	AEP (%)
Average	5.00	3.97	14.95
Min	4.24	3.40	13.11
Max	5.81	4.48	16.68

The analysis of the Monte Carlo simulation sensitivity analysis presented above in Table 4.4, Table 4.5 and Table 4.6 suggest that although the model is sensitive to density and dynamic Young's Modulus, the proposed model is more sensitive to the dynamic Young's modulus. A greater uncertainty in the dynamic Young's Modulus resulted in greater errors and uncertainties in the estimation of the static Young's Modulus. Table 4.6 shows that the error margin and uncertainty is increased when both density and dynamic Young's Modulus input data contain uncertainties.

The initial statistical analysis performed on the data set provided RMSE, AAE and AEP of 4.14, 3.38 and 13% respectively. By including a -/+ 10% uncertainty to the dynamic Young's Modulus, the average RMSE, AAE and AEP of 1001 random simulations provided 4.69, 3.75 and 14% respectively. Similarly, by including a -/+ 10% percent uncertainty to the density, the average RMSE, AAE and AEP of 1001 random simulations provided 4.51, 3.63 and 14% respectively. In addition, by combining the uncertainties to both the density and dynamic Young's Modulus, the average RMSE, AAE and AEP of 1001 random simulations provided 5, 3.97 and 15% respectively. The change in the statistical analysis is less than 10% in each case thereby demonstrating the robustness of the model to be applied in the estimation of static Young's Modulus with reasonable certainty of the results.

4.5 Conclusion

In this study, a new model to estimate the static modulus from Young's modulus considering a lithology-porosity dependent variable is proposed. The model is tested on a dataset compiled from different sources covering a wide range of lithologies from different parts of the world. Therefore, the model can be applied widely in the various geological setting for several lithologies.

The present study demonstrates that previous models for estimating static Young's modulus from the dynamic modulus do not adequately capture the non-linear relationship between the static and dynamic relationship.

The performance of the proposed model is compared to existing models from different sources. The coefficient of determination, the root mean square, the average absolute error, and average percentage error are used to statistically analyze the predictions from all models. The proposed model outperforms all the previous existing models.

The proposed model is robust and provides reasonable estimates of static Young's Modulus with even with combined uncertainties from the input data. Using the proposed model, engineers will have a more reliable method of estimating static modulus from dynamic modulus to determine the mechanical properties of a formation for geomechanical analysis.

It is recommended that the proposed model should be tested on formations in different parts of the world irrespective of the lithology. Precise initial estimates can save companies substantial amounts in cost, time and personnel over the course of drilling several wells in a region.

To improve the proposed model, other formation specific dependent parameters like confining pressure and fluid saturation may be included in the analysis.

Acknowledgments

The authors thankfully acknowledge the financial support provided by the Natural Science and Engineering Council of Canada and the Canada Research Chair (CRC) Program, the Hibernia Management and Development Company (HMDC), Chevron Canada, and Innovate NL for the support without which this work could not have been performed.

Nomenclature

K	Bulk modulus (MPa)
R^2	Coefficient of determination
V_p	Compressional velocity (km/s)
Δt_c	Compressional wave travel time (µsec/ft)
E_d	Dynamic Young's modulus (GPa)
ρ, ρ_b	Formation density (g/cc)
Δt_{fl}	Formation fluid compressional wave travel time (µsec/ft)
MAE	Mean absolute error
MPE	Mean percentage error
Δt_{log}	Measured compressional wave travel time (µsec/ft)
ϑ	Poisson's ratio
RMSE	Root mean square error
G	Shear modulus (MPa)
V_s	Shear velocity (km/s)
Δt_s	Shear wave travel time (µsec/ft)
E_s	Static Young's modulus (GPa)
E	Young's modulus (MPa)

References

Al-Ameri, N.J., Al-Kattan, W., 2012. Estimation of the Rock Mechanical Properties Using Conventional Log Data in North Rumaila Field. Iraqi J. Chem. Pet. Eng. 13, 27–33.

Al-Shayea, N.A., 2004. Effects of testing methods and conditions on the elastic properties of limestone rock. Eng. Geol. 74, 139–156. https://doi.org/10.1016/j.enggeo.2004.03.007

Al-Tahini, A.M., Sondergeld, C.H., Rai, C.S., 2004. The Effect of Cementation on Static and Dynamic Properties in Jauf and Unayzah Formations at Saudi Arabia. SPE Annu. Tech. Conf. Exhib. https://doi.org/10.2118/90448-MS

Appendino, P., Ferraris, M., Matekovits, I., Salvo, M., 2004. Production of glass–ceramic bodies from the bottom ashes of municipal solid waste incinerators. J. Eur. Ceram. Soc. 24, 803–810.

Balarabe, T., Isehunwa, S., 2017. Evaluation of Sand Production Potential using Well Logs. SPE Niger. Annu. Int. Conf. Exhib. https://doi.org/10.2118/189107-MS

Deere, D.U., Miller, R.., 1966. Engineering classification and index properties for intact rock. Tech. Report, Air Force Weapons Lab. 1, 65–116.

Eissa, E.A., Kazi, A., 1988. Relation between static and dynamic Young's moduli of rocks. Int. J. Rock Mech. Min. Sci. 25, 479–482. https://doi.org/10.1016/0148-9062(88)90987-4

Elkatatny, S., Mahmoud, M., Mohamed, I., Abdulraheem, A., 2018. Development of a new correlation to determine the static Young's modulus. J. Pet. Explor. Prod. Technol. 8, 17–30. https://doi.org/10.1007/s13202-017-0316-4

Fiona, T., Cook, J., 1995. Effects of stress cycles on static and dynamic Young's moduli in Castlegate sandstone, in: Rock Mechanics: Proceedings of the 35th US Symposium. p. 155.

Fjaer, E., 2008. Petroleum related rock mechanics. Elsevier.

Fjaer, E., Holt, R.M., Raaen, A.M., 1989. Rock Mechanics And Rock Acoustics. ISRM Int. Symp.

Ghasemi, E., Kalhori, H., Bagherpour, R., Yagiz, S., 2018. Model tree approach for predicting uniaxial compressive strength and Young's modulus of carbonate rocks. Bull. Eng. Geol. Environ. 77, 331–343.

Goodway, B., Perez, M., Varsek, J., Abaco, C., 2010. Seismic petrophysics and isotropic-anisotropic AVO methods for unconventional gas exploration. Lead. Edge 29, 1500–1508. https://doi.org/10.1190/1.3525367

Hahn, F., Brüggemann, N., Bracke, R., Alber, M., 2017. Geomechanical characterization of the Upper Carboniferous under thermal stress for the evaluation of a High Temperature-Mine Thermal Energy Storage (HT-MTES), in: EGU General Assembly Conference Abstracts. p. 14506.

Heerden, W.L., 1987. General relations between static and dynamic moduli of rocks. Int. J. Rock Mech. Min. Sci. 24, 381–385. https://doi.org/10.1016/0148-9062(87)92262-5

Holt, R.M., Nes, O.-M., Stenebraten, J.F., Fjaer, E., 2012. Static Vs. Dynamic Behavior of Shale. 46th U.S. Rock Mech. Symp.

King, M.S., 1983. Static and dynamic elastic properties of rocks from the Canadian shield. Int. J. Rock Mech. Min. Sci. https://doi.org/10.1016/0148-9062(83)90004-9

Kılıç, A., Teymen, A., 2008. Determination of mechanical properties of rocks using simple methods. Bull. Eng. Geol. Environ. 67, 237–244. https://doi.org/10.1007/s10064-008-0128-3

Lacy, L.L., 1997. Dynamic Rock Mechanics Testing for Optimized Fracture Designs. SPE Annu. Tech. Conf. Exhib. https://doi.org/10.2118/38716-MS

Ledbetter, H., 1993. Dynamic vs. static Young's moduli: A case study. Mater. Sci. Eng. A 165, L9–L10.

Mavko, G., Mukerji, T., Dvorkin, J., 2009. The Rock Physics Handbook: Tools for Seismic Analysis of Porous Media, Book. https://doi.org/http://dx.doi.org/10.1017/CBO9780511626753

McCann, D., McCann, C., 1977. Application of borehole acoustic logging techniques in engineering geology, Log Analyst.

McCann, D.M., Entwisle, D.C., 1992. Determination of Young's modulus of the rock mass from geophysical well logs. Geol. Soc. London, Spec. Publ. 65, 317–325.

Mockovčiaková, A., Pandula, B., 2003. Study of the relation between the static and dynamic moduli of rocks. Metalurgija 42, 37–39.

Morales, R.H., Marcinew, R.P., 1993. Fracturing of High-Permeability Formations: Mechanical Properties Correlations. SPE Annu. Tech. Conf. Exhib. https://doi.org/10.2118/26561-MS

Mullen, M.J., Roundtree, R., Turk, G.A., 2007. A Composite Determination of Mechanical Rock Properties for Stimulation Design (What to Do When You Don't Have a Sonic Log). Rocky Mt. Oil Gas Technol. Symp. https://doi.org/10.2118/108139-MS

Najibi, A.R., Ghafoori, M., Lashkaripour, G.R., Asef, M.R., 2015. Empirical relations between strength and static and dynamic elastic properties of Asmari and Sarvak limestones, two main oil reservoirs in Iran. J. Pet. Sci. Eng. 126, 78–82. https://doi.org/10.1016/j.petrol.2014.12.010

Ohen, H.A., 2003. Calibrated Wireline Mechanical Rock Properties Model for Predicting and Preventing Wellbore Collapse and Sanding. SPE Eur. Form. Damage Conf. https://doi.org/10.2118/82236-MS

Onalo, D., Adedigba, S., Khan, F., James, L., Butt, S., 2018. Data-driven model for sonic well log prediction. J. Pet. Sci. Eng. https://doi.org/10.1016/j.petrol.2018.06.072

Pan, Z., Connell, L.D., Camilleri, M., 2010. Laboratory characterization of coal reservoir permeability for primary and enhanced coalbed methane recovery. Int. J. Coal Geol. 82, 252–261.

Price, R.H., Boyd, P.J., Noel, J.S., Martin III, R.J., 1994. Relationship between static and dynamic rock properties in welded and nonwelded tuff, in: 1st North American Rock Mechanics Symposium. American Rock Mechanics Association.

Rahimi, R., Nygaard, R., 2014. What Difference Does Selection of Failure Criteria Make in Wellbore Stability Analysis? 48th U.S. Rock Mech. Symp.

Ramcharitar, K., Hosein, R., 2016. Rock Mechanical Properties of Shallow Unconsolidated Sandstone. SPE Trinidad Tobago Sect. Energy Resour. Conf. https://doi.org/10.2118/180803-MS

Savich, A.I., 1984. Generalized relations between static and dynamic indices of rock

deformability. Hydrotechnical Constr. 18, 394–400. https://doi.org/10.1007/BF01426714

Tixier, M.P., Loveless, G.W., Anderson, R.A., 1975. Estimation of Formation Strength From the Mechanical-Properties Log. SPE J. Pet. Technol. 27, 283–293. https://doi.org/10.2118/4532-pa

Yale, D.P., Jamieson, W.H., 1994. Static and Dynamic Rock Mechanical Properties in the Hugoton and Panoma Fields, Kansas. Proc. SPE Mid-Continent Gas Symp. SPE 27939, 209–219. https://doi.org/10.2523/27939-MS

Yale, D.P., Swami, V., 2017. Conversion of dynamic mechanical property calculations to static values for geomechanical modeling. Am. Rock Mech. Assoc. 17-0644.

Zhou, Y., Gao, J., Sun, Z., Qu, W., 2015. A fundamental study on compressive strength, static and dynamic elastic moduli of young concrete. Constr. Build. Mater. 98, 137–145. https://doi.org/10.1016/j.conbuildmat.2015.08.110

Zoback, M.D., 2010. Reservoir Geomechanics. Cambridge University Press.

Zong, Z., Yin, X., Wu, G., 2013. Elastic impedance parameterization and inversion with Young's modulus and Poisson's ratio with Young and Poisson. Geophysics 78, N35–N42.

Chapter 5 Data-driven model for sonic well log prediction

Preface

A version of this chapter has been published in the ***Journal of Petroleum Science and Engineering 2018.*** *I am the primary author. Co-author. Dr. Sunday Adedigba was the subject matter expert on artificial neural networks and helped in formulating the concept of the paper, and review of the first draft. Co-author Dr. Faisal Khan is a subject matter expert on artificial neural networks. He provided valuable insights on necessary sections to include to make the work publishable. Co-author Dr. Lesley James provided technical assistance, proper formatting and representation of the well log data, expert analysis and review. She provided financial support to carry out the research. Co-author Dr. Stephen Butt provided technical assistance, review and financial support during the research, as well as analyzing the well log format used in the paper. I and Dr. Sunday Adedigba carried out most of the data collection and analysis. The first draft of the manuscript was prepared by me, and I subsequently revised the manuscript, based on the feedback from the co-authors and also a peer review process. The co-authors assisted in the development of the concept and testing the model, reviewed and corrected the model and results. They also contributed to the review and revision of the manuscript.*

Abstract

Near wellbore failure during the exploration of hydrocarbon reservoirs presents a serious concern to the oil and gas industry. To predict the probability of these undesirable phenomena, engineers study the mechanical rock properties of the formation such as Young's modulus, Bulk modulus, shear modulus and Poisson's ratio. Conventionally, these are measured indirectly using the established petrophysical relationship from sonic wave velocities which can be obtained from sonic well logs. Unfortunately, reliable sonic well logs are not always available due to poor borehole conditions (wash out), damaged tools and offset well data. Most offset well log data are not acquired with dipole sonic tools; they are acquired with a borehole compensated logging tool. This limits the application of the acoustic measurements to estimate the mechanical rock properties.

In this study, a three-layer feedforward multilayered perceptron artificial neural network model is presented. This model aims to estimate compressional wave transit time and shear wave transit time using real gamma-ray and formation density logs. The validation of the model is confirmed on an oil and gas offshore shaley sandstone reservoir located in West Africa. The results of the validation show that the model presented in this study can be used to determine the sanding potential of the formation without carrying compressive geoscientific analysis in the absence of sonic well logs. The developed model effectiveness is tested by comparing the predicted results with results obtained from the measured well log. The paper provides a tool to give preliminary recommendations of the likelihood of the formation to produce sand. Implementation of the proposed model would serve as a cost-effective and reliable alternative for the oil and gas industry.

Keywords: Artificial neural network, Sand production, wellbore failure, well log, sonic velocity

5.1 Introduction

Petroleum remains one of the most important sources of energy in the world and will continue to play a vital role in the world energy mix in the near future. The drive to produce more hydrocarbons to increase production from hydrocarbon reservoirs is crucial, due to the increasing demand for energy and the rising global population. Sanding, wellbore stability and collapse can lead to a reduction in both production and injection (Kalgaonkar et al., 2017). According to Bianco and Halleck (2001), clastic formations represent 90% of the world's hydrocarbon reservoirs, of which 70% may be in reservoirs prone to sand production and wellbore failure (Balarabe and Isehunwa, 2017; Bianco and Halleck, 2001). Hence, the ability to increase production from these reservoirs is often limited by the wellbore stability and collapse from the production of sand (Ranjith et al., 2014). The Gulf of Guinea, Gulf of Mexico, Alberta, Niger Delta and Iran are some of the regions where these phenomena have been reported (Aadnoy et al., 2013; Najibi et al., 2015; Perera et al., 2017; Santarelli et al., 1989). Sand production and wellbore failure present major challenges for the petroleum industry (Ranjith et al., 2013). The consequences of neglecting sand production in hydrocarbon reservoirs include the damage of mechanical equipment like the wellhead, Christmas tree, tubing hangers, valves, separators, casing pipes and flowlines (Balarabe and Isehunwa, 2017). This results in the limitation of the injection rate, production rate, well collapse, well plugging and even the total abandonment of a well (Perera et al., 2017). The oil and gas industry dedicates a huge amount of resources to tackle sand production and near wellbore failure (Ranjith et al., 2013). Sand control techniques such as sand screening, gravel packing, expandable screens and chemical sand consolidation increase the operating cost of hydrocarbon reservoirs (Kalgaonkar et al., 2017). Remedial operations, equipment repair and workover interventions lead to costly downtime during

drilling, completion, production and injection operations (Balarabe and Isehunwa, 2017; Ukaonu et al., 2017).

The formation strength, stress-state, and failure mechanism around the wellbore often provide good indications of the susceptibility of the formation to sand production and wellbore failure (Alloush et al., 2017; Balarabe and Isehunwa, 2017; Geertsma, 1985; Perera et al., 2017). Tixier et al. (1975) proved that sonic velocity measurements are able to provide accurate, reliable and continuous indications of the formation strength and mechanical rock properties through several correlations. Santarelli et al. (1989) suggested that simple log analysis on well log data is useful in predicting sand production when the full wave sonic data are available (McPhee et al., 2014). Wu et al. (2006) conducted a geo-mechanical study to predict wellbore instability and sanding; their results buttress the need for reliable petrophysical and rock mechanical properties. Very recently, Ukaonu et al. (2017) proposed using the relationship between formation strength and porosity from compressional sonic logs as a reliable real-time indication of sanding in hydrocarbon reservoirs in the Niger Delta. Balarabe and Isehunwa (2017) developed a sand prediction model from the mechanical rock properties estimated from sonic logs to serve as an effective management tool for reservoir development.

Mechanical rock properties are some of the most important factors affecting wellbore stability and sanding (Tariq et al., 2017; Zeynali, 2012). In combination with the formation density, the formation sonic velocity is perhaps the most reliable and common indirect method for estimating rock mechanical properties of a formation. This may be due to the fact that they are both functions of lithology, saturating pore fluid, overburden pressure, porosity and clay content (Castagna et al., 1985; Eberhart‐Phillips et al., 1989; Gardner et al., 1974; Hossain et al., 2012; Raymer et al., 1980; Wyllie et al., 1956). One of the primary advantages of indirect estimations of mechanical

rock properties from sonic velocity is their success in weakly consolidated formations where other direct measurements have failed (Fjær, 2009; Tixier et al., 1975). However, in the absence of sonic logs, how do we obtain sonic velocity measurements for mechanical rock property estimations for the various studies and operations? Geologists and engineers try to predict the values from correlations, models and offset data from adjacent wells. Some popular estimations of sonic velocity using empirical techniques include the models of Castagna et al. (1985), Han et al. (1986), Eberhert-Phillip et al. (1989) (Castagna et al., 1985; Eberhart‐Phillips et al., 1989; Han et al., 1986). More recent research has shown that more accurate predictions of formation sonic velocity could be estimated from neural networks (Ramcharitar and Hosein, 2016).

Models derived from systems which attempt to mimic the process by which the human brain solves complex problems are often referred to as intelligent systems (Asoodeh and Bagheripour, 2012). Intelligent systems have been used to improve the prediction and accuracy of sonic wave velocity prediction where sonic logs have been lost due to poor storage, poor logging, failure of logging instruments and bad hole condition (Akhundi et al., 2014; Al-Dousari et al., 2016; Aleardi, 2015; Asoodeh and Bagheripour, 2014, 2013; Bagheripour et al., 2015; Cranganu and Bautu, 2010; Kazatchenko et al., 2006b, 2006a; Maleki et al., 2014; Rajabi et al., 2010; Rajabi and Tingay, 2013; Rezaee et al., 2007; Zoveidavianpoor et al., 2013).

The application of artificial neural networks in the petroleum industry is rapidly growing because of their ability to predict complex non-linear relationships by a parallel computing scheme that resembles the process in the human brain (Prieto et al., 2016; Saputro et al., 2016; Verma et al., 2012). ANN has been used to generate petrophysical properties like formation density for reservoir characterization in wells where the density log was only run for a short interval in the well due to the financial implications (Long et al., 2016). ANN models have been developed to estimate

Young's modulus and Poisson's ratio from density and sonic logs (Tariq et al., 2017). Elkatatny et al. (2017) adopted the same model to estimate the static Poisson's ratio to be used in analyzing the stress-state in formations where it is not possible to extract cores continuously for static laboratory testing. Ketmalee and Bandyopadhyay (2018) employed ANN to predict sanding from sonic and density logs, thereby evaluating the sanding risk from producing reservoirs. The application of ANN in the petroleum industry as presented is vast and there are still more emerging areas in which ANN can be used as a tool to aid predictions and analysis.

Ramcharitar and Hosein (2016) developed a 10-hidden layer artificial neural network using depth, porosity, clay content and bulk density to estimate compressional and shear interval travel times. They concluded that results from the ANN model presented lower absolute average errors when compared with the empirical correlations developed and were thus more appropriate for mechanical rock properties estimations.

In older offset wells and in the absence of sufficient reliable data well logs, gamma ray and formation bulk density logs can be used to train and develop effective models for predicting the sonic velocities to determine the mechanical rock properties for sand prediction, as proposed in this study. Recently, Tariq et al. (2017) proposed empirical correlations from ANN models to estimate sonic wave velocity from density, gamma ray and neutron porosity; the model is adapted from the original model (Tariq et al., 2016). Unlike the proposed model in this study, in the absence of the neutron porosity or sufficient data, the models become inapplicable.

The paper aims to provide a simple but robust ANN model for field engineers to determine the compressional wave and shear wave transit time during hydrocarbon exploration from limited well logs, and without knowledge of the porosity of the formation. The results of these predictions can

be used as a reliable tool to predict geomechanical reservoir properties including the sanding potential of the reservoir. The main objective of the paper is to provide a rugged method to determine the sanding potential of a formation in the field in real-time with limited data or where sonic logs are not available. The significance of this model to the industry is that limited log data will not have to be transmitted offsite for geoscientific analysis for initial determination of the likelihood of sand production thereby reducing cost and time of exploration operations

Table 5.1 highlight the difference between the current work and the following intelligent system articles.

The chapter is structured as follows: section 5.2 introduces the concept of ANN and how the algorithm is applied to train the model. In section 5.3, the methodology to develop the ANN architecture is presented. The proposed model is also applied to a case study in section 5.4 and used to estimate the rock mechanical properties. The results of the model predictions are analyzed in section 5.5. The conclusions based on the analysis are finalized in section 5.6.

Table 5.1. The differences between the current work and the following intelligent system articles

S/N	Articles	Intelligent System	Formation Type	Input data	Output data	Nos of layers	Area of Application	Region
1	Rajabi et al.(2010)	Genetic Algorithm Fuzzy logic Neuro-Fuzzy technique	Carbonate	NPHI, RHOB & RESD	Compressional velocity, Shear wave velocity, & Stoneley wave velocity	5	Petrophysical, geophysical & geomechanical studies	Iran
2	Maleki et al. (2014)	Support Vector Machine, Back Propagation Neural Network	Carbonate	DTCO, RHOB & GR	Shear wave velocity	3	Estimation of rock formation mechanical properties	Iran
3	Zoveidavianpoor (2014)	Artificial Neural Network Adaptive Neuro-fuzzy Inference System	Carbonate	Depth, GR, NPHI & RHOB	Compressional wave velocity	4 & 5	Prediction of p-wave	Middle Eastern
4	Rajabi and Tingay (2013)	Genetic Algorithm	Shales Sandstone	GR, RHOB & NPHI	Compressional velocity Shear wave velocity	N/A	Rock mechanical properties	Australia
		Mamdani fuzzy inference systems	Shales Sandstone	GR, RHOB & NPHI	Bulk Modulus Young's Modulus, Shear Modulus, Poisson's Ratio	N/A	Rock mechanical properties	Australia
		Adaptive Neuro-fuzzy Inference System	Carbonate	Porosity logs (DT, NPHI & RHOB)	Bulk Modulus Young's Modulus, Shear Modulus, Poisson's Ratio	N/A	Rock mechanical properties	Australia

5	Asoodeh and Bagheripour (2012)	Genetic Algorithm Fuzzy logic Neuro-Fuzzy technique	Carbonate	NPHI, RHOB, RESD & Vsh	Compressional velocity, Shear wave velocity, & Stoneley wave velocity	3	Improvement of sonic velocity predictions	Iran
		Genetic Algorithm (GA)	Shale-sand	Depth, GR, RHOB and RESD	Shear wave velocity	N/A	Prediction Optimization	N/A
		Genetic Algorithm (GA)	Shale-sand	Depth, GR & RHOB	Compressional wave velocity	N/A	Prediction Optimization	N/A
6	Aleardi (2015)	Genetic Algorithm (GA)	Shale-sand	Depth, Vp & RESD	Shear wave velocity	N/A	Prediction Optimization	N/A
7	Rezaee et al. (2007)	Fuzzy logic Neuro-Fuzzy	Sandstone	Vp, GR, FDC, RESD & NPHI	Shear wave velocity	N/A	Reservoir characterization	Australia
8	Cranganu and Bautu (2010)	Gene Expression Programming	sandy shales	GR, RESD	Compressional wave velocity	N/A	Estimating the presence of overpressure zones	Oklahoma
9	Zoveidavianpoor et al. (2013)	Artificial Neural Network	Carbonate	Depth, GR, NPHI & RHOB	Compressional wave velocity	3	Reservoir exploration & development activities	Middle Eastern
10	Akhundi et al. (2014)	Artificial Neural Network	Carbonate	Vp, NPHI, GR, RHOB & RESD	Shear wave velocity	3	Geo-mechanical, petrophysical & geophysical studies	Iran
11	Asoodeh and Bagheripour (2014)	Alternative Condition Expectation Stimulated Neural Network (ACESNN)	Carbonate	NPHI, Vp, RHOB & RESD	Shear wave velocity	3	Geo-mechanical, geophysical, & reservoir characterization studies	Iran

		General Regression Neural Network (GRNN)	Sandstones, shaley sands & carbonate	Porosity, clay content, grain density, permeability & cementation exponent	Shear wave velocity	4	Predict shear wave velocity	Broad spectrum
12	Al-Dousari et al. (2016)	General Regression Neural Network (GRNN)	Sandstones, shaley sands, & carbonate	Compressional wave velocity	Shear wave velocity	4	Predict shear wave velocity	Broad spectrum
13	Kazatchenko et al. (2006b)	Joint Inversion Technique	Carbonate	Δtp, micro-resistivity, total porosity & density	Shear wave velocity	N/A	Reconstructing double porosity carbonate formations	Mexico
14	Bagheripour et al. (2015)	Support Vector Regression (SVR)	Carbonate	Δtp, RHOB, NPHI, RT, PEF, RS & GR	Shear wave velocity	N/A	Geomechanical & geophysical studies	Iran
15	Ramcharitar and Hosein (2016)	Artificial Neural Network	Unconsolidated Sandstone	Porosity, clay content & bulk density	DTCO & DTSH (Independently)	10	Rock mechanical properties	Trinidad
16	Tariq et al. (2017)	Artificial Neural Network	Limestone	GR, NPHI & RHOB	DTCO & DTSH (Independently)	3	Construction of earth models	N/A
17	Tariq et al. (2016)	Feed forward Neural Network & Radial Basic Function	Carbonate	GR, NPHI & RHOB	DTCO & DTSH (Independently)	3	Rock elastic parameters	N/A
18	Current work	Artificial Neural Network	Sandstone and shale	GR, RHOB & Vsh	DTCO & DTSM	3	Sanding Potential	West Africa

5.2 Artificial Neural Network (ANN)

ANN is a robust and effective computational tool for establishing relationships between complex non-linear parameters without much knowledge of the system structure. ANN probably started in the 1940s (Buhulaigah et al., 2017). ANN uses strong, complex and parallel correlations that provide a mathematical approximation for these non-linear relationships by imitating the behavior of the system's input and output data (Chitsazan et al., 2015; Prieto et al., 2016). ANN imitates behavioral patterns; thus, ANN can grow and learn to develop and establish non-linear patterns between input and output data, even for systems with no known mathematical relationship (Azizi et al., 2016). Historical data are effective resources for ANN because they provide examples from which ANN can learn from previous scenarios and past experiences (Ashtiani and Shahsavari, 2016).

The artificial neural network can be classified by the input data feeding direction into feedforward and feedback neural networks. Feedforward networks are used more often in engineering applications (Benardos and Vosniakos, 2007; Mhaskar, 1993; Razavi and Tolson, 2011; Sperduti, 2015). Feedforward neural ANNs are further sub-classified as a single-layer perceptron, multilayer perceptron and radial basis function neural networks (Gardner and Dorling, 1998; Razavi and Tolson, 2011). A perceptron can be viewed as interconnected neurons (nodes) through which functions (signals) are transmitted through the network chain.

5.2.1 Multi-layer perceptron artificial neural network

A class of feedforward ANN is the multilayer perceptron ANN. A multilayer perceptron network is made up of an input layer, hidden layers and an output layer; more than two layers is typical for ANN (Basheer and Hajmeer, 2000; Gardner and Dorling, 1998; Prieto et al., 2016; Schmidhuber, 2015). A multilayer perceptron neural network consists of a network of interconnected neurons

between the input and output layers; these interconnected neurons map out and establish relationships between the vectors in the layers (Dorofki et al., 2012; Gardner and Dorling, 1998). The multilayered perceptron modeling process involves the resolution of the respective weights to approximately establish the relationship between the input and output layer. The initial weights are a set of random values to begin the cycle (Gardner and Dorling, 1998). The calculated errors at the end of each epoch are plotted to determine the smallest error using the gradient descent technique. The initialized weights are passed through activation (transfer) functions for the forward pass and the errors backpropagated to reinitialize the weights. The activation transfer functions common applied are logistic, hyperbolic tangent and pure linear functions (Dorofki et al., 2012).

A major advantage of multilayer perceptron is that they can learn; therefore, they can be trained to determine simple and complex non-linear pattern functions. However, the network must be furnished with reliable data for the input and target layers that adequately represent the existing relationship between the parameters in the provided dataset. In addition, the ANN is generalized so that it is suitable for use with a similar data format (Chitsazan et al., 2015; Gardner and Dorling, 1998). A detailed and comprehensive breakdown of how feedforward ANNs are developed with examples has been presented in literature (Adedigba et al., 2017; Chitsazan et al., 2015; Gardner and Dorling, 1998; Lawrence et al., 1997; Ruck et al., 1990; White and Rosenblatt, 1963). A summary of the implementation of the ANN in the proposed model is presented in section 5.3.3.

5.3 **Methodology to develop the ANN model**

The framework for the proposed methodology is presented in Figure 5.1

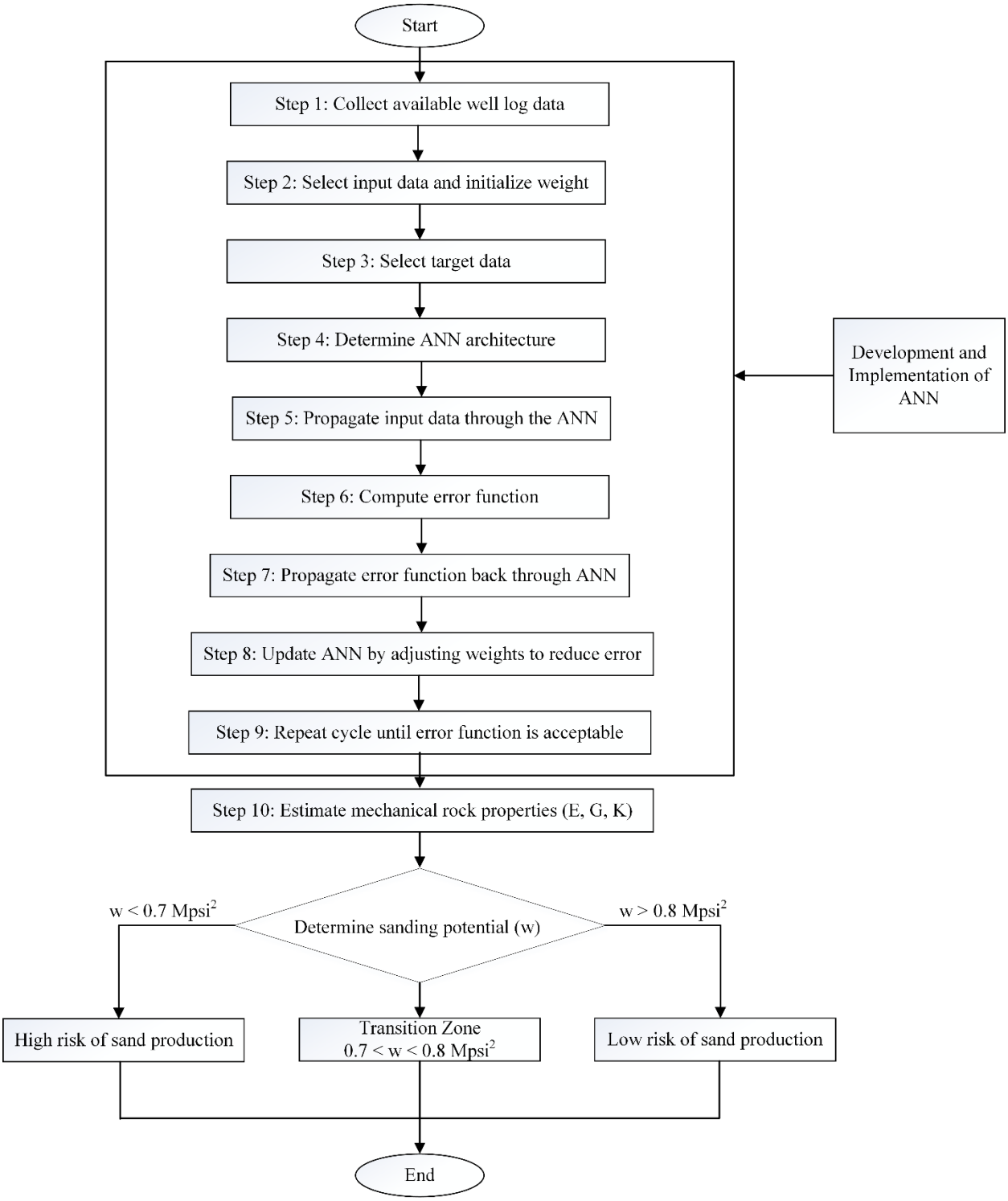

Figure 5.1. Proposed ANN model methodology flowchart

5.3.1 Data collection and determination for ANN

The data for the proposed methodology is obtained from actual well logs. Firstly, the data is analyzed to identify the suitable depth range that provides an accurate representation of the well. The chosen interval for the network was 7100 feet to 8400 feet. The data contains the depths, caliper, resistivity, bulk density, gamma ray, neutron and sonic logs.

5.3.2 Quality assurance and quality checks (QAQC)

Quality assurance and quality control (QAQC) were performed on the well log dataset to ensure the reliability of the data. Firstly, shallow sections of the data with null sets were removed from the dataset. Secondly, washout and key-seat sections were eliminated by cross-referencing with the caliper logs for adjacent formation sections. Poisson's ratio was used as a final quality check to ensure all data fell within possible Poisson's ratio estimates.

5.3.3 ANN model and architecture

The general architecture to be implemented for the proposed model is presented in Figure 5.2. The neural network model is a three-layered feedforward artificial neural network which uses a backpropagation algorithm. The ANN is made up of three layers, input, hidden and output layers. Advances in deep space learning have provided the ability to create more than one hidden layer in between the input and output layer, though an extra computational cost (Prieto et al., 2016). The input layer consists of three inputs vectors (X_1, X_2, X_3) while the output layer consists of two output vectors (Y_1 and Y_2). The hidden layer is made up three hidden layers. The sigmoid function used on the first sub-hidden layer is a logsig function while the hyperbolic tangent function is used for the second sub-hidden layer and output hidden layer. For training, cross-validation and testing, the Levenberg-Marquardt optimization function is used with the mean square error (MSE) loss function. The main features of the ANN architecture are presented in Table 5.2.

Table 5.2. Main features of the proposed ANN model

ANN model	Parameters
Training method	Feedforward backpropagation
Input data	Well log data
Number of layers	3
Output data	Sonic well log data
Optimization algorithm	Levenberg-Marquardt
Activation function	Logsig-Tansig-Tansig
Loss function	MSE

5.3.4 **Learning and training of the ANN**

In order for the ANN to adequately capture the relationship, linear or non-linear, that exists within the dataset, the neural network must be trained with a sample dataset. The purpose of training the ANN is to allow the network to locate the best permutation sequence of weights and their corresponding input vectors that offer the closest fit to the corresponding target vector (Gardner and Dorling, 1998; Ma et al., 2017; Rolon et al., 2009). The ANN teaches itself by learning; the learning can be supervised, unsupervised or reinforced. In supervised learning, the network is provided with input data and target data for the output data. The target data serve as a guide and correction for the network; hence, the term supervised. With the target values available to the neural network, the ANN is able to attempt to establish the tightest fit to the data. Supervised learning remains the most common methodology adopted for most applications (Khandelwal and Singh, 2010; Rolon et al., 2009; Saputro et al., 2016). Backpropagation is the most common supervised neural network; it is adopted in many operationally driven and geological systems. The backpropagation algorithm is implemented firstly with a forward activation for the target solution, and then a backward propagation to reinitialize the weight from the computed error gradient. This is done in two sweeps (Adedigba et al 2017). The backpropagation algorithm determines the epoch with the least errors by calculating the local error gradient and locating the minimum point

on the error surface (Chen et al., 2017; Chitsazan et al., 2015). The local error gradient descent learning for the implementation of the backpropagation algorithm is an iterative process which is corrected with the help of adjustable parameters such as the learning rate and momentum term (Gardner and Dorling, 1998). The error function can be determined with performance functions such as mean square error (MSE), sum square error (SSE) and mean absolute deviation (MAD) which are back-propagated into the network to re-initialize the weights (Adedigba et al., 2017; Ashtiani and Shahsavari, 2016; Hsu et al., 1995).

For the proposed ANN to learn the best permutation sequence between the input and target vectors, the well log data are sub-divided into a training set, a validation set and a test set. 70% of the input well log data is used to train the ANN model, 15% is used to validate the model and 15% is used to test the ANN model.

The steps used to develop and implement the proposed model are summarized below:

1. Determine the architecture of the ANN: This involves establishing the number of layers that adequately predicts the corresponding pattern recognition. The neurons in each layer must also be determined at this stage. The schematic of the proposed ANN architecture is presented in Figure 5.2.

2. Select network vectors and data: The input vector and data for the network and target data are specified. A range of input data available for the model is presented in Figure 5.3.

3. Initialize the weight values of the input parameters and biases: The initial values are initially assumed and redistributed as a continuous process of the learning and growth of the network.

4. Propagate the input vector or data: The input vector is propagated through the neural network to estimate the output data.

5. Compute error: The error between the target value and output values is calculated by calculating their differences. The error function of each set point is determined.

6. Back pass the error terms: The error term is passed back into the neural network

7. Update network: The neural network is updated based on the error function determined in order to reduce the error between the target and output values.

8. Repeat all stages: The weights and biases are re-initialized to begin the loop again. This process is cycled until the limiting criteria are reached. This can be the minimum error, validation step or the number of cycles, known as epochs.

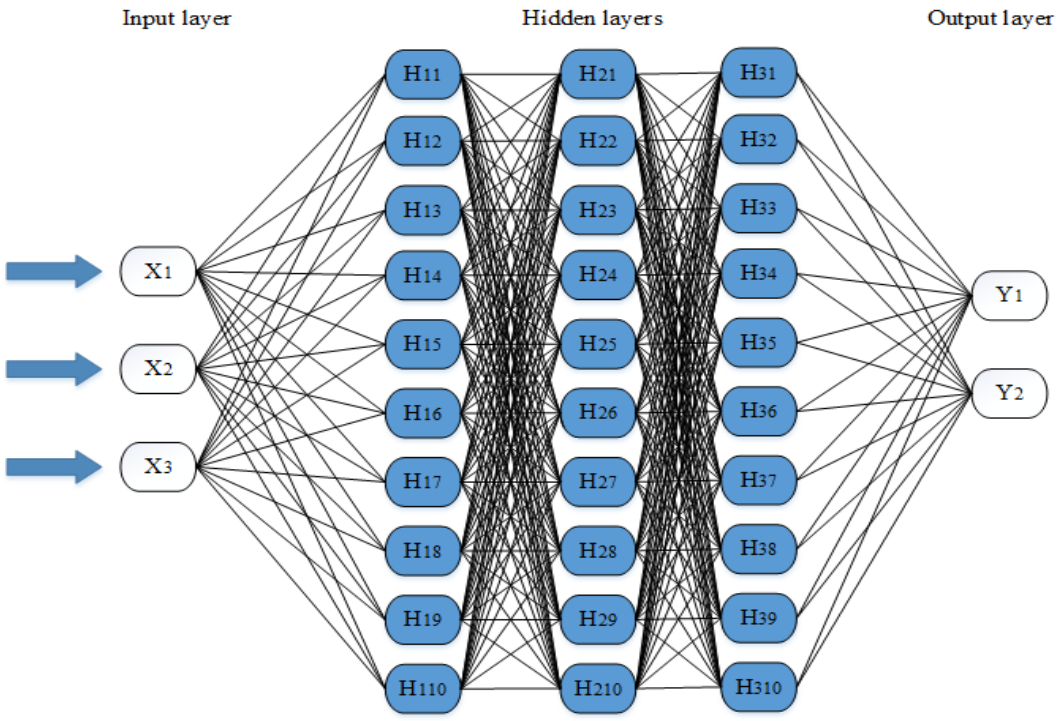

Figure 5.2. Schematic of the proposed ANN architecture

5.3.5 Generalization of the ANN

The essence of using a reliable dataset to develop an ANN model is the ability to generalize the model so that it is applicable to a dataset outside the data used to train the model. The proposed model is trained with a section of the dataset and generalized by applying the model to estimate the desired properties from a different section of the dataset.

5.4 Case Study

The proposed methodology framework in section 5.3 is applied to an actual well log dataset. The case study presented in this work is actual well log data from an offshore oil and gas well located in West Africa. Information containing the details and location of the offshore well has not been made public due to confidentiality and proprietary issues. However, for interested users, the well log data is presented in Figure 5.3 and Table 5A 1 in Appendix 5A. The input data available from the well log dataset are presented below.

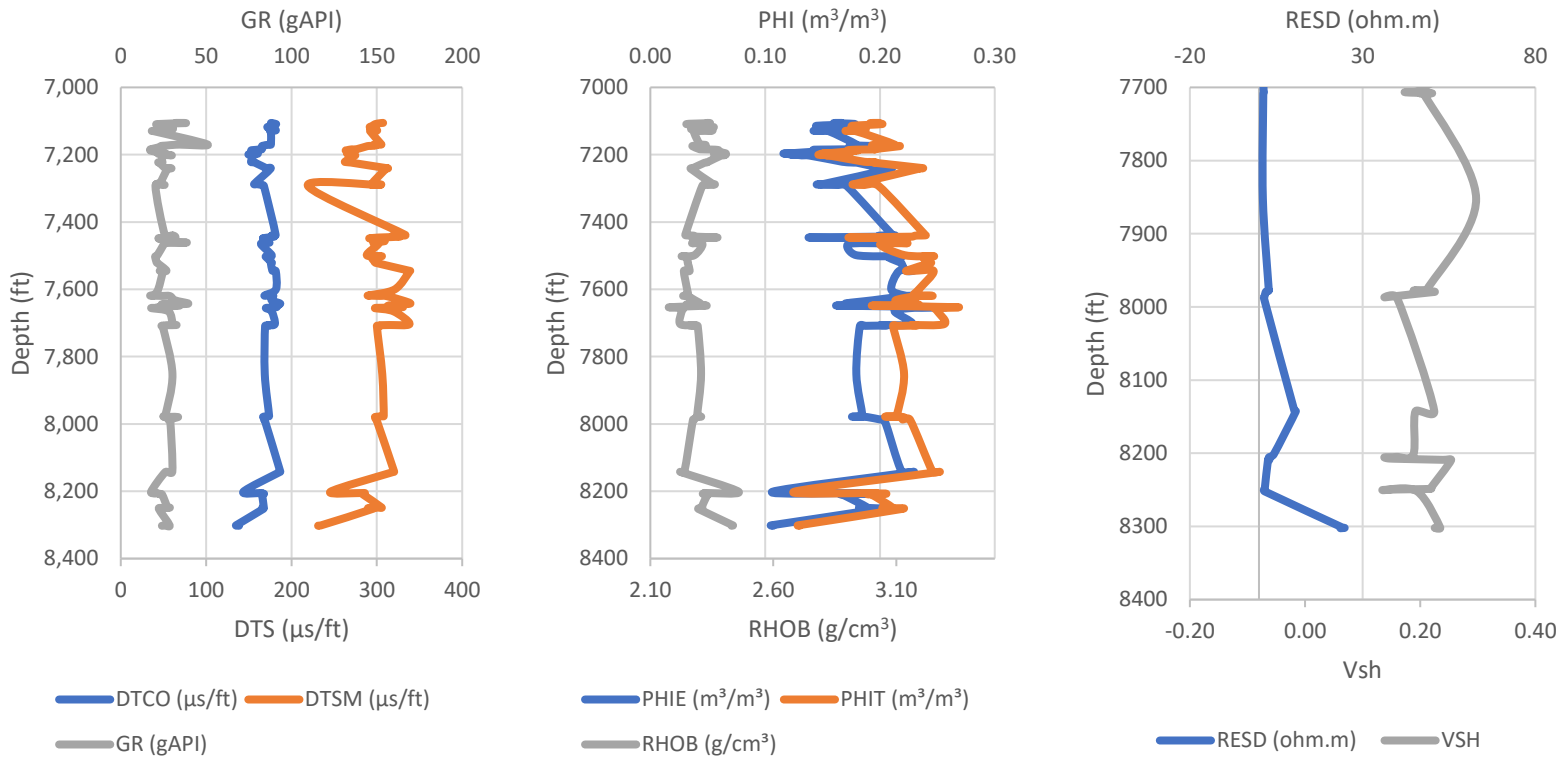

Figure 5.3. Well Log Data

5.4.1 **Input parameters**

- Gamma ray log (GR)
- Bulk density log (RHOB)

$$\phi_{den} = \frac{\rho_{ma} - \rho_b}{\rho_{ma} - \rho_{fl}} \tag{5.1}$$

- Deep resistivity log (RESD)
- Neutron log (NPHI)

$$\phi_N = \phi * \phi_{N,fl} + (1 - \phi) * ((1 - V_{sh}) * \phi_{N,ma} + V_{sh} * \phi_{N,sh}) \tag{5.2}$$

- Shale Volume (Vsh)

$$V_{sh} = \frac{GR - GR_{min}}{GR_{max} - GR_{min}} \tag{5.3}$$

- Total porosity (PHIT)
- Effective porosity (PHIE)

$$PHIE = PHIT - V_{sh} \tag{5.4}$$

5.4.2 **Output parameters**

- Compressional wave sonic transit time log (DTCO)
- Shear wave sonic transit time log (DTSM)

5.4.3 **Selection of Models**

Several models were developed to determine the best model for carrying out on the spot determination of compressional transit time and shear transit time to be used to determine the likelihood of the formation to sand. All the models developed were trained, tested and validated.

The well log data set is divided into three sections based on best practices. 70% of the data was used for training, 15% was used for testing and the rest of the data was used to validate the model. The training set is used to compute the gradient and predict the weight values and biases. The validation set is used to certify the precision and generalization capability of the developed network in the process of the training. The test set is used to verify the performance of the network. The coefficients of determination (R^2) of 0.9904, 0.9957 and 0.993 were obtained for the training set, testing set and validation set respectively. The results obtained showed the model fits your data. The proposed ANN Model

Based on the ANN architecture proposed in section 5.3.3, different combinations of input vectors were studied. Gamma-ray, density log, and shale volume were observed to adequately predict the sonic transit time from the well log data. Thus, they were chosen as input vectors for the ANN model and applied to the ANN framework in Figure 5.2. The adopted ANN framework for this case study is presented in Figure 5.4.

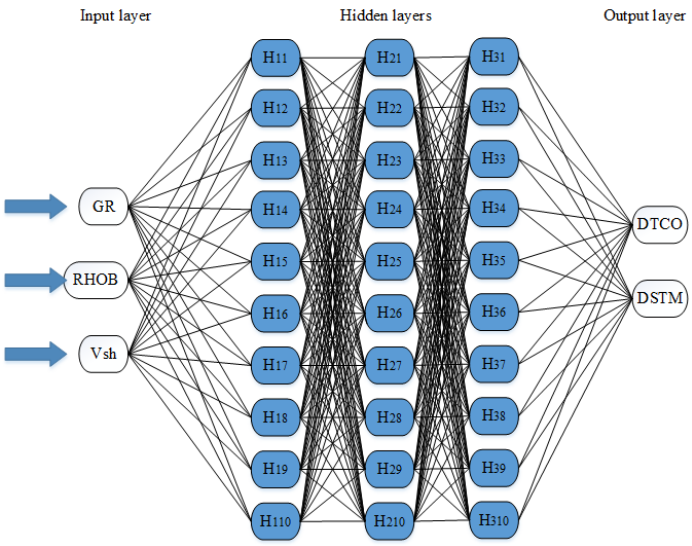

Figure 5.4. Schematic diagram of ANN architecture for sonic interval travel time

5.4.4 **Estimated Formation Mechanical Properties**

Most rock elastic constants and mechanical rock properties can be obtained directly from the sonic wave interval travel time through the formations. The correlations commonly used to determine these properties in isotropic and homogeneous formation are presented below (Mullen et al., 2007; Tixier et al., 1975).

5.4.4.1 Young's Modulus (E)

The ratio of the uniaxial stress to strain is known as Young's modulus. It is the measure of the stiffness of the formation, its ability to resist uniaxial deformation and compression. It is estimated from sonic transit time by equation (5.5).

$$E = \frac{\rho}{{\Delta t_s}^2} * \left(\frac{3{\Delta t_s}^2 - 4{\Delta t_c}^2}{{\Delta t_s}^2 - {\Delta t_c}^2} \right) * 1.34 * 10^{10} \tag{5.5}$$

5.4.4.2 Bulk Modulus (K)

The ratio of hydrostatic stress to the volumetric strain is given by the bulk modulus and can be estimated from the sonic transit times using equation (5.6). The bulk modulus measures the ability of the formation to resist hydrostatic deformation and compression (Fjaer, 2008).

$$K = \rho * \left(\frac{3{\Delta t_s}^2 - 4{\Delta t_c}^2}{3{\Delta t_s}^2 * {\Delta t_c}^2} \right) * 1.34 * 10^{10} \tag{5.6}$$

5.4.4.3 Shear Modulus (G)

The shear modulus measures the ability of the formation to resist shear deformation and is estimated from the sonic transit time using equation (5.7). It is also known as the modulus of rigidity (Fjaer, 2008).

$$G = \frac{\rho}{\Delta t_s{}^2} * 1.34 * 10^{10} \quad (5.7)$$

5.4.4.4 Sonic Porosity:

One of the common uses of the sonic interval travel time through a formation during well logging is the estimation of porosity, known as sonic porosity. Porosity from sonic logs can be estimated from Wyllie's time-average equation (Wyllie et al., 1956).

$$\phi_s = \frac{\Delta t_{log} - \Delta t_{ma}}{\Delta t_{fl} - \Delta t_{ma}} \quad (5.8)$$

However, Raymer-Hunt et. al. (1980) modified Wyllie's equation to account for compaction (Raymer et al., 1980).

$$\phi_s = \frac{5}{8} * \frac{\Delta t_{log} - \Delta t_{ma}}{\Delta t_{log}} \quad (5.9)$$

Wyllie's porosity model fails to provide accurate estimations in unconsolidated or loosely consolidated formations. To compensate for this error, a term known as the compaction factor (C_p) is added to the equation.

$$\phi_s = \frac{\Delta t_{log} - \Delta t_{ma}}{\Delta t_{fl} - \Delta t_{ma}} * \frac{1}{C_p} \quad (5.10)$$

$$C_p = \frac{\Delta t_{sh}}{100} \quad (5.11)$$

Table 5.3. Interval Travel times of some formations and fluids (after (Asquith and Gibson, 2004))

Formation/Fluid	Interval travel time (µsec/ft)
Sandstone	51 – 55.5
Limestone	47.6
Dolomite	43.5
Freshwater	189
Saltwater	185

Table 5.3 presents the interval travel time of some formations. The presence of hydrocarbon and gas can alter the measured values of the interval travel time by increasing the measured value (Nourafkan and Kadkhodaie-Ilkhchi, 2015; Tixier et al., 1975). This leads to errors in the derived sonic porosity. To correct for this increase, the convention is to multiply the derived sonic porosity by 0.7 for gas and by 0.9 for oil.

5.4.4.5 Sanding potential:

According to Tixier et al. (1975), sanding potential (ω) can be determined from the product of the shear modulus and bulk modulus. If the product is greater than 0.8 $Mpsi^2$, then the probability of sand production is said to be highly unlikely; however, if the product is less than 0.7 $Mpsi^2$, then the probability of sanding is said to be highly likely (Tixier et al., 1975; Veeken et al., 1991). Therefore, high values of sanding potential are desirable.

$$\omega = \mathrm{G} * \mathrm{K} \tag{5.12}$$

In this study, the unconfined compressive strength was not estimated from the sonic velocities because generalization of the unconfined compressive strength (UCS) correlation tends to be highly inconsistent from region to region. A correlation valid in the Gulf of Mexico may fail totally in the Alberta sands; therefore, adequate care must be taken prior to selecting the best correlation for a particular region. Najibi et al. (2015) provide a comprehensive list of possible UCS correlations that could be used to estimate unconfined compressive strength from sonic logs.

5.5 Results and discussion

5.5.1 Sonic transit time log estimation

The primary objective of developing the ANN model is to provide a reliable tool capable of developing sonic transit time logs in the absence of reliable sonic well logs with a limited number of well log data. The recommended input well logs for the ANN model are gamma ray and formation density logs, from which the shale volume can be calculated. The actual values from the well logs are given in Table 5A 1. A sample of the target measured sonic log data and the predicted output sonic transit log data is presented in Table 5.5. It may be observed that the predicted sonic transit time demonstrates a close match with actual measured values. This is further evident in Figure 5.5, where the measured and ANN predicted compressional wave sonic transit time is plotted versus depth on the left-hand side. On the right-hand side of Figure 5.5, the measured and ANN predicted shear wave sonic transit times is plotted versus depth. Figure 5.5 confirms a closer match of the measured and ANN predicted values for compressional wave sonic transit time than for shear wave sonic transit time. This may be due to the fact that ANN input vectors like bulk density are affected by both the matrix and the saturating fluid. The compressional wave travels through both the matrix and saturating fluid of the formation; however, the shear wave travels only through the matrix of the formation. Perhaps input parameters that are affected by only the matrix (matrix density, porosity) would provide a better fit for shear wave sonic transit time prediction. The model fails to predict accurately a section (7200 – 7400 feet) of the shear sonic log; however, this has been left in this paper to draw attention to this section. This could be as a result of the presence of gas or formation anisotropy, especially as a result of clay. The measurement of sonic transit time varies depending on the orientation of the clay anisotropy along its path. The difference in the match is not so evident in the cross-plot comparison of measured compressional transit time

with ANN compressional transit time in Figure 5.6, and the cross-plot comparison of measured compressional transit time with ANN compressional transit time in Figure 5.7. To further provide a qualitative analysis of the model prediction, the root mean square error (RMSE), the mean absolute error (MAE) and the average percentage error (MPE) are calculated for the model. The RMSE was 2.62 and 5.29, while the MAE was 2.14 and 3.77 for compressional and shear transit time respectively. The MPE was 3% for both compressional and shear transit time. A summary of the mean average error and mean percentage error of the sonic logs and mechanical rock properties is presented in Table 5.4.

Table 5.4. Summary of statistical analysis

Formation property	RMSE	MAE	MPE
DTCO	2.62	2.14	0.03
DTSC	5.29	3.77	0.03
Young's modulus	0.21	0.15	0.04
Bulk modulus	0.28	0.21	0.09
Shear modulus	0.13	0.08	0.05
Sonic porosity	0.01	0.01	0.06
Sanding potential	0.50	0.38	0.09

The ANN model provides an alternative of using overgeneralized empirical correlations which are not robust enough to be applied to every well. The ANN is relatively cheap, cost-effective and computationally less rigorous than other well log data analysis tools. Due to the dynamic nature of the well log matching, severe deviations from the ANN predicted values should be investigated for formation anomalies.

Table 5.5. Sample measured sonic well log and ANN derived values

Depth (ft)	DTCO (µsec/ft)		DTSM (µsec/ft)	
	Measured	Predicted	Measured	Predicted
8142.00	93.45	91.60	160.15	161.88
8142.50	93.27	93.06	159.73	164.44
8201.50	71.81	68.32	122.82	111.49
8205.00	82.57	80.39	142.48	139.20
8205.50	82.37	78.61	143.04	135.20
8207.00	83.20	80.10	142.78	138.56
8207.50	83.96	81.32	142.68	141.23
8209.00	82.85	81.55	142.01	141.75
8209.50	82.73	82.31	141.88	143.39
8248.00	83.78	86.56	152.76	152.26
8248.50	83.00	87.26	150.86	153.66
8249.00	82.93	85.30	147.91	149.70
8249.50	83.18	84.28	145.73	147.58
8250.50	83.11	82.21	144.74	143.18
8252.00	83.63	83.95	147.76	146.90
8301.50	67.41	70.03	117.19	115.34
8302.00	68.02	70.44	115.69	116.29
8302.50	69.26	70.95	115.58	117.46

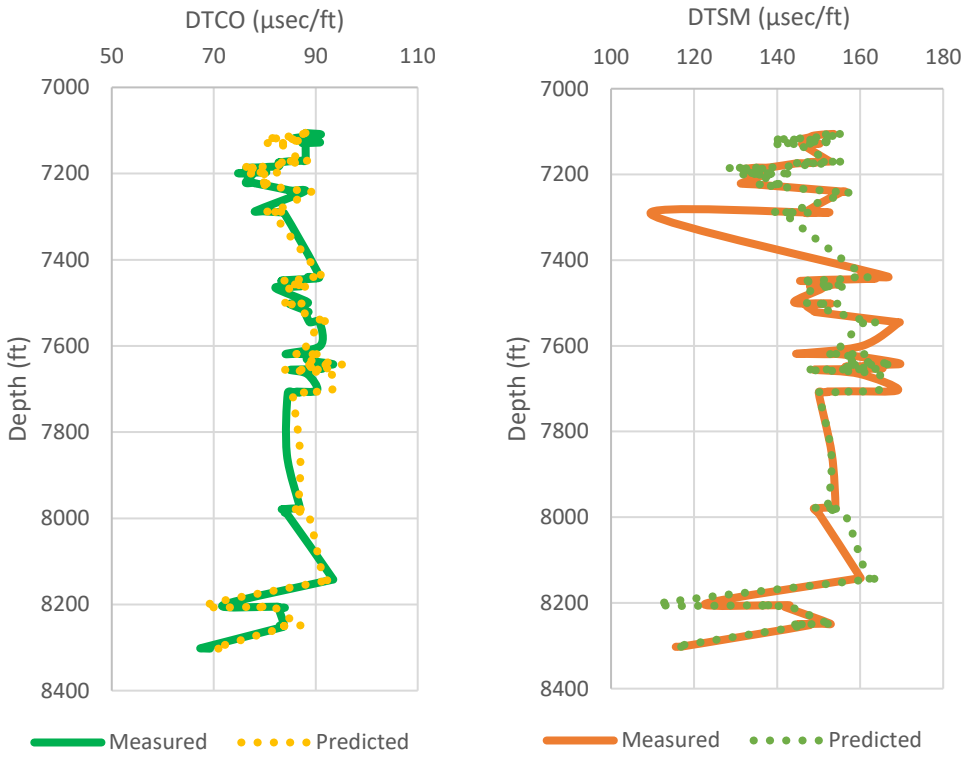

a) Compressional wave travel time (DTCO) b) Shear wave travel time (DTSM)

Figure 5.5. Depth vs Interval Travel Time

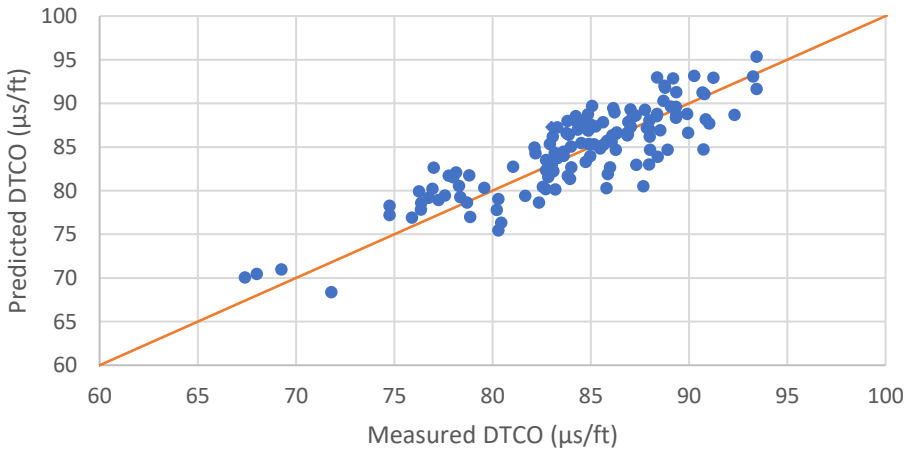

Figure 5.6. Comparison of measured and predicted compressional wave travel time

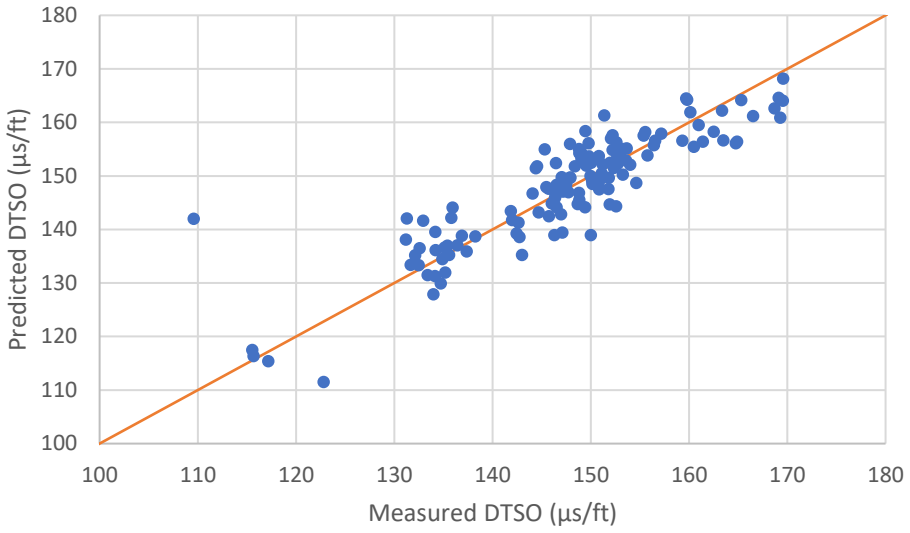

Figure 5.7. Comparison of measured and predicted shear wave travel time

5.5.2 **Formation Mechanical Property Prediction**

The effectiveness of the ANN model as a reliable and cost-effective alternative to an actual sonic well log is demonstrated by comparing the estimations of the typical rock mechanical properties that are estimated from sonic logs in the oil and gas industry. The results of the mechanical rock properties estimations are presented in Table 5.6.

Table 5.6. Sample measured well log and ANN derived mechanical rock properties

Dept (ft)	Young's Modulus		Bulk Modulus		Shear Modulus		Sonic Porosity		Sanding Potential	
	Measured	Predicted	Measured	Predicted	Measured	Predicted	Measured	Predicted	Measured	Predicted
8142.0	2.9	2.89	1.88	2.05	1.17	1.14	0.25	0.25	2.19	2.34
8142.5	2.9	2.79	1.87	1.97	1.17	1.1	0.25	0.26	2.18	2.17
8201.5	5.42	6.36	3.48	3.52	2.18	2.65	0.14	0.1	7.59	9.34
8205.0	3.82	4.01	2.52	2.67	1.53	1.6	0.2	0.19	3.85	4.28
8205.5	3.81	4.23	2.56	2.76	1.52	1.7	0.2	0.18	3.89	4.70
8207.0	3.79	4.04	2.46	2.68	1.52	1.62	0.2	0.19	3.74	4.34
8207.5	3.76	3.89	2.37	2.62	1.52	1.55	0.21	0.19	3.60	4.06
8209.0	3.86	3.9	2.49	2.63	1.55	1.56	0.2	0.19	3.87	4.10
8209.5	3.86	3.81	2.5	2.59	1.55	1.52	0.2	0.19	3.88	3.93
8248.0	3.41	3.36	2.64	2.35	1.33	1.33	0.21	0.22	3.50	3.13
8248.5	3.49	3.31	2.68	2.32	1.36	1.31	0.2	0.22	3.65	3.04
8249.0	3.6	3.48	2.62	2.41	1.42	1.38	0.2	0.22	3.70	3.34
8249.5	3.66	3.57	2.53	2.46	1.45	1.42	0.2	0.21	3.67	3.49
8250.5	3.69	3.77	2.5	2.55	1.47	1.5	0.2	0.2	3.67	3.83
8252.0	3.56	3.58	2.52	2.46	1.41	1.42	0.21	0.21	3.55	3.51
8301.5	5.96	5.93	4.02	3.38	2.38	2.45	0.11	0.12	9.54	8.31
8302.0	6.02	5.84	3.8	3.36	2.44	2.41	0.11	0.12	9.26	8.09
8302.5	5.95	5.72	3.54	3.32	2.44	2.36	0.12	0.13	8.62	7.84

These values are used to produce cross-plot comparisons of the measured versus ANN model estimates of the mechanical rock properties. The Young's modulus is presented in Figure 5.8; the root mean square error, the mean absolute error and mean percentage error were 0.21, 0.15 and 4% respectively. Typical values of Young's modulus in sandstone formation are between can be found in Table 5.7 (Deere and Miller, 1966; Nauroy, 2011). The values in the case study vary from 2.7 Mpsi to 6 Mpsi, with a majority of the values less than 4.7 along the well. This suggests that the formation is moderately weak and well consolidated. The stress state of the formation expected can also be assumed for initial analysis. A moderately high confining stress state that is capable of confining the formation into a consolidated state would thus be expected upon further geomechanical investigation.

Table 5.7. Formation classification table

Formation classification		**Ed (GPa)**	**Ed (Mpsi)**
(Deere and Miller, 1966)	**Nauroy (2011)**		
Very weak formation	Poorly consolidated formation	<1	0.145
weak formation	Poorly cemented formation	5 - 10	0.725 - 1.45
Moderately weak formation	Consolidated formation	10 – 50	1.45 - 7.25
Hard formation	Highly consolidated formation	50 - 100	7.25 - 14.5
Very hard formation	Hard formation	>100	>14.5

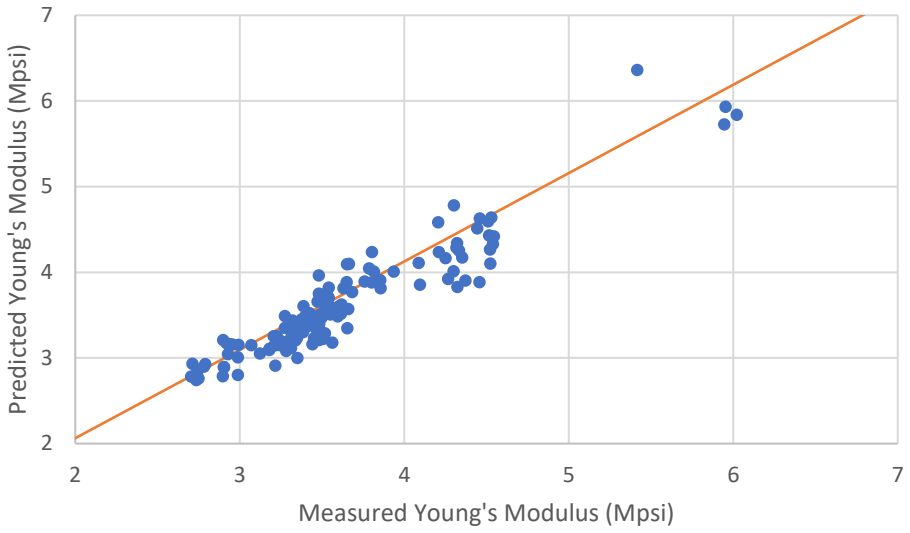

Figure 5.8. Comparison of measured and predicted Young's modulus

Most of the predicted bulk modulus values did not fall on the perfect linear trendline. Nevertheless, the root mean square error was found to be 0.28, the mean absolute error was found to be 0.21, while the mean percentage error was 9%. The trendline is also seen to be very close to the unity line, indicating that the predictions are not biased positively or negatively.

The values of the bulk modulus presented in Figure 5.9 suggests that the formation has a moderate resistance to external pressure, and more specifically, stresses induced from drilling or production operations. The presence of liquid hydrocarbon or water may increase the bulk modulus; therefore, the values may also be initially indicative of a gas hydrocarbon-bearing formation. High compressibility may be desirable to squeeze more hydrocarbon out of the fluid pore space where the failure can be controlled. Compaction and subsidence may be challenges not expected to be encountered in such formations; hence, surface facilities may be designed to cater to this scenario over time.

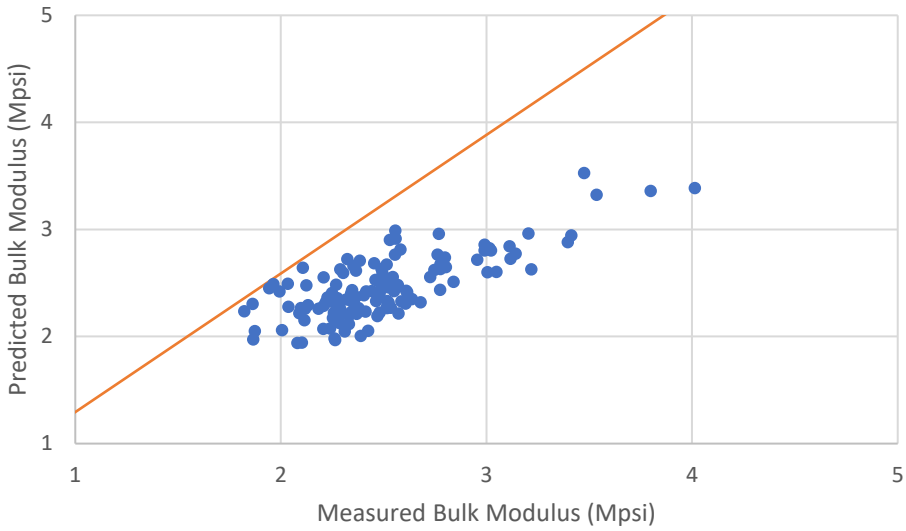

Figure 5.9. Comparison of measured and predicted bulk modulus

The analysis of the cross plot of the shear modulus in Figure 5.10 revealed the root mean square error to be 0.13, the mean absolute error to be 0.07 and the mean percentage error to be approximately 5%. The shear modulus of quartz has been reported to be approximately 44 GPa while clay is approximately 6.85 GPa at confining pressures between 5 MPa and 40 MPa (Lee, 2005). The shear modulus values presented in Figure 5.10 are significantly lower, which is in line with the observed Young's modulus and shear modulus in the case study. This confirms that the formation is moderately susceptible to both compressional and shear deformation; thus, wellbore failure is not anticipated during controlled exploration. The completion engineer is able to anticipate and plan an effective completion program to ensure the well is intact after initial drilling and ready for production.

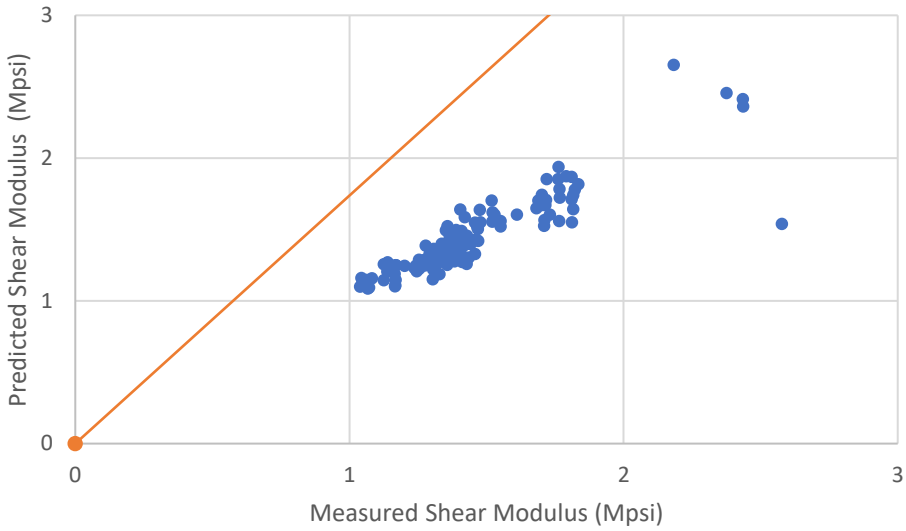

Figure 5.10. Comparison of measured and predicted shear modulus

The sonic porosity presented in Figure 5.11 mainly ranges between 0.15 to 0.25, confirming that the formation is potentially a good reservoir with significant pore volume to store the desired hydrocarbons. The statistical model analysis showed that RMSE = 0.01, MAE = 0.01 and MPE = 5.8%. The values of the sonic porosity in the case study are similar to the values obtained from the density porosity logs and neutron porosity logs, which help to validate the authenticity of the model.

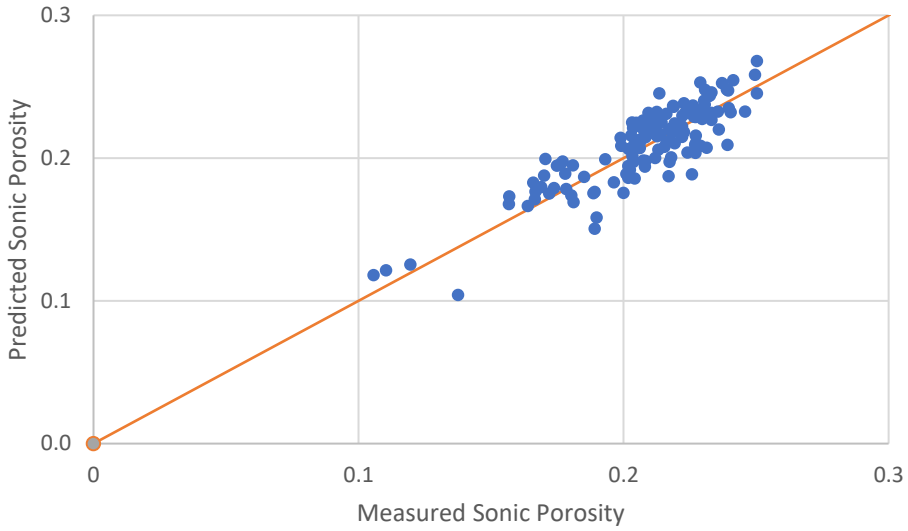

Figure 5.11. Comparison of measured and predicted sonic porosity

The sanding potential of the well is also estimated and plotted in Figure 5.12. The model analysis demonstrated that the root mean square error was 0.5, the mean absolute error was 0.37 and the mean percentage error was 9%. All values of the sanding potential from both the measured and predicted sanding potential are above 0.8 $Mpsi^2$; therefore, the formation is not susceptible to sand production and an adequate sanding control program is not critical at this stage of the field development.

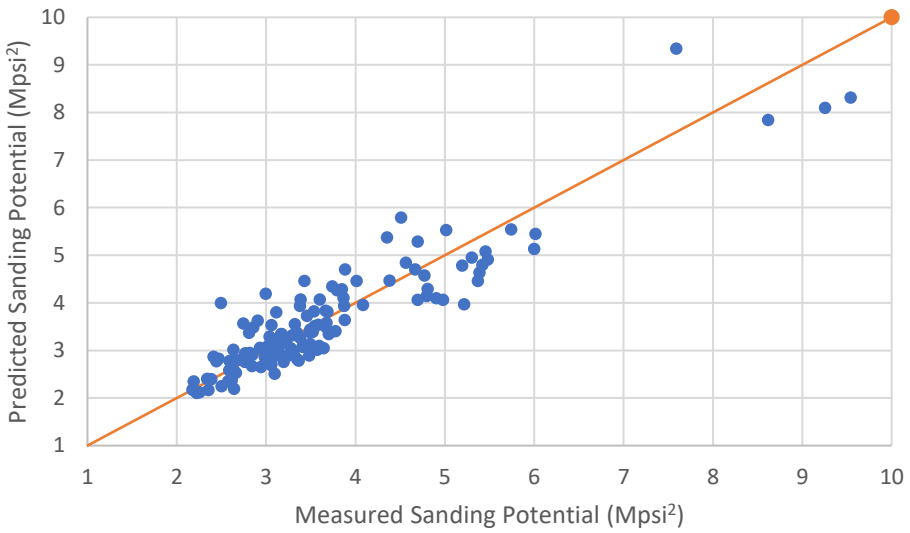

Figure 5.12 Comparison of measured and predicted sanding potential

The application of the proposed methodology on the well log data is a major step forward. To the best of the authors' knowledge, there is no available ANN model which predicts sonic travel transit time from gamma rays, formation density and shale volume. Most available ANN models from well logs predict reservoir parameters such as porosity, fracture porosity and permeability (Al-Kattan and Jasim Al-Ameri, 2012; Banchs and Michelena, 2002; Bhatt, 2002; Kohli and Arora, 2014; Ma et al., 2017; Rafik and Kamel, 2017; Saputro et al., 2016; Tixier et al., 1975; Verma et al., 2012). Though the ANN is a promising tool, it is of paramount importance to state some of the limitations of ANN modeling. ANN predicting accuracy may be affected by overfitting. Increasing the data not only increases the computational time and power, it also increases the chances of overfitting the data (Lawrence et al., 1997). This reduces the accuracy of the ANN for use with outset data and is a major drawback of the method (Chitsazan et al., 2015). It is important that the limitations of ANN-based models be emphasized because they can affect the output predicted by the model. The output vectors are affected by the quality of the well log input vectors. The output

can vary based on the training algorithm, the training method and transfer functions. A higher number of neurons or layers does not guarantee a better model; therefore, adequate time should be dedicated to determining a suitable architecture. Most importantly, there is no set rule on how an ANN derived model should be designed or developed to get the best results (Adedigba et al., 2017). For this reason, it is recommended to adopt simple ANN architecture except in cases where complex correlations will better describe the existing structure between the input and target values (Franses and Draisma, 1997). Noteworthy is that increasing the number of input vectors or data is not synonymous with a better prediction as it is possible to overfit the data.

5.6 Conclusions

The present study has demonstrated the use of an artificial neural network in modeling sonic transit time logs from limited well log data. In this study, an ANN is proposed as a robust and reliable tool to define sonic logs from gamma ray and formation density logs. The proposed methodology provides the oil and gas industry with the following advantages:

- The ANN model offers a solution to estimating sonic transit time from old wells with missing well log data, erroneous data due to faulty or damaged tools, and lost tools in a well.

- The ANN model offers a solution where there is no sufficient well log dataset to develop formation property log tables for a geological area.

- The ANN model offers a considerably cheaper alternative to running actual sonic logging tools like borehole compensated and dipole sonic logging tools.

- The ANN model provides an alternative to using empirical correlation and offset data to determine shear wave velocity for calculating rock mechanical properties.

The ANN model accurately predicts whether the well has a high sanding potential value meaning the probability of sanding is low. This is consistent with actual field observations. The well is an actual well with very little sanding issue, as accurately predicted by the ANN model.

In general, the modeling flexibility of the ANN allows for the prediction of various kinds of relationship from well logs that cannot be readily determined from other correlations. The effectiveness of the proposed ANN is demonstrated by estimating parameters which can also be

measured with sonic logs. The ANN model is recommended for establishing relationships for formation evaluation and characterization, especially for properties with no existing correlation.

By adopting the proposed methodology, engineers will be able to estimate sonic transit times with a limited amount of well log data. The application of this models is that it provides field engineers with a means of determining the potential of a formation to produce sand in real time without having to send the data for comprehensive analysis by the geoscientists, thereby enabling the engineers to make quick, efficient and effective recommendations for field development.

As future work, compressional wave transit time could be added or combined with the available well logs to improve the estimation of shear wave sonic transit time. This would be useful for offset wells with only compressional wave transit time or logs from borehole compensated sonic logs.

Acknowledgment

The authors thankfully acknowledge the financial support provided by the Natural Science and Engineering Council of Canada and the Canada Research Chair (CRC) Program, the Hibernia Management and Development Company (HMDC), Chevron Canada, and Innovate NL for the support without which this work could not have been performed.

Nomenclature

RHOB	Bulk density log (g/cm^3)
K	Bulk modulus (Mpsi)
DTCO	Compressional wave travel time (µsec/ft)
Δt_c	Compressional wave travel time (µsec/ft)
RESD	Deep resistivity log (ohm.m)
PHIE	Effective porosity log (m^3/m^3)
ϕ_{den}	Electron density porosity (g/cc)
ρ_{fl}	Fluid density (g/cc)
ρ, ρ_b	Formation density (g/cc)
Δt_{fl}	Formation fluid compressional wave travel time (µsec/ft)
Δt_{ma}	Formation matrix compressional wave travel time (µsec/ft)
GR_{min}	Gamma-ray in clean sandstone
GR_{min}	Gamma-ray in shale
GR	Gamma-ray log (gAPI)
GR	Gamma-ray log reading
ρ_{ma}	Matrix density (g/cc)
MAE	Mean absolute error
MPE	Mean percentage error
Δt_{log}	Measured compressional wave travel time (µsec/ft)
ϕ_N	Neutron porosity
NPHI	Neutron porosity
$\phi_{N,fl}$	Neutron response of the fluid
$\phi_{N,ma}$	Neutron response of the matrix
PEF	Photoelectric factor
ϑ	Poisson's ratio
ϕ	Rock porosity
w	Sanding potential (Mpsi^2)
Vsh	Shale volume
RS	Shallow resistivity
G	Shear modulus (Mpa)
DTSM	Shear wave travel time (µsec/ft)
Δt_s	Shear wave travel time (µsec/ft)
ϕ_s	Sonic porosity
PHIT	Total porosity log (m^3/m^3)
RT	True resistivity
E	Young's modulus (Mpsi)

References

Aadnoy, B.S., Kaarstad, E., Gonsalves, C.J. de C., 2013. Obtaining Both Horizontal Stresses from Wellbore Collapse. SPE/IADC Drill. Conf. https://doi.org/10.2118/163563-MS

Adedigba, S.A., Khan, F., Yang, M., 2017. Dynamic failure analysis of process systems using neural networks. Process Saf. Environ. Prot. 111, 529–543. https://doi.org/10.1016/J.PSEP.2017.08.005

Akhundi, H., Ghafoori, M., Lashkaripour, G.-R., 2014. Prediction of Shear Wave Velocity Using Artificial Neural Network Technique, Multiple Regression and Petrophysical Data: A Case Study in Asmari Reservoir (SW Iran). Open J. Geol. 04, 303–313. https://doi.org/10.4236/ojg.2014.47023

Al-Dousari, M., Garrouch, A.A., Al-Omair, O., 2016. Investigating the dependence of shear wave velocity on petrophysical parameters. J. Pet. Sci. Eng. 146, 286–296. https://doi.org/10.1016/J.PETROL.2016.04.036

Al-Kattan, W., Jasim Al-Ameri, N., 2012. Estimation of the Rock Mechanical Properties Using Conventional Log Data in North Rumaila Field. Iraqi J. Chem. Pet. Eng. 13, 27–33.

Aleardi, M., 2015. Seismic velocity estimation from well log data with genetic algorithms in comparison to neural networks and multilinear approaches. J. Appl. Geophys. 117, 13–22. https://doi.org/10.1016/J.JAPPGEO.2015.03.021

Alloush, R.M., Elkatatny, S.M., Mahmoud, M.A., Moussa, T.M., Ali, A.Z., Abdulraheem, A., 2017. Estimation of Geomechanical Failure Parameters from Well Logs Using Artificial Intelligence Techniques. SPE Kuwait Oil Gas Show Conf. https://doi.org/10.2118/187625-

MS

Ashtiani, H.R.R., Shahsavari, P., 2016. A comparative study on the phenomenological and artificial neural network models to predict hot deformation behavior of AlCuMgPb alloy. J. Alloys Compd. 687, 263–273. https://doi.org/10.1016/J.JALLCOM.2016.04.300

Asoodeh, M., Bagheripour, P., 2014. ACE stimulated neural network for shear wave velocity determination from well logs. J. Appl. Geophys. 107, 102–107. https://doi.org/10.1016/J.JAPPGEO.2014.05.014

Asoodeh, M., Bagheripour, P., 2013. Neuro-fuzzy reaping of shear wave velocity correlations derived by hybrid genetic algorithm-pattern search technique. Open Geosci. 5, 272–284. https://doi.org/10.2478/s13533-012-0129-4

Asoodeh, M., Bagheripour, P., 2012. Prediction of Compressional, Shear, and Stoneley Wave Velocities from Conventional Well Log Data Using a Committee Machine with Intelligent Systems. Rock Mech. Rock Eng. 45, 45–63. https://doi.org/10.1007/s00603-011-0181-2

Asquith, G., Gibson, C., 2004. Basic well log analysis for geologists, American Association of Petroleum Geologists Methods in Exploration. https://doi.org/82-73052

Azizi, S., Ahmadloo, E., Awad, M.M., 2016. Prediction of void fraction for gas–liquid flow in horizontal, upward and downward inclined pipes using artificial neural network. Int. J. Multiph. Flow 87, 35–44. https://doi.org/10.1016/J.IJMULTIPHASEFLOW.2016.08.004

Bagheripour, P., Gholami, A., Asoodeh, M., Vaezzadeh-Asadi, M., 2015. Support vector regression based determination of shear wave velocity. J. Pet. Sci. Eng. 125, 95–99. https://doi.org/10.1016/J.PETROL.2014.11.025

Balarabe, T., Isehunwa, S., 2017. Evaluation of Sand Production Potential using Well Logs. SPE Niger. Annu. Int. Conf. Exhib. https://doi.org/10.2118/189107-MS

Banchs, R.E., Michelena, R.J., 2002. From 3D seismic attributes to pseudo-well-log volumes using neural networks: Practical considerations. Lead. Edge 21, 996–1001. https://doi.org/10.1190/1.1518436

Basheer, I.., Hajmeer, M., 2000. Artificial neural networks: fundamentals, computing, design, and application. J. Microbiol. Methods 43, 3–31. https://doi.org/10.1016/S0167-7012(00)00201-3

Benardos, P.G., Vosniakos, G.-C., 2007. Optimizing feedforward artificial neural network architecture. Eng. Appl. Artif. Intell. 20, 365–382. https://doi.org/10.1016/j.engappai.2006.06.005

Bhatt, A., 2002. Reservoir properties from well logs using neural networks.

Bianco, L.C.B., Halleck, P.M., 2001. Mechanisms of Arch Instability and Sand Production in Two-Phase Saturated Poorly Consolidated Sandstones. SPE Eur. Form. Damage Conf. https://doi.org/10.2118/68932-MS

Buhulaigah, A., Al-Mashhad, A.S., Al-Arifi, S.A., Al-Kadem, M.S., Al-Dabbous, M.S., 2017. Multilateral Wells Evaluation Utilizing Artificial Intelligence. SPE Middle East Oil Gas Show Conf. https://doi.org/10.2118/183688-MS

Castagna, J.P., Batzle, M.L., Eastwood, R.L., 1985. Relationships between compressional-wave and shear-wave velocities in clastic silicate rocks. Geophysics 50, 571–581. https://doi.org/10.1190/1.1441933

Chen, Z., Ma, W., Wei, K., Wu, J., Li, S., Xie, K., Lv, G., 2017. Artificial neural network modeling for evaluating the power consumption of silicon production in submerged arc furnaces. Appl. Therm. Eng. 112, 226–236. https://doi.org/10.1016/J.APPLTHERMALENG.2016.10.087

Chitsazan, N., Nadiri, A.A., Tsai, F.T.-C., 2015. Prediction and structural uncertainty analyses of artificial neural networks using hierarchical Bayesian model averaging. J. Hydrol. 528, 52–62. https://doi.org/10.1016/J.JHYDROL.2015.06.007

Cranganu, C., Bautu, E., 2010. Using Gene Expression Programming to estimate sonic log distributions based on the natural gamma ray and deep resistivity logs: A case study from the Anadarko Basin, Oklahoma. J. Pet. Sci. Eng. 70, 243–255. https://doi.org/10.1016/J.PETROL.2009.11.017

Deere, D.U., Miller, R.., 1966. Engineering classification and index properties for intact rock. Tech. Report, Air Force Weapons Lab. 1, 65–116.

Dorofki, M., Elshafie, A.H., Jaafar, O., Karim, O.A., Mastura, S., 2012. Comparison of Artificial Neural Network Transfer Functions Abilities to Simulate Extreme Runoff Data, in: 2012 International Conference on Environment, Energy and Biotechnology. pp. 39–44.

Eberhart-Phillips, D., Han, D.-H., Zoback, M., 1989. Empirical relationships among seismic velocity, effective pressure, porosity, and clay content in sandstone. Geophysics 54, 82–89. https://doi.org/10.1190/1.1442580

Elkatatny, S.M., Tariq, Z., Mahmoud, M.A., Abdulraheem Abdelwahab, Z.A., Woldeamanuel, M., Mohamed, I.M., 2017. An Artificial Intelligent Approach to Predict Static Poisson's Ratio. 51st U.S. Rock Mech. Symp.

Fjaer, E., 2008. Petroleum related rock mechanics. Elsevier.

Fjær, E., 2009. Static and dynamic moduli of a weak sandstone. Geophysics 74, WA103. https://doi.org/10.1190/1.3052113

Franses, P.H., Draisma, G., 1997. Recognizing changing seasonal patterns using artificial neural networks. J. Econom. 81, 273–280. https://doi.org/10.1016/S0304-4076(97)00047-X

Gardner, G.H.F., Gardner, L.W., Gregory, A.R., 1974. Formation velocity and density—the diagnostic basics for stratigraphic traps. Geophysics 39, 770–780. https://doi.org/10.1190/1.1440465

Gardner, M.W., Dorling, S.R., 1998. Artificial neural networks (the multilayer perceptron) - a review of applications in the atmospheric sciences. Atmos. Environ. 32, 2627–2636. https://doi.org/10.1016/S1352-2310(97)00447-0

Geertsma, J., 1985. Some Rock - Mechanical Aspects of Oil and Gas Well Completions. Soc. Pet. Eng. 848–856. https://doi.org/10.2118/8073-PA

Han, D., Nur, A., Morgan, D., 1986. Effects of porosity and clay content on wave velocities in sandstones. Geophysics 51, 2093–2107. https://doi.org/10.1190/1.1442062

Hossain, Z., Mukerji, T., Fabricius, I.L., 2012. Vp-Vs relationship and amplitude variation with offset modeling of glauconitic greensand‡. Geophys. Prospect. 60, 117–137. https://doi.org/10.1111/j.1365-2478.2011.00968.x

Hsu, K., Gupta, H.V., Sorooshian, S., 1995. Artificial Neural Network Modeling of the Rainfall-Runoff Process. Water Resour. Res. 31, 2517–2530. https://doi.org/10.1029/95WR01955

Kalgaonkar, R., Chang, F., Ballan, A.N.A., Abadi, A., Tan, X., 2017. New Advancements in Mitigating Sand Production in Unconsolidated Formations. SPE Kingdom Saudi Arab. Annu. Tech. Symp. Exhib. https://doi.org/10.2118/188043-MS

Kazatchenko, E., Markov, M., Mousatov, A., Pervago, E., 2006b. Prediction of the s-wave velocity in carbonate formation using joint inversion of conventional well logs. J. Geophys. Eng. 3, 386–399. https://doi.org/10.1088/1742-2132/3/4/010

Kazatchenko, E., Markov, M., Mousatov, A., Pervago, E., 2006a. Prediction of the s-wave velocity in carbonate formation using joint inversion of conventional well logs. J. Geophys. Eng. 3, 386–399. https://doi.org/10.1088/1742-2132/3/4/010

Ketmalee, T., Bandyopadhyay, P., 2018. Application of Neural Network in Formation Failure Model to Predict Sand Production. Offshore Technol. Conf. Asia. https://doi.org/10.4043/28506-MS

Khandelwal, M., Singh, T.N., 2010. Artificial neural networks as a valuable tool for well log interpretation. Pet. Sci. Technol. 28, 1381–1393. https://doi.org/10.1080/10916460903030482

Kohli, A., Arora, P., 2014. Application of Artificial Neural Networks for Well Logs, in: International Petroleum Technology Conference. International Petroleum Technology Conference. https://doi.org/10.2523/IPTC-17475-MS

Lawrence, S., Giles, C.L., Tsoi, A.C., 1997. Lessons in neural network training: overfitting may be harder than expected. 14th Natl. Conf. Artificial Intell. 540–545.

Lee, M., 2005. Proposed Moduli of Dry Rock and Their Application to Predicting Elastic

Velocities of Sandstones. Usgs 14.

Long, W., Chai, D., Aminzadeh, F., 2016. Pseudo Density Log Generation Using Artificial Neural Network. SPE West. Reg. Meet. https://doi.org/10.2118/180439-MS

Ma, Y.Z., Gomez, E., Luneau, B., 2017. Integration of seismic and well-log data using statistical and neural network methods. Lead. Edge 36, 324–329. https://doi.org/10.1190/tle36040324.1

Maleki, S., Moradzadeh, A., Riabi, R.G., Gholami, R., Sadeghzadeh, F., 2014. Prediction of shear wave velocity using empirical correlations and artificial intelligence methods. NRIAG J. Astron. Geophys. 3, 70–81. https://doi.org/10.1016/J.NRJAG.2014.05.001

McPhee, C.A., Webster, C., Daniels, G., Reed, C., Mulders, F.M.M., Howat, C., Britton, A., 2014. Developing an Integrated Sand Management Strategy for Kinabalu Field, Offshore Malaysia. SPE Annu. Tech. Conf. Exhib. https://doi.org/10.2118/170749-MS

Mhaskar, H.N., 1993. Approximation properties of a multilayered feedforward artificial neural network. Adv. Comput. Math. 1, 61–80. https://doi.org/10.1007/BF02070821

Mullen, M.J., Roundtree, R., Turk, G.A., 2007. A Composite Determination of Mechanical Rock Properties for Stimulation Design (What to Do When You Don't Have a Sonic Log). Rocky Mt. Oil Gas Technol. Symp. https://doi.org/10.2118/108139-MS

Najibi, A.R., Ghafoori, M., Lashkaripour, G.R., Asef, M.R., 2015. Empirical relations between strength and static and dynamic elastic properties of Asmari and Sarvak limestones, two main oil reservoirs in Iran. J. Pet. Sci. Eng. 126, 78–82. https://doi.org/10.1016/J.PETROL.2014.12.010

Nauroy, J.-F., 2011. Geomechanics applied to the petroleum industry. Editions Technip.

Nourafkan, A., Kadkhodaie-Ilkhchi, A., 2015. Shear wave velocity estimation from conventional well log data by using a hybrid ant colony-fuzzy inference system: A case study from Cheshmeh-Khosh oilfield. J. Pet. Sci. Eng. 127, 459–468. https://doi.org/10.1016/j.petrol.2015.02.001

Perera, M., Granjith, P., Rathnaweera, T., De Silva, G., Liu, T., 2017. An experimental study to quantify sand production during oil recovery from unconsolidated quicksand formations. Pet. Explor. Dev. 44, 860–865. https://doi.org/10.1016/S1876-3804(17)30097-6

Prieto, A., Prieto, B., Ortigosa, E.M., Ros, E., Pelayo, F., Ortega, J., Rojas, I., 2016. Neural networks: An overview of early research, current frameworks and new challenges. Neurocomputing 214, 242–268. https://doi.org/10.1016/J.NEUCOM.2016.06.014

Rafik, B., Kamel, B., 2017. Prediction of permeability and porosity from well log data using the nonparametric regression with multivariate analysis and neural network, Hassi R'Mel Field, Algeria. Egypt. J. Pet. 26, 763–778. https://doi.org/10.1016/J.EJPE.2016.10.013

Rajabi, M., Bohloli, B., Gholampour Ahangar, E., 2010. Intelligent approaches for prediction of compressional, shear and Stoneley wave velocities from conventional well log data: A case study from the Sarvak carbonate reservoir in the Abadan Plain (Southwestern Iran). Comput. Geosci. 36, 647–664. https://doi.org/10.1016/J.CAGEO.2009.09.008

Rajabi, M., Tingay, M., 2013. Applications of Intelligent Systems in Petroleum Geomechanics-Prediction of Geomechanical Properties in Different Types of Sedimentary Rocks, in: International EAGE Workshop on Geomechanics and Energy.

Ramcharitar, K., Hosein, R., 2016. Rock Mechanical Properties of Shallow Unconsolidated

Sandstone. SPE Trinidad Tobago Sect. Energy Resour. Conf. https://doi.org/10.2118/180803-MS

Ranjith, P.G., Perera, M.S.A., Perera, W.K.G., Choi, S.K., Yasar, E., 2014. Sand production during the extrusion of hydrocarbons from geological formations: A review. J. Pet. Sci. Eng. https://doi.org/10.1016/j.petrol.2014.10.017

Ranjith, P.G., Perera, M.S.A., Perera, W.K.G., Wu, B., Choi, S.K., 2013. Effective parameters for sand production in unconsolidated formations: An experimental study. J. Pet. Sci. Eng. 105, 34–42. https://doi.org/10.1016/j.petrol.2013.03.023

Raymer, L.L., Hunt, E.R., Gardner, J.S., 1980. An Improved Sonic Transit Time-to-Porosity Transform. SPWLA Annu. Logging Symp. 1–13.

Raymer, L.L.L., Hunt, E.R.R., Gardner, J.S., 1980. An Improved Sonic Transit Time to Porosity-to-Porosity transform. 21st SPWLA Logging Symp. Trans. 1–13.

Razavi, S., Tolson, B. a, 2011. A new formulation for feedforward neural networks. IEEE Trans. Neural Netw. 22, 1588–98. https://doi.org/10.1109/TNN.2011.2163169

Rezaee, M.R., Kadkhodaie Ilkhchi, A., Barabadi, A., 2007. Prediction of shear wave velocity from petrophysical data utilizing intelligent systems: An example from a sandstone reservoir of Carnarvon Basin, Australia. J. Pet. Sci. Eng. 55, 201–212. https://doi.org/10.1016/J.PETROL.2006.08.008

Rolon, L., Mohaghegh, S.D., Ameri, S., Gaskari, R., McDaniel, B., 2009. Using artificial neural networks to generate synthetic well logs. J. Nat. Gas Sci. Eng. 1, 118–133. https://doi.org/10.1016/J.JNGSE.2009.08.003

Ruck, D.W., Rogers, S.K., Kabrisky, M., Oxley, M.E., Suter, B.W., 1990. Letters: The Multilayer Perceptron as an Approximation to a Bayes Optimal Discriminant Function. IEEE Trans. Neural Networks 1, 296–298. https://doi.org/10.1109/72.80266

Santarelli, F.J., Detienne, J.L., Zundel, J.P., 1989. Determination of the Mechanical Properties of Deep Reservoir Sandstones to Assess the Likelihood of Sand Production. ISRM Int. Symp.

Saputro, O.D., Maulana, Z.L., Latief, F.D.E., 2016. Porosity Log Prediction Using Artificial Neural Network, in: Journal of Physics: Conference Series. IOP Publishing, p. 012092. https://doi.org/10.1088/1742-6596/739/1/012092

Schmidhuber, J., 2015. Deep learning in neural networks: An overview. Neural Networks 61, 85–117. https://doi.org/10.1016/J.NEUNET.2014.09.003

Sperduti, A., 2015. Equivalence results between feedforward and recurrent neural networks for sequences, in: IJCAI International Joint Conference on Artificial Intelligence. pp. 3827–3833.

Tariq, Z., Elkatatny, S., Mahmoud, M., Abdulraheem, A., 2016. A New Artificial Intelligence Based Empirical Correlation to Predict Sonic Travel Time. Int. Pet. Technol. Conf. https://doi.org/10.2523/IPTC-19005-MS

Tariq, Z., Elkatatny, S.M., Mahmoud, M.A., Abdulraheem, A., Abdelwahab, A.Z., Woldeamanuel, M., 2017. Estimation of Rock Mechanical Parameters Using Artificial Intelligence Tools. 51st U.S. Rock Mech. Symp.

Tixier, M.P., Loveless, G.W., Anderson, R.A., 1975. Estimation of Formation Strength From the Mechanical-Properties Log. SPE J. Pet. Technol. 27, 283–293. https://doi.org/10.2118/4532-pa

Ukaonu, C., Odubanjo, T., Lawal, K.A., Eyitayo, S.I., Ovuru, M.I., Anyadike, E., Matemilola, S., 2017. Use of Petro-Elastic Analysis to Evaluate Potential for Sand Production in Petroleum Reservoirs, in: Nigeria Annual International Conference and Exhibition. https://doi.org/10.2118/189177-MS

Veeken, C.A.M., Davies, D.R., Kenter, C.J., Kooijman, A.P., 1991. Sand Production Prediction Review: Developing an Integrated Approach. SPE Annu. Tech. Conf. Exhib. https://doi.org/10.2118/22792-MS

Verma, A., Cheadle, B., … A.R., 2012. Porosity and permeability estimation using neural network approach from well log data, in: SPE Annual Technical Conference and Exhibition. pp. 1–6.

White, B.W., Rosenblatt, F., 1963. Principles of Neurodynamics: Perceptrons and the Theory of Brain Mechanisms. Am. J. Psychol. 76, 705. https://doi.org/10.2307/1419730

Wu, B., Mohamed, N., Tan, C.P., Sukahar, M.W., Hong, T.Y., Viswanathan, C., Hon, V., 2006. An Integrated Wellbore Stability and Sand Production Prediction Study for a Multi-Field Gas Development. SPE Asia Pacific Oil Gas Conf. Exhib. https://doi.org/10.2118/101087-MS

Wyllie, M.R.J., Gregory, A.R., Gardner, L.W., 1956. Elastic wave velocities in heterogeneous and porous media. Geophysics 21, 41–70. https://doi.org/10.1190/1.1438217

Zeynali, M.E., 2012. Mechanical and physico-chemical aspects of wellbore stability during drilling operations. J. Pet. Sci. Eng. 82–83, 120–124. https://doi.org/10.1016/J.PETROL.2012.01.006

Zoveidavianpoor, M., 2014. A comparative study of artificial neural network and adaptive neuro-fuzzy inference system for prediction of compressional wave velocity. Neural Comput. Appl.

25, 1169–1176. https://doi.org/10.1007/s00521-014-1604-2

Zoveidavianpoor, M., Samsuri, A., Shadizadeh, S.R., 2013. Prediction of compressional wave velocity by an artificial neural network using some conventional well logs in a carbonate reservoir. J. Geophys. Eng. 10, 045014. https://doi.org/10.1088/1742-2132/10/4/045014

Appendix 5A

Table 5A 1. 100 feet of the Actual well log data

Depth (ft)	DTCO (µsec /ft)	DTSM (µsec /ft)	GR (gAPI)	PHIE (m3/m3)	PHIT (m3/m3)	RESD (ohm.m)	RHOB (g/cm3)	Vsh
7105.5	88.00	153.67	64.37	0.17	0.20	16.16	2.33	0.23
7106	88.02	152.38	76.51	0.16	0.19	10.32	2.34	0.23
7109	91.04	149.02	42.23	0.18	0.20	44.99	2.25	0.17
7114	88.03	147.53	50.99	0.14	0.18	77.66	2.34	0.22
7117.5	85.88	145.78	45.08	0.16	0.18	43.15	2.35	0.19
7118	85.81	146.32	42.53	0.16	0.18	38.45	2.36	0.17
7118.5	86.00	146.54	47.95	0.15	0.18	32.54	2.35	0.18
7119	86.28	146.56	53.50	0.16	0.18	30.01	2.35	0.18
7123	87.05	149.10	61.06	0.17	0.18	26.11	2.32	0.05
7123.5	88.93	147.39	41.34	0.17	0.18	25.01	2.29	0.05
7124	89.98	146.47	41.79	0.18	0.19	28.79	2.27	0.06
7124.5	92.44	146.55	40.36	0.18	0.19	27.95	2.26	0.07
7125	93.21	147.25	38.47	0.18	0.19	37.42	2.24	0.10
7128	90.75	150.21	52.98	0.15	0.18	23.49	2.35	0.24
7129	87.33	148.71	46.24	0.14	0.17	20.12	2.33	0.20
7129.5	87.69	147.15	36.27	0.15	0.17	41.30	2.30	0.16
7130	87.98	146.06	38.50	0.16	0.18	49.40	2.28	0.17
7169.5	87.98	152.68	101.59	0.18	0.21	5.06	2.30	0.24
7170	87.29	152.64	68.93	0.17	0.20	6.14	2.31	0.20
7170.5	86.88	150.06	63.38	0.18	0.20	9.91	2.32	0.16
7171	85.66	147.95	60.89	0.18	0.20	9.60	2.33	0.15
7171.5	84.76	148.87	57.77	0.17	0.19	8.53	2.32	0.14
7172.5	84.02	149.44	54.37	0.18	0.20	9.30	2.32	0.14

7174	82.74	146.39	47.10	0.19	0.21	14.60	2.29	0.15
7174.5	83.07	144.42	49.75	0.20	0.22	14.42	2.27	0.14
7183.5	82.72	138.27	35.57	0.17	0.19	7.46	2.30	0.16
7184	81.67	135.44	34.51	0.17	0.20	6.90	2.30	0.21
7184.5	80.45	134.74	36.59	0.16	0.19	3.77	2.33	0.26
7185	80.31	134.00	38.00	0.14	0.18	3.07	2.36	0.26
7186.5	76.76	132.61	41.48	0.14	0.17	2.83	2.38	0.22
7187	76.39	132.16	37.75	0.15	0.18	1.77	2.37	0.19
7187.5	76.36	131.70	34.48	0.16	0.18	1.61	2.36	0.18
7196	78.87	133.43	50.05	0.12	0.15	3.01	2.41	0.23
7196.5	80.23	132.51	52.98	0.12	0.15	2.91	2.41	0.24
7197	80.31	134.23	43.74	0.13	0.16	2.85	2.38	0.24
7197.5	78.82	135.85	44.86	0.14	0.17	2.91	2.36	0.21
7198	77.03	135.97	49.16	0.15	0.17	2.88	2.36	0.18
7199	74.78	134.92	51.35	0.13	0.15	2.93	2.40	0.13
7199.5	74.77	135.20	47.85	0.13	0.15	3.37	2.40	0.14
7200	75.92	134.16	49.01	0.12	0.15	3.62	2.41	0.17

Disclaimer

The well log data presented in this study is solely for educational purposes. To ensure the confidentiality and prevent any proprietary issue, the source of the data has been withheld. The authors take no liability for linking this data to any source, group, persons or organizations.

Chapter 6 Data Driven Model for Shear wave Transit Time Prediction

Preface

A version of this chapter has been submitted to the Journal of Petroleum Exploration and Production Technology. I am the primary author. Co-author. Dr. Sunday Adeshina helped in formulating the concept of the paper, and review of the first draft. Co-author Dr. Faisal Khan availed us with support in implementing the concept and testing the model to make the work publishable. Co-author Dr. Lesley James provided technical assistance, proper formatting and representation of the well log data, expert analysis and review. She provided financial support to carry out the research. Co-author Dr. Stephen Butt provided technical assistance, review and financial support during the research, as well as analyzing the well log format used in the paper. I and Dr. Sunday Adedigba carried out most of the data collection and analysis. The first draft of the manuscript was prepared by me, and I subsequently revised the manuscript, based on the feedback from the co-authors and also a peer review process. The co-authors assisted in the development of the concept and testing the model, reviewed and corrected the model and results. They also contributed to the review and revision of the manuscript.

Abstract

Shear wave velocity in conjunction with compressional wave velocity provides a cost-effective and efficient non-destructive tool for estimating the mechanical rock properties of reservoir formations. In the exploration and production of oil and gas reservoirs, shear wave velocity is obtained from sonic well logging of the formation transit time. The shear wave velocities are used to provide continuous evaluation of the reservoir formation. However, shear sonic logs are not acquired in all oil and gas exploration wells. More so, many offset wells are not run with the most recent sonic logging tools capable of measuring both shear and compressional sonic transit times due to the relatively high costs of running such equipment. Such offset wells lack shear wave velocity measurements

In this study, an exponential Gaussian process regression model is presented. The model accurately predicts the shear wave transit times in the formations which lack reliable shear wave transit time measurements. The proposed model is developed from five predictors namely: depth, density, porosity, gamma-ray and compressional transit time. The shear sonic transit time predictions are used to calculate the dynamic Young's Modulus and Poisson's Ratio of a reservoir formation. A sensitivity analysis is conducted to compare the results of the measured and predicted Young's Modulus and Poisson's Ratio of the formation. The proposed model provides a reliable and cost-effective tool for the oil and gas formation evaluation.

Keywords: Gaussian process, exploration, sonic log, well logging, velocity, reservoir formation

6.1 Introduction

Sonic well logs have been around since the 1900's in the petroleum industry (Alford et al., 2012; Doh and Alger, 1958). Over the years, geologists, petrophysicist, and petroleum engineers have come to see the reliability and usefulness of sonic well logs in the exploration and production of hydrocarbon reservoirs. Onalo et al. (2018a) use an artificial neural network to predict the compressional and shear wave sonic logs along a wellbore from a producing well. Drilling engineers use sonic data to improve drilling efficiency and reduce target offset margins (Alford et al., 2012). The transmission of the sonic wave through the formation, "sonic well logging", provides valuable data such as compressional transit time and shear transit time that is used in formation evaluation (Minear and Fletcher, 1983). Sonic logging was the first tool that provided the industry with a means to estimate formation porosity without knowledge of the fluid saturation (Raymer et al., 1980). As far back as 1958, researchers like Doh and Alger (1958) perceived formation porosity estimation to be the major advantage of sonic logs. The transit arrival times of the sonic waves have evolved and now being used for formation porosity determination, lithology identification, fluid saturation indication, formation strength characterization, hydrocarbon indication, and much more (Khazanehdari and Mccann, 2005; Williams, 1990). This is due to the fact that the sonic transit interval times are affected by reservoir properties that include compaction, porosity, anisotropy density, lithology, cementation, consolidation, overburden stress and pore pressure (Khazanehdari and Mccann, 2005; Krief et al., 1990; Thomsen, 1986; Toksöz et al., 1976; Williams, 1990). A good understanding of how these properties change over the life of the reservoir is essential for proper reservoir planning, development and management (Khazanehdari and Mccann, 2005).

Well-calibrated and reliable sonic logging tools are necessary to acquire accurate measurements of the compressional and shear wave transit time, otherwise, the formation evaluations and estimation become false and misleading (Onalo et al., 2018a). This may result in the development of non-potential reservoirs and the abandonment of potential reservoir formations. Sonic logging tools have also evolved over the years. From single transmitters and receivers to two-receivers to compensate for discrepancies from the transmission source due to the borehole and mud. This known as the borehole effect. (Doh and Alger, 1958). The spacing between the receivers is usually about one feet to ensure proper description of the transit formation medium. To correct the errors generated as a result of the irregularities of the borehole, borehole compensated sonic tools were developed (Kokesh et al., 1965). To further improve the quality of the sonic measurements, array sonic logging tools were adopted that contains an array of transmitters and receivers (Hsu et al., 1987). The above mentioned sonic logging tools are mainly monopole sonic logging as they do not provide measurements of the shear wave especially in fast formations (Alford et al., 2012; Harrison et al., 1990). Fast formations are formations in which the shear wave response of the formation arrives at the receivers before the compressional wave response of the wellbore fluid. In situations where the compressional wave response of the borehole fluid arrives before the shear wave response of the formation, the formation is known as a slow formation. More modern sonic logging tools include dipole sonic and multipole sonic logging tools which are capable of measuring both compressional and shear wave properties directly or indirectly by generating flexural waves (Alford et al., 2012; Market and Canady, 2006).

Shear wave transit time is vital for many geophysical and engineering analysis including, seismic interpretations and bright spot analysis (Greenberg and Castagna, 1992a; Onalo et al., 2018b). The lack of shear wave transit time data limits the amount of valuable relationships and correlations

that can be derived from sonic logging especially for lithology identification, fluid saturation identification and porosity estimation (Domenico, 1984; Onalo et al., 2018a). Shear wave transit time alone is not sufficient to provide a full description of the diversity across the reservoir formation (Greenberg and Castagna, 1992a).

Empirical relationships have been developed to estimate the shear wave velocity from compressional wave velocity in situations where the shear wave data were missing (Bailey, 2012; Castagna et al., 1985; Domenico, 1984; Eberhart‐Phillips et al., 1989; Gardner et al., 1974; Greenberg and Castagna, 1992b; Hamada, 2004; Han et al., 1986; Jorstad et al., 1999; Krief et al., 1990; Lee, 2006; Miller and Stewart, 1990, 1974; Oloruntobi et al., 2018; Ramcharitar and Hosein, 2016; Raymer et al., 1980; Takahashi et al., 2000; Vernik et al., 2002). Though these estimations provide simple correlation for quick estimations, they are not as robust as modern day machine learning techniques that have been applied in several engineering applications (Kumar et al., 2014; Nourafkan and Kadkhodaie-Ilkhchi, 2015; Ramcharitar and Hosein, 2016; Reichel et al., 2012).

Gaussian process (GP) is a powerful technique for predicting and modeling complex mathematical and engineering data-driven problems. GP involves defining a finite vector space function of infinite dimension over a Gaussian distribution. GP has been used in many engineering applications due to its flexibility to model non-linear complex patterns between dataset variables (MacKay, 2005). GP has been adopted in solving many engineering and real-life problems because of their ability to handle data in various forms and sizes (Ebden, 2008). GP regression has been used to predict Young's modulus of jointed formations from the formation joint roughness parameter, inclination, frequency and elastic modulus (Kumar et al., 2014). Deformations around the reservoir formations are non-linear (Yin et al., 2009). GP-based models have been used to predict non-linear time deformations around mining tunnels and caves from prior of past formation

deformation history as training sample data (Su, 2009). More recently, the rock strength of intact formations has been predicted from the in-situ stresses acting on the formation (Huang et al., 2017).

GP has been used to stabilize multivariate geological data to optimize the computational efficiency in the geostatistical analysis (Silva and Deutsch, 2016). GP has been used to model regions with potential ore deposits in geostatistical modeling by locating regions with high probabilistic errors (Adeli et al., 2017). A GP that was used to develop 3D models of heterogeneities in reservoir formations with the aim of better portraying the permeability and potential production index (Dubrule and Damsleth, 2001).

In reservoir modeling, GP has been used to classify the uncertainties associated with the reservoir formation properties (Iglesias et al., 2013). A Gaussian continuum process model has been developed to model the reservoir stimulation by induced seismicity to improve reservoir permeability (Izadi and Elsworth, 2014). History matching is an essential aspect of reservoir modeling which involves a lot of trial and error (Abdollahzadeh et al., 2012). Abdollahzadeh et al. (2012) used a set of Gaussian-based process algorithm estimations to provide optimized solutions to continuous history matching for numerical reservoir models.

Gaussian-based process has been used in the hydrocarbon indication to distinguish between hydrocarbon bearing formations and water-bearing formations (Williams, 1990). Reservoir fluids have been characterized using GP models (Rostami et al., 2013). The total organic carbon (TOC) of shale gas reservoirs have been estimated using GP regression for reservoir characterization (Yu et al., 2016). Rostami and Khaksar Manshad (2013) developed a GP regression to determine the amount of asphaltene precipitation from crude oil using the properties of the crude oil like hydrocarbon composition, temperature, pressure, specific gravity and solvent molecular weight

establishing which crude oil properties played a higher role in determining the likelihood of asphaltene precipitation.

Considering the success that Gaussian-based processes have had in several petroleum engineering applications, the objective of the paper is to develop a reliable model that predicts shear wave sonic logs using a Gaussian-based process from available well log data. The importance of such a model to the industry is invaluable for offset wells that have been drilled and logged without dipole or multipole sonic logging tools and therefore do not have the corresponding shear wave sonic logs. Also, in formations where the inaccurate log data have been obtained due to damaged equipment or calibration (human) error. Sonic logs are essentials components for drilling, exploration and reservoir management. The shear wave sonic logs provide a means of accurate continuous predictions of the reservoir properties for better reservoir planning and management.

This paper comprises of seven sections. A brief introduction to GP is introduced in section 6.2. In section 6.3, the methodology for the model development is presented. The model is applied to a case study in section 6.4. The results are presented in section 6.5. A sensitivity analysis is also conducted in section 6.6. In section6.7, the conclusions from the study are highlighted.

6.2 Gaussian Process (GP)

Modeling complex engineering problems present a real challenge in the petroleum industry. The GP is a probabilistic modeling technique that is nonparametric, meaning that, the prior is placed in space and the actual distribution that fits the data is not known before the initialization (Huang et al., 2017; Kuss and Rasmussen, 2006). GP has been recognized as a promising data mining technique in machine learning due to its ability to handle large amounts of data (Han and Kamber, 2010). GP is generally classified into supervised and unsupervised. Simply put, supervised GP involves establishing functions of input datasets used for the training to predict the corresponding output dataset (Rostami et al., 2013). In unsupervised, there is no prediction as there are no target output dataset or prior history to establish functions from. Nonetheless, this is a very useful functionality for classifying large datasets. When the GP is used for prediction, it is referred to as a GP regression. On the other hand, if the GP is used for classification, it is referred to as GP classification (Rostami et al., 2013). GP captures set finite random variables attempting to represent them by a joint Gaussian distribution; this process is known as the GP regression (Rasmussen, 2004). GP is defined fully by their mean and covariance functions (Seeger, 2004). Gaussian process-based models are highly capable of establishing non-linear relationships from non-parametric data and deriving algorithms for future predictions (Abdollahzadeh et al., 2012).GP is highly universal and can be adapted to various problems presented; however, the care must be taken to select the best covariance, kernel and hyperparameters describing the multi-dimensional distribution (Kuss and Rasmussen, 2006).

6.2.1 **Gaussian process theory**

A description of the GP is presented below; however, a more detailed explanation can be found in Rasmussen (2004) and Williams and Rasmussen (2006).

Assume a set of data is provided in the following format (Kumar et al., 2014):

$$D = \{x_i, y_i\}_{i=1}^{n}, \qquad x_i \in R^d and\ y_i \in R \tag{6.1}$$

x_i = input data, y_i= output data, n = number of data points, R = 1-dimensional vector space, R^d= d-dimensional vector space. In this study, the input data are depth (ft), RHOB (g/cc), PHIT, GR (GAPI) and DTCO (µs/ft). The output is DTSM (µs/ft). Mathematically: x = [depth, RHOB, PHIT, GR and DTCO] and y = [DSTM].

The GP can be defined by the mean (m(x)) and the covariance function (k(x, x$'$)) for the function (f(x)) (Rostami and Khaksar Manshad, 2013).

$$\mathrm{m(x)} = \mathrm{E[f(x)]} \tag{6.2}$$

$$\mathrm{k(x, x')} = \mathrm{E[(f(x)] - m(x))(f(x') - m(x'))}, \qquad x\ and\ x' \in R^d \tag{6.3}$$

Thus, the GP is written as follows (Rostami et al., 2013)

$$\mathrm{f(x)} = \mathrm{GP(m(x), k(x, x'))} \tag{6.4}$$

The GP regression is then expressed similarly to a linear regression with the main function and Gaussian noise (ε) function as follows (Yu et al., 2016):

$$\mathrm{y} = \mathrm{f(x)} + \varepsilon \tag{6.5}$$

The Gaussian noise has a mean of 0 and a variance of σ.

$$\varepsilon \sim N(0, \sigma) \tag{6.6}$$

For a new input data set (x^*) and output data set (y^*), the GP prior distribution is given as follows (Kumar et al., 2014):

$$\begin{pmatrix} y \\ y^* \end{pmatrix} \sim N(0, k^*) \tag{6.7}$$

$$k^* = \begin{bmatrix} k & k(x, x^*) \\ k(x, x^*)^T & k(x^*, x^*) \end{bmatrix} \tag{6.8}$$

$k(x, x^*)$ = the covariance between the training inputs data and test input data; $k(x, x^*)^T$ = the transpose of $k(x, x^*)$; $k(x^*, x^*)$ = the covariance of the test data.

Thus, the mean and variance of the posterior Gaussian distribution of (y^*) can be written as follows respectively (Yu et al., 2016):

$$m^* = k(x, x^*)^T k^{-1} y \tag{6.9}$$

$$\sigma^* = k(x^*, x^*) - k(x, x^*)^T \, k^{-1} y \, k(x, x^*) \tag{6.10}$$

6.2.2 **Covariance and kernel Function**

The covariance function can be defined by the kernel functions in order to provide better response across the dataset to which they are similar (Ebden, 2008). A set of kernel functions or hyperparameters ($\theta = \{\sigma_f, \sigma_l\}$) parameterizes the covariance function. The kernel functions are needed to reduce the error and improve the accuracy by smoothening the data set predictions. The dependency of the covariance function is written as $k(x, x'|\theta)$. Most problems can be presented as GP distribution; however, the accuracy and efficiency are improved by the kernel and hyperparameter functions. Therefore, to ensure an adequate model is attributed to a problem, the

most suitable kernel function that describes the non-linear relationship should be chosen. Although, Ebden (2008) suggests that squared exponential kernel is the popular choice, in this study the following set of kernel functions are explored to provide a justification for the model selection (Matlab Documentation, 2018).

6.2.2.1 Exponential kernel:

$$k(x_i, x_j|\theta) = {\sigma^2}_f \exp[-\frac{(x_i - x_j)^T(x_i - x_j)}{\sigma_l}] \tag{6.11}$$

σ_f = the standard deviation, σ_l = the characteristic length and a = positive scale mixture parameter

6.2.2.2 Squared exponential kernel:

$$k(x_i, x_j|\theta) = {\sigma^2}_f \exp[-\frac{1}{2}(\frac{(x_i - x_j)^T(x_i - x_j)}{{\sigma^2}_l})] \tag{6.12}$$

6.2.2.3 Matern 5/2 kernel:

$$\begin{aligned} k(x_i, x_j|\theta) = {\sigma^2}_f (1 + \frac{\sqrt{5}(x_i - x_j)^T(x_i - x_j)}{\sigma_l} \\ + \left(\frac{\sqrt{5}(x_i - x_j)^T(x_i - x_j)}{\sqrt{3}\sigma_l}\right)^2) \exp[-(\frac{\sqrt{5}(x_i - x_j)^T(x_i - x_j)}{\sigma_l})] \end{aligned} \tag{6.13}$$

6.2.2.4 Rational quadratic kernel:

$$k(x_i, x_j|\theta) = {\sigma^2}_f [1 + \left(\frac{(x_i - x_j)^T(x_i - x_j)}{2a{\sigma^2}_l}\right)^{-a}] \tag{6.14}$$

The process of finding the most suitable values of the hyperparameters is the GP regression learning that illustrates how the GPR trains the model to define the problem with the least errors (Huang et al., 2017).

6.3 Model Development Methodology

The framework of the proposed model development and testing is presented in Figure 6.1.

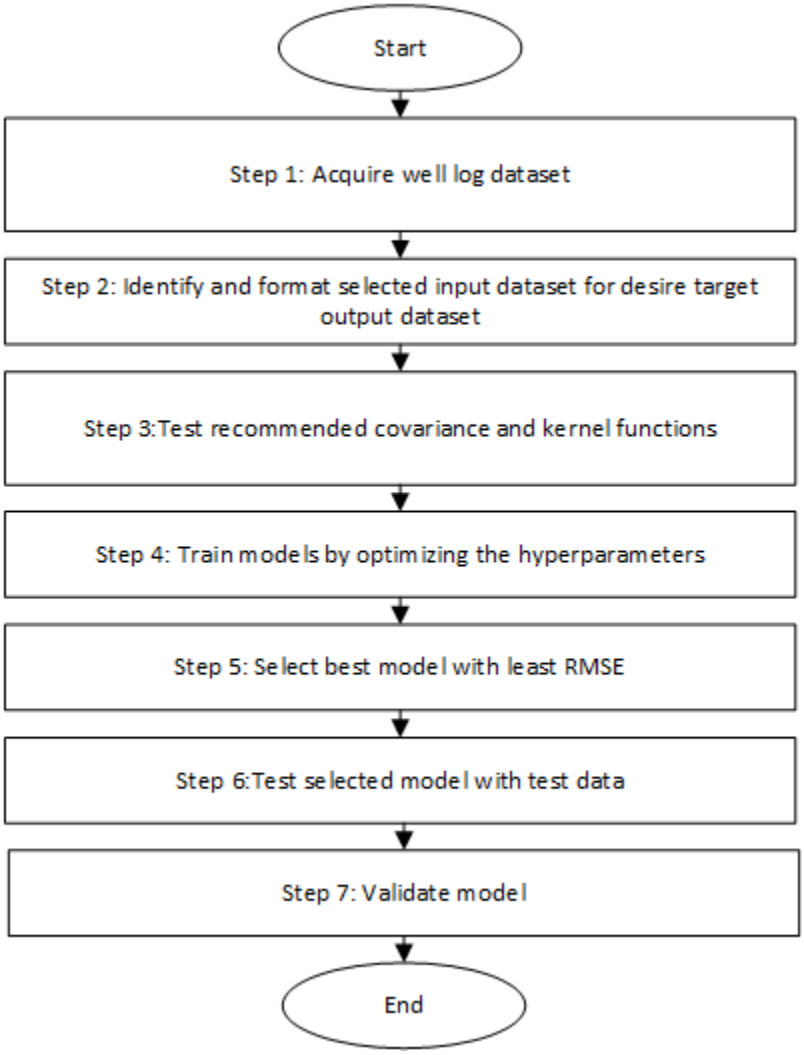

Figure 6.1. Framework for the proposed model development

6.3.1 Data collection and preparation

The data required for the proposed methodology are actual well logs. The data should contain the relevant logs required for the proposed model namely: depth (ft), RHOB (g/cc), PHIT, GR (GAPI), DTCO (µs/ft) as input predictors and DTSM (µs/ft) as the target response.

6.3.2 **Quality assurance and quality checks (QAQC)**

Quality assurance and quality control (QAQC) were performed on the suite of well logs to ensure the reliability of the data. Firstly, the logs are analyzed to identify null readings where the logging tools failed to accurately record the corresponding measurements. Secondly, the sections were washout and key-seat sections were observed were removed for the model development by referencing with the caliper logs for adjacent formation sections. Poisson's Ratio calculations where used to ensure only valid sections were represented in the dataset.

6.3.3 **Gaussian process model development**

For the model development, well log data from 2850 ft to 6000 ft and from 8000 ft to 12500 ft of a sandstone reservoir is used to build and train the model. To test the model, the section from 6000 ft to 8000 ft is used to test the model. The prepared data is formatted to match the initial model set up with five predictors and one response. The actual target response is presented in Figure 6.2.

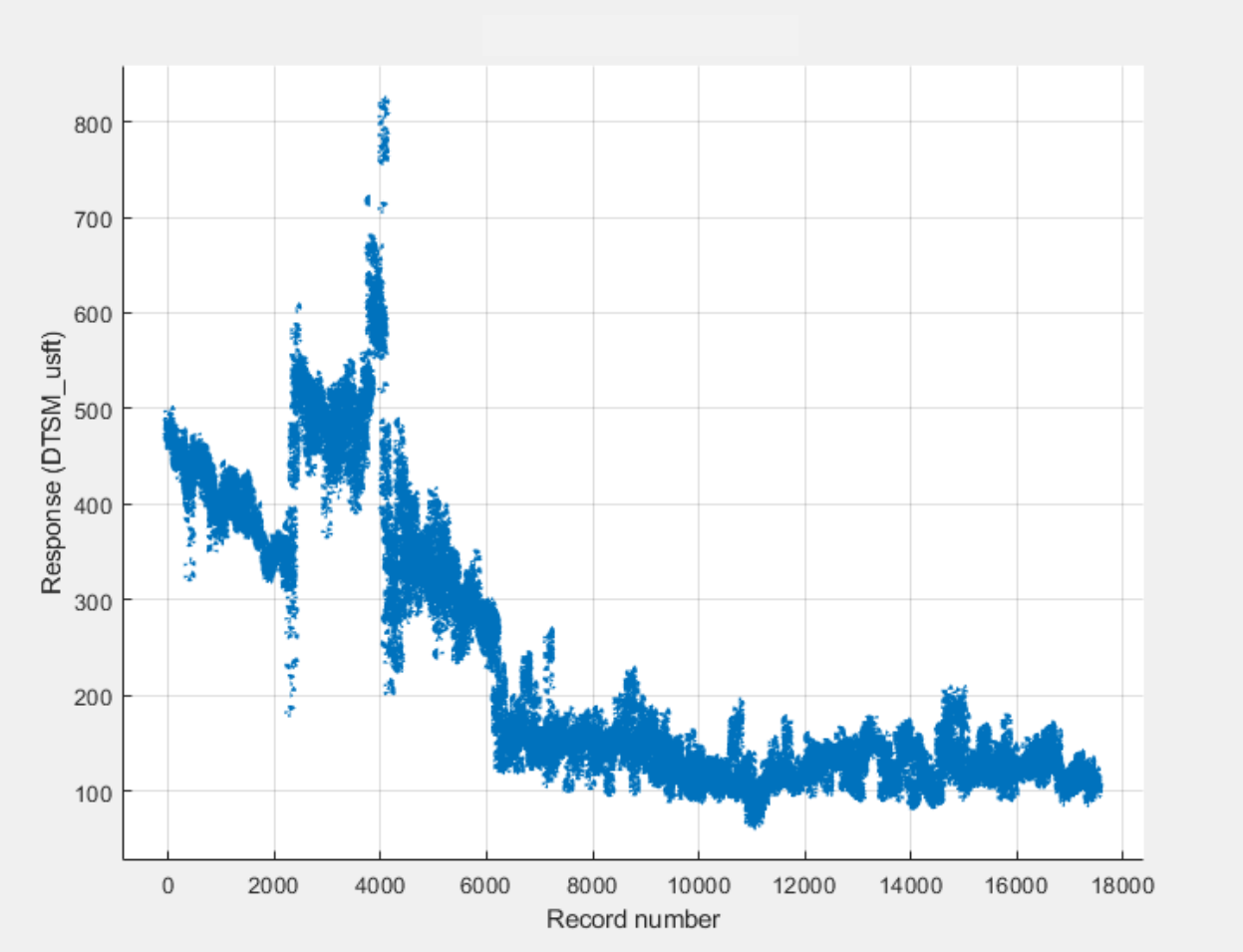

Figure 6.2. Actual target response

The GP distribution is applied to the dataset; however, the kernel function that best represents the distribution function is not known. Therefore, a set of kernel functions were applied to the data set to ascertain which kernel function was able to best smoothen the dataset and provide the least errors. The squared exponential kernel, exponential kernel, Matern 5/2 kernel and rational quadratic kernel were applied to the dataset. Each GP model and kernel function were trained by constantly updating the hyperparameters until the best match describing the well log correlation was reached by the respective models.

6.3.4 **Gaussian process selection**

The test results of each model are presented in Table 6.1. In Figure 6.3, the prediction response of each model is presented. All models performed well and were able to represent the data with a relatively high degree of accuracy; however, the exponential GP regression model seemed to better follow the actual plotted response (see Figure 6.2) more closely. The predicted responses of the models are plotted against the actual responses in a cross plot in Figure 6.4 to validate the model prediction accuracy. All the tested models alluded have coefficients of determination (R^2) of 0.99. This proved that GP regressions were highly capable of predicting the responses and would thus provide relatively sufficient models. Nonetheless, the coefficient of determination could not be used as a basis for the selection of the optimum GP regression model. Therefore, the errors of the models were plotted in Figure 6.5 and the exponential GP regression model presented the least error through the dataset.

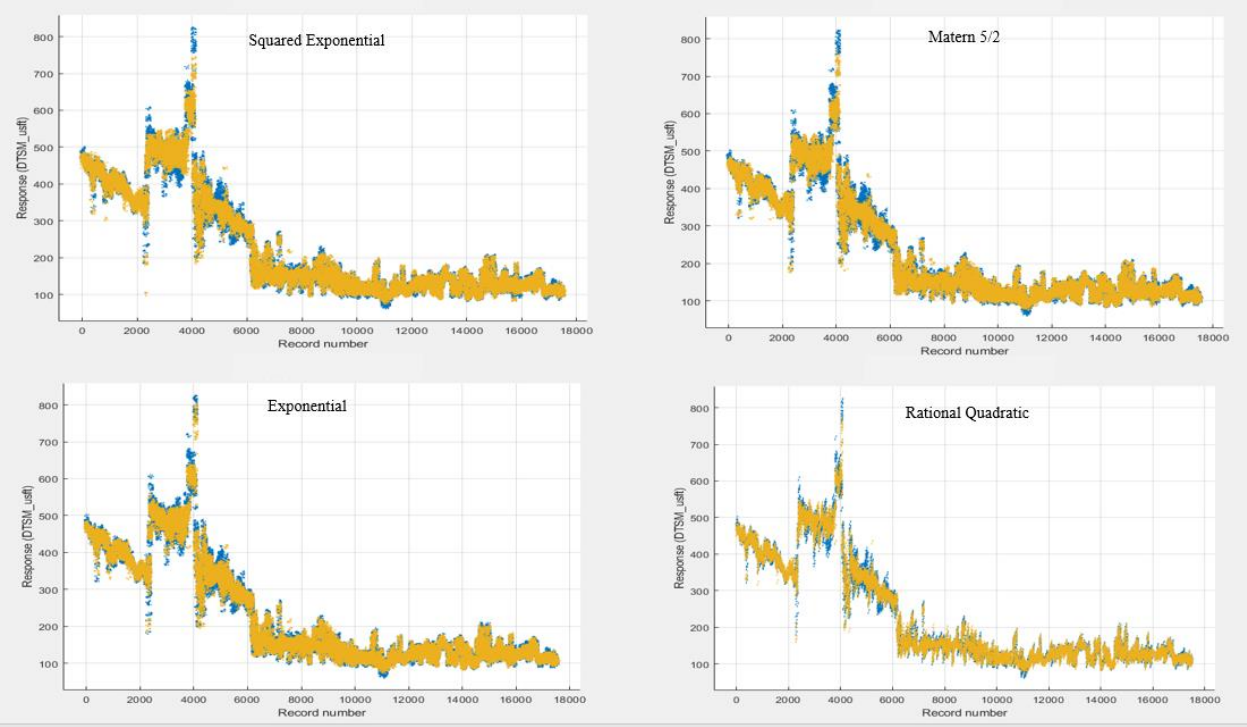

Figure 6.3. The response of the tested GP model

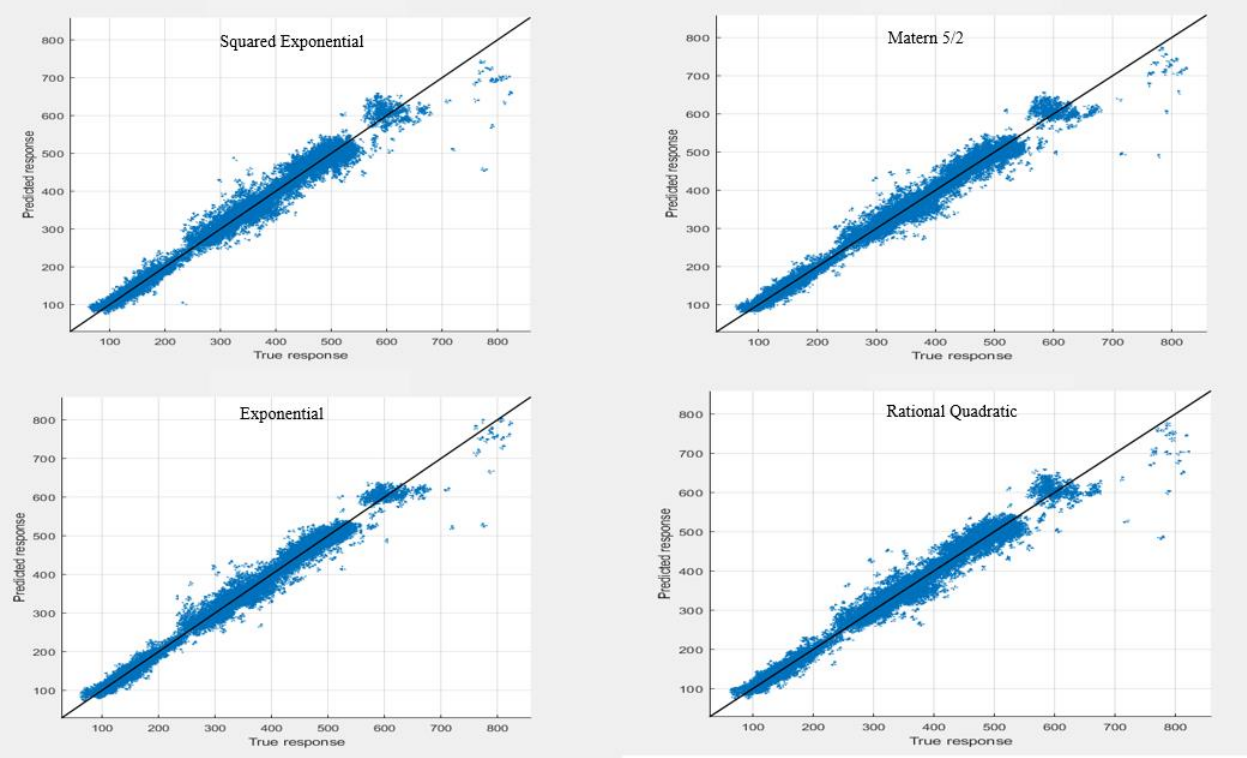

Figure 6.4 Cross-plot of the tested GP models

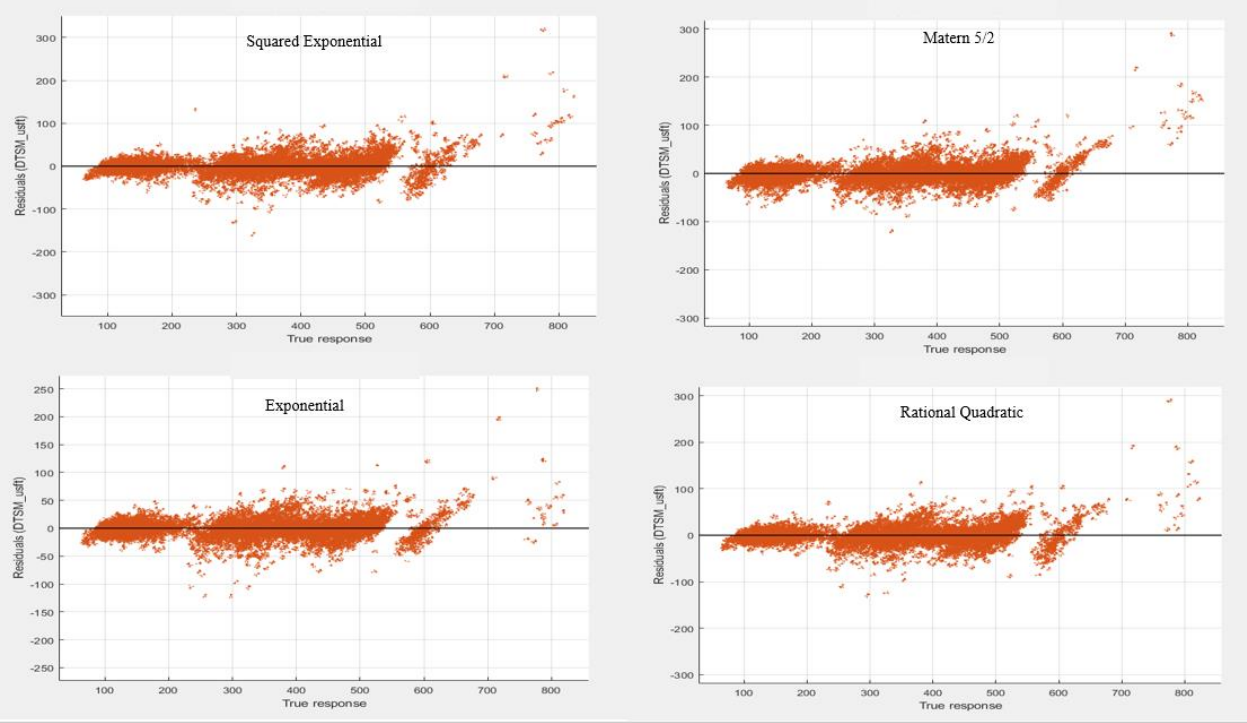

Figure 6.5. Errors of the tested GP models

The exponential GP model had the least root mean square (RMSE) with a value of 11.147. This was followed by the Matern 5/2 GP model with an RMSE = 12.718, then the rational quadratic Gaussian model with an RMSE = 12.786. The squared exponential Gaussian model, though popular, presented the highest error with an RMSE = 13.774. The mean square error (MSE) and mean average error (MAE) follow the same trend with the root mean square error. A summary of the results of the tested models is presented in Table 6.1. The exponential Gaussian regression model was selected as the best of the four models tested. In Table 6.2, the properties of the features of the selected model are presented,

Table 6.1. Summary of the results of the GP regression model selection

Model type	RMSE	R-squared	MSE	MAE
Exponential GPR	11.147	0.99	124.26	6.6046
Squared Exponential GPR	13.774	0.99	189.71	8.0162
Matern 5/2 GPR	12.718	0.99	161.74	7.4618
Rational Quadratic GPR	12.786	0.99	163.48	7.5401

Table 6.2. Main features of the proposed GP regression model

Parameter	Feature
Model type	Exponential
Basis function	constant
Use isotropic kernel	automatic
Kernel scale	automatic
Sigma	automatic
Standardize	true
Optimize numeric parameters	true

Observations	17526
Predictors	5
Response	1

6.3.5 **Generalization of the GP**

GP machine learning is adaptive in nature and can be generalized for datasets in a similar format as the original training data. To validate and ensure that the proposed model is generalized, it is applied to the section of the well log data that was omitted in the development of the model in section 6.4.

6.4 **Application of the developed Model**

The proposed shear wave transit time model is validated by applying the proposed model to actual well logs. The well log data presented in this study is a 2000 feet section, from 6000 feet to 8000 feet of an actual oil and gas sandstone reservoir This is an improvement to most studies conducted on a section of only several hundred feet. The location and details of the well log data have been withheld in this study due to protect the privacy and confidentiality of the logging company. Nevertheless, the first 100 feet of the data is presented in the Appendices in Table 6.3 for interested users. A plot of the well log data available for the study is presented in Figure 6.6.

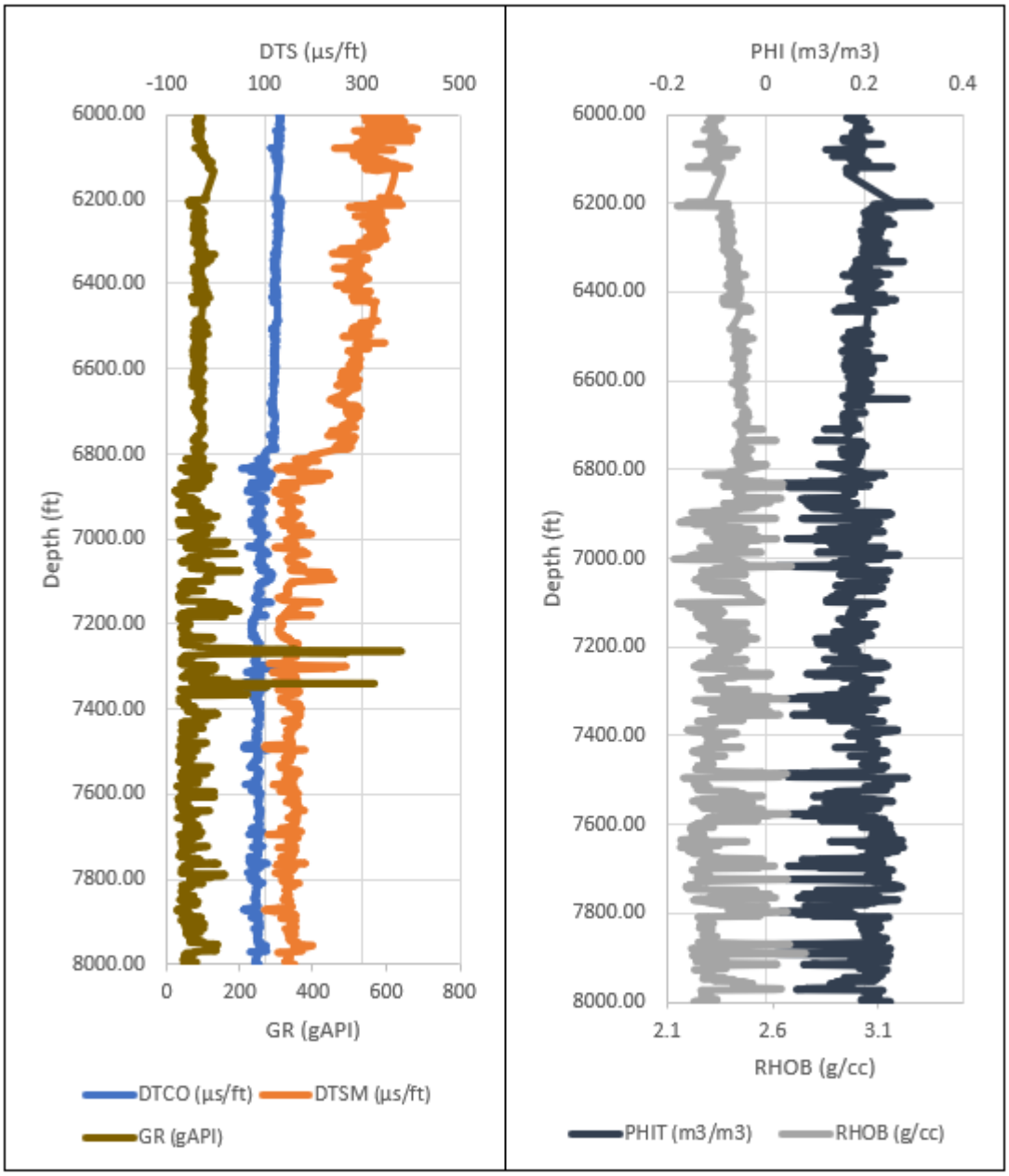

Figure 6.6. Available well log data

6.5 Results and discussion

6.5.1 Shear Sonic transit time log estimation

The primary objective of developing a Gaussian-based process regression model from well log data is to provide a tool adequate enough to furnish reliable shear sonic transit time logs in wells from offset wells run with monopole sonic logging tools. More so, in wells with corrupted datasets or erroneous readings from faulty equipment. In Figure 6.7, the measured shear sonic transit log is plotted against the depth profile of the wells used for the case study from 6000 feet to 8000 feet. This is followed by a plot of the shear sonic transit log along the same depth in Figure 6.7. The predicted shear sonic log closely matches the measured shear sonic log values. The most disparity is seen from 6010 feet to 6050 feet with less than a 5% difference in value. What is very intriguing is that the proposed model is relatively conservative in the sense that it tries to follow the measured shear sonic log trend, without going out of the measured shear sonic log boundaries in the well. This ensures that analysis conducted using the models are reliable and safe as they do not venture away from or to the extreme boundary scenarios of the formation. To further depict the success of the model in predicting the shear sonic transit log from the well logs proposed in the previous section, a cross-validation plot of the predicted shear sonic transit time versus the measured shear sonic transit time log is presented in Figure 6.8. The proposed model does a good job of almost matching the measured shear sonic logs with a coefficient of determination of 0.9923. The trend line in Figure 6.8 also falls on the perfect unity slope line the figure thereby portraying a non-bias in the predictions of the proposed model. The results show that the proposed model achieves the desired objective of the proposed model by accurately predicting shear sonic transit log of the well.

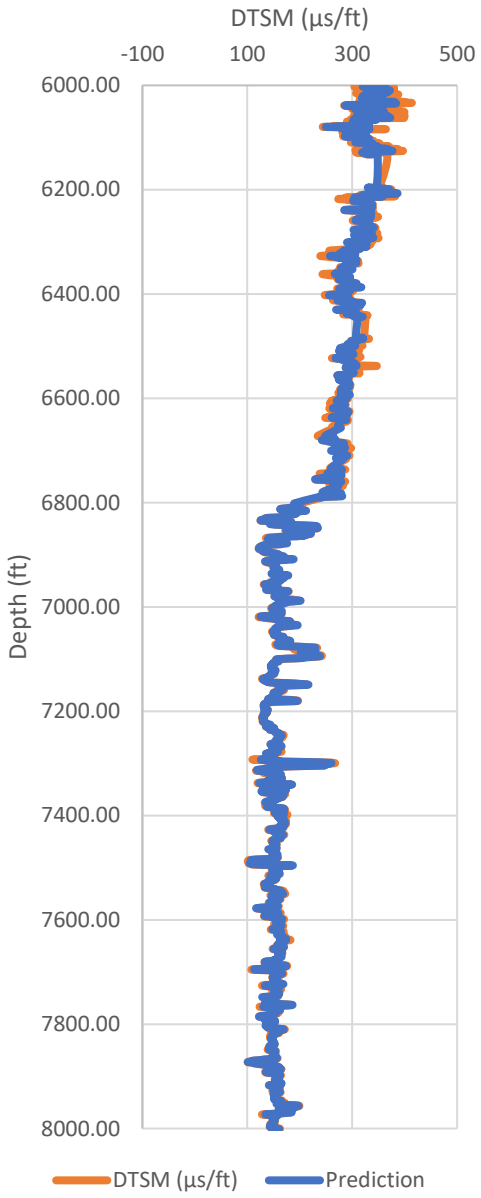

Figure 6.7. Shear wave transit time versus depth

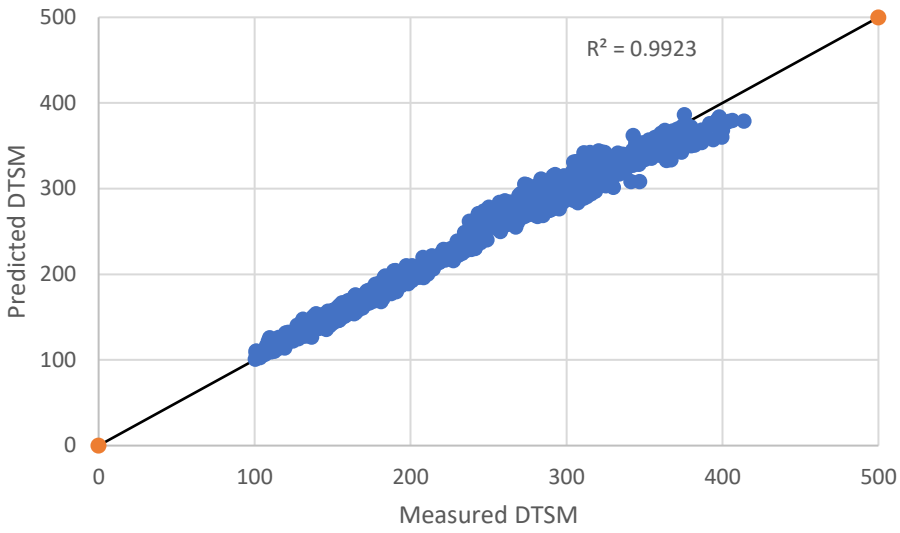

Figure 6.8. Predicted shear wave transit time versus measured shear wave transit time

6.6 Predicting Dynamic Geomechanical properties

In this section illustrate the common uses of sonic logs in the evaluation of formation mechanical properties. To illustrate these uses, the dynamic Young's Modulus and Poisson's Ratio are estimated from the measured sonic logs and compared the dynamic Young's Modulus and Poisson's Ratio estimated from the proposed model sonic log predictions.

6.6.1 Dynamic Young's Modulus

Young's Modulus commonly known as the modulus of elasticity because it is a measure of the stiffness of the formation can be estimated using equation (6.15) (Mullen et al., 2007).

$$E = \frac{\rho}{{\Delta t_s}^2} * \left(\frac{3{\Delta t_s}^2 - 4{\Delta t_c}^2}{{\Delta t_s}^2 - {\Delta t_c}^2} \right) * 1.34 * 10^{10} \qquad (6.15)$$

The results of the estimation of dynamic Young's Modulus from the measured sonic logs and proposed model predicted sonic logs are presented and compared in Figure 6.9. The cross-validation of the Young's Modulus from the predicted and measured sonic logs presented in Figure 6.9 show very good agreement with a coefficient of determination of 0.9953. The trendline line through the zero intercept of the measured and predicted estimations matches the perfect slope increases indicating unbiased in the predictions. As the dynamic Young's Modulus increases, the deviation from the perfect slop increases. The estimation from the proposed model sonic logs slightly underpredicts Young's Modulus from approximately 40 GPa to 70 GPa. The highest deviation is observed at a depth of 7480-7490 feet with the average dynamics Young's Modulus of 55 GPa and 50 GPa which both signify a good consolidation at such depths for measured and predicted respectively.

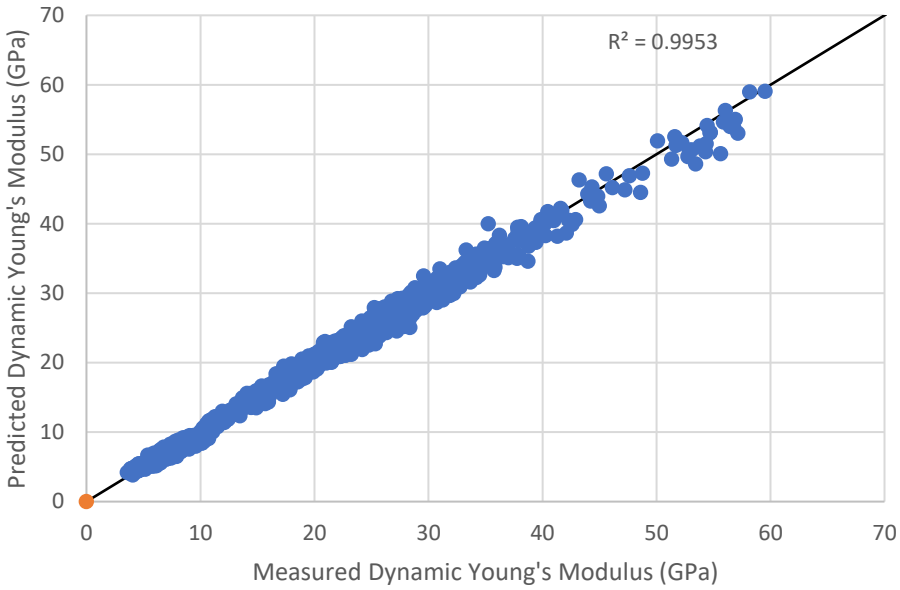

Figure 6.9. Cross-validation plot of predicted and measured dynamic Young's Modulus

6.6.2 **Poisson's Ratio (PR)**

Poisson's Ratio is another rock mechanical property that is estimated during formation evaluation. It is literally the ratio of the lateral to the vertical strain of a specimen and is estimated from sonic logs as follows (Mullen et al., 2007).

$$\vartheta = 0.5 * \left(\frac{\Delta t_s{}^2 - 2\Delta t_c{}^2}{\Delta t_s{}^2 - \Delta t_c{}^2} \right) \tag{6.16}$$

The results of the estimation of Poisson's Ratio from the measured sonic logs and proposed model predicted sonic logs are presented and compared in Figure 6.10. The cross-validation of the Young's Modulus from the predicted and measured sonic logs presented in Figure 6.10 portrays a good match with a coefficient of determination of 0.9413. The trendline line through the zero intercept of the measured and predicted estimations almost perfectly follows the perfect unity slope line indicating a general non-bias in the predictions. As the Poisson's Ratio increases, the deviation

from the perfect slop decreases. The estimations from the proposed model overpredict points of Poisson' Ratio values below 0.25. The accuracy of the estimations from the predicted model is increased as the formation weakens.

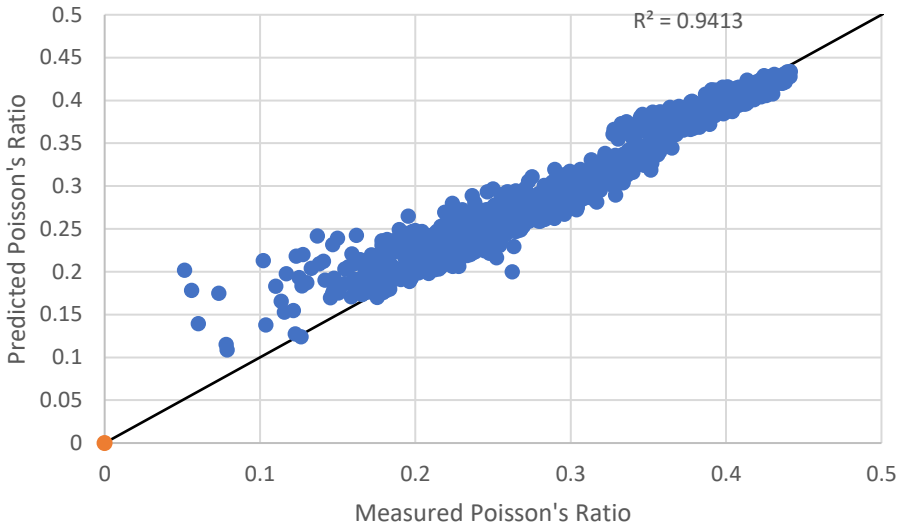

Figure 6.10. Cross-validation plot of predicted and measured Poisson's Ratio

The main reason why the Young's Modulus and Poisson's Ratio predictions are reasonably accurate is that of the accuracy of the Shear Velocity predictions which are then used in the theoretical and empirical relationships given in Equations (6.15) and (6.16). In general, both estimation of Young's Modulus and Poisson's Ratio from the measured and predicted sonic logs allude to a good agreement in the sensitivity analysis. Therefore the model can be used in place of actual sonic logs with a high confidence level.

6.7 Conclusions

The present study has demonstrated that in the absence of shear sonic transit logs, a GP regression model can be used to model the shear sonic logs from the depth, density, gamma-ray, porosity and compressional transit time logs. The new model can be particularly useful in wells where accurate or continuous shear wave transit times are missing or where borehole compensated sonic tool has not been used.

The proposed GP model development offers the following benefits to the oil and gas industry:

- The GP model offers operators with offset wells that only contain compressional sonic wells a reliable tool to predict the shear sonic log for better formation evaluation analysis.

- The GP model provides a cost-effective and safe tool to operators by offering a reliable means of predicting shear transit time in a field instead of carrying out more expensive diploe and multipole sonic logging on several wells in the field. This leads to cost savings and human (work hours) reduction leading to higher days without accidents (Day since last accident or hazard exposure) on projects.

- The Gaussian model provides a cheap method of establishing mechanical rock formation property tables for several geographical regions and geological settings.

- The GP model provides a calibration and validation tool for cross-checking already measured and acquired sonic shear logs from sonic loggers that may be faulty or run in complicated hole sections.

The GP model accurately predicts shear sonic time log for the case study with an R^2 of 0.99. The model is also used to estimate some mechanical formation properties namely; Young's Modulus

and Poisson's Ratio in a sensitivity analysis. The results are compared to the same mechanical rock properties using the measured sonic logs. The coefficients of determination between the measured and predicted sonic logs used for the estimations of Young's Modulus and Poison's Ratio are 0.99 and 0.94 respectively.

Generally, the GP models are highly efficient in recognizing non-linear patterns with complex dataset including well logs used in the oil and gas industry as is evident in this study. GP models are recommended for developing non-parametric correlations between other well log dataset of interest.

The present study provides the oil and gas industry with a roadmap for estimating shear sonic well logs and also validating measured shear sonic transit time logs. Future work can be done to estimate both compressional and shear sonic transit logs from a Gaussian model, thereby eliminating the need to run countless expensive sonic logging tools in the formation. The significance of such a future model will be highly valuable in terms of cost saving gains and man-hours resources that could potentially be saved.

Acknowledgment

The authors thankfully acknowledge the financial support provided by the Natural Science and Engineering Council of Canada and the Canada Research Chair (CRC) Tier I Program, the Hibernia Management and Development Company (HMDC), Chevron Canada, and Innovate NL for the support without which this work could not have been performed.

Nomenclature

RHOB	Bulk density log (g/cm3)
DTCO	Compressional wave travel time (µsec/ft)
Δt_c	Compressional wave travel time (µsec/ft)
RESD	Deep resistivity log (ohm.m)
PHIE	Effective porosity log (m3/m3)
ϕ_{den}	Electron density porosity (g/cc)
ρ_{fl}	Fluid density (g/cc)
ρ, ρ_b	Formation density (g/cc)
Δt_{fl}	Formation fluid compressional wave travel time (µsec/ft)
Δt_{ma}	Formation matrix compressional wave travel time (µsec/ft)
GR_{min}	Gamma-ray in clean sandstone
GR_{min}	Gamma-ray in shale
GR	Gamma-ray log (gAPI)
GR	Gamma-ray log reading
ρ_{ma}	Matrix density (g/cc)
MAE	Mean absolute error
MPE	Mean percentage error
Δt_{log}	Measured compressional wave travel time (µsec/ft)
ϕ_N	Neutron porosity
$\phi_{N,fl}$	Neutron response of the fluid
$\phi_{N,ma}$	Neutron response of the matrix
ϑ	Poisson's Ratio
ϕ	Rock porosity
Vsh	Shale volume
DTSM	Shear wave travel time (µsec/ft)
Δt_s	Shear wave travel time (µsec/ft)
ϕ_s	Sonic porosity
PHIT	Total porosity log (m3/m3)
E	Young's Modulus (MPa)

References

Abdollahzadeh, A., Christie, M.A., Corne, D., 2012. Gaussian-based Estimation of Distribution Algorithms for History Matching. Abu Dhabi Int. Pet. Conf. Exhib. https://doi.org/10.2118/161951-MS

Adeli, A., Emery, X., Dowd, P., 2017. Geological Modelling and Validation of Geological Interpretations via Simulation and Classification of Quantitative Covariates. https://doi.org/10.3390/min8010007

Alford, J., Blyth, M., Tollefsen, E., Crowe, J., Loreto, J., Mohammed, S., Pistre, V., Rodriguez-Herrera, A., 2012. Sonic logging while drilling-shear answers. Oil. Rev. 24, 4–15.

Bailey, T., 2012. An empirical Vp/Vs shale trend for the Kimmeridge Clay of the Central North Sea, in: 74th EAGE Conference & Exhibition Incorporating SPE EUROPEC 2012. Copenhagen, Denmark, pp. 4–7.

Castagna, J.P., Batzle, M.L., Eastwood, R.L., 1985. Relationships between compressional-wave and shear-wave velocities in clastic silicate rocks. Geophysics 50, 571–581. https://doi.org/10.1190/1.1441933

Doh, C.A., Alger, R.P., 1958. Sonic Logging, A New Petrophysical Tool.

Domenico, S.N., 1984. Rock lithology and porosity determination from shear and compressional wave velocity. Geophysics 49, 1188–1195. https://doi.org/10.1190/1.1441748

Dubrule, O., Damsleth, E., 2001. Achievements and challenges in petroleum geostatistics. Pet. Geosci. 7, S1–S7.

Ebden, M., 2008. Gaussian processes for regression: A quick introduction. Website Robot. Res. Gr. Dep. Eng. Sci. Univ. Oxford.

Eberhart-Phillips, D., Han, D.-H., Zoback, M.D., 1989. Empirical relationships among seismic velocity, effective pressure, porosity, and clay content in sandstone. Geophysics. https://doi.org/10.1190/1.1442580

Gardner, G.H.F., Gardner, L.W., Gregory, A.R., 1974. Formation velocity and density—the diagnostic basis for stratigraphic traps. Geophysics 39, 770–780. https://doi.org/10.1190/1.1440465

Greenberg, M.L., Castagna, J.P., 1992a. Shear-Wave Velocity Estimation in Porous Rocks: Theoretical Formulation, Preliminary Verification and Applications1. Geophys. Prospect. 40, 195–209. https://doi.org/10.1111/j.1365-2478.1992.tb00371.x

Greenberg, M.L., Castagna, J.P., 1992b. Shear-Wave Estimation in Porous Rocks: Theoretical Formulation Preliminary Verification and Application. Geophys. Prospect. 40, 195–209. https://doi.org/10.1111/j.1365-2478.1992.tb00371.x

Hamada, G.M., 2004. Reservoir Fluids Identification Using Vp /Vs Ratio. Oil Gas Sci. Technol. – Rev. IFP 59, 649–654.

Han, D., Nur, A., Morgan, D., 1986. Effects of porosity and clay content on wave velocities in sandstones. Geophysics 51, 2093–2107. https://doi.org/10.1190/1.1442062

Han, I., Kamber, M., 2010. Data Mining: Concepts and Techniques. Morgan Kaufinann (2006).

Harrison, A.R., Randall, C.J., Aron, J.B., Morris, C.F., Wignall, A.H., Dworak, R.A., Rutledge, L.L., Perkins, J.L., 1990. Acquisition and Analysis of Sonic Waveforms From a Borehole

Monopole and Dipole Source for the Determination of Compressional and Shear Speeds and Their Relation to Rock Mechanical Properties and Surface Seismic Data. SPE Annu. Tech. Conf. Exhib. https://doi.org/10.2118/20557-MS

Hsu, K., Brie, A., Plumb, R.A., 1987. A New Method for Fracture Identification Using Array Sonic Tools. https://doi.org/10.2118/14397-PA

Huang, X.B., Zhang, Q., Zhu, H.H., Zhang, L.Y., 2017. An Estimated Method of Intact Rock Strength Using Gaussian Process Regression. 51st U.S. Rock Mech. Symp.

Iglesias, M.A., Law, K.J.H., Stuart, A.M., 2013. Evaluation of Gaussian approximations for data assimilation in reservoir models. Comput. Geosci. 17, 851–885. https://doi.org/10.1007/s10596-013-9359-x

Izadi, G., Elsworth, D., 2014. Reservoir stimulation and induced seismicity: Roles of fluid pressure and thermal transients on reactivated fractured networks. Geothermics 51, 368–379. https://doi.org/10.1016/J.GEOTHERMICS.2014.01.014

Jorstad, A., Mukerji, T., Mavko, G., 1999. Model-based shear-wave velocity estimation versus empirical regressions. Geophys. Prospect. 47, 785–797. https://doi.org/10.1046/j.1365-2478.1999.00154.x

Khazanehdari, J., Mccann, C., 2005. Acoustic and petrophysical relationships in low-shale sandstone reservoir rocks. Geophys. Prospect. 53(4), 447–461.

Kokesh, F.P., Schwartz, R.J., Wall, W.B., Morris, R.L., 1965. A New Approach to Sonic Logging and Other Acoustic Measurements. https://doi.org/10.2118/991-PA

Krief, M., Garat, J., Stellingwerf, J., Ventre, J., 1990. A Petrophysical Interpretation Using The

Velocities Of P And S Waves (full-waveform Sonic). Log Anal. 31, 355–369.

Kumar, M., Bhatt, M.R., Samui, P., 2014. Modeling of Elastic Modulus of Jointed Rock Mass: Gaussian Process Regression Approach. Int. J. Geomech. 14, 06014001. https://doi.org/10.1061/(ASCE)GM.1943-5622.0000318

Kuss, M., Rasmussen, C.E., 2006. Assessing Approximations for Gaussian Process Classification. Adv. Neural Inf. Process. Syst. 18 Proc. 2005 Conf. 699–706.

Lee, M.W., 2006. A simple method of predicting S-wave velocity. Geophysics 71, F161–F164. https://doi.org/10.1190/1.2357833

MacKay, D.J.C., 2005. Information Theory, Inference, and Learning Algorithms David J.C. MacKay, Learning. https://doi.org/10.1198/jasa.2005.s54

Market, J., Canady, W.J., 2006. Dispersion Corrections Are Not Just for LWD Dipole Sonic Tools. SPE Annu. Tech. Conf. Exhib. https://doi.org/10.2118/102345-MS

Matlab Documentation, 2018. The MathWorks Inc.

Miller, S., Stewart, R., 1990. Effects of lithology, porosity and shaliness on the P and S-wave velocities from sonic logs. J. Can. Soc. Expl. Geophys. 26, 94–103.

Miller, S.L.M., Stewart, R.R., 1974. The relationship between elastic-wave velocities and density in sedimentary rocks: A proposal. Crewes Res. Rep. 260–273.

Minear, J.W., Fletcher, C.R., 1983. Full-Wave Acoustic Logging. SPWLA 24th Annu. Logging Symp.

Mullen, M.J., Roundtree, R., Turk, G.A., 2007. A Composite Determination of Mechanical Rock

Properties for Stimulation Design (What to Do When You Don't Have a Sonic Log). Rocky Mt. Oil Gas Technol. Symp. https://doi.org/10.2118/108139-MS

Nourafkan, A., Kadkhodaie-Ilkhchi, A., 2015. Shear wave velocity estimation from conventional well log data by using a hybrid ant colony-fuzzy inference system: A case study from Cheshmeh-Khosh oilfield. J. Pet. Sci. Eng. 127, 459–468. https://doi.org/10.1016/j.petrol.2015.02.001

Oloruntobi, O., Onalo, D., James, L., Chunduru, R., Butt, S., Adedigba, S., 2018. The New Shear – Compressional Velocity Relationship for Siliciclastic Rocks. Submitted to J. Rock Mech. Geotech. Eng.

Onalo, D., Adedigba, S., Oloruntobi, O.S., Khan, F., James, L., Butt, S., 2018a. Data Driven Model for Sonic Well Log Prediction. Submitted to J. Pet. Sci. Eng.

Onalo, D., Oloruntobi, O., Adedigba, S., Khan, F., James, L., Butt, S., 2018b. Static Young's modulus model for drilling operation planning. Submitted to J. Pet. Sci. Eng.

Ramcharitar, K., Hosein, R., 2016. Rock Mechanical Properties of Shallow Unconsolidated Sandstone. SPE Trinidad Tobago Sect. Energy Resour. Conf. https://doi.org/10.2118/180803-MS

Rasmussen, C.E., 2004. Gaussian processes in machine learning, in: Advanced Lectures on Machine Learning. Springer, pp. 63–71.

Raymer, L.L.L., Hunt, E.R.R., Gardner, J.S., 1980. An Improved Sonic Transit Time to Porosity-to-Porosity transform. 21st SPWLA Logging Symp. Trans. 1–13.

Reichel, N., Evans, M., Allioli, F., Mauborgne, M.-L., Nicoletti, L., Haranger, F., Stoller, C.,

Schlumberger, V.C., El, E., Sipetrol, H., 2012. Neutron-Gamma Density (Ngd): Principles, Field Test Results And Log Quality Control Of A Radioisotope-Free Bulk Density Measurement, in: SPWLA 53rd Annual Logging Symposium. Society of Petrophysicists and Well-Log Analysts, pp. 1–15.

Rostami, H., Azin, R., Dianat, R., 2013. Prediction of Undersaturated Crude Oil Density Using Gaussian Process Regression. Pet. Sci. Technol. 31, 418–427. https://doi.org/10.1080/10916466.2010.531346

Rostami, H., Khaksar Manshad, A., 2013. Prediction of Asphaltene Precipitation in Live and Tank Crude Oil Using Gaussian Process Regression. Pet. Sci. Technol. 31, 913–922. https://doi.org/10.1080/10916466.2010.531349

Seeger, M., 2004. Gaussian processes for machine learning. Int. J. Neural Syst. 14, 69–106.

Silva, D.S.F., Deutsch, C. V., 2016. Multivariate data imputation using Gaussian mixture models. Spat. Stat. https://doi.org/10.1016/J.SPASTA.2016.11.002

Su, G., 2009. Modeling Non-linear Deformation Time Series of Tunnel Using Gaussian Process Machine Learning. ISRM Int. Symp. Rock Mech. - SINOROCK 2009.

Takahashi, I., Mukerji, T., Mavko, G., 2000. Vp - Vs relations of sandstones and carbonates:Implications about the pore structure, in: SEG Technical Program Expanded Abstracts 2000. Society of Exploration Geophysicists, pp. 1838–1841. https://doi.org/10.1190/1.1815786

Thomsen, L., 1986. Weak elastic anisotropy. Geophysics 51, 1954–1966. https://doi.org/10.1190/1.1442051

Toksöz, M.N., Cheng, C.H., Timur, A., 1976. VELOCITIES OF SEISMIC WAVES IN POROUS ROCKS. Geophysics 41, 621–645. https://doi.org/10.1190/1.1440639

Vernik, L., Fisher, D., Bahret, S., 2002. Estimation of net-to-gross from P and S impedance in deep-water turbidites. Lead. Edge 21, 380–387. https://doi.org/10.1190/1.1471602

Williams, C.K.I., Rasmussen, C.E., 2006. Gaussian processes for machine learning. MIT Press 2, 4.

Williams, D.M., 1990. The Acoustic Log Hydrocarbon Indicator. Soc. Petrophysicists Well-Log Anal.

Yin, S., Dusseault, M.B., Rothenburg, L., 2009. Multiphase poroelastic modeling in semi-space for deformable reservoirs. J. Pet. Sci. Eng. 64, 45–54. https://doi.org/10.1016/j.petrol.2008.12.003

Yu, H., Wang, Z., Rezaee, R., Zhang, Y., Xiao, L., Luo, X., Wang, X., Zhang, L., 2016. The Gaussian Process Regression for TOC Estimation Using Wireline Logs in Shale Gas Reservoirs. Int. Pet. Technol. Conf. https://doi.org/10.2523/IPTC-18636-MS

Appendices

Table 6.3. 50 feet of available well log data for the study

Depth (ft)	DTCO (µs/ft)	DTSM (µs/ft)	GR (gAPI)	PHIT (m3/m3)	RHOB (g/cc)
6000.00	131.82	324.03	87.14	0.19	2.32
6000.50	133.00	349.97	87.44	0.20	2.31
6001.00	134.20	363.23	86.52	0.20	2.30
6001.50	133.26	342.61	86.24	0.20	2.31
6002.00	131.83	312.74	86.66	0.19	2.32
6002.50	130.86	304.08	85.50	0.18	2.33
6003.00	130.94	304.68	84.60	0.18	2.33
6003.50	129.35	315.31	85.13	0.18	2.34
6004.00	129.85	338.09	85.31	0.18	2.33
6004.50	131.38	363.53	87.60	0.19	2.32
6005.00	133.30	379.96	88.31	0.19	2.32
6005.50	133.26	379.00	91.86	0.19	2.32
6006.00	132.83	373.47	92.08	0.19	2.32
6006.50	132.59	361.99	89.04	0.19	2.32
6007.00	131.24	358.47	86.43	0.18	2.34
6007.50	131.50	361.11	88.95	0.17	2.35
6008.00	132.92	371.02	94.94	0.17	2.36
6008.50	132.07	374.90	97.52	0.17	2.36
6009.00	133.00	378.18	95.00	0.17	2.35
6009.50	133.95	379.63	89.53	0.18	2.34
6010.00	133.47	350.07	85.95	0.18	2.33
6010.50	133.49	332.87	84.92	0.19	2.32
6011.00	134.39	346.93	85.52	0.19	2.31
6011.50	133.68	367.18	84.63	0.19	2.32
6012.00	133.95	363.88	82.08	0.18	2.33
6012.50	132.86	356.71	86.91	0.18	2.34
6013.00	132.95	363.06	93.85	0.18	2.34
6013.50	131.60	342.72	94.98	0.19	2.32
6014.00	131.81	316.72	91.16	0.19	2.31
6014.50	131.79	311.10	85.44	0.20	2.31
6015.00	131.07	307.31	82.28	0.19	2.31
6015.50	132.31	310.24	77.20	0.19	2.31
6016.00	131.97	322.17	77.37	0.19	2.32
6016.50	130.74	364.35	83.84	0.19	2.31
6017.00	132.42	385.76	86.86	0.20	2.30
6017.50	133.16	387.82	86.94	0.21	2.29
6018.00	133.07	372.00	82.35	0.20	2.30

6018.50	132.27	335.59	81.35	0.20	2.30
6019.00	131.38	323.30	80.80	0.20	2.30
6019.50	131.01	318.53	80.37	0.20	2.31
6020.00	130.82	319.37	82.46	0.19	2.32
6020.50	130.81	330.04	80.39	0.19	2.32
6021.00	130.69	366.92	82.67	0.19	2.32
6021.50	131.93	373.65	81.17	0.19	2.31
6022.00	131.37	366.63	87.45	0.19	2.31
6022.50	130.85	326.51	88.73	0.19	2.31
6023.00	131.18	315.40	92.32	0.19	2.31
6023.50	128.95	315.07	91.10	0.19	2.31
6024.00	130.31	319.97	91.63	0.19	2.32
6024.50	130.17	323.64	89.42	0.19	2.32
6025.00	129.66	317.45	86.47	0.19	2.32
6025.50	129.85	321.53	82.90	0.19	2.31
6026.00	130.95	333.50	81.50	0.20	2.30
6026.50	130.85	341.21	82.07	0.20	2.31
6027.00	131.47	336.61	83.38	0.19	2.31
6027.50	132.42	332.92	85.78	0.19	2.32
6028.00	132.36	324.53	87.77	0.19	2.32
6028.50	132.19	320.65	91.52	0.19	2.32
6029.00	132.28	315.04	91.68	0.19	2.32
6029.50	132.71	313.44	87.51	0.19	2.32
6030.00	132.55	316.99	85.33	0.19	2.32
6030.50	132.35	324.50	87.06	0.19	2.32
6031.00	131.76	357.34	92.97	0.19	2.33
6031.50	132.15	396.80	95.18	0.19	2.33
6032.00	131.76	401.90	95.50	0.19	2.33
6032.50	132.21	402.31	95.32	0.19	2.32
6033.00	133.53	406.33	93.26	0.20	2.31
6033.50	134.37	413.76	89.90	0.20	2.29
6034.00	135.44	404.15	89.06	0.21	2.28
6034.50	135.84	398.00	91.33	0.21	2.28
6035.00	131.67	392.08	96.32	0.21	2.28
6035.50	130.85	387.02	97.00	0.20	2.29
6036.00	130.95	354.82	96.31	0.20	2.30
6036.50	129.68	339.62	88.86	0.20	2.31
6037.00	129.51	329.55	83.93	0.19	2.32
6037.50	125.87	307.18	77.83	0.19	2.32
6038.00	126.05	292.21	78.55	0.19	2.31
6038.50	122.92	284.44	79.17	0.19	2.31

6039.00	125.14	290.37	81.78	0.19	2.32
6039.50	128.86	307.30	84.62	0.19	2.33
6040.00	128.77	322.01	82.73	0.18	2.34
6040.50	129.55	365.22	83.52	0.18	2.34
6041.00	130.52	354.40	84.58	0.18	2.33
6041.50	130.84	315.02	89.45	0.19	2.32
6042.00	131.80	356.62	93.99	0.19	2.32
6042.50	132.12	322.97	92.13	0.19	2.31
6043.00	130.62	317.84	89.23	0.19	2.32
6043.50	128.64	310.26	84.82	0.18	2.33
6044.00	126.87	309.84	84.66	0.18	2.34
6044.50	126.66	305.22	82.88	0.18	2.34
6045.00	127.37	299.49	80.86	0.18	2.33
6045.50	128.29	305.08	81.14	0.19	2.32
6046.00	129.59	311.22	82.66	0.19	2.32
6046.50	129.64	320.78	85.12	0.19	2.33
6047.00	129.81	327.75	82.91	0.18	2.33
6047.50	129.74	352.66	82.84	0.18	2.34
6048.00	130.00	358.57	81.03	0.18	2.34
6048.50	130.38	324.24	81.19	0.18	2.33
6049.00	131.37	323.73	81.31	0.19	2.32
6049.50	132.51	377.43	84.68	0.20	2.31
6050.00	132.55	386.24	91.19	0.20	2.31
6050.50	132.55	393.98	90.16	0.19	2.31
6051.00	132.75	399.55	88.44	0.19	2.32

Table 6.4. Sensitivity analysis data (Dynamic Young's Modulus and Poisson's Ratio)

Depth (ft)	Measured Ed (GPa)	Predicted Ed (GPa)	Measured PR	Measured PR
6000.00	5.71	5.55	0.40	0.40
6000.50	4.92	4.91	0.42	0.42
6001.00	4.58	4.76	0.42	0.42
6001.50	5.13	5.06	0.41	0.41
6002.00	6.10	5.69	0.39	0.40
6002.50	6.45	5.87	0.39	0.40
6003.00	6.44	5.54	0.39	0.41
6003.50	6.08	5.67	0.40	0.41
6004.00	5.33	5.62	0.41	0.41
6004.50	4.63	5.37	0.42	0.41
6005.00	4.24	4.94	0.43	0.42
6005.50	4.26	4.59	0.43	0.42

6006.00	4.38	4.70	0.43	0.42
6006.50	4.66	4.87	0.42	0.42
6007.00	4.78	5.16	0.42	0.41
6007.50	4.74	4.93	0.42	0.42
6008.00	4.52	4.62	0.43	0.42
6008.50	4.43	4.74	0.43	0.42
6009.00	4.33	4.52	0.43	0.43
6009.50	4.28	4.45	0.43	0.43
6010.00	4.97	5.01	0.41	0.41
6010.50	5.44	5.24	0.40	0.41
6011.00	5.01	4.91	0.41	0.41
6011.50	4.52	4.94	0.42	0.41
6012.00	4.63	4.99	0.42	0.41
6012.50	4.83	4.81	0.42	0.42
6013.00	4.66	4.54	0.42	0.43
6013.50	5.16	4.65	0.41	0.42
6014.00	5.94	5.30	0.40	0.41
6014.50	6.12	5.16	0.39	0.41
6015.00	6.28	5.46	0.39	0.41
6015.50	6.17	5.57	0.39	0.40
6016.00	5.78	5.66	0.40	0.40
6016.50	4.58	5.07	0.43	0.42
6017.00	4.09	4.67	0.43	0.42
6017.50	4.03	4.66	0.43	0.42
6018.00	4.37	4.96	0.43	0.41
6018.50	5.32	5.19	0.41	0.41
6019.00	5.70	5.42	0.40	0.41
6019.50	5.88	5.60	0.40	0.40
6020.00	5.87	5.56	0.40	0.41
6020.50	5.54	5.86	0.41	0.40
6021.00	4.54	5.41	0.43	0.41
6021.50	4.37	5.14	0.43	0.41
6022.00	4.53	5.16	0.43	0.41
6022.50	5.63	5.48	0.40	0.41
6023.00	5.99	5.44	0.40	0.41
6023.50	6.02	5.88	0.40	0.40
6024.00	5.86	5.70	0.40	0.40
6024.50	5.75	5.78	0.40	0.40
6025.00	5.95	5.92	0.40	0.40
6025.50	5.79	5.56	0.40	0.41
6026.00	5.39	5.39	0.41	0.41

6026.50	5.17	5.32	0.41	0.41
6027.00	5.32	5.22	0.41	0.41
6027.50	5.43	5.43	0.41	0.41
6028.00	5.71	5.17	0.40	0.41
6028.50	5.83	5.12	0.40	0.41
6029.00	6.01	5.16	0.39	0.41
6029.50	6.06	5.27	0.39	0.41
6030.00	5.95	5.44	0.39	0.41
6030.50	5.71	5.37	0.40	0.41
6031.00	4.78	4.75	0.42	0.42
6031.50	3.92	4.25	0.44	0.43
6032.00	3.83	4.34	0.44	0.43
6032.50	3.81	4.30	0.44	0.43
6033.00	3.72	4.24	0.44	0.43
6033.50	3.57	4.22	0.44	0.43
6034.00	3.70	4.19	0.44	0.43
6034.50	3.81	4.08	0.43	0.43
6035.00	3.94	4.32	0.44	0.43
6035.50	4.06	4.52	0.44	0.43
6036.00	4.80	4.76	0.42	0.42
6036.50	5.23	5.43	0.41	0.41
6037.00	5.55	5.76	0.41	0.40
6037.50	6.36	6.56	0.40	0.39
6038.00	6.94	6.65	0.39	0.39
6038.50	7.31	7.25	0.39	0.39
6039.00	7.04	6.93	0.39	0.39
6039.50	6.34	6.15	0.39	0.40
6040.00	5.85	5.67	0.40	0.41
6040.50	4.63	5.22	0.43	0.42
6041.00	4.88	5.41	0.42	0.41
6041.50	6.04	5.56	0.40	0.41
6042.00	4.78	4.75	0.42	0.42
6042.50	5.74	5.14	0.40	0.41
6043.00	5.93	5.66	0.40	0.40
6043.50	6.25	6.02	0.40	0.40
6044.00	6.30	6.28	0.40	0.40
6044.50	6.48	6.31	0.40	0.40
6045.00	6.66	6.48	0.39	0.39
6045.50	6.42	6.35	0.39	0.39
6046.00	6.17	5.94	0.40	0.40
6046.50	5.86	5.95	0.40	0.40

6047.00	5.64	5.77	0.41	0.40
6047.50	4.94	5.25	0.42	0.42
6048.00	4.79	5.25	0.42	0.42
6048.50	5.75	5.65	0.40	0.41
6049.00	5.73	5.58	0.40	0.40
6049.50	4.28	4.79	0.43	0.42
6050.00	4.10	4.68	0.43	0.42

Disclaimer

The well log data presented in this paper is strictly for educational application. To protect the confidentiality and avoid any proprietary issue, the origin of the data has been withheld. The authors accept no liability for relating this data to any source, group, persons or organizations.

Chapter 7 Dynamic Data Driven Sonic Well Log Model for Formation Evaluation

Preface

A version of this chapter has been published in the Journal of Petroleum Science and Engineering. I am the primary author. Co-author Olalere Oloruntobi helped in formulating the petrophysical concept of the paper. Co-author Dr. Sunday Adeshina helped in formulating the intelligent system concept of the paper, and review of the first draft. Co-author Dr. Faisal Khan provided the much-needed support in formulating and implementing the concept and testing the model to make the work publishable. Co-author Dr. Lesley James provided technical assistance, proper formatting and representation of the well log data, expert analysis and review. She provided financial support to carry out the research. Co-author Dr. Stephen Butt provided technical assistance, review and financial support during the research, as well as analyzing the well log format used in the paper. I and Dr. Sunday Adedigba carried out most of the data collection and analysis. The first draft of the manuscript was prepared by me, and I subsequently revised the manuscript, based on the feedback from the co-authors and also a peer review process. The co-authors assisted in the development of the concept and testing the model, reviewed and corrected the model and results. They also contributed to the review and revision of the manuscript.

Abstract

The lack of acoustic measurements places severe limitations on the application of well log data to analyze rock physics. In such conditions, other petrophysical data can be used to predict the shear and compressional sonic travel time. This study presents a novel data-driven model based on a nonlinear autoregressive neural network with exogenous (NARX) input to estimate the shear and compressional sonic travel time due to its ability to accurately determine nonlinearity in sequential and temporal data. The architecture of the model comprises three-layers and ten hidden neurons with gamma ray log as exogenous inputs. The proposed NARX methodology is developed using 11 wells, six from the Norwegian continental shelf and five from West Africa. The results show that the wells provide sufficiently accurate predictions of the actual sonic well logs using the NARX model. The predicted sonic logs are used to estimate formation property parameters like sonic ratio, sonic difference, sonic porosity, and Poisson's ratio. This paper proves NARX is an affordable, efficient and accurate means to reproduce sonic well logs for formation evaluation.

Keywords: Recurrent neural network, intelligent systems, well log, sonic log prediction

7.1 Introduction

Well logs have proven to be very valuable in the petroleum industry due to their use in reservoir evaluation (Avseth and Odegaard, 2004; Krief et al., 1990; Minear and Fletcher, 1983; Onalo et al., 2018b; Reichel et al., 2012). With the help of well log data, engineers have been able to predict with reasonable certainty the type of formation being encountered, the fluids in the formation, the rock mechanical properties, wellbore stability and potential hydrocarbon plays (Asquith and Gibson, 2004; Ellis, 2003; Lindseth, 1979; Luffel and Guidry, 1989; Oloruntobi et al., 2018; Onalo et al., 2018a; Reichel et al., 2012; Schön, 2015; Williams, 1990; Wisniak and Jing, 2001). Sonic logs, along with density and neutron logs, are referred to as porosity logs; therefore, sonic logs can be used as a check and validation tool of other porosity logs (Ellis, 2003; Pickett, 1963; Raymer et al., 1980; Wyllie et al., 1956). Sonic logs have been used to develop stratigraphic correlations identifying the different lithological beds along the formation (Domenico, 1984; Miller and Stewart, 1990). The ratio of compressional to shear sonic log has been reported to be more sensitive to lithology and fluid changes (Bailey, 2012; Domenico, 1984; Eastwood and Castagna, 1983; Hamada, 2004; Han et al., 1986; Tatham, 1982). Sonic logs can be used to estimate the formation pore pressure and identify overpressure zones by observing a sudden increase in sonic transit time in shale formations (Saleh et al., 2013; Walls et al., 2000). Cracks and fractures can be identified using sonic logs (Hsu et al., 1987; Iy et al., 1976; Lacy, 1997; Onalo et al., 2018b; Tatham, 1982).

In the absence of sonic logs or where the readings are erroneous due to faults inherent in the sonic logging tool or in formations where sonic logs have not been run due to financial constraints, there is a need for reliable and accurate methods of estimating these logs for formation evaluation (Onalo et al., 2018a). In such scenarios, empirical correlations have been deployed (Bailey and Dutton, 2012; Castagna et al., 1985; Eberhart‐Phillips et al., 1989; Gregory, 1977; Hossain et al., 2012;

Johnston and Christensen, 1993; Miller and Stewart, 1991, 1974). However, empirical correlations have limitations in terms of their accuracy and specificity to certain lithologies and geographical regions (Onalo et al., 2018a; Ramfcharitar and Hosein, 2016).

Machine learning and intelligent systems have been employed in several industries, including the petroleum industry to help analyze data, find patterns and predict target variables (Adedigba et al., 2017; Onalo et al., 2018a). Such machine learning techniques and intelligent systems range from using artificial neural networks (ANN), to generic algorithms (GA), to particle swarm optimization (PSA), to fuzzy logic (FL), to neuro-fuzzy inference system (ANFIS) and to recurrent neural networks (Akin et al., 2008; Ali Ahmadi and Golshadi, 2012; Asadisaghandi and Tahmasebi, 2011; Ashoori et al., 2010; Babakhani et al., 2015; Derakhshanfard and Mehralizadeh, 2018; Huang et al., 2003; Iturrarán-Viveros and Molero, 2013; Kelechukwu et al., 2013; Riazi et al., 2014; Sheremetov et al., 2014; Vaferi et al., 2014). Some examples of the intelligent systems that have been developed to solve several problems in the industry are presented in Table 7.1.

Table 7.1: Examples of intelligent systems used in the petroleum industry

S/N	Reference	Intelligent System or Method	Input data	Output data	Application
1	Smaoui and Garrouch (1997)	Karhunen-Lorve-ANN (KLANN)	Effective porosity mean pore size, weight fractions	Permeability	Estimation of permeability in tight sands
2	Huang et al. (2003)	BPANN	Molecular weight, reservoir temperature, and concentrations	CO_2 Minimum miscibility pressure	Impure and pure CO_2 minimum miscibility pressures oil prediction
3	Akin et al. (2008)	Feedforward neural network (FFNN)	SP, RHOB, GR, deep resistivity and NPHI	Pore type	Population of the reservoir with multiphase flow functions

4	Ashoori et al. (2010)	Artificial Neural Network (ANN)	Dilution ratio, temperature and molecular weight of alkanes	Asphaltene precipitation	Asphaltene precipitation prediction
5	Asadisaghandi and Tahmasebi, (2011)	Back propagation learning algorithms (BPLA)	Oil relative density (API), temperature, relative gas gravity (γg) and solution gas oil ratio (Rs)	Formation volume factor bubble point (Bob) and bubble point pressure (Pb)	PVT oil properties estimation
6	Ali Ahmadi and Golshadi (2012)	Hybrid genetic algorithm and particle swarm optimization (HGAPSO), feedforward neural network (FFNN), GA and PSO	Pressure & Temperature	Amount of asphaltene precipitation	Asphaltene precipitation
7	Kelechukwu et al. (2013)	Feedforward neural network (FFNN)	Temperature differential, flow rate and residence time	Wax deposition	Paraffin wax problems during hydrocarbon production
8	Sheremetov et al. (2014)	Nonlinear autoregressive neural network with exogenous input (NARX)	Maximum depth of completed intervals, latitude, longitude, bottom-hole flowing pressure, fracture permeability, VDOL and VLIS	Flow rate	Modeling of naturally fractured reservoir
9	Vaferi et al. (2014)	Artificial neural network (ANN)	Oil saturation Temperature, fluid density, porosity, pressure and bulk density	Thermal conductivity (TC)	Evaluation of the efficiency of the thermal EOR and reservoir thermal simulation
10	Riazi et al. (2014)	Particle swarm optimization (PSO), generic algorithm (GA), & imperialist Competitive Algorithm	Temperature & pressures	Hydrate formation	Prevention of hydrate formation
11	Masoudi et al. (2014)	Conventional cut-off-based method and ANN	Shale volume, porosity and water saturation	Net pay	Pay zone determination

12	Babakhani et al. (2015)	Multilayer perceptron neural network (MLPNN)	Critical pressure, critical temperature, molecular weight, temperature & composition	Pressure	Hydrate pressure of binary mixtures estimation
13	Masoudi et al. (2015)	Bayesian Network (BN) and K2 algorithm	RHOB, GR, DT, resistivity, PEF	Porosity, permeability, vug and fracture, and net pay	Petrophysical reservoir characterization
14	Salehinia et al. (2016)	NARX, Hammerstein-Wiener (HW), Adaptive Neuro-Fuzzy Inference System (ANFIS)	Temperature, resistivity, oil density, specific gravity and bubble point pressure	Density and oil formation volume factor	Reservoir fluid characterization
15	Masoudi et al. (2017)	Fuzzy membership function	GR, RHOB, NPHI, and DT	Vertical resolution	Volume of investigation study
16	Masoudi et al. (2018)	Hybrid clustering-fuzzy arithmetic algorithm	NPHI, DT and RHOB	Porosity, permeability and water saturation	Quantification of uncertainty in estimations
17	Derakhshanfard and Mehralizadeh (2018)	Radial basis function neural network (RBFNN)	FeO_3, NiO, ZnO, TiO_2, & WO_3 nanoparticles	Viscosity	The effect of temperature and mass fraction of nanoparticles on crude oil viscosity
18	(Zhang et al., 2018)	Long Short-term Memory (LSTM)	Micro potential and gradient difference, caliper, SP and GR	Acoustic log, borehole compensated sonic and density	Well auto completion and missing synthetic logs generation
19	Current work	NARX RNN	NPHI & GR	Sonic logs	Formation evaluation

Onalo et al. (2018a) provide a comprehensive list of intelligent systems that have been developed to predict sonic logs. Previous neural networks used in the estimation of sonic logs have been mostly fully connected neural networks, which involves taking input data only from the same depth as the output data; the previous neural networks are not able to store memory of previous iterations (Zhang et al., 2018).

An advancement of these neural networks is recurrent neural networks (Zhang et al., 2018). Recurrent neural networks have a memory capacity and are therefore able to include previous data and iterations in their development for a better model (Bianchi et al., 2017). Bhatt and Helle (2002) were able to improve an artificial neural network model for facies identification from well logs by using a recurrent neural network. However, in recent times, not a lot of effort and research has gone into the development of recurrent neural networks in the industry besides minor scale tasks (Sak et al., 2014). Recently, Zhang et al. (2018) utilized a long short-term memory recurrent neural network (LSTM) to develop synthetic logs, thereby demonstrating the viability of recurrent neural networks in the estimation of sonic well logs.

The main objective of this paper is to develop a simple, yet robust, recurrent neural network model to accurately estimate sonic logs with the least amount of input data (well log). The results of these predictions can be used in place of actual sonic well logs for the evaluation of reservoir formations. The industrial significance of this model is that in scenarios where sonic logs data are not continuous and where there are missing data, costly sonic well logging tools would not have to be deployed, thereby reducing the operational cost of acquiring reliable sonic log data for formation evaluation.

7.2 Recurrent Neural Network (RNN)

RNN is a special category of neural networks capable of handling dynamic and spatial nonlinear dependencies (Bianchi et al., 2017). RNNs have demonstrated significant success in prediction, pattern identification and filtering of dynamic data (Obst and Riedmiller, 2012). An intrinsic characteristic of neural networks is that neural networks try to imitate the brain's ability to develop and establish patterns among variables (Onalo et al., 2018a). Complex network maps are created between the input elements, neurons and output elements by implementing certain activation functions (Hammer, 2000). RNNs are able to process sequential data better than feedforward neural networks due to the cyclic connections that RNNs establish (Sak et al., 2014). This allows the RNN to develop independent temporal activation functions even without input data. Hence, the term dynamic (Lukoševičius and Jaeger, 2009) The transfer functions are applied over each sequential input datum to predict the desired output. In addition, at each time step, RNN considers previous inputs, output and computational weight functions which are mapped through the hidden layer neurons (Bianchi et al., 2017). This demonstrates the superior quality of the RNN to store information, indicating a memory function. The memory capacity of RNN is not infinite; it is limited in size, depending on the specific RNN model adopted (Weston et al., 2015). Some RNN which capture the nonlinearity and dynamic nature of a dataset in neural networks include Elman, long short-term memory, gated recurrent unit, echo state network and nonlinear autoregressive RNNs (Bianchi et al., 2017). In this study, a nonlinear auto-regressive RNN model with exogenous inputs is proposed for the dynamic prediction of sequential sonic well log data from minimal well logs.

7.2.1 **Nonlinear auto-regressive with exogenous inputs (NARX)**

The NARX model refers to a dynamic RNN developed after nonlinear discrete-time models (Leontaritis and Billings, 1985; Siegelmann et al., 1997). In contrast to other RNNs, NARX does not depend on the entire internal network state to establish long-term dependencies, but on the output feedback (Menezes Jr and Barreto, 2008). NARX is based on autoregressive models that have an external estimator and regressor (Matlab Documentation, 2018). The NARX state is controlled by the set of tapped delay lines (TDL), usually two, one for the input vector and one for the output vectors (Siegelmann et al., 1997). The TDL contains the current and past time-step data. In NARX, when the predicted output is fed back as input into the neural network to estimate the new output, this is referred to as a parallel architecture, as shown Figure 7.1 (Menezes and Barreto, 2008). In series-parallel architecture, the actual output, which is available for the training, is used directly as inputs to estimate the output as illustrated in Figure 7.2.

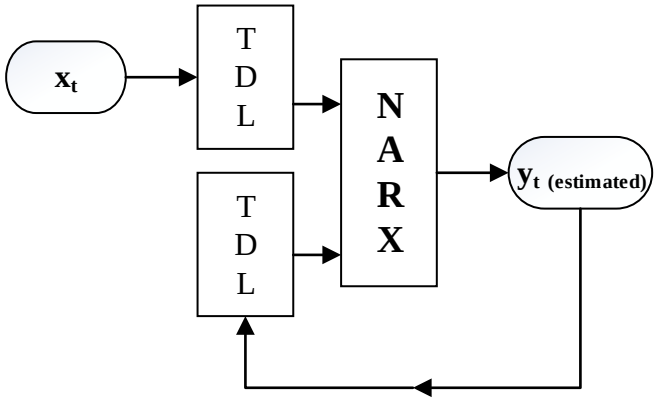

Figure 7.1: Parallel NARX architecture

In the parallel architecture, once the network parameters have been learned and established by the network, or in scenarios where the output is missing or incomplete, the output can be disconnected.

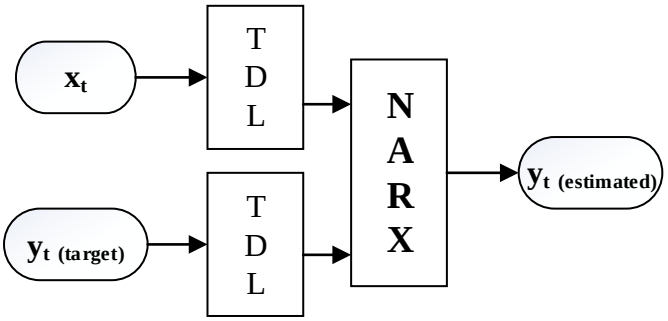

Figure 7.2: Series-parallel NARX architecture

This presents a major advantage of the NARX network. In addition, two taped layered delay lines of NARX models enable them to apply the gradient descent techniques to learn long-term temporal dependencies of large datasets (Diaconescu, 2008; Menezes and Barreto, 2008). In many instances, NARX has been equated to Turing machines (Bianchi et al., 2017; Diaconescu, 2008; Siegelmann et al., 1997). These models are very efficient at predicting and estimating the value of dynamic time series data; they converge and generalize data faster than other RNN (Çoruh et al., 2014).

7.3 **Methodology to develop the NARX model**

The outline for the suggested methodology is presented in Figure 7.3

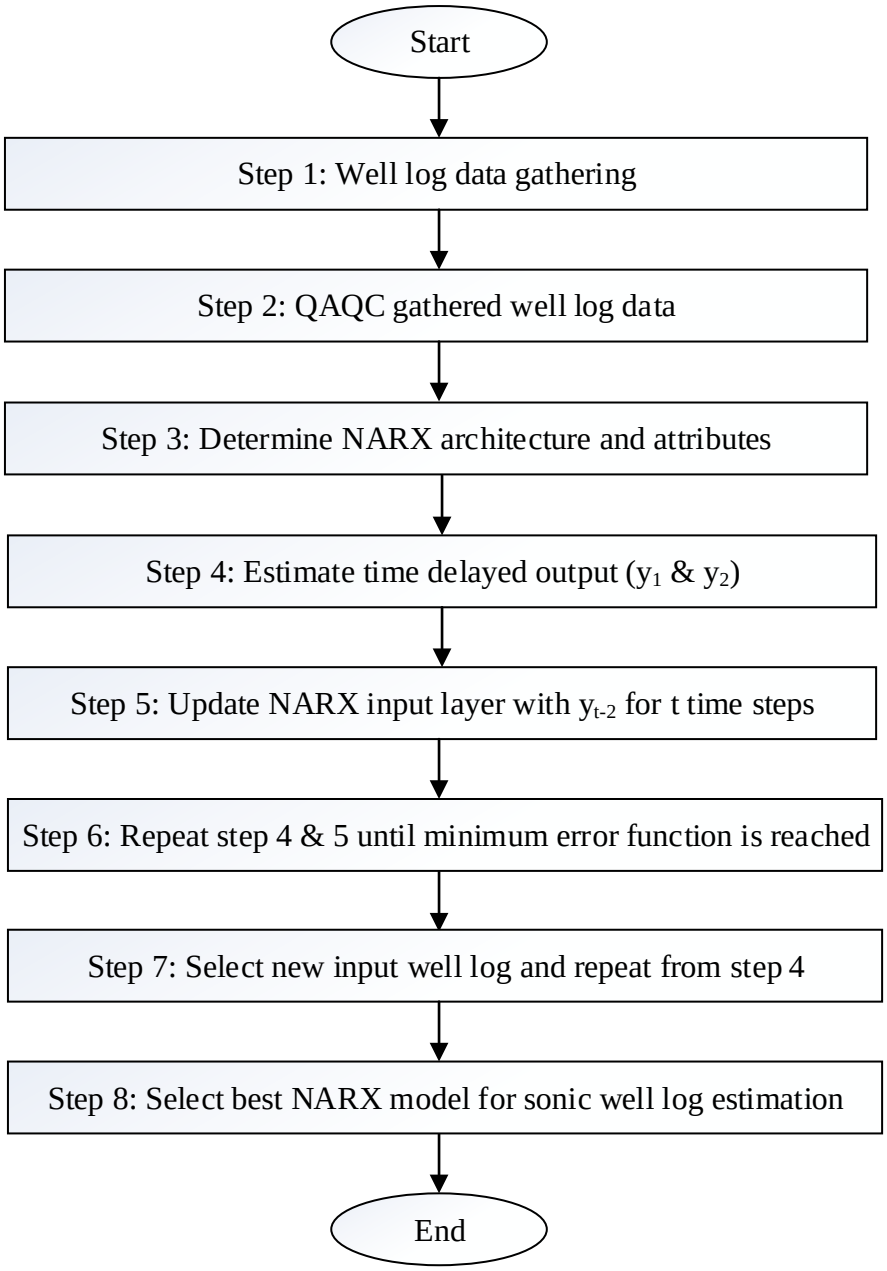

Figure 7.3: Proposed NARX model methodology flowchart

7.3.1 Collection and determination of data for NARX

In order to investigate the suitability of the NARX model for the prediction of sonic well logs, actual well log data is needed for the development of the models. Well logs from eleven wells were acquired, six from Norway and five from West Africa. The data contains the respective depths, sonic, bulk density, gamma ray, caliper, resistivity and neutron logs.

7.3.2 Quality assurance and quality control (QAQC)

The well log data have had quality assurance and quality control (QAQC) performed on all the selected datasets that have been used in this study to ensure that the data were reliable and accurate. Caliper logs were used to eliminate borehole irregularities, key seats and wash out sections where the tools may have generated false readings. Shallow sections of the data without the corresponding required logs were also eliminated from the dataset. Poisson's ratio was used to quality check the well log data to ensure the data were within acceptable limits, except in cases were anisotropic formations were suspected.

7.3.3 Development of NARX model architecture

An illustration of the proposed NARX model is presented in Figure 7.4.

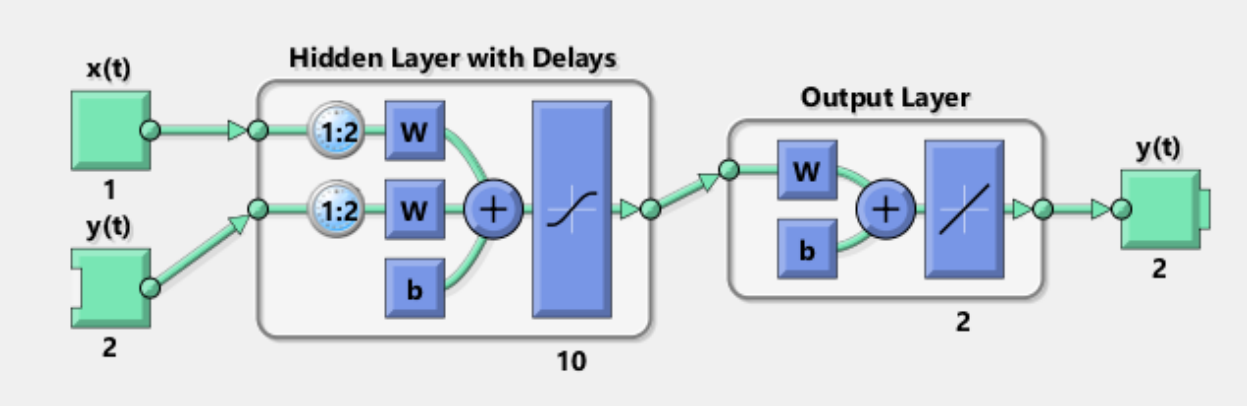

Figure 7.4: Proposed NARX network model adopted from MATLAB documentation

The proposed NARX architecture chosen for this study is a parallel architecture with three layers and 10 hidden neurons which has been implemented using MATLAB. The NARX model is a three-layer recurrent neural architecture implemented by a feedforward neural network. The NARX layers consist of input, hidden and output layers. The input layer is made up of one or two inputs matrices ($x_{GR} \in x_t$) while the output layer is made up of two output matrices ($y_{DTC}\ and\ y_{DTS}\ \in y_t$). The data should be configured for the input and target layers, which includes the normalization of the data to values ranging between 0 - 1.

The output equation can be written as follows (Bianchi et al., 2017):

$$y_t = f(x_{t-2}, x_{t-1}, x_t, y_{t-2}, y_{t-1}, \lambda) \tag{7.1}$$

Where f () is the nonlinear function, λ are trainable hyperparameters, 1 and 2 represent the dx and dy which are the input and output time delays respectively.

Therefore, the input layer would consist of the two tapped delay lines (TDL) as follows:

$$i_t = \begin{bmatrix} (x_{t-2}, x_{t-1})^T \\ (y_{t-2}, y_{t-1})^T \end{bmatrix}^T \tag{7.2}$$

The following equations govern the output network (Bianchi et al., 2017)

$$h_t[1] = f(i_t, \theta_i) \tag{7.3}$$

$$h_t[2] = f(h_{t-1}[1], \theta_h[1]) \tag{7.4}$$

$$y_t = g(h_{t-1}[2], \theta_o) \tag{7.5}$$

$$\lambda = \{\theta_i, \theta_h, \theta_o\} \tag{7.6}$$

$$\theta_i = \{w_i^{h1}, b_{h1}\} \quad (7.7)$$

$$\theta_o = \{w_{h2}^{o}, b_o\} \quad (7.8)$$

$$\theta_h = \{w_{h1}^{h2}, b_h\} \quad (7.9)$$

Where g () is a linear function applied to the output of the last hidden layer to produce the output, $h_t[1]$ is the first hidden layer at time t; w and b are the weight and bias of the neuron connections (θ) for the respective layers. w_i^{h1} is the weight for the h1 with a previous layer-i.

The Levenberg-Marquardt function is used as the optimization function for the feedforward network hidden layer to train, validate and test the model. The loss error function is updated based on the mean square error (MSE) performance. The main features of the NARX architecture are presented in Table 7.2.

Table 7.2. Main features of the proposed NARX model

NARX model	Parameters
Network architecture	Parallel Feedforward
Input data	Gamma-ray and/or neutron porosity
Number of layers	3
Number of neurons	10
Input time delay	2
Output time delay	2
Output data	Sonic well log data
Optimization algorithm	Levenberg-Marquardt
Loss function	MSE

7.3.4 **Learning and training of the NARX**

The process by which the model updates the current inputs, previous inputs and outputs to predict future outputs is referred to as the learning process of the model. The model learns with the aim of minimizing the loss function, including the differential error between the outputs (actual and

estimated) and regularization parameters (Bianchi et al., 2017). The proposed model uses a dynamic feed forward back propagation algorithm to determine the gradients. Dynamic backpropagation algorithms are more complex than static backpropagation because the error surfaces of dynamic networks are more complicated and could be stuck in a local minima (Diaconescu, 2008). The input data set should be analyzed to avoid overfitting. The Levenberg-Marquardt algorithm is applied to the model for fast convergence of the model. This is especially beneficial in real-time predictive models. For the proposed NARX model development, the gamma ray is initialized as input to the first model.

7.3.5 **Generalization of the NARX**

Generalization of a model is an important feature of any model. The developed model must be able to adequately describe the relationship in the training dataset such that, the relationship is applicable for a dataset outside the training dataset. If the model successfully describes the relationship in the training dataset but fails to validate and test the model on an external dataset, the model is said to be poor. To avoid this, the dataset has been divided into three sets namely, training (70%), validation (15%) and testing (15%). In addition, a 5-V fold cross-validation is applied to the dataset to improve the model. This involves the partitioning of the data in five random equal subsets where four sets are used to train, and one is used to validate the model (Arlot and Celisse, 2010). More so, the methodology is applied to different well logs from different geographical regions.

7.4 Results and discussion

To test and validate the proposed NARX model presented in section 7.3, real well log data from actual reservoir formations have been gathered. Recently, Equinor, an operator in the North Sea and Volve license partners released subsurface and operating data to the public from the Volve field located in the Norwegian continental shelf. Six wells from the field have been selected for this study along with five well from West African fields. All the well from the Nigerian reservoirs are from different fields located onshore and offshore in Nigeria. Details of the wells are presented in Table 7.3.

Table 7.3. Available Well Data Summary

Well	Log interval (ft)	Lithology	Well type	Location
1A	8592 - 11949	Shale - sand	Oil	Offshore North Sea Norway
1B	9839 - 11235	Shale - sand	Water	Offshore North Sea Norway
11A	8474 - 12215	Shale - sand	Oil	Offshore North Sea Norway
11T2	8474 - 14807	Shale - sand	Oil	Offshore North Sea Norway
14	9128 - 12175	Shale - sand	Oil	Offshore North Sea Norway
4	9064 - 11395	Shale - sand	Water	Offshore North Sea Norway
AJ	2856 - 12563	Shale - sand	Gas condensate	Offshore Nigeria
AS	7974 - 10392	Shale - sand	Gas	Onshore Port-Harcourt Nigeria
EJ	1023 - 8095	Shale - sand	Gas	Onshore Port-Harcourt Nigeria
KC	6033 - 16608	Shale - sand	Oil	Offshore Port-Harcourt Nigeria
OK	8983 - 16161	Shale - sand	Oil	Offshore Warri Nigeria

7.4.1 Model development and calibration

Well 1A of the Volve field has been used for the calibration of the model applying the parameters presented in Table 4.2. The details of this well are described in section 7.5.1. The model is developed using the Levenberg-Marquardt (LM) algorithm; however, the LM model performance has been compared with the performance of the Bayesian Regularization (BR) algorithm using the same input parameters. This is to verify that the model has not been overtrained which is a major

problem with small data using LM algorithm due to the fact that LM stops once MSE has been minimized (Demuth et al., 2008). BR, on the contrary, provides a suitable generalization of the model by continually optimizing the weights and bias. The performance of the models is analyzed based on the MSE and is presented in Figure 7.5 and summarized in Table 4.4.

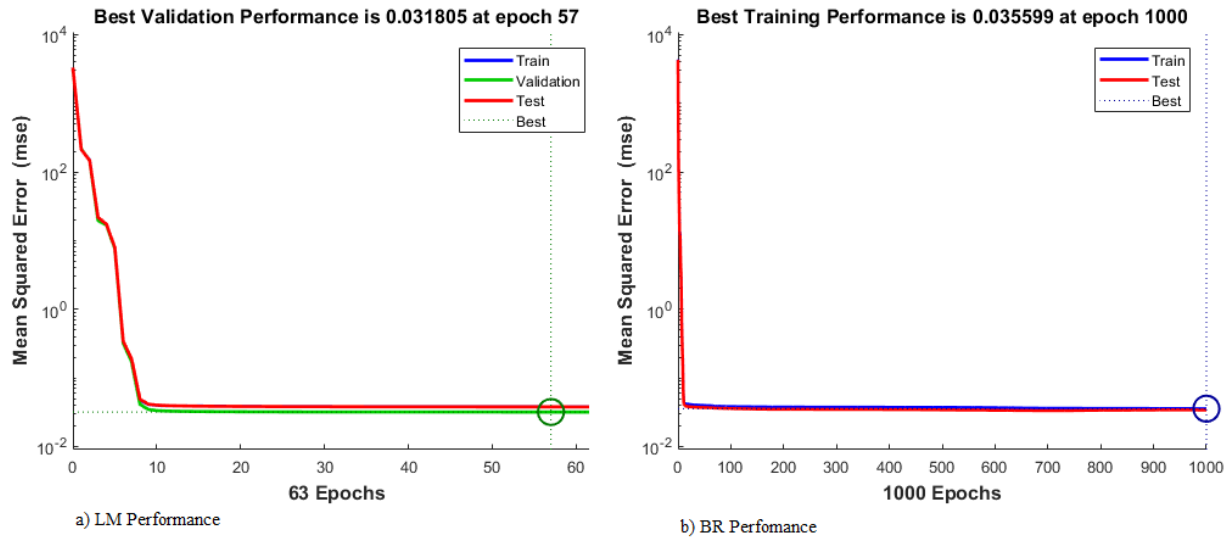

Figure 7.5. LM and BR model performance

The iteration stops as rightly pointed out once the MSE of verification set minimized at 57 epochs for Levenberg-Marquardt. For BR, it continued until the set maximum number of iterations (1000). However, the overall MSE value for the LM and BR algorithm are very similar indicating the LM was not over trained.

Table 7.4. Model Development and calibration

Model	Stage	Datapoints	MSE	MSE
Training algorithm			Levenberg-Marquardt	Bayesian-Regularization
GR1A	Training	7150	0.038	0.038
	Validation	1532	0.032	
	Testing	1532	0.038	0.034
	All	10214	0.032	0.032

7.4.2 **Model parameter selection**

The simulation package used in the development of the NARX model provides standard network architectural parameters to help new users build reliable models. Users can optimize these parameters such as layers, time delays and neurons. To demonstrate this, the base LM model which contains 10 neurons is compared with models containing 5 and 20 neurons respectively. The MSE performance is also provided in Figure 7.6. Figure 7.6 shows that 10 neurons perform better than the 5 and 20 neurons. Similarly, the number of time delays in the base model is two. It is compared with 5- and 10-time delays, and the performance of the models is seen in Figure 7.7. Figure 7.7 points to 5-time delays as the better choice. However, the two-time delay has been chosen for further model development to simulate less available reliable data in the field.

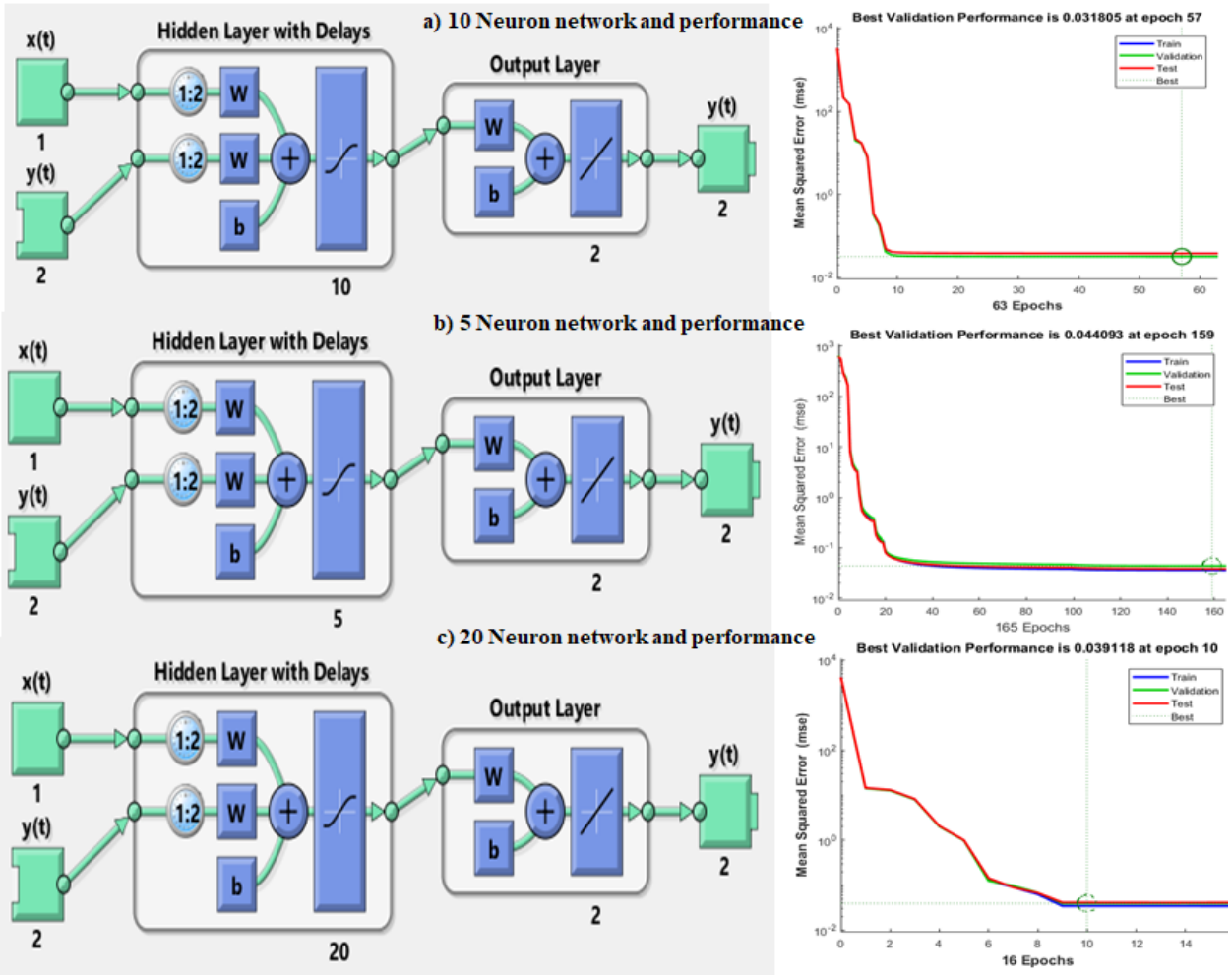

Figure 7.6. Model parameter selection based on the number of hidden layer neurons

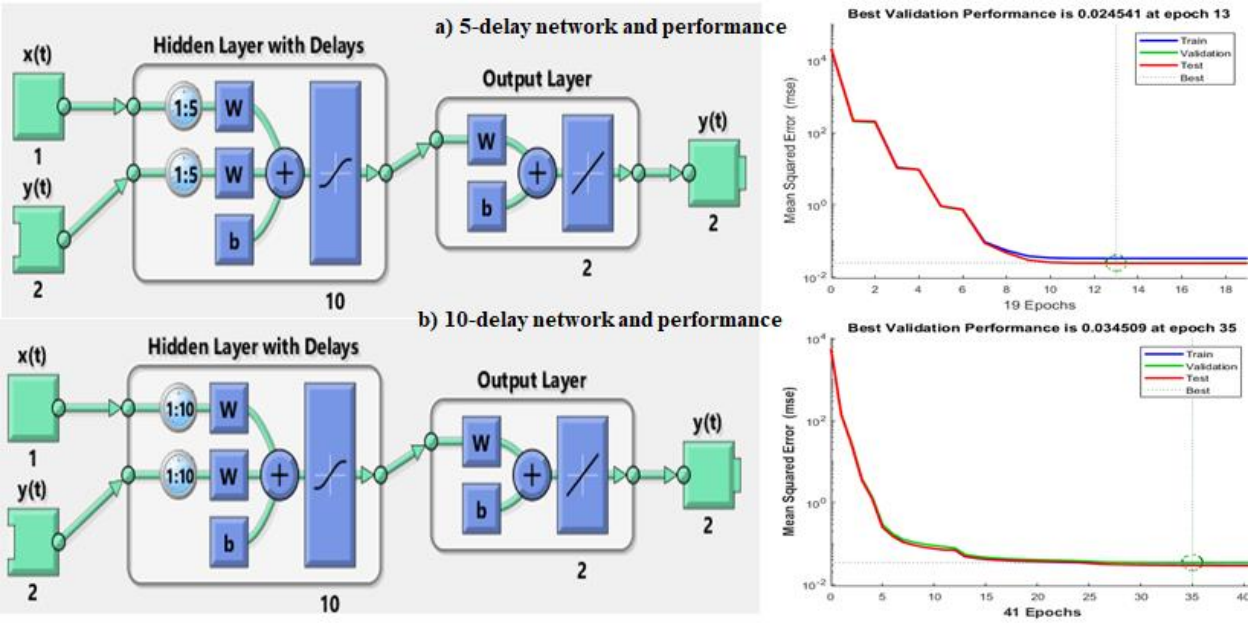

Figure 7.7. Model parameter selection based on the number of time delays

7.4.3 **Model testing and validation**

To test the calibrated model, the model is applied to external data from ten wells. Five wells are from the Volve field located in the Norwegian continental shelf and five wells, each from different fields, are found in West Africa. Both the LM and BR models are applied to test the robustness of each model. A summary of the test and validation is presented in Table 7.5. The Models are named as follows. For example GR1B means model developed with Gamma ray exogenous input from well 1B.

Table 7.5. Testing of the model on external data

Training algorithm		Levenberg-Marquardt	Bayesian Regularization
Model	Datapoints	MSE	MSE
GR1B	3808	0.39	0.42
GR11A	11084	0.45	12.46
GR11T2	18721	0.41	12.14
GR14	6094	0.258	2.55
GR4	4246	0.38	0.38

GRAJ	17526	1604.23	3535.22
GRAS	4273	14.97	29.58
GREJ	16923	2869.43	5624.42
GRKC	16608	11.59	21.15
GROK	16161	0.46	0.48

As postulated, the model accurately models the sonic logs in the Volve field in Norway but with less accuracy in the wells located in the West African region. However, Well-OK was modeled accurately by the model. The model fails in wells AJ and EJ. This could be due to the fact that the calibration model is from a well located in the Volve field. This suggests that localized models can be developed with more well data from a particular field thereby eliminating the need for continuous sonic logging in new wells in the same field. This confirms that both compressional and shear travel time logs are sequential and temporal in formation sonic logging. It can also be observed that the LM based models outperformed the BR models in all wells; therefore, LM is recommended for subsequent models in this paper.

7.5 Case study

In an attempt to provide the reader with the use of such models, a demonstration of sonic formation evaluation has been conducted on three wells namely, 1A, 1B and OK.

7.5.1 First Case study - Well 1A.

The well used for the first case study is referred to as Well 1A, corresponding to wellbore name – 15/9-F-1A of the Norwegian Volve field. The operators state that the well is an observation well drilled into a sandstone formation from the Jurassic age Hugin formation. It is an offshore well with a water depth of 91 meters and a total depth of 3240 meters. The fluid content of the reservoir formation is oil; therefore, it is referred to as an oil observation well. For this study, an interval of 8600 feet to 11900 feet has been chosen (Equinor, 2018a). The well log data gathered for the study are presented in Figure 7.8 and the data can be accessed via the Equinor website (Equinor, 2018b). The NARX model framework described in section 7.3 is utilized on the well log data. The target values for the NARX model include a matrix containing the sonic compressional travel time and sonic shear travel time logs of the formation**.**

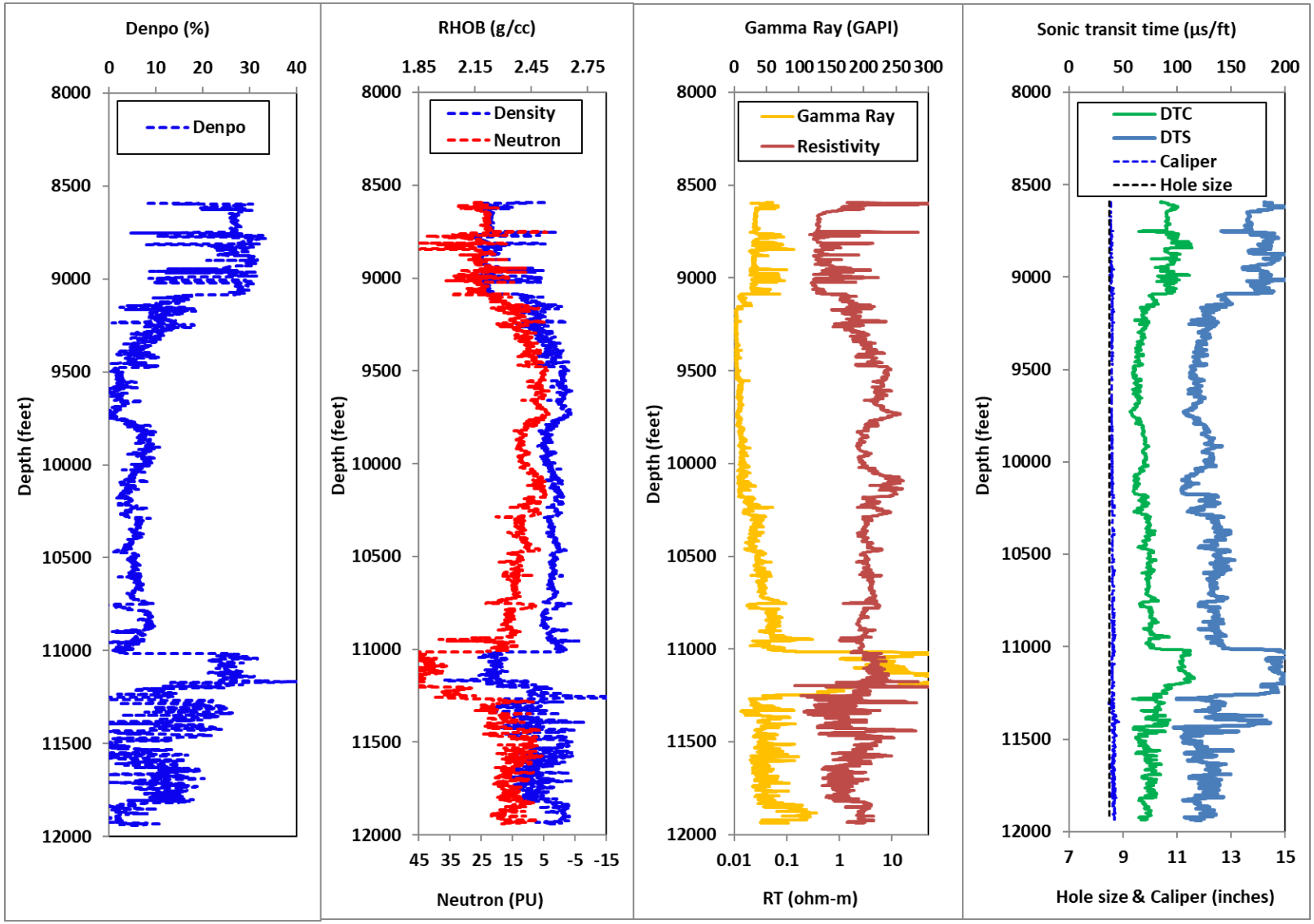

Figure 7.8. Well 1A log data

The predicted sonic log from the NARX model is plotted over the measured sonic log versus the corresponding formation depth in Figure 7.9. Figure 7.9 denotes that the model accurately follows the measured trend of the sonic logs for Well A.

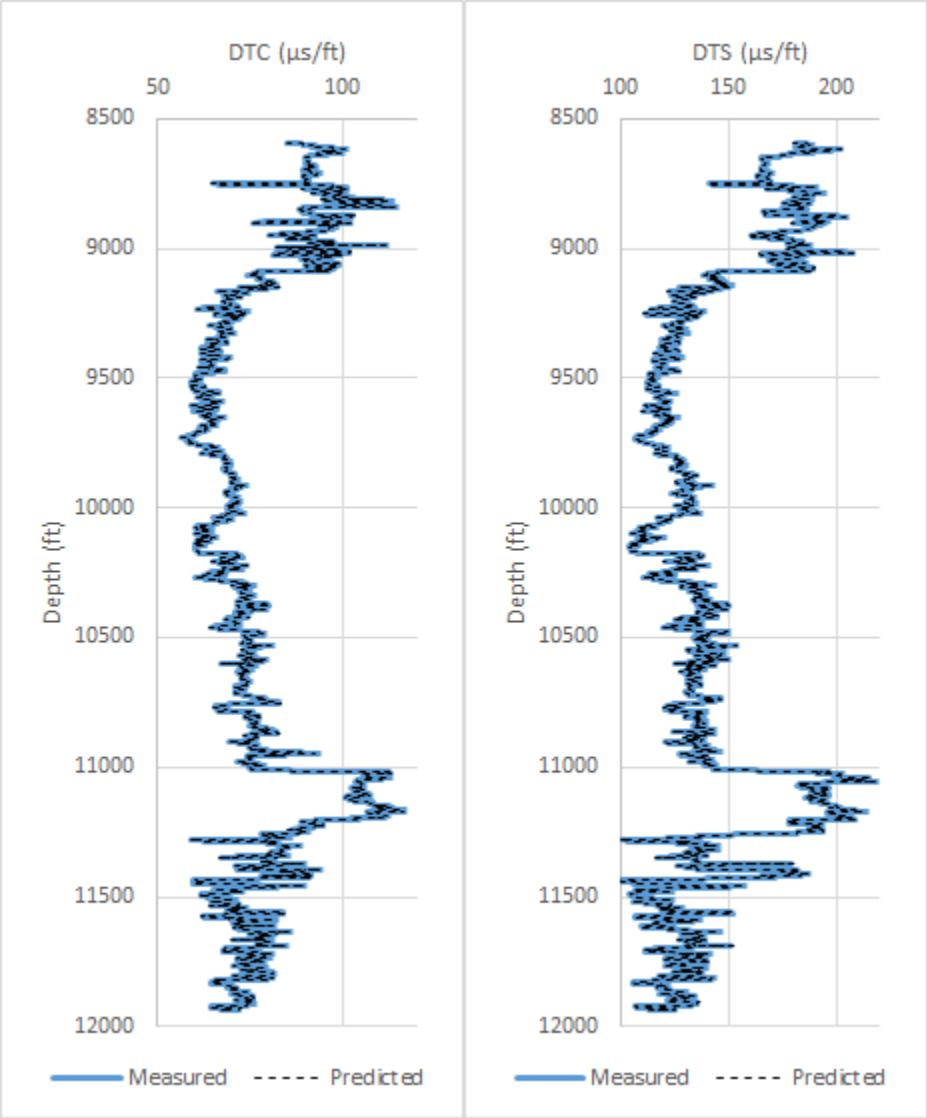

Figure 7.9. Measured and predicted sonic well logs versus depth

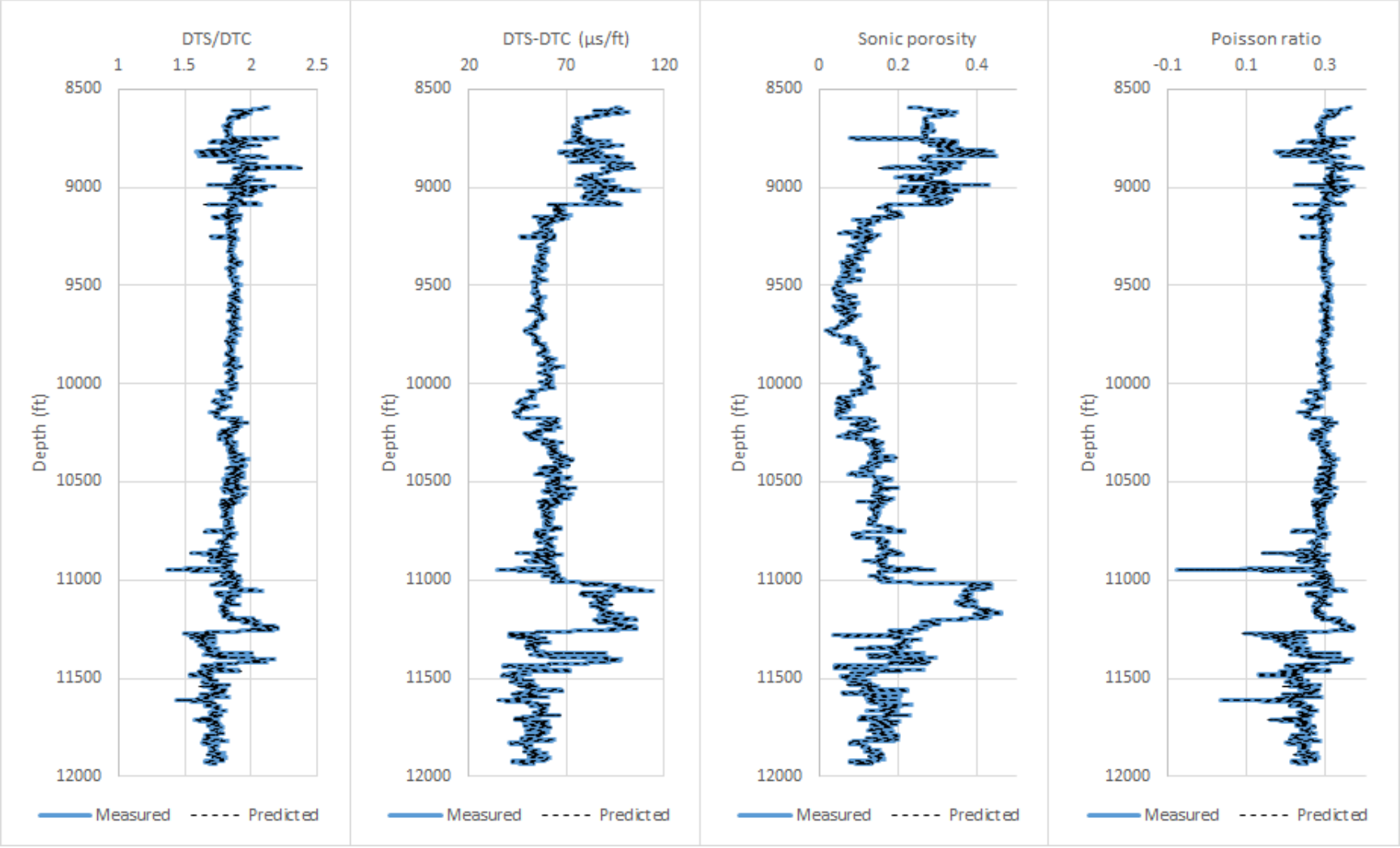

Figure 7.10. Well 1A formation evaluation properties

Table 7.6. Statistical analysis of Well 1A formation evaluation properties

Formation property	MSE	AAE
DTS/DTC	0.000	0.002
DTS-DTC	0.049	0.116
Sonic porosity	0.000	0.001
Poisson ratio	0.000	0.001

The sonic formation evaluation properties for well A are illustrated in Figure 7.10. Table 7.6 shows that the MSE and AAE for the sonic parameters are reasonably low. Evaluation based on Figure 7.8 and Figure 7.10 shows that the top section is a shaley water saturated formation from 8600 feet to 9100 feet, hence, the increase in sonic difference and sonic ratio. 8600 feet to 10200 feet is comprised of a sandstone reservoir formation with typical sonic ratios of 1.7 – 1.8 (Domenico, 1984; Tatham, 1982). The sonic porosity reduction is as a result of compaction with depth.

7.5.2 **Second Case study -Well 1B**

The investigated well in the second case study is referred to as Well 1B and corresponds to the wellbore name 15/9-F-1 B of the Volve field in Norway. The well is an injection water well, located offshore in the North Sea. The formation is also a water saturated sandstone (Equinor, 2018a). The well log data for Well 1B is presented in

Figure 7.11 and can also be found on the Equinor website (Equinor, 2018b). Logging of this well begins at about 9842 feet up until about 11155 feet. An interval from 10240 feet to 10390 feet has been quality checked for this study. The NARX model framework is applied to Well 1B using

gamma ray logs as the exogenous input log to reproduce the sonic logs of the well. However, several sections of the gamma ray well log data have been intentionally omitted as highlighted in

Figure 7.11 to simulate missing data**.** Figure 7.12 suggests that the NARX model with gamma ray logs as exogenous inputs which have missing data to predict sonic well logs is feasible, as shown by the success of the model. Furthermore, the predictions confirm that sonic well logs are sequential along the wellbore and thus, their predictions can be better modeled with time sequential techniques. The sonic formation evaluation properties for Well 1B are illustrated in

Figure 7.13. The MSE and AAE of Well 1B sonic parameters are provided in Table 7.7, indicating minimal errors between the model predicted parameters and actual sonic log parameters.

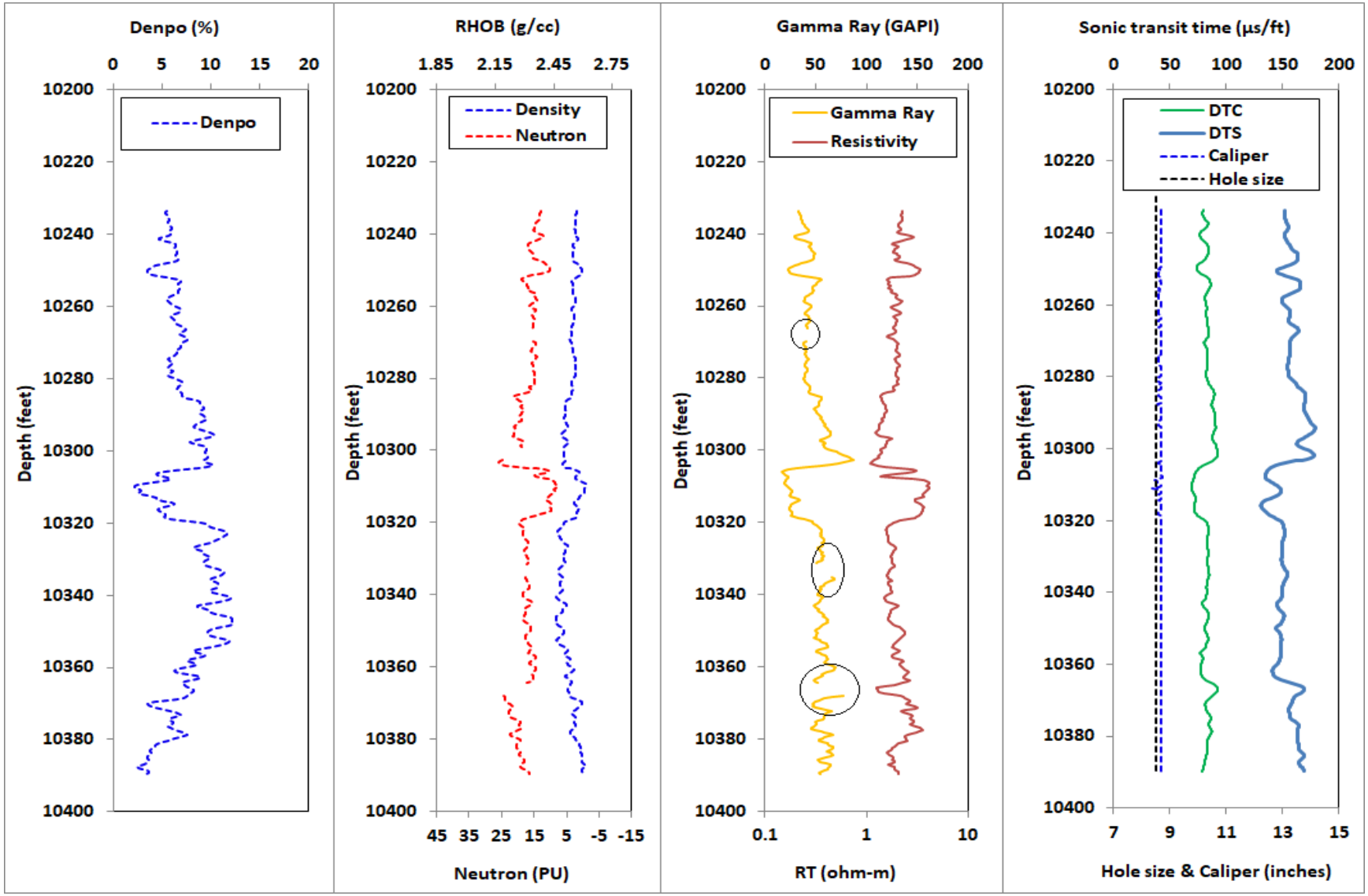

Figure 7.11. Well 1B well log data

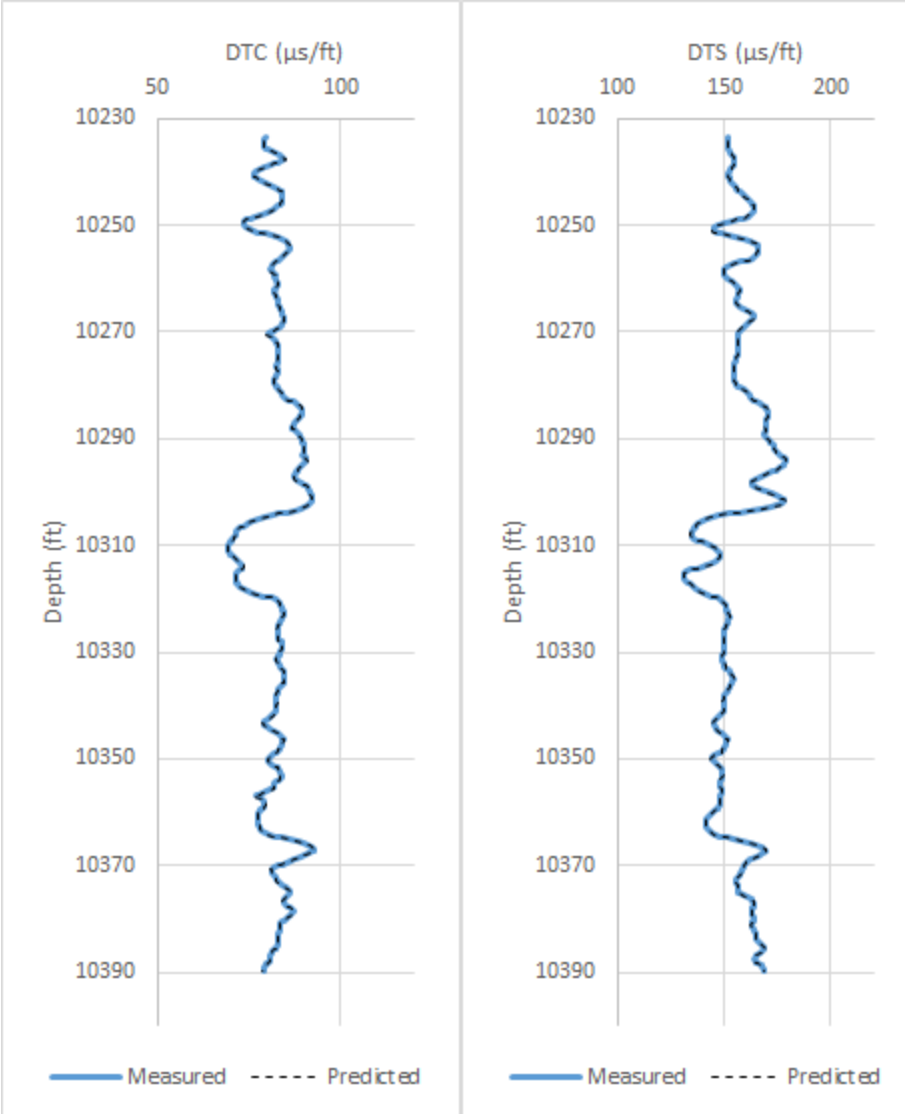

Figure 7.12. Measured and predicted sonic well logs versus depth

Figure 7.11 and

Figure 7.13 indicate a water saturated shaley formation from the top of the well section to 10300 feet, where a sandstone reservoir begins with possibly hydrocarbon, present for 20 feet. This section appears to be denser with lower porosity. The lower section of the formation appears to be water saturated shaley sands.

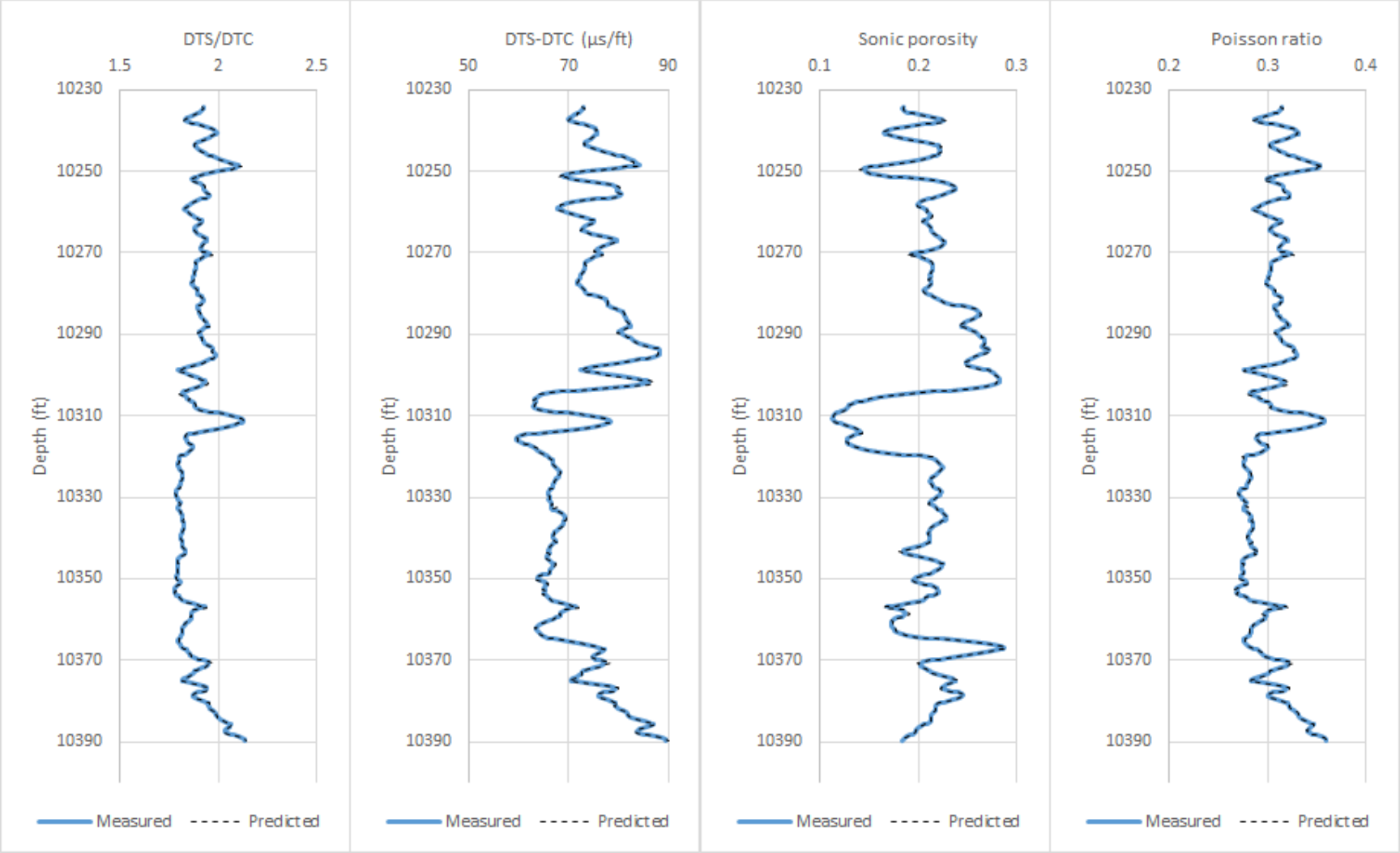

Figure 7.13. Well 1B formation evaluation properties

Table 7.7. Statistical analysis of Well 1B formation evaluation properties

Formation property	MSE	AAE
DTS/DTC	0.000	0.004
DTS-DTC	0.157	0.265
Sonic porosity	0.000	0.001
Poisson ratio	0.000	0.001

7.5.3 **Third Case study – Well OK**

The third case study well is marked as Well OK, to ensure that the success of the NARX model observed in the Volve field is not only applicable to the Norwegian continental shelf. A formation in the Niger Delta basin of West Africa is chosen as the third case study and called Well OK. The well investigated in this case study is an offshore oil well located in a shaley-sandstone formation. An interval of 9000 feet to 13000 feet of well log data has been made available for this study. Due to proprietary issues and to respect the confidentiality of the owners of the well, further details of the well have not been made public in this study.

Similar to the previous case studies, the different configurations of the NARX model framework are applied to Well OK. The results of the prediction of the optimum NARX model are plotted for the measured sonic logs versus the depths in Figure 7.15. This points to the fact that the model is also sufficient and accurate in that field in West Africa. The sonic formation evaluation properties for Well OK are presented in Figure 7.16. The sonic parameters' statistical properties like MSE and AAE for Well OK are provided in Table 7.8, demonstrating a close match between the model predicted parameters and actual sonic log parameters. Figure 7.14 and

Figure 7.16 suggest a shaley formation with interbedded sands saturated with water to a depth of about 10900 feet. A water-saturated sandstone reservoir is seen from 11000 feet to 11500 feet. A

100-foot interval of potential hydrocarbon sandstone reservoir play begins around 12100 feet. The sonic ratio and difference suggest this also. In addition, the sonic porosity suggests a normal compaction trend with depth.

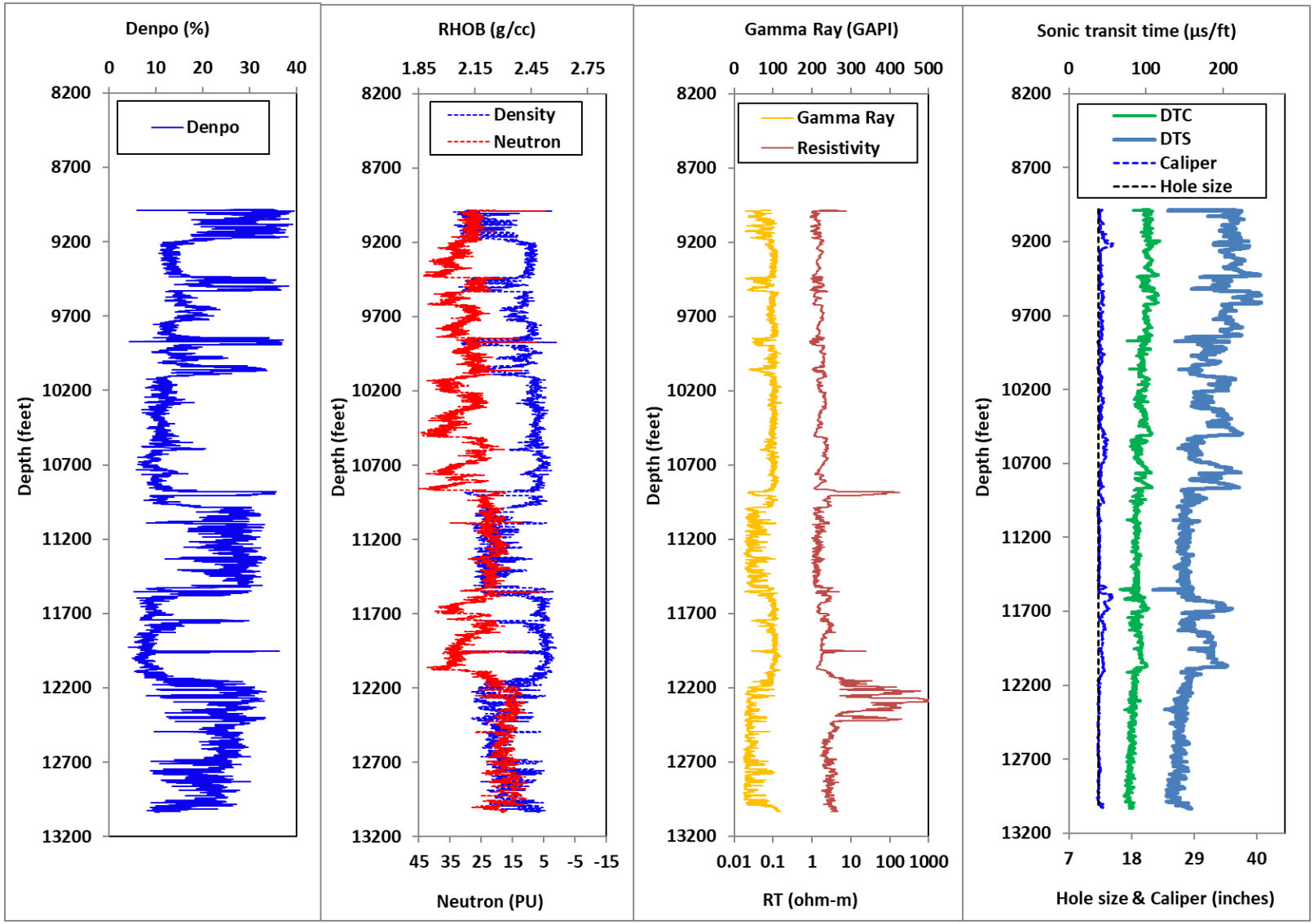

Figure 7.14. Well OK well log data

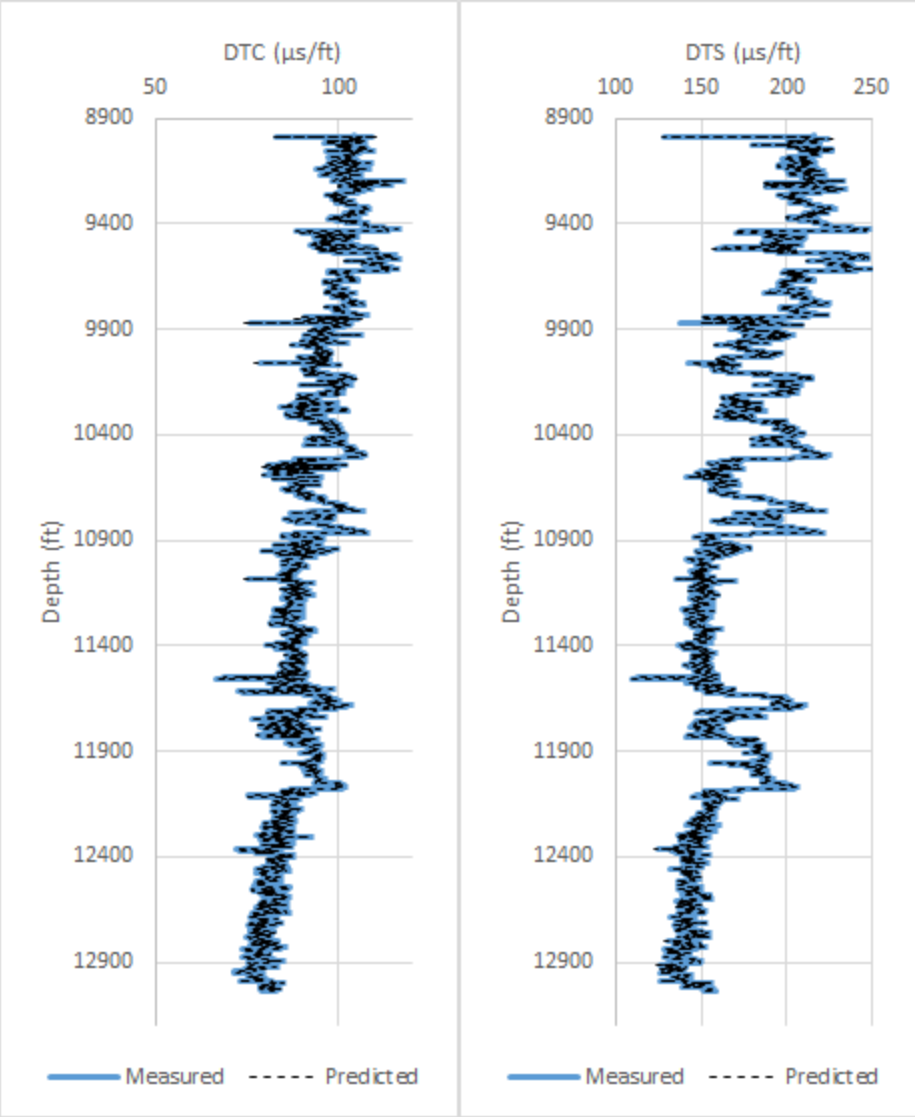

Figure 7.15. Well OK measured and predicted sonic well logs versus depth

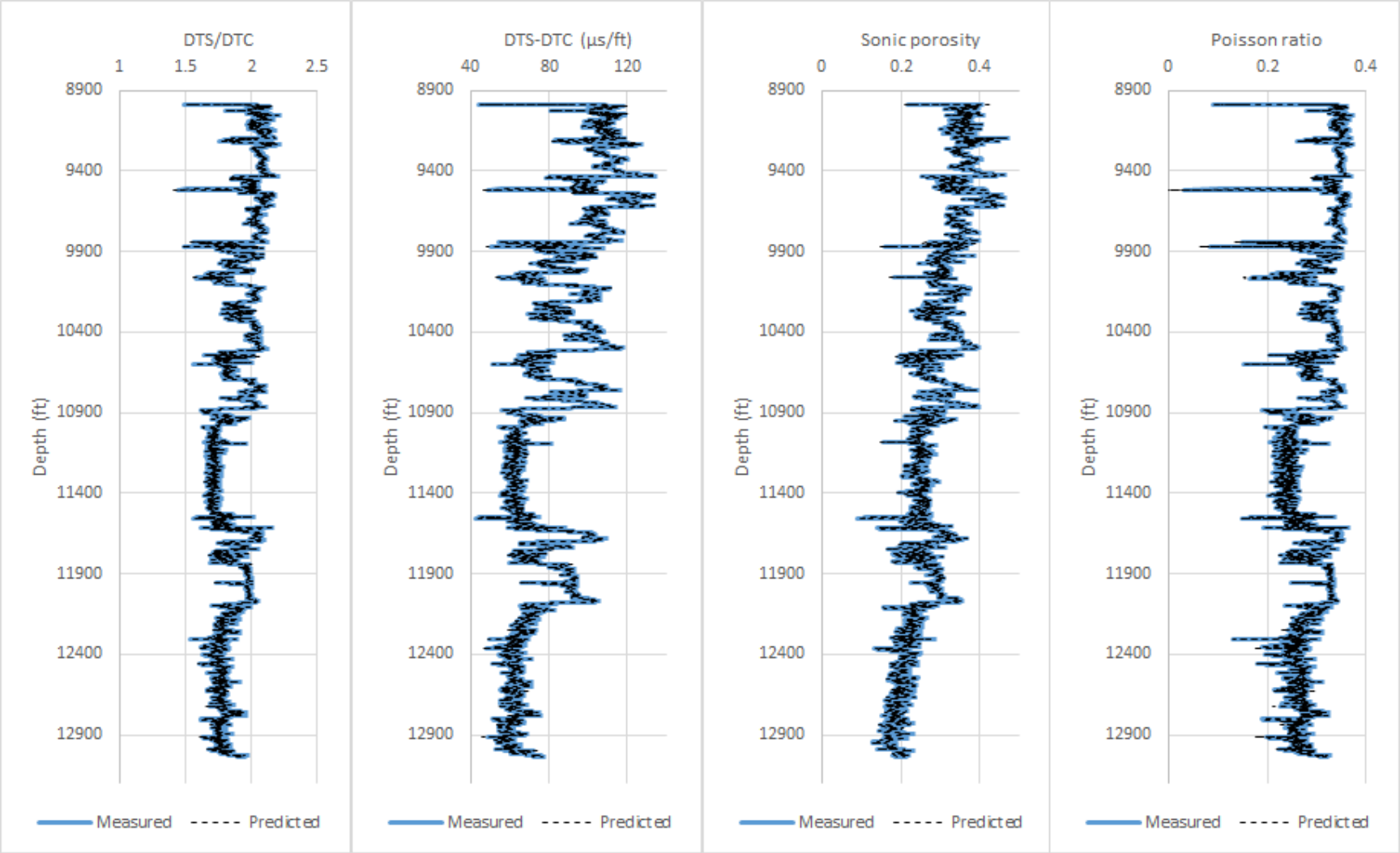

Figure 7.16. Well OK formation evaluation properties

Table 7.8. Statistical analysis of Well OK formation evaluation properties

Formation property	MSE	AAE
DTS/DTC	0.000	0.003
DTS-DTC	0.512	0.290
Sonic porosity	0.000	0.001
Poisson's ratio	0.000	0.001

The application of the suggested framework methodology on the well log data is a significant step forward. The authors are not aware of any NARX RNN model which reproduces sonic logs from neutron and/or gamma ray logs. Nevertheless, the application of RNN comes with certain challenges. Learning the long-term dataset dependencies presents a challenge of the model over time; therefore, the training optimization might become limited (Salehinejad et al., 2017). RNNs are still subject to vanishing and exploding gradient issues. Although more data and deep networks enhance memory function, the challenge becomes obvious when previous data beyond the memory capacity have to be reintroduced back into the network (Bianchi et al., 2017). Overfitting is another challenge encountered in RNN development; however, this is often addressed with regularization techniques such as activation preservation, dropout and activation stabilization (Salehinejad et al., 2017). The tested models capture the complexity and diversity in their respective reservoir formations. However, care must be exercised in applying the model to other geological settings different from those presented in this paper. The codes and data format have been provided to aid interested users. A sample of the codes used to develop the models has been provided in the supplementary data for potential users. The essence of the three case studies, codes and sample

data provided in this paper is to encourage learning and the extension of the model by other researchers with access to more data to test the methodology on their formations.

7.6 Conclusions

The current study has confirmed that compressional and shear sonic logs are sequential data that can be accurately modeled with recurrent neural networks. Particularly, the NARX model proved to be highly capable of predicting and reproducing sonic logs of reservoir formations with one or two exogenous inputs.

The results of the NARX model applied to all wells has shown the efficiency of the model as an effective and reliable dynamic technique for reproducing actual sonic well logs.

. The suggested methodology offers the petroleum industry benefits such as:

- The NARX model proffers a solution to estimating sonic logs where there are missing well log data sections.
- The NARX model offers the ability to reproduce and regenerate sonic well logs for the recalibration and quality check of actual sonic logs.
- The NARX model provides a cheap and efficient solution for formations where sonic logging has not been budgeted for, due to economic or time constraints.
- The NARX model provides the ability to determine several sonic derived formation property evaluation parameters to analyze reservoir formations.

In general, recurrent neural networks such as NARX are very efficient at determining nonlinear patterns in sequential and temporal data. Sonic well logs are no exception. In place of running several sonic logging tools when erroneous or misleading sonic data have been recorded or where the sonic logging tools have been damaged, the NARX RNN model presented in this study can be an economical and risk-free method of accurately reproducing the sonic well logs of the formation.

Acknowledgment

The primary author thankfully acknowledges the financial support provided by the Hibernia Management and Development Company (HMDC), the Natural Science and Engineering Council of Canada and the Canada Research Chair (CRC) Program, Innovate NL and Chevron Canada for their support. We also wish to thank Equinor who made the data available via their website (Equinor, 2018b) As stated on the website, “The Volve Data were approved for data sharing in 2018 by the initiative of the last Operating company, Equinor and approved by the license partners ExxonMobil E&P Norway AS and Bayerngas Norge AS in the end of 2017”.

Nomenclature

ANN	Artificial neural network
RHOB	Bulk density log (g/cm^3)
K	Bulk modulus (Mpsi)
DT	Travel time (µsec/ft)
DTC or DTCO (Δt_c)	Compressional travel time (µsec/ft)
y_{DT}	Compressional sonic log target data
RESD	Deep log resistivity (ohm.m)
Denpo (ϕ_{den})	Electron density porosity (g/cm^3)
GR_{min}	Gamma ray in clean sandstone
x_{GR}	Gamma ray input data
GR_{min}	Gamma ray in shale
GR	Gamma ray log (gAPI)
x_t	Input layer
ρ_{ma}	Density of matrix (g/cm^3)
AAE	Absolute average error
MPE	Mean percentage error
Δt_{log}	Measured compressional travel time (µsec/ft)
x_N	log input data
NPHI (ϕ_N)	Neutron porosity
$\phi_{N,fl}$	Neutron response of the fluid
$\phi_{N,ma}$	Neutron response of the matrix
NARX	Nonlinear autoregressive neural network with exogenous
PEF	Photoelectric factor
ϑ	Poisson's ratio
RNN	Recurrent neural network
ϕ	Porosity of rock
Vsh	Volume of shale
G	Shear modulus (Mpa)
y_{DTS}	Shear sonic log target data
DTS or DTSM (Δt_s)	Shear wave travel time (µsec/ft)
ϕ_s	Sonic porosity
TDL	Tapped delay lines
E	Young's modulus (Mpsi)

Appendix: Supplementary data and information

Supplementary data and information which include sample well log data which contains the input and output data, the model predictions and sonic formation evaluation properties are presented in this document. The full data can be found on Equinor website (Equinor, 2018b). A sample code has also been provided for potential users.

Table 7.9. Actual and predicted sonic evaluation properties of 10 feet of well 1A

Depth (ft)	Sonic ratio		Sonic difference		Sonic porosity		Poisson's ratio	
	Actual	Predicted	Actual	Predicted	Actual	Predicted	Actual	Predicted
8600.16	2.08	2.08	97.41	97.56	0.27	0.27	0.35	0.35
8600.49	2.07	2.07	97.16	97.08	0.27	0.27	0.35	0.35
8600.82	2.07	2.07	96.89	96.85	0.27	0.27	0.35	0.35
8601.14	2.06	2.06	96.15	96.55	0.27	0.27	0.35	0.35
8601.47	2.05	2.05	95.41	95.37	0.27	0.27	0.34	0.34
8601.80	2.04	2.04	94.67	94.63	0.28	0.28	0.34	0.34
8602.13	2.03	2.03	94.26	93.90	0.28	0.28	0.34	0.34
8602.46	2.02	2.02	93.85	93.82	0.28	0.28	0.34	0.34
8602.78	2.02	2.02	93.45	93.43	0.28	0.28	0.34	0.34
8603.11	2.01	2.01	93.27	93.03	0.28	0.28	0.34	0.34
8603.44	2.01	2.01	93.11	93.08	0.28	0.28	0.34	0.34
8603.77	2.01	2.01	92.94	92.92	0.28	0.28	0.34	0.34
8604.10	2.01	2.01	92.93	92.75	0.28	0.28	0.34	0.34
8604.42	2.01	2.01	92.93	92.87	0.28	0.28	0.34	0.34
8604.75	2.01	2.01	92.92	92.89	0.28	0.28	0.34	0.34
8605.08	2.01	2.02	92.80	92.90	0.28	0.28	0.34	0.34
8605.41	2.01	2.01	92.65	92.66	0.28	0.28	0.34	0.34
8605.74	2.01	2.01	92.51	92.49	0.28	0.28	0.34	0.34
8606.06	2.01	2.01	92.40	92.34	0.28	0.27	0.34	0.34
8606.39	2.01	2.01	92.31	92.26	0.28	0.28	0.34	0.34
8606.72	2.01	2.01	92.21	92.16	0.28	0.28	0.34	0.34
8607.05	2.00	2.01	91.85	92.07	0.28	0.28	0.33	0.34
8607.38	2.00	2.00	91.40	91.46	0.28	0.28	0.33	0.33
8607.70	1.99	1.99	90.96	90.96	0.28	0.28	0.33	0.33
8608.03	1.97	1.98	90.26	90.52	0.29	0.28	0.33	0.33
8608.36	1.96	1.96	89.46	89.59	0.29	0.29	0.32	0.32
8608.69	1.95	1.95	88.66	88.70	0.29	0.29	0.32	0.32

8609.02	1.93	1.93	87.72	87.89	0.30	0.30	0.32	0.32
8609.34	1.91	1.91	86.72	86.82	0.30	0.30	0.31	0.31
8609.67	1.90	1.90	85.71	85.75	0.31	0.31	0.31	0.31
8610.00	1.88	1.88	85.01	84.76	0.31	0.31	0.30	0.30
8610.33	1.88	1.87	84.49	84.36	0.31	0.31	0.30	0.30
8610.66	1.87	1.87	83.97	84.03	0.32	0.32	0.30	0.30
8610.98	1.86	1.86	83.83	83.53	0.32	0.32	0.30	0.30

Sample MATLAB generated code for modeling sonic well logs

A sample of a MATLAB generated code of the modeling is presented below. The input data for the model are neuron logs and the output data are compressional and shear wave sonic logs.

Code

```
% The solution of an Autoregression task with an Exogenous Input with a NARX Neural Network
% The script has been generated by MATLAB Neural Time Series application
% 03-Aug-2018 23:57:19
%
% The variables are defined as follows:
%
%   Anp – The input time series.
%   Adtds – The feedback time series.

X = tonndata(Anp,true,false);
T = tonndata(Adtds,true,false);

% 'trainlm' training function is chosen

trainFcn = 'trainlm';  % Levenberg-Marquardt backpropagation.

% Model creation
inputDelays = 1:2;
feedbackDelays = 1:2;
hiddenLayerSize = 10;
net = narxnet(inputDelays,feedbackDelays,hiddenLayerSize,'open',trainFcn);

% Training and simulation data preparation
[x,xi,ai,t] = preparets(net,X,{},T);

% Divide the data for training, validation and testing
net.divideParam.trainRatio = 70/100;
```

```
net.divideParam.valRatio = 15/100;
net.divideParam.testRatio = 15/100;

% Network training
[net,tr] = train(net,x,t,xi,ai);

% Network testing
y = net(x,xi,ai);
e = gsubtract(t,y);
performance = perform(net,t,y)

% Network view
view(net)

% Plots
figure, plotperform(tr)
figure, plottrainstate(tr)
figure, ploterrhist(e)
figure, plotregression(t,y)
figure, plotresponse(t,y)
figure, ploterrcorr(e)
figure, plotinerrcorr(x,e)

% Closed Loop Network
netc = closeloop(net);
netc.name = [net.name ' - Closed Loop'];
view(netc)
[xc,xic,aic,tc] = preparets(netc,X,{},T);
yc = netc(xc,xic,aic);
closedLoopPerformance = perform(net,tc,yc)

% Step-Ahead Prediction Network
nets = removedelay(net);
nets.name = [net.name ' - Predict One Step Ahead'];
view(nets)
[xs,xis,ais,ts] = preparets(nets,X,{},T);
ys = nets(xs,xis,ais);
stepAheadPerformance = perform(nets,ts,ys)
```

References

Adedigba, S.A., Khan, F., Yang, M., 2017. Dynamic failure analysis of process systems using neural networks. Process Saf. Environ. Prot. 111, 529–543. https://doi.org/10.1016/J.PSEP.2017.08.005

Akin, S., Ross, C.M., Kovscek, A.R., 2008. Combination of well log and pore-scale data to predict petrophysical properties of diatomite. J. Pet. Sci. Eng. 60, 133–149. https://doi.org/10.1016/J.PETROL.2007.05.013

Ali Ahmadi, M., Golshadi, M., 2012. Neural network based swarm concept for prediction asphaltene precipitation due to natural depletion. J. Pet. Sci. Eng. 98–99, 40–49. https://doi.org/10.1016/J.PETROL.2012.08.011

Asadisaghandi, J., Tahmasebi, P., 2011. Comparative evaluation of back-propagation neural network learning algorithms and empirical correlations for prediction of oil PVT properties in Iran oilfields. J. Pet. Sci. Eng. 78, 464–475. https://doi.org/10.1016/J.PETROL.2011.06.024

Ashoori, S., Abedini, A., Abedini, R., Nasheghi, K.Q., 2010. Comparison of scaling equation with neural network model for prediction of asphaltene precipitation. J. Pet. Sci. Eng. 72, 186–194. https://doi.org/10.1016/J.PETROL.2010.03.016

Asquith, G., Gibson, C., 2004. Basic well log analysis for geologists, American Association of Petroleum Geologists Methods in Exploration. https://doi.org/82-73052

Avseth, P.A., Odegaard, E., 2004. Well log and seismic data analysis using rock physics templates. First Break 22, 37–43. https://doi.org/10.3997/1365-2397.2004017

Babakhani, S.M., Bahmani, M., Shariati, J., Badr, K., Balouchi, Y., 2015. Comparing the capability of artificial neural network (ANN) and CSMHYD program for predicting of hydrate formation pressure in binary mixtures. J. Pet. Sci. Eng. 136, 78–87. https://doi.org/10.1016/J.PETROL.2015.11.002

Bailey, T., 2012. An empirical Vp/Vs shale trend for the Kimmeridge Clay of the Central North Sea, in: 74th EAGE Conference & Exhibition Incorporating SPE EUROPEC 2012. Copenhagen, Denmark, pp. 4–7.

Bailey, T., Dutton, D., 2012. An Empirical Vp/Vs Shale Trend for the Kimmeridge Clay of the Central North Sea. https://doi.org/10.3997/2214-4609.20148426

Bhatt, A., Helle, H.B., 2002. Determination of facies from well logs using modular neural networks. Pet. Geosci. 8, 217–228.

Bianchi, F.M., Maiorino, E., Kampffmeyer, M.C., Rizzi, A., Jenssen, R., 2017. Recurrent Neural Networks for Short-Term Load Forecasting, SpringerBriefs in Computer Science. Springer International Publishing, Cham. https://doi.org/10.1007/978-3-319-70338-1

Castagna, J.P., Batzle, M.L., Eastwood, R.L., 1985. Relationships between compressional-wave in elastic silicate. Geophysics 50, 571–581. https://doi.org/10.1190/1.1441933

Çoruh, S., Geyikçi, F., Kılıç, E., Çoruh, U., 2014. The use of NARX neural network for modeling of adsorption of zinc ions using activated almond shell as a potential biosorbent. Bioresour. Technol. 151, 406–410. https://doi.org/10.1016/J.BIORTECH.2013.10.019

Derakhshanfard, F., Mehralizadeh, A., 2018. Application of artificial neural networks for viscosity of crude oil-based nanofluids containing oxides nanoparticles. J. Pet. Sci. Eng. 168, 263–272.

https://doi.org/10.1016/J.PETROL.2018.05.018

Diaconescu, E., 2008. The use of NARX neural networks to predict chaotic time series. WSEAS Trans. Comput. Res.

Domenico, S.N., 1984. Rock lithology and porosity determination from shear and compressional wave velocity. GEOPHYSICS 49, 1188–1195. https://doi.org/10.1190/1.1441748

Eastwood, R.L., Castagna, J.P., 1983. Basis for interpretation of Vp/Vs ratios in complex lithologies. SPWLA 24th Annu. logging Symp. 1–17.

Eberhart-Phillips, D., Han, D.-H., Zoback, M.D., 1989. Empirical relationships among seismic velocity, effective pressure, porosity, and clay content in sandstone. Geophysics. https://doi.org/10.1190/1.1442580

Ellis, D., 2003. Formation Porosity Estimation from Density Logs.

Equinor, 2018a. Volve field [WWW Document]. URL http://factpages.npd.no/ReportServer?/FactPages/PageView/field&rs:Command=Render&rc:Toolbar=false&rc:Parameters=f&NpdId=3420717&IpAddress=142.134.216.81&CultureCode=en (accessed 8.8.18).

Equinor, 2018b. Equinor Dataset [WWW Document]. URL https://data-equinor-com.azurewebsites.net/dataset/volve

Gregory, A.R., 1977. Aspects of Rock Physics From Laboratory and Log Data that are Important to Seismic Interpretation: Section 1. Fundamentals of Stratigraphic Interpretation of Seismic Data 165, 15–46.

Hamada, G.M., 2004. Reservoir Fluids Identification Using V p /V s Ratio. Oil Gas Sci. Technol. – Rev. IFP 59, 649–654.

Hammer, B., 2000. Learning with recurrent neural networks, Lecture Notes in Control and Information Sciences. Springer London, London. https://doi.org/10.1007/BFb0110016

Han, D., Nur, A., Morgan, D., 1986. Effects of porosity and clay content on wave velocities in sandstones. GEOPHYSICS 51, 2093–2107. https://doi.org/10.1190/1.1442062

Hossain, Z., Mukerji, T., Fabricius, I.L., 2012. Vp-Vs relationship and amplitude variation with offset modelling of glauconitic greensand‡. Geophys. Prospect. 60, 117–137. https://doi.org/10.1111/j.1365-2478.2011.00968.x

Hsu, K., Brie, A., Plumb, R.A., 1987. A New Method for Fracture Identification Using Array Sonic Tools. https://doi.org/10.2118/14397-PA

Huang, Y.F., Huang, G.H., Dong, M.Z., Feng, G.M., 2003. Development of an artificial neural network model for predicting minimum miscibility pressure in CO2 flooding. J. Pet. Sci. Eng. 37, 83–95. https://doi.org/10.1016/S0920-4105(02)00312-1

Iturrarán-Viveros, U., Molero, M., 2013. Simulation of sonic waves along a borehole in a heterogeneous formation: Accelerating 2.5-D finite differences using [Py]OpenCL. Comput. Geosci. 56, 161–169. https://doi.org/10.1016/J.CAGEO.2013.03.014

Iy, A., Toksoz, N., Velocities, A.T., 1976. VELOCITIES OF SEISMIC WAVES IN POROUS ROCKS I : 41.

Johnston, J.E., Christensen, N.I., 1993. Compressional to Shear Velocity Ratios in Sedimentary-Rocks. Int. J. Rock Mech. Min. Sci. Geomech. Abstr. 30, 751–754.

Kelechukwu, E.M., Said Al-Salim, H., Saadi, A., 2013. Prediction of wax deposition problems of hydrocarbon production system. J. Pet. Sci. Eng. 108, 128–136. https://doi.org/10.1016/j.petrol.2012.11.008

Krief, M., Garat, J., Stellingwerf, J., Ventre, J., 1990. A Petrophysical Interpretation Using The Velocities Of P And S Waves (full-waveform Sonic). Log Anal. 31, 355–369.

Lacy, L.L., 1997. Dynamic Rock Mechanics Testing for Optimized Fracture Designs. SPE Annu. Tech. Conf. Exhib. https://doi.org/10.2118/38716-MS

Leontaritis, I.J., Billings, S.A., 1985. Input-output parametric models for non-linear systems part I: deterministic non-linear systems. Int. J. Control 41, 303–328.

Lindseth, R.O., 1979. Synthetic sonic logs—a process for stratigraphic interpretation. Geophysics 44, 3. https://doi.org/10.1190/1.1440922

Luffel, D.L., Guidry, F.K., 1989. Reservoir rock properties of Devonian shale from core and log analysis 1989.

Lukoševičius, M., Jaeger, H., 2009. Reservoir computing approaches to recurrent neural network training. Comput. Sci. Rev. 3, 127–149. https://doi.org/10.1016/J.COSREV.2009.03.005

Masoudi, P., Aifa, T., Memarian, H., Tokhmechi, B., 2018. Uncertainty assessment of porosity and permeability by clustering algorithm and fuzzy arithmetic. J. Pet. Sci. Eng. 161, 275–290.

Masoudi, P., Arbab, B., Mohammadrezaei, H., 2014. Net pay determination by artificial neural network: Case study on Iranian offshore oil fields. J. Pet. Sci. Eng. 123, 72–77.

Masoudi, P., Asgarinezhad, Y., Tokhmechi, B., 2015. Feature selection for reservoir characterisation by Bayesian network. Arab. J. Geosci. 8, 3031–3043.

Masoudi, P., Memarian, H., Aifa, T., Tokhmechi, B., 2017. Geometric modelling of the volume of investigation of well logs for thin-bed characterization. J. Geophys. Eng. 14, 426.

Matlab Documentation, 2018. The MathWorks Inc.

Menezes, J.M.P., Barreto, G.A., 2008. Long-term time series prediction with the NARX network: An empirical evaluation. Neurocomputing 71, 3335–3343. https://doi.org/10.1016/J.NEUCOM.2008.01.030

Menezes Jr, J.M.P., Barreto, G.A., 2008. Long-term time series prediction with the NARX network: an empirical evaluation. Neurocomputing 71, 3335–3343.

Miller, S., Stewart, R., 1990. Effects of lithology, porosity and shaliness on the P and S-wave velocities from sonic logs. J. Can. Soc. Expl. Geophys. 26, 94–103.

Miller, S.L.M., Stewart, R.R., 1991. The relationship between elastic-wave velocities and density in sedimentary rocks: A proposal. Crewes Res. Rep. 260–273.

Miller, S.L.M., Stewart, R.R., 1974. The relationship between elastic-wave velocities and density in sedimentary rocks: A proposal. Crewes Res. Rep. 260–273.

Minear, J.W., Fletcher, C.R., 1983. Full-Wave Acoustic Logging. SPWLA 24th Annu. Logging Symp.

Obst, O., Riedmiller, M., 2012. Taming the reservoir: Feedforward training for recurrent neural networks, in: The 2012 International Joint Conference on Neural Networks (IJCNN). IEEE,

pp. 1–7. https://doi.org/10.1109/IJCNN.2012.6252506

Oloruntobi, O., Adedigba, S., Khan, F., Chunduru, R., Butt, S., 2018. Overpressure prediction using the hydro-rotary specific energy concept. J. Nat. Gas Sci. Eng. 55, 243–253.

Onalo, D., Adedigba, S., Khan, F., James, L.A., Butt, S.D., 2018a. Data Driven Model for Sonic Well Log Prediction. J. Pet. Sci. Eng. https://doi.org/10.1016/j.petrol.2018.06.072

Onalo, D., Oloruntobi, O., Adedigba, S., Khan, F., James, L., Butt, S., 2018b. Static Young's modulus model for drilling operation planning. J. Pet. Sci. Eng.

Pickett, G.R., 1963. Acoustic Character Logs and Their Applications in Formation Evaluation. J. Pet. Technol. 15, 659–667. https://doi.org/10.2118/452-PA

Ramcharitar, K., Hosein, R., 2016. Rock Mechanical Properties of Shallow Unconsolidated Sandstone. SPE Trinidad Tobago Sect. Energy Resour. Conf. https://doi.org/10.2118/180803-MS

Raymer, L.L., Hunt, E.R., Gardner, J.S., 1980. An Improved Sonic Transit Time-to-Porosity Transform. SPWLA Annu. Logging Symp. 1–13.

Reichel, N., Evans, M., Allioli, F., Mauborgne, M.-L., Nicoletti, L., Haranger, F., Stoller, C., Schlumberger, V.C., El, E., Sipetrol, H., 2012. Neutron-Gamma Density (Ngd): Principles, Field Test Results And Log Quality Control Of A Radioisotope-Free Bulk Density Measurement, in: SPWLA 53rd Annual Logging Symposium. Society of Petrophysicists and Well-Log Analysts, pp. 1–15.

Riazi, S.H., Heydari, H., Ahmadpour, E., Gholami, A., Parvizi, S., 2014. Development of novel correlation for prediction of hydrate formation temperature based on intelligent optimization

algorithms. J. Nat. Gas Sci. Eng. 18, 377–384. https://doi.org/10.1016/J.JNGSE.2014.03.012

Sak, H., Senior, A., Beaufays, F., 2014. Long short-term memory recurrent neural network architectures for large scale acoustic modeling, in: Fifteenth Annual Conference of the International Speech Communication Association.

Saleh, S., Williams, K., Rizvi, A., 2013. Predicting Subsalt Pore Pressure with Vp/Vs. Pap. OTC 24157 Proc. 2013 Offshore Technol. Conf. held Houston, Texas, USA, 6–9 May.

Salehinejad, H., Sankar, S., Barfett, J., Colak, E., Valaee, S., 2017. Recent Advances in Recurrent Neural Networks. arXiv Prepr. arXiv1801.01078.

Schön, J., 2015. Basic Well Logging and Formation Evaluation Basic Well Logging and Formation Evaluation 4 Contents, 1st ed.

Sheremetov, L., Cosultchi, A., Martínez-Muñoz, J., Gonzalez-Sánchez, A., Jiménez-Aquino, M.A., 2014. Data-driven forecasting of naturally fractured reservoirs based on nonlinear autoregressive neural networks with exogenous input. J. Pet. Sci. Eng. 123, 106–119. https://doi.org/10.1016/J.PETROL.2014.07.013

Siegelmann, H.T., Horne, B.G., Giles, C.L., 1997. Computational capabilities of recurrent NARX neural networks. IEEE Trans. Syst. Man, Cybern. Part B 27, 208–215.

Tatham, R.H., 1982. VP / VS and lithology. Geophysics 47, 336–344.

Vaferi, B., Gitifar, V., Darvishi, P., Mowla, D., 2014. Modeling and analysis of effective thermal conductivity of sandstone at high pressure and temperature using optimal artificial neural networks. J. Pet. Sci. Eng. 119, 69–78. https://doi.org/10.1016/J.PETROL.2014.04.013

Walls, J., Dvorkin, J., Mavko, G., Nur, A., 2000. Use of Compressional and Shear Wave Velocity for Overpressure Detection. Pap. OTC 11912 Proc. 2000 Offshore Technol. Conf. held Houston, Texas, 1–4 May.

Weston, J., Chopra, S., Bordes, A., 2015. Memory networks. Int. Conf. Learn. Represent. https://doi.org/v0

Williams, D.M., 1990. The Acoustic Log Hydrocarbon Indicator. Soc. Petrophysicists Well-Log Anal.

Wisniak, M., Jing, X., 2001. Integration of Core , Log and Test Data To Improve the Characterisation of a Thinly. Test 1–11.

Wyllie, M.R.J., Gregory, A.R., Gardner, L.W., 1956. Elastic wave velocities in heterogeneous and porous media. Geophysics 21, 41–70. https://doi.org/10.1190/1.1438217

Zhang, D., Yuntian, C., Jin, M., 2018. Synthetic well logs generation via Recurrent Neural Networks. Pet. Explor. Dev. 45, 629–639.

Chapter 8 Are ANN model reliable Well Log Tools?

Preface

A version of this chapter has been submitted to the Journal of Petroleum Science and Engineering. I am the primary author. Co-author Dr. Sunday Adeshina helped in formulating the concept of the paper, and review of the first draft. Co-author Dr. Faisal Khan provided the much-needed support in directing and improving the quality of work. Co-author Dr. Lesley James provided technical assistance, proper formatting and representation of the well log data, expert analysis and review. Co-author Dr. Stephen Butt provided technical assistance and review, as well as, analyzing the well log format used in the paper. I and Dr. Sunday Adedigba carried out most of the data collection and analysis. The first draft of the manuscript was prepared by me, and I subsequently revised the manuscript, based on the feedback from the co-authors and also a peer review process. The co-authors assisted in the development of the concept and testing the model, reviewed and corrected the model and results. They also contributed to the review and revision of the manuscript.

Abstract

Artificial neural networks (ANN) have increasingly been used to estimate sonic well logs in the oil and gas industry because running sonic logging tools downhole is challenging, costly, and time-consuming.

ANN models are seen as reliable, cost-effective and efficient alternative. However, the challenges associated with ANN models for sonic well prediction are not well understood and considered. This paper is meant to shed light on these important topics. The paper is focused on highlighting the challenges and pitfalls encountered in the development of ANN models for sonic well log prediction. The points are explained with the help of a case study of developing sonic logs for a well located on the Norwegian continental shelf. Recommendations are suggested to resolve some of the challenges encountered in ANN model development.

Keywords: Artificial neural network, sonic well log, challenges, transit time, prediction

8.1 Introduction

Reliable, continuous and accurate data are invaluable for formation evaluation when using well logs (Deo et al., 2009). Formation evaluation analysis performed based on quantitative measurements of the well logs of a reservoir formation is associated with a certain degree of error and uncertainty (Gimbe and Lippard, 2015; Yashrakshita, 2013). Formation evaluation is based on the inherent characteristic properties of the formation such as bulk density, acoustic travel time, resistivity, hydrogen index and gamma rays (Onalo et al., 2018a). From these measurements, porosity, volume of shale, permeability, fluid saturation and geomechanical elastic properties are deduced (Akin et al., 2008; Derakhshanfard and Mehralizadeh, 2018; Elkatatny et al., 2018; Kazatchenko et al., 2006a; Maleki et al., 2014; TAO and KING, 1993; Yashrakshita, 2013; Zendehboudi et al., 2012, 2014). Uncertainties may originate from input data, well logging tools, calibration charts for the tools (especially when quality checks have not been performed), equations and methodologies used to estimate the well log properties and irregularities in the borehole (Al-Ameri and Al-Kattan, 2012; Asquith and Gibson, 2004; Balarabe and Isehunwa, 2017; Kohli and Arora, 2014; William R. Moore, 2011; Williams, 1990). Additionally, the petrophysical measurements from logging tools are not direct measurements of the formation's geomechanical properties; hence, another degree of error and uncertainty is introduced (Moore et al., 2011). These uncertainties lead to errors in the well logs used for formation evaluation and petrophysical interpretations during exploration and development.

Apart from the errors in the acquired well logs from a reservoir formation, gaps in the data may exist in certain regions along the entire length of the wellbore (Yu et al., 2008). In other wells, the entire formation may not be logged deliberately, due to financial constraints or regions of particular interest (Mullen et al., 2007). When data from these sections are required for further field

development and analysis, the missing well logs are inferred from adjacent well logs and offset wells (Lopes and Jorge, 2017; Yu et al., 2008). This leads to more uncertainty and error generation. Alternatively, well logging tools may be deployed to re-log the missing well log section; however, this presents additional cost and environmental risks (Lopes and Jorge, 2017). Logs are not run at all depth and especially not along shallow sections. This is mainly due to the fact that these sections do not represent the zones of interest and are not potential hydrocarbon reservoirs (Ramcharitar and Hosein, 2016).

The data required to infer the values of the missing well log regions are not always available due to the fact that the full suite of possible well logs may not have been logged and therefore are not available for indirect estimation or completion of the missing logs (Saggaf and Nebrija, 2000). For example, many offset wells that contain compressional wave sonic logs do not have corresponding shear wave sonic logs (Hossain et al., 2012; Mullen et al., 2007; Nourafkan and Kadkhodaie-Ilkhchi, 2015; Onalo et al., 2018a). Estimating these logs for geomechanical analysis and formation evaluation has been the central focus of a plethora of research (Anemangely et al., 2017; Greenberg and Castagna, 1992; Henning, 2000; Jørstad et al., 1999; Maleki et al., 2014; Rezaee et al., 2007). The petro-physicist and engineer must assess if the errors and uncertainties present in the available data are negligible enough to carry out reliable interpretation and evaluation of the reservoir's formation (Moore et al., 2011; Onalo et al., 2018b). Alternatively, they must find techniques that can help resolve these challenges by providing useable well logs for their analysis.

To solve these challenges inherent in the use of well logs for formation evaluation, interpretation and analysis, several methods have been used, such as empirical correlations, intelligent systems and hybrid models (Al-Dousari et al., 2016; Asoodeh and Bagheripour, 2013; Bagheripour et al., 2015; Bahrpeyma et al., 2015; Bhatt, 2002; Cranganu and Bautu, 2010; Ibrahim and Potter, 2004;

Kazatchenko et al., 2006b; Maleki et al., 2014; Rajabi et al., 2010; Rajabi and Tingay, 2013; Rolon et al., 2009; Saputro et al., 2016; Sbiga and Potter, 2017; Ukaonu et al., 2017). In particular, artificial neural networks are gaining popularity for estimating and reproducing missing logs (Khandelwal and Singh, 2010; Kohli and Arora, 2014; Onalo et al., 2018a; Verma et al., 2012).

It is assumed that the reader is familiar with ANN techniques and its use in the petroleum industry. For example, Handhal (2017) was able to deduce missing sonic, neutron, and density well logs in an oil field located in Southern Iraq by developing an artificial neural network (ANN); Handhal emphasized the high synthesizing capability of ANN. Saputro et al. (2016) developed a model to predict porosity from sonic and gamma ray logs using ANN. Rolon et al. (2009) analyzed the properties of four reservoir wells using synthetic well logs that were developed from an ANN model. Kohli and Arora (2014) estimated the permeability of three reservoir formations using gamma ray, density, resistivity, and porosity logs as inputs.

Although ANN is a powerful computational tool to model nonlinear complex relationships, researchers are beginning to recognize that it has its shortcomings and pitfalls, such as overfitting and over parametrization of weights and bias (Chitsazan et al., 2015; Shahin et al., 2009). Ma et al. (2017) attempted to resolve some of the issues by introducing a principal component analysis (PCA) to classify the lithology and integrated this into the ANN model. This improved the selection of relevant data for model development. Yu et al. (2012) took the use of ANN a step further by generating an algorithm to select the best well logs and intervals for training the ANN in order to improve the accuracy of ANN model predictions. Very recently, Onalo et al. (2018a) developed an ANN model to predict compressional and shear wave sonic logs from a combination of gamma rays, formation bulk density, and the volume of shale. The results of the model were used for on the spot field analysis of sanding potential and geomechanical properties. However,

similar to other researchers mentioned above, several challenges and limitations were observed during the development of the ANN models. Some of these challenges are discussed in this work.

The aim of this paper is to highlight and discuss some of the challenges and pitfalls often encountered in the development of ANN models for sonic well prediction. Although the application in this paper is for sonic well log prediction, similar challenges are encountered in the prediction of other well logs using this tool. The objective of the paper is to buttress the need for solutions and possible future directions to resolve these challenges so as to improve ANN as a viable technique for the oil and gas industry. To do this, the following assumptions have been made:

- As researchers, the authors have used ANN techniques for data-driven modeling in the oil and gas industry; nevertheless, the authors understand that ANNs have limitations.
- The reader understands ANN and is familiar with its use in the petroleum industry, including some of the published work by the authors (Adedigba et al., 2017; Khakzad et al., 2011; Onalo et al., 2018a).
- The current work is not to provide a critique of ANN; but to provide a direction for its future use as a means to interpret and interpolate well logs as well as predict formation properties from well log data.
- The application of ANN for formation evaluation in this study has genuine bases; therefore, the work does not comment or criticize the validity of ANN for this application.

The paper has been divided into four sections. The first section introduces the problems and need for ANN. The second section considers the application of ANN to an actual well in a case study.

The third section discusses the challenges that were encountered in the development of the ANN model. The fourth section provides a summary of the conclusions from the investigation.

8.2 Case Study

In this case study, ANN has been applied to predict the sonic logs of the Volve field located on the Norwegian continental shelf. The data is made available through the recent release of subsurface data by Equinor to the public in order to aid academicians in their research efforts. The well considered in this case study is well-15/9-F-1A in the Volve field in Norway. The well is located in a sandstone formation under water of up to 91 meters depth. The reservoir is considered to be an oil reservoir due to its fluid content and was initially drilled as an observation well (Equinor, 2018). For the purpose of this study, a controllable dataset size from 3400 to 3650 meters is considered. The control section is predominately water saturated sandstone; however, potential oil reservoirs can be observed in Figure 8.1 at depths of 3435, 3480 and 3530 m respectively. The input data available for the ANN model development is presented in Figure 8.1. The statistical distribution of the data, showing the maximum, minimum, mean and range of the well log data used for the case study is presented in Table 8.1.

Table 8.1 Statistical representation of the well log data

	Depth (m)	Caliper (in)	GR (API)	NPHI	RHOB (g/cm^3)	RT (ohm.m)	VSH	DTC (µs/ft)	DTS (µs/ft)
Max	3640.00	8.87	126.90	0.41	2.93	29.49	1.00	93.41	186.09
Min	3429.40	8.47	10.35	0.05	2.24	0.19	0.01	58.71	96.90
Mean	3534.70	8.65	52.20	0.16	2.50	2.40	0.36	75.02	129.57
Range	210.60	0.41	116.55	0.35	0.69	29.30	0.99	34.70	89.19

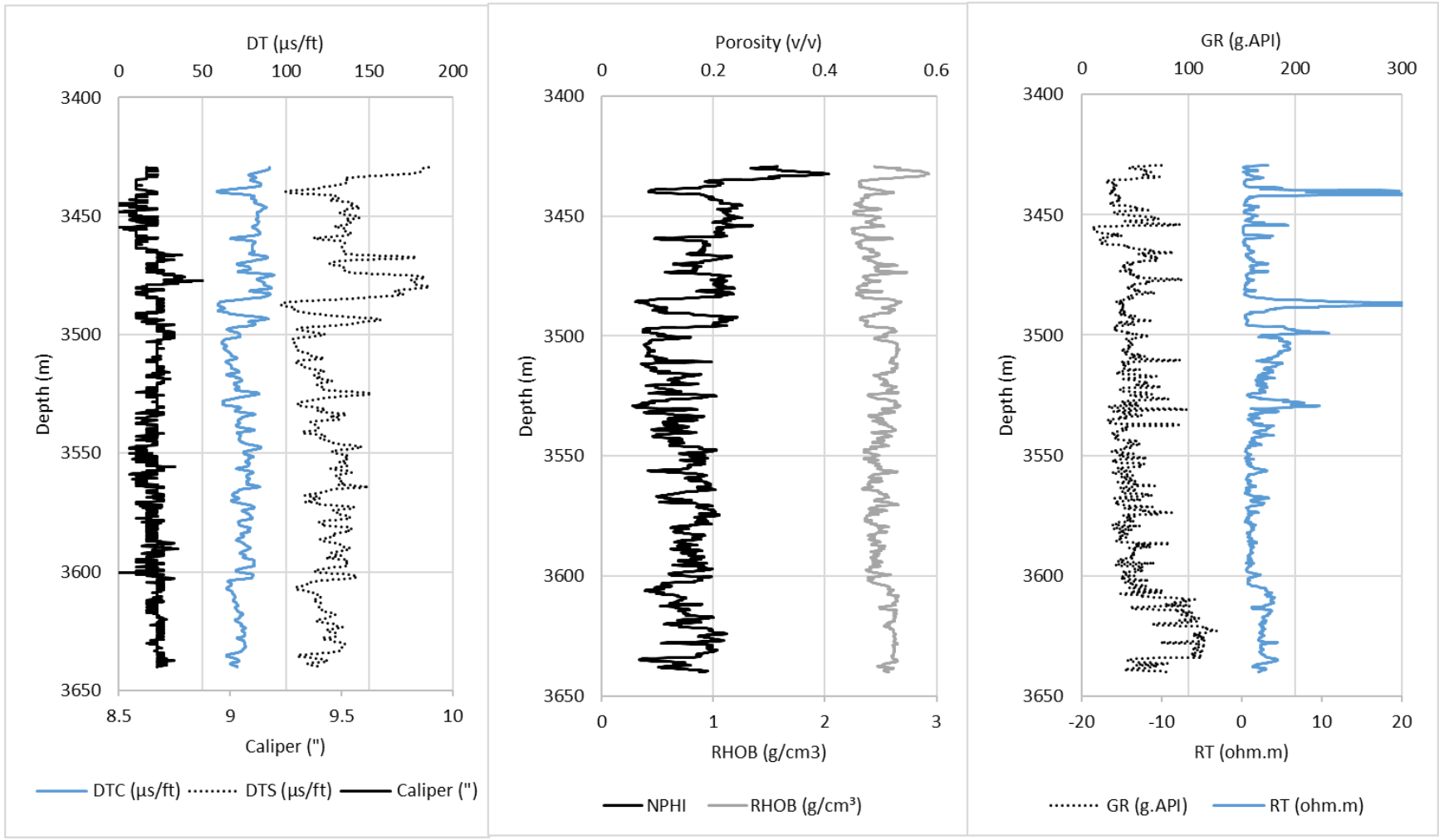

Figure 8.1. Well log data from Well 15/9-F-1A, Volve Field, Norway (Equinor, 2018)

8.2.1 **Development of ANN model**

A base model is established to serve as a model for comparison to help the reader observe the changes as the parameters are adjusted during the model development. Consider a scenario where there is available data, meaning that all the available well log data provided can be used for the model development. The multilayered perceptron artificial neural network (MLP-ANN) is applied to the entire dataset using the backpropagation algorithm. The base model is a three-layered network with 10 neurons. The logistic activation function has been applied to the dataset. 70% of the data was used for training while 30% was used for validation and testing of the models. For easy identification of the model developed, the input data are abbreviated as follows: gamma ray - GR, neutron porosity – N, resistivity – RT, depth – Dep, bulk density – RHOB, and volume of shale – VSH. A summary of the features in the initial model is presented in Table 8.2.

Table 8.2. The features of the base model

Main features of the model	Parameters
Architecture of the network	Feedforward
Input data	All (GR, N, Dep, RT, RHOB, VSH)
Number of layers	3
Number of neurons	10
Activation function	Logistic
Training algorithm	Backpropagation
Output data	Compressional and shear sonic transit time
Optimization algorithm	Levenberg-Marquardt
Performance function	MSE

The results of the model indicate that the coefficient of determination of the model is 0.991 and the MSE is 15.52 overall. This alludes to a sufficiently accurate model; however, caution should

be exercised because the results provide the overall performance of the model based on the output vector (combined compressional and shear sonic logs). It is useful to extract the individual values of the model prediction for a cross-validation. To demonstrate this, the individual cross-validation of the model is presented in Figure 8.2.

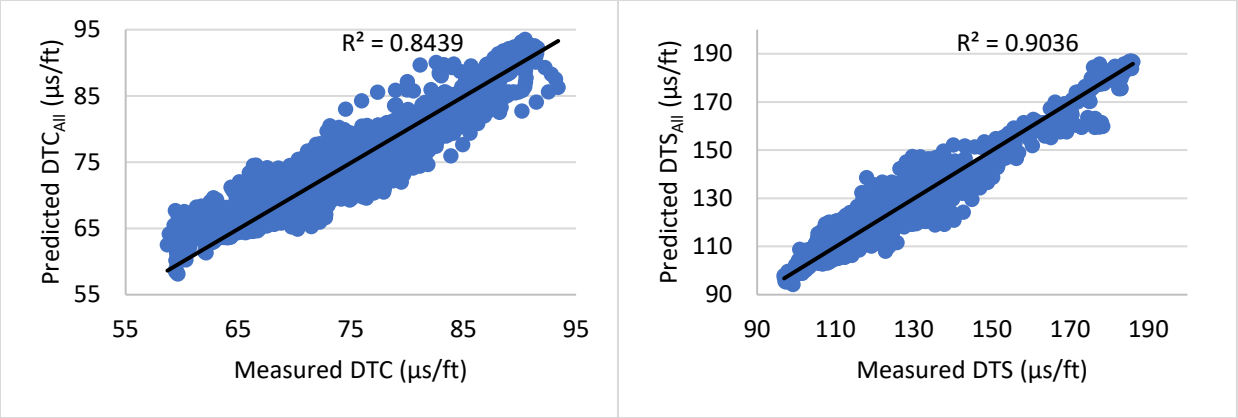

Figure 8.2. Cross-validation of All-model

The R^2 of compressional sonic transit log and shear sonic transit log is 0.844 and 0.904 respectively. This is lower than the overall output vector R^2 presented by the model initially. This also applies to the MSE; however, since this is only for demonstration, the overall output vector is used as the basis for comparison except when it is necessary to explain a challenge or short coming of ANN.

8.3 Challenges and limitations of ANN model development

In this section, some of the challenges, shortcomings and pitfalls which were encountered during the model development are presented. In addition, some shortcomings which have been reported to be issues encountered when developing ANN models by other researchers are also presented.

8.3.1 Input data

The input data plays a significant role in model definition. All the data available in the well log dataset are not always available in most wells. The full suite of logs is not always run; sometimes, the data contain errors or missing sections. The most suitable selection of data in one well may very well differ in another well, but determining this for a particular region will prove useful for wells in that region. It is voluminous and unnecessary to consider all permutations of the available well log data set; hence, an input layer with three input well logs is considered for the development of models with limited data where only three input well logs are available and reliable. Applying the same training parameters as in the base model, several combinations of input well logs were considered. A summary of the models is presented in Table 8.3. A legend for the models can be found in the nomenclature.

Table 8.3. Summary the model performance based on the selected input data

Sn	Model	Stage	R^2	MSE	Epoch
1	GRRHOBVSH (Gamma ray, density and shale volume)	Training	0.968	55.83	7
		Validation	0.966	58.99	
		Testing	0.963	69.83	
		Overall	0.967	58.99	
2	GRRHOBN (Gamma ray, density and neutron)	Training	0.974	45.78	8
		Validation	0.973	48.60	
		testing	0.974	47.23	
		Overall	0.974	48.59	
3	GRRHOBRT (Gamma ray, density and resistivity)	Training	0.976	42.98	65
		Validation	0.970	51.75	

		Testing	0.960	72.15	
		Overall	0.973	51.75	
4	GRRHOBDep (Gamma ray, density and depth)	Training	0.977	41.90	47
		Validation	0.979	36.72	
		Testing	0.969	54.28	
		Overall	0.976	36.72	
5	GRNDep (Gamma ray, neutron and depth)	Training	0.986	25.48	36
		Validation	0.981	35.09	
		Testing	0.985	27.88	
		Overall	0.985	35.08	
6	GRNRT (Gamma ray, neutron and resistivity)	Training	0.973	48.26	11
		Validation	0.976	43.18	
		Testing	0.977	39.55	
		Overall	0.974	43.18	
7	GRNVSH (Gamma ray, neutron and shale volume)	Training	0.972	50.05	41
		Validation	0.972	51.76	
		Testing	0.971	53.07	
		Overall	0.972	51.75	
8	DepGRRT (Depth, gamma ray and resistivity)	Training	0.977	41.08	24
		Validation	0.976	41.61	
		Testing	0.975	45.12	
		Overall	0.977	41.62	
9	DepGRVSH (Depth, gamma ray and shale volume)	Training	0.972	50.41	39
		Validation	0.973	50.38	
		Testing	0.972	49.87	
		Overall	0.972	50.38	
10	NRHOBRT (Neutron, density and resistivity)	Training	0.971	51.98	11
		Validation	0.974	45.73	
		Testing	0.964	68.11	
		Overall	0.970	45.73	
11	NRHOBDep (Neutron, density and depth)	Training	0.982	32.91	27
		Validation	0.981	34.30	
		Testing	0.978	41.54	
		Overall	0.980	34.30	
12	NRHOBVSH (Neutron, density and shale volume)	Training	0.974	46.83	13
		Validation	0.975	43.14	
		Testing	0.974	48.98	
		Overall	0.974	43.14	
13	NRTVSH (Neutron, resistivity and shale volume)	Training	0.975	45.00	32
		Validation	0.977	41.23	
		Testing	0.974	46.07	

		Overall	0.975	41.23	
14	NRTDep (Neutron, resistivity and depth)	Training	0.989	19.85	50
		Validation	0.989	19.28	
		Testing	0.989	20.67	
		Overall	0.989	19.28	

Table 8.3 suggests that NRTDep-model had the best performance of the models tested with an overall R^2 of 0.989 and MSE of 19.28 respectively. NRTDep-model is considered as the base model henceforth for comparative consistency.

ANNs are good approximators and are probably able to provide a solution for almost any dataset. To develop a good model, the input data must be selected carefully. Data which describe subtle changes in the target data are usually a good choice for model development (Gardner and Dorling, 1998; Shahin et al., 2009). Often, there may be more than one input data; different input data, suggesting changes in the target data at different points in the training may proffer a better solution when combined to form an input vector. For sonic well prediction, different input data vectors have been considered. Examples include gamma ray, neutron, density, volume of shale (Akhundi et al., 2014; Kazatchenko et al., 2006b; Khandelwal and Singh, 2010; Kohli and Arora, 2014; Ma et al., 2017; Maleki et al., 2014; Onalo et al., 2018a; Ramcharitar and Hosein, 2016; Rolon et al., 2009; Zoveidavianpoor et al., 2013). However, there is no consensus on the best set of input data for prediction of sonic well logs.

8.3.2 **Target data**

For the ANN model developed from the case study, compressional sonic transit time and shear sonic transit time were concurrently predicted as the target data.

ANN models are capable of estimating more than one output target data at a time. Depending on the objective of the model, the target data is set. When the objective is speed and quick analysis, a set of target data may be combined to form a target vector for quick and on the spot analysis. In contrast, when the objective is accuracy, separate models may be developed with their target data forming the basis of each model. The model results can be analyzed individually. The target data of a sonic well log may be compressional sonic transit time, shear sonic time and/or Stoneley sonic transit time (Rajabi et al., 2010). These can be combined to suit the objective of the model. For geomechanical formation analysis, compressional and shear sonic logs are usually sufficient and can be the target data (Khandelwal and Singh, 2010; Kohli and Arora, 2014; Onalo et al., 2018a; Ramcharitar and Hosein, 2016). In offset wells, where compressional sonic logs are available, only shear sonic logs are required for model predictions (Akhundi et al., 2014; Asoodeh and Bagheripour, 2014; Kazatchenko et al., 2006b; Maleki et al., 2014). Another pitfall of BP is that the more dimensions or input data introduced into the model, the larger the dataset required to describe the model; this increases convergence time (Gardner and Dorling, 1998).

8.3.3 **Data quality**

The data in the case study have been quality checked by filtering the noise observed. Without this initial step, any result from the model would be misleading. Details of this process can be found in literature (Oloruntobi et al., 2018; Onalo et al., 2018a).

ANN models may appear to model a given problem and pass the optimization criteria in the training data and sometimes, even the validation data, but still fail when applied to a fresh set of test data. One of the reasons for this ANN shortcoming is the quality of the data. The data may contain errors or false readings, which are carried into the model development and training. For example, during the acquisition of well log data, irregular wellbore surfaces are sources of error

which must be monitored to access the suitable data for model development. Pad type tools such as density and resistivity logs, which measure the distance of a rock property from the surface of the wellbore, produce erroneous results when the drilling mud and mud filter cake limit the contact between the tool and the formation (Bjorlykke, 2010). These false readings are noise in the data and need to be filtered from the data prior to use.

8.3.1 **Data size**

The initial model was developed with 2107 data points; however, the developer must decide if the data size considered is sufficient or if the model can be developed with a small data size. To investigate the influence of the data size on the model developed, datasets of 500 and 100 are developed based on the same parameters as the base model. The results are presented in Table 8.4.

Table 8.4. Model performance summary based on data size

Sn	Model (Size)		R^2	MSE	Epoch	Samples
1	2107	Training	0.989	19.85	50	1475
		Validation	0.989	19.28		316
		Testing	0.989	20.67		316
		Overall	0.989	19.28		2107
2	500	Training	0.997	6.26	48	350
		Validation	0.996	8.91		75
		Testing	0.998	5.4		75
		Overall	0.998	8.91		500
3	100	Training	0.999	0.03	50	75
		Validation	0.999	0.06		15
		Testing	0.999	0.06		15
		Overall	0.999	0.06		100

At first glance, it appears that reducing the data size improves the performance of the model. This is true if this is the only dataset possible for sonic well prediction i.e. if the data size is representative of the problem. To investigate this, the model must be tested for generalization.

ANN is a data-driven technique that relies heavily on the dataset presented for the training and development of the model. The data must be representative and include an extensive description of the problem (Gardner and Dorling, 1998). If the data are not representative of the problem or too few, the model will fail to generalize the problem and will not be able to handle a new dataset. On the other hand, if the data are too copious, the model might be subjected to overfitting. Caution should be exercised when training ANN models; a data set which has been trained may indicate good results in the training, validation and testing and still be poor in generalization. This begets another question. How should the training, validation and testing data size be decided? If this is done randomly, representative data may be omitted in the training data, which will reduce the model's performance (Gardner and Dorling, 1998). Some researchers take a trial and error, fuzzy clustering or self-organizing approach to dividing the data (Dorofki et al., 2012; Shahin et al., 2009). MATLAB documentation recommends 70% for training, 15% for validation and 15% for testing. This is consistent with recommendations found in the literature (Basheer and Hajmeer, 2000; Chen et al., 2017; Dorofki et al., 2012). To reduce the risk of not having a representative dataset for model training, they can be divided into exclusive subsets, which are trained separately; the results are analyzed for convergence. If they are similar, then the confidence level is said to be high and the data are representative of the problem. This is known as the V-fold cross-validation (Gardner and Dorling, 1998; Matlab Documentation, 2018).

8.3.2 **Generalization of the ANN**

Generalization refers to the ability of a model to adequately model the underlying relationship that has been observed in a training dataset and use the modeled relationship to determine output values of a different dataset exclusive of the training data set (Chitsazan et al., 2015). The ability of the developed model to generalize based on the available data is evaluated based on the models

presented in Table 8.4. The results are shown in Figure 8.3. As depicted in Figure 8.3, although the models appeared to have good performance values as the data size was reduced, when the models were applied to the entire dataset, they performed poorly. The dataset most likely does not account for the lithology, which may have different relationships. This alludes to the fact that the smaller datasets were not representative of the problem; in this case, the input well logs used to predict the compressional and shear transit logs were not representative of the entire reservoir formation.

From a well logging perspective, formation interval dependent variables like the pressure regime (overpressure), fluid saturation, lithology, temperature, stress, porosity and permeability vary along the wellbore. If the dataset selected does not contain datasets with these variables, then the model will fail to adequately represent the formation. Thus, it may be prudent to assume that different ANN models could be considered for different lithologies and only combined if separate modeling indicates that it is appropriate to develop one model.

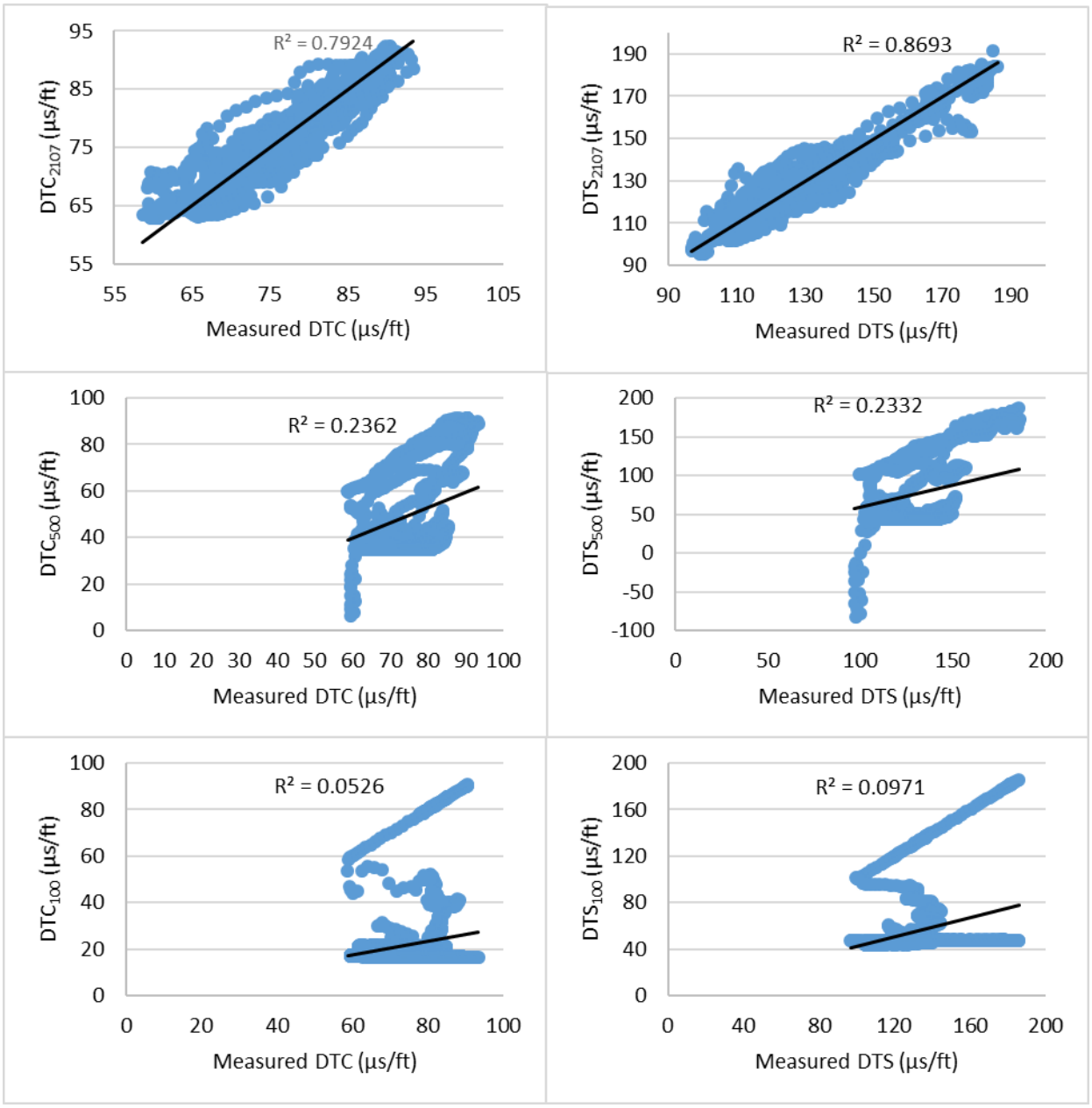

Figure 8.3. Cross-validation of models based on data size generalization

Generalization is essential to any model development and should be of high priority when developing predictive ANN models. With the aim to improve the generalization capability of models, developers fall into the trap of increasing the number of data and neurons; unfortunately, this may not solve the problem. The model identifies all previously existing training patterns and

parameters in the training data set and applies them blindly to the new dataset, thereby leading to overfitting (Gardner and Dorling, 1998). The idea of dividing the dataset into training data, validation data and test data has the aim of improving the ability of the model to generalize unseen data (Briggs and Circi, 2017). Sometimes the dataset is also divided into batches to help with the generalization.

8.3.1 Model Architecture

The architecture applied for model development in the case study is a three-layered network with 10 neurons. This has been selected based on best industry practices. In most networks, the initial challenge that becomes obvious to the developer is the architecture of the model. Many researchers admit to adopting a trial and error basis when trying to select the best architecture for the model (Briggs and Circi, 2017; Gardner and Dorling, 1998). This is due to the fact that there are no hard and fast rules or procedures for developing an ANN model.

8.3.1.1 Model neurons

Although 10 neurons were selected for the development of the base model, based on past experiences, choice of the number of neurons in each layer is evaluated. The number of neurons considered in the evaluation is 1, 5, 10 and 20, to give a representative variation from the base case of 10 neurons. The summary of the evaluation is presented in Table 8.5. It may be tempting to assume that by increasing the number of neurons, the performance of the model can be improved. Although this may be accurate to some extent, if errors exist in the model, then the reverse will be the case. In this case study, the data have been quality checked prior to evaluation. Increasing the number of neurons increases the number of epochs and thus, the speed of convergence. Therefore, it is redundant to keep increasing the number of neurons infinitely.

Table 8.5 Summary of model performance based on the number of neurons

Sn	Number of neurons	Stage	R^2	MSE	Epoch
1	1	Training	0.967	58.97	6
		Validation	0.967	57.48	
		Testing	0.963	67.39	
		Overall	0.966	57.48	
2	5	Training	0.985	26.26	21
		Validation	0.986	25.93	
		Testing	0.982	32.07	
		Overall	0.985	25.93	
3	10	Training	0.989	19.85	50
		Validation	0.989	19.28	
		Testing	0.989	20.67	
		Overall	0.989	19.28	
4	20	Training	0.992	14.31	125
		Validation	0.991	14.73	
		Testing	0.992	15.41	
		Overall	0.992	14.73	

As they are the building blocks of ANN, selecting the appropriate number of neurons is critical to successful ANN model development. The number of neurons is dependent on the actual problem, the data available and the noise present in the data. Few neurons will cause the BP algorithm not to converge at the minimum error function surface, which will lead to underfitting. Excess neurons will render the BP algorithm redundant, which will cause overfitting (Elkatatny et al., 2017; Van der Aalst et al., 2010). Limiting the number of neurons and layers has been used to reduce the tendency for the model to overfit the dataset by filtering data that are considered to be noisy and ignoring them (Gardner and Dorling, 1998).

8.3.1.2 Model Layers

The model presented in the case study has been developed with one hidden layer, making a total of three layers; however, the hidden layers can be increased to give a better description of the relationship. For this case study, one, two and three hidden layers have been considered.

The results are presented in Table 8.6. Increasing the number of layers does not necessarily increase the accuracy of the model, as can been seen in Table 8.6. The model performance suggests that a model with two hidden layers provides a better predictive model.

Table 8.6 Summary of model performance based on the number of layers

Sn	Number of hidden layers	Stage	R^2	MSE	Epoch
1	1	Train	0.967	57.48	6
		Validation	0.967		
		Test	0.963		
		Overall	0.966		
2	2	Train	0.990	21.13	130
		Validation	0.988		
		Test	0.987		
		Overall	0.989		
3	3	Train	0.979	36.41	38
		Validation	0.980		
		Test	0.977		
		Overall	0.979		

ANN architectures typically consist of neurons in the input, hidden and output layers of the networks (Shahin et al., 2009). For simple and less complex problems, a three-layer network is often sufficient to produce a smooth function (Gardner and Dorling, 1998). This implies an input layer, a hidden layer and an output layer.

8.3.2 **Training of ANN models**

The manner and method ANN models adopt in adjusting and updating the weights assigned to the neurons in the layers is known as the training of the model (Briggs and Circi, 2017; Shahin et al., 2009). The training algorithm considered in this work is the backpropagation algorithm, which is a first-order algorithm. MATLAB offers a range of training optimization algorithm options for the development of ANN models that adopt a backpropagation algorithm. The Levenberg-Marquardt second order optimization algorithm was applied to the case study.

MATLAB offers other second order algorithms to optimize the training, such as Bayesian regularization (BR) and the scaled conjugate gradient (SCD) technique. The second order algorithms significantly increase the training speed of the models, optimize the selection of the learning rate and momentum and prevent overfitting (Kayri, 2016; Wilamowski and Yu, 2010). LM optimizes by trying to reduce the sum of the square error function (Sapna et al., 2012). LM is considered to be the fastest; however, it requires more memory (Matlab Documentation, 2018). BR incorporates a probability distribution of a combination of the weights and square errors and attempts to reduce the error function (Kayri, 2016). Conjugate gradient descent techniques have been known to reduce the iterative process of the first order algorithm (Møller, 1993). SCD is a faster alternative to the line search technique, where the learning rate does not have to be estimated at each iteration. This is achieved by using a scaling mechanism The main advantage of SCD is that model parameters like rate and momentum do not need to be defined by the developer (Møller, 1993). Selecting the best training optimization algorithm is again dependent on the problem at hand.

To evaluate how this feature can be an issue in model development, these optimization algorithms were applied to the base model. The results are presented in

Table 8.7

Table 8.7. Summary of model performance based on the optimization algorithm

Sn	Training optimization algorithm	Stage	R^2	MSE	Epoch
1	Levenberg-Marquardt	Training	0.989	19.85	50
		Validation	0.989	19.28	
		Testing	0.989	20.67	
		Overall	0.989	19.28	
2	Bayesian regularization	Training	0.991	16.48	213
		Validation	0	0	
		Testing	0.990	16.48	
		Overall	0.990	17.01	
3	Scaled conjugate gradient	Train	0.972	49.48	56
		Validation	0.973	47.54	
		Training	0.968	57.57	
		Overall	0.972	47.54	

Besides the training optimization function, the following should also be considered when training a model.

8.3.2.1 Activation function

Selecting and deciding which activation function to use is often confusing. It is recommended to use bounded functions to increase the level of control over the output (Gardner and Dorling, 1998). More importantly, for BP, the function must be differentiable. MATLAB offers the logistic function, hyperbolic tangent function and purelin functions (Matlab Documentation, 2018). The logistic and hyperbolic tangent functions are non-linear functions, but the purelin, a linear function can be applied to the last output layer (Matlab Documentation, 2018). Normalizing the input data (0 – 1) is a redundant practice as the ANN adjusts the data based on the weights and bias; the data can be divided by the standard deviation to standardize the data (Chen et al., 2017; Gardner and Dorling, 1998).

8.3.2.2 Training parameters

Adjusting the learning rate and momentum help when training a model. The learning rate determines the step size the algorithm or activation function employs in updating in the model. A small learning rate will result in a longer convergence time; however, a large learning rate may result in the model failing to converge at the minimum error surface. The learning momentum is another training parameter which can help prevent the model from getting stuck at a false local error gradient minimum. It considers a portion or percentage of the previous layer in updating the next layer. Decreasing the learning rate has been found to aid models that fail to converge either due to instability or oscillation over a local error surface minimum (Gardner and Dorling, 1998).

8.3.2.3 Performance criteria

Depending on the actual problem and the reason behind developing the model, the performance criteria must be established prior to development. If the emphasis is on speed, then training speed should be monitored and optimized in model development; however, this may reduce model accuracy and generalization capacity. The size of the data and dimensionality may also be reduced to improve speed. However, if the emphasis is accuracy, then the reverse is true. Developers may decide to use the coefficient of determination as the basis for selecting the better model. This is sometimes statistically misleading. Hence, the regression coefficient should be combined with the selected error function to ascertain the model performance. Another important aspect of deciding the performance criteria is deciding when the model ends, the stopping criteria (Jaksa et al., 2008). This can be based on the number of epochs, the error function, or cross-validation; otherwise, the model training may run infinitely. A common fix is to select the limit for each performance stopping criterion so that the model ends whenever any of the criteria is reached. For the models

presented in this study, there was no time limitation; however, 1000 Epochs, MSE of 0 or 6 validation checks, whichever occurred first ended the model.

8.3.2.4 Epoch

The epoch refers to the number of iterations it takes for the ANN model to converge to a solution; that is, to find the global minimum error surface. Lower epochs are more desirable provided the models are equally or more accurate than models with more epochs. Levenberg-Marquardt often provides the models with the least epochs because Levenberg-Marquardt tends to solve faster as observed in

Table 8.7 Table 8.5 also alludes to the fact that the more neurons in the model architecture, the more the number of epochs. This is due to the fact that the algorithm becomes more complicated with more neurons that have to be solved to reach a solution. Hence, if adding more neurons does not improve the model, the model should not be slowed down by adding more neurons (epochs).

8.3.3 **Repeatability**

ANN models are difficult to repeat and regenerate. Even when the all model parameters are kept constant, the weight initialization process selects random values to initiate the training of the model. To demonstrate this, the base model is repeated three times and the results are shown in Table 8.8. It can be observed that none of the performance parameters are repeated in the repeat models. Although the model deviations are not severe in this case, it is recommended that as soon as a representative model is developed, the model should be saved, as the probability of obtaining the same model is slim.

Table 8.8 Summary of model performance based on model repetition

Sn	Repeatability models		R^2	MSE	Epoch

1	A	Training	0.989	19.85	50
		Validation	0.989	19.28	
		Testing	0.989	20.67	
		Overall	0.989	19.28	
2	B	Training	0.989	20.27	110
		Validation	0.986	23.48	
		Testing	0.988	20.73	
		Overall	0.988	23.48	
3	C	Training	0.990	18.64	111
		Validation	0.990	18.90	
		Testing	0.989	19.99	
		Overall	0.990	18.90	

MLP randomly selects the initial weights and adjusts the weights based on the feedback error signal sweep. As a result of this, most model training is not repeatable. The training takes a different path each time during the gradient descent to reach the local error minimum surface. A model that has just been trained and developed can be retrained, but the performance results and the weights will vary at each iteration. This is one of the reasons that ANN is referred to as a black box (Adedigba et al., 2017; Gardner and Dorling, 1998; Prieto et al., 2016). Jaksa et al. (2008) suggest that this is a major limitation of ANN as it limits model transparency and hence, the extraction of valuable knowledge from the model.

8.3.4 **Uncertainty**

Though uncertainty has been identified as a challenge of ANN models, attempts can be made to quantify the uncertainty using Monte Carlo simulation (Onalo et al., 2018b; Yashrakshita, 2013). The weights, bias and prediction of the ANN model present difficulties in obtaining consistent models, even when all model developments are kept constant. However, this is beyond the scope of this work. The aim of this work is to show that this challenge exists.

According to Chitsazan et al. (2015), the source of the uncertainty found in ANN is mainly associated with weights, bias, and inputs. The ANN structure also contributes significantly to the

uncertainty. Unfortunately, uncertainty in ANN models is rarely quantified due to the nature of the task (Jaksa et al., 2008). Whenever it is possible, it is important to identify the individual sources of uncertainty, and if possible, quantify them (Chitsazan et al., 2015; Wagener and Gupta, 2005). At the very least, this limitation should be stated in the development of the model. Optimization with the Bayesian technique has been suggested by some researchers as a means to improve the uncertainty in ANN development (Jaksa et al., 2008; Shahin et al., 2009).

In general, there is no one way or consensus on how to go about training every model. ANN models may never be able to overcome all these challenges. Combining ANN techniques with other techniques such as genetic algorithms, fuzzy logic and PCA to form ANN hybrids may provide more accurate models which do not suffer from these challenges (Akhundi et al., 2014; Asoodeh and Bagheripour, 2014, 2013, 2012; Babakhani et al., 2015; Bagheripour et al., 2015; Bianchi et al., 2017; Chung et al., 2014; Cranganu and Bautu, 2010; Kadkhodaie-Ilkhchi et al., 2009; Maleki et al., 2014; Zoveidavianpoor, 2014). Genetic algorithms are reported to not suffer from the black box syndrome; hence, knowledge extraction from the model is possible. Therefore, the models can be built upon and improved (Shahin et al., 2009; Waszczyszyn and Słoński, 2010). A summary of the challenges and pitfalls discussed in the paper is presented in Table 8.9.

8.4 Conclusions

ANN in its current form may not be the most appropriate tool for well log prediction in the petroleum industry. ANN suffers from many challenges and pitfalls of which the developer must be conscious.

In this study, a case study is presented to demonstrate the use of ANN models in sonic well log prediction in the petroleum industry. An actual oil field (Volve field) located in the Norwegian continental shelf has been evaluated in the study.

Some of the challenges and pitfalls encountered in the development of ANN for the case study are evaluated and discussed.

Table 8.9. A list of the challenges and limitations discussed

Sn	Challenges and limitations
1	Input data
2	Target data
3	Data quality
4	Data size
5	Generalization
6	Model Architecture • Neurons • layers
7	Training • Activation function • Training parameters • Performance criteria
8	Repeatability
9	Uncertainty

In addition, some of the recommended solutions to some of the common issues are presented.

In general, ANNs are highly capable, robust and reliable computing tools for sonic well log prediction; however, to remain relevant, the technique of choice when estimating sonic logs, the

current challenges and pitfalls need to be resolved. Otherwise, other techniques may with time surpass the functionality of ANN. Hybrid models that resolve some of the pitfalls of ANN may be the way forward. It is recommended that researchers look to resolving these pitfalls and challenges encountered in ANN model development.

Acknowledgments

The authors would like to thank and acknowledge the financial support of Innovate NL, the Natural Science and Engineering Research Council of Canada (NSERC), Hibernia Management and Development Company (HMDC), and Chevron Canada for their tremendous support during this work. We would also like to thank the management of Equinor for making the data for this research available on their website https://data-equinor-com.azurewebsites.net/dataset/volve.

Nomenclature

ANN	Artificial neural network
BP	Backpropagation
BR	Bayesian regularization
RHOB	Bulk density log (g/cm^3)
DTC	Compressional wave travel time (μsec/ft)
RES or RT	Deep resistivity log (ohm.m)
Dep	Depth (m)
DepGRRT	Depth, gamma ray and resistivity input well logs
DepGRVSH	Depth, gamma ray and shale volume input well logs
GR	Gamma ray log (gAPI)
GRRHOBDep	Gamma ray, density and depth input well logs
GRRHOBN	Gamma ray, density and neutron input well logs
GRRHOBRT	Gamma ray, density and resistivity input well logs
GRRHOBVSH	Gamma ray, density and shale volume input well logs
GRNDep	Gamma ray, neutron and depth input well logs
GRNRT	Gamma ray, neutron and resistivity input well logs
GRNVSH	Gamma ray, neutron and shale volume input well logs
All	Gamma ray, neutron, depth, resistivity, density and shale volume
LM	Levenberg-Marquardt
MAE	Mean absolute error
MPE	Mean percentage error
MLP	Multi-layer perceptron
NPHI or N	Neutron porosity (m^3/m^3)
NRHOBDep	Neutron, density and depth input well logs
NRHOBRT	Neutron, density and resistivity input well logs
NRHOBVSH	Neutron, density and shale volume input well logs
NRTDep	Neutron, resistivity and depth input well logs
NRTVSH	Neutron, resistivity and shale volume input well logs
SCD	Scaled conjugate descent
Vsh	Shale volume
DTS	Shear wave travel time (μsec/ft)
RT	True resistivity (ohm.m)

References

Adedigba, S.A., Khan, F., Yang, M., 2017. Dynamic failure analysis of process systems using neural networks. Process Saf. Environ. Prot. 111, 529–543. https://doi.org/10.1016/J.PSEP.2017.08.005

Akhundi, H., Ghafoori, M., Lashkaripour, G.-R., 2014. Prediction of Shear Wave Velocity Using Artificial Neural Network Technique, Multiple Regression and Petrophysical Data: A Case Study in Asmari Reservoir (SW Iran). Open J. Geol. 04, 303–313. https://doi.org/10.4236/ojg.2014.47023

Akin, S., Ross, C.M., Kovscek, A.R., 2008. Combination of well log and pore-scale data to predict petrophysical properties of diatomite. J. Pet. Sci. Eng. 60, 133–149. https://doi.org/10.1016/J.PETROL.2007.05.013

Al-Ameri, N.J., Al-Kattan, W., 2012. Estimation of the Rock Mechanical Properties Using Conventional Log Data in North Rumaila Field. Iraqi J. Chem. Pet. Eng. 13, 27–33.

Al-Dousari, M., Garrouch, A.A., Al-Omair, O., 2016. Investigating the dependence of shear wave velocity on petrophysical parameters. J. Pet. Sci. Eng. 146, 286–296. https://doi.org/10.1016/J.PETROL.2016.04.036

Anemangely, M., Ramezanzadeh, A., Tokhmechi, B., 2017. Shear wave travel time estimation from petrophysical logs using ANFIS-PSO algorithm: A case study from Ab-Teymour Oilfield. J. Nat. Gas Sci. Eng. 38, 373–387.

Asoodeh, M., Bagheripour, P., 2014. ACE stimulated neural network for shear wave velocity determination from well logs. J. Appl. Geophys. 107, 102–107.

https://doi.org/10.1016/J.JAPPGEO.2014.05.014

Asoodeh, M., Bagheripour, P., 2013. Neuro-fuzzy reaping of shear wave velocity correlations derived by hybrid genetic algorithm-pattern search technique. Open Geosci. 5, 272–284. https://doi.org/10.2478/s13533-012-0129-4

Asoodeh, M., Bagheripour, P., 2012. Prediction of Compressional, Shear, and Stoneley Wave Velocities from Conventional Well Log Data Using a Committee Machine with Intelligent Systems. Rock Mech. Rock Eng. 45, 45–63. https://doi.org/10.1007/s00603-011-0181-2

Asquith, G., Gibson, C., 2004. Basic well log analysis for geologists, American Association of Petroleum Geologists Methods in Exploration. https://doi.org/82-73052

Babakhani, S.M., Bahmani, M., Shariati, J., Badr, K., Balouchi, Y., 2015. Comparing the capability of artificial neural network (ANN) and CSMHYD program for predicting of hydrate formation pressure in binary mixtures. J. Pet. Sci. Eng. 136, 78–87. https://doi.org/10.1016/J.PETROL.2015.11.002

Bagheripour, P., Gholami, A., Asoodeh, M., Vaezzadeh-Asadi, M., 2015. Support vector regression based determination of shear wave velocity. J. Pet. Sci. Eng. 125, 95–99. https://doi.org/10.1016/J.PETROL.2014.11.025

Bahrpeyma, F., Cranganu, C., Dadaneh, B.Z., 2015. Active learning method for estimating missing logs in hydrocarbon reservoirs, in: Artificial Intelligent Approaches in Petroleum Geosciences. pp. 209–224. https://doi.org/10.1007/978-3-319-16531-8_7

Balarabe, T., Isehunwa, S., 2017. Evaluation of Sand Production Potential using Well Logs. SPE Niger. Annu. Int. Conf. Exhib. https://doi.org/10.2118/189107-MS

Basheer, I.., Hajmeer, M., 2000. Artificial neural networks: fundamentals, computing, design, and application. J. Microbiol. Methods 43, 3–31. https://doi.org/10.1016/S0167-7012(00)00201-3

Bhatt, A., 2002. Reservoir properties from well logs using neural networks.

Bianchi, F.M., Maiorino, E., Kampffmeyer, M.C., Rizzi, A., Jenssen, R., 2017. Recurrent Neural Networks for Short-Term Load Forecasting, SpringerBriefs in Computer Science. Springer International Publishing, Cham. https://doi.org/10.1007/978-3-319-70338-1

Bjorlykke, K., 2010. Petroleum Geoscience from Sedimentary Enviroments to Rock Physics, Petroleum Geoscience. https://doi.org/10.1007/978-3-642-02332-3

Briggs, D.C., Circi, R., 2017. Challenges to the Use of Artificial Neural Networks for Diagnostic Classifications with Student Test Data. Int. J. Test. 17, 302–321. https://doi.org/10.1080/15305058.2017.1297816

Chen, Z., Ma, W., Wei, K., Wu, J., Li, S., Xie, K., Lv, G., 2017. Artificial neural network modeling for evaluating the power consumption of silicon production in submerged arc furnaces. Appl. Therm. Eng. 112, 226–236. https://doi.org/10.1016/J.APPLTHERMALENG.2016.10.087

Chitsazan, N., Nadiri, A.A., Tsai, F.T.-C., 2015. Prediction and structural uncertainty analyses of artificial neural networks using hierarchical Bayesian model averaging. J. Hydrol. 528, 52–62. https://doi.org/10.1016/J.JHYDROL.2015.06.007

Chung, J., Gulcehre, C., Cho, K., Bengio, Y., 2014. Empirical Evaluation of Gated Recurrent Neural Networks on Sequence Modeling.

Cranganu, C., Bautu, E., 2010. Using Gene Expression Programming to estimate sonic log

distributions based on the natural gamma ray and deep resistivity logs: A case study from the Anadarko Basin, Oklahoma. J. Pet. Sci. Eng. 70, 243–255. https://doi.org/10.1016/J.PETROL.2009.11.017

Deo, P., Xue, D., Mendez, F., 2009. Managing Uncertainty of Well Log Data in Reservoir Characterization. Proc. Eur. Conf. Exhib. i, 8–11. https://doi.org/10.2118/118980-MS

Derakhshanfard, F., Mehralizadeh, A., 2018. Application of artificial neural networks for viscosity of crude oil-based nanofluids containing oxides nanoparticles. J. Pet. Sci. Eng. 168, 263–272. https://doi.org/10.1016/J.PETROL.2018.05.018

Dorofki, M., Elshafie, A.H., Jaafar, O., Karim, O.A., Mastura, S., 2012. Comparison of Artificial Neural Network Transfer Functions Abilities to Simulate Extreme Runoff Data, in: 2012 International Conference on Environment, Energy and Biotechnology. pp. 39–44.

Elkatatny, S., Mahmoud, M., Mohamed, I., Abdulraheem, A., 2018. Development of a new correlation to determine the static Young's modulus. J. Pet. Explor. Prod. Technol. 8, 17–30. https://doi.org/10.1007/s13202-017-0316-4

Elkatatny, S.M., Tariq, Z., Mahmoud, M.A., Abdulraheem Abdelwahab, Z.A., Woldeamanuel, M., Mohamed, I.M., 2017. An Artificial Intelligent Approach to Predict Static Poisson's Ratio. 51st U.S. Rock Mech. Symp.

Equinor, 2018. Volve field [WWW Document]. URL http://factpages.npd.no/ReportServer?/FactPages/PageView/field&rs:Command=Render&rc:Toolbar=false&rc:Parameters=f&NpdId=3420717&IpAddress=142.134.216.81&CultureCode=en (accessed 8.8.18).

Gardner, M.W., Dorling, S.R., 1998. Artificial neural networks (the multilayer perceptron) - a review of applications in the atmospheric sciences. Atmos. Environ. 32, 2627–2636. https://doi.org/10.1016/S1352-2310(97)00447-0

Gimbe, M., Lippard, S., 2015. Formation evaluation and uncertainty analysis of the Ormen Lange Field, Norwegian sea offshore Norway. Dep. Geol. Miner. Resour. Eng. Norwegian University of Science and Technology.

Greenberg, M.L., Castagna, J.P., 1992. Shear-Wave Estimation in Porous Rocks: Theoretical Formulation Prelimary Verification and Application. Geophys. Prospect. 40, 195–209. https://doi.org/10.1111/j.1365-2478.1992.tb00371.x

Handhal, A.M., 2017. Synthesis of missing openhole well log data through artificial neural networks, JOURNAL OF KUFA-PHYSICS.

Henning, A., 2000. Shear-wave velocity estimation in the deepwater Gulf of Mexico, in: SEG Technical Program Expanded Abstracts 2000. Society of Exploration Geophysicists, pp. 1723–1726. https://doi.org/10.1190/1.1815753

Hossain, Z., Mukerji, T., Fabricius, I.L., 2012. Vp-Vs relationship and amplitude variation with offset modelling of glauconitic greensand‡. Geophys. Prospect. 60, 117–137. https://doi.org/10.1111/j.1365-2478.2011.00968.x

Ibrahim, M.A., Potter, D.K., 2004. Prediction of Residual Water Saturation Using Genetically Focused Neural Nets. SPE Asia Pacific Oil Gas Conf. Exhib. https://doi.org/10.2118/88457-MS

Jaksa, M., Maier, H., A Shahin, M., 2008. Future Challenges for Artificial Neural Network

Modelling in Geotechnical Engineering, 12th International Conference on Computer Methods and Advances in Geomechanics 2008.

Jørstad, A., Mukerji, T., Mavko, G., 1999. Model-based shear-wave velocity estimation versus empirical regressions. Geophys. Prospect. 47, 785–797. https://doi.org/10.1046/j.1365-2478.1999.00154.x

Kadkhodaie-Ilkhchi, A., Rezaee, M.R., Rahimpour-Bonab, H., 2009. A committee neural network for prediction of normalized oil content from well log data: An example from South Pars Gas Field, Persian Gulf. J. Pet. Sci. Eng. 65, 23–32. https://doi.org/10.1016/J.PETROL.2008.12.012

Kayri, M., 2016. Predictive abilities of bayesian regularization and Levenberg–Marquardt algorithms in artificial neural networks: a comparative empirical study on social data. Math. Comput. Appl. 21, 20.

Kazatchenko, E., Markov, M., Mousatov, A., Pervago, E., 2006a. Prediction of the s-wave velocity in carbonate formation using joint inversion of conventional well logs. J. Geophys. Eng. 3, 386–399. https://doi.org/10.1088/1742-2132/3/4/010

Kazatchenko, E., Markov, M., Mousatov, A., Pervago, E., 2006b. Prediction of the s-wave velocity in carbonate formation using joint inversion of conventional well logs. J. Geophys. Eng. 3, 386–399. https://doi.org/10.1088/1742-2132/3/4/010

Khakzad, N., Khan, F., Amyotte, P., 2011. Safety analysis in process facilities: Comparison of fault tree and Bayesian network approaches. Reliab. Eng. Syst. Saf. 96, 925–932. https://doi.org/10.1016/j.ress.2011.03.012

Khandelwal, M., Singh, T.N., 2010. Artificial neural networks as a valuable tool for well log interpretation. Pet. Sci. Technol. 28, 1381–1393. https://doi.org/10.1080/10916460903030482

Kohli, A., Arora, P., 2014. Application of Artificial Neural Networks for Well Logs, in: International Petroleum Technology Conference. International Petroleum Technology Conference. https://doi.org/10.2523/IPTC-17475-MS

Lopes, R.L., Jorge, A.M., 2017. Mind the Gap: a Well Log Data Analysis.

Ma, Y.Z., Gomez, E., Luneau, B., 2017. Integration of seismic and well-log data using statistical and neural network methods. Lead. Edge 36, 324–329. https://doi.org/10.1190/tle36040324.1

Maleki, S., Moradzadeh, A., Riabi, R.G., Gholami, R., Sadeghzadeh, F., 2014. Prediction of shear wave velocity using empirical correlations and artificial intelligence methods. NRIAG J. Astron. Geophys. 3, 70–81. https://doi.org/10.1016/J.NRJAG.2014.05.001

Matlab Documentation, 2018. The MathWorks Inc.

Møller, M.F., 1993. A scaled conjugate gradient algorithm for fast supervised learning. Neural networks 6, 525–533.

Moore, W., Ma, Z., Urdea, J., Bratton, T., 2011. Uncertainty analysis in well log and petrophysical interpretations, in: Uncertainty Analysis and Reservoir Modeling. AAPG Special Volumes, pp. 17–28. https://doi.org/10.1306/13301405M963478

Mullen, M.J., Roundtree, R., Turk, G.A., 2007. A Composite Determination of Mechanical Rock Properties for Stimulation Design (What to Do When You Don’t Have a Sonic Log). Rocky Mt. Oil Gas Technol. Symp. https://doi.org/10.2118/108139-MS

Nourafkan, A., Kadkhodaie-Ilkhchi, A., 2015. Shear wave velocity estimation from conventional well log data by using a hybrid ant colony-fuzzy inference system: A case study from Cheshmeh-Khosh oilfield. J. Pet. Sci. Eng. 127, 459–468. https://doi.org/10.1016/j.petrol.2015.02.001

Oloruntobi, O., Adedigba, S., Khan, F., Chunduru, R., Butt, S., 2018. Overpressure prediction using the hydro-rotary specific energy concept. J. Nat. Gas Sci. Eng. 55, 243–253.

Onalo, D., Adedigba, S., Khan, F., James, L.A., Butt, S.D., 2018a. Data Driven Model for Sonic Well Log Prediction. J. Pet. Sci. Eng. https://doi.org/10.1016/j.petrol.2018.06.072

Onalo, D., Oloruntobi, O., Adedigba, S., Khan, F., James, L., Butt, S., 2018b. Static Young's modulus model for drilling operation planning. J. Pet. Sci. Eng.

Prieto, A., Prieto, B., Ortigosa, E.M., Ros, E., Pelayo, F., Ortega, J., Rojas, I., 2016. Neural networks: An overview of early research, current frameworks and new challenges. Neurocomputing 214, 242–268. https://doi.org/10.1016/J.NEUCOM.2016.06.014

Rajabi, M., Bohloli, B., Gholampour Ahangar, E., 2010. Intelligent approaches for prediction of compressional, shear and Stoneley wave velocities from conventional well log data: A case study from the Sarvak carbonate reservoir in the Abadan Plain (Southwestern Iran). Comput. Geosci. 36, 647–664. https://doi.org/10.1016/J.CAGEO.2009.09.008

Rajabi, M., Tingay, M., 2013. Applications of Intelligent Systems in Petroleum Geomechanics-Prediction of Geomechanical Properties in Different Types of Sedimentary Rocks, in: International EAGE Workshop on Geomechanics and Energy.

Ramcharitar, K., Hosein, R., 2016. Rock Mechanical Properties of Shallow Unconsolidated

Sandstone. SPE Trinidad Tobago Sect. Energy Resour. Conf. https://doi.org/10.2118/180803-MS

Rezaee, M.R., Kadkhodaie Ilkhchi, A., Barabadi, A., 2007. Prediction of shear wave velocity from petrophysical data utilizing intelligent systems: An example from a sandstone reservoir of Carnarvon Basin, Australia. J. Pet. Sci. Eng. 55, 201–212. https://doi.org/10.1016/J.PETROL.2006.08.008

Rolon, L., Mohaghegh, S.D., Ameri, S., Gaskari, R., McDaniel, B., 2009. Using artificial neural networks to generate synthetic well logs. J. Nat. Gas Sci. Eng. 1, 118–133. https://doi.org/10.1016/J.JNGSE.2009.08.003

Saggaf, M.M., Nebrija, L., 2000. Estimation of lithologies and depositional facies from wire-line logs. Am. Assoc. Pet. Geol. Bull. 84, 1633–1646.

Sapna, S., Tamilarasi, A., Kumar, M.P., 2012. Backpropagation learning algorithm based on Levenberg Marquardt Algorithm. Comp Sci Inf. Technol (CS IT) 2, 393–398.

Saputro, O.D., Maulana, Z.L., Latief, F.D.E., 2016. Porosity Log Prediction Using Artificial Neural Network, in: Journal of Physics: Conference Series. IOP Publishing, p. 012092. https://doi.org/10.1088/1742-6596/739/1/012092

Sbiga, H.M., Potter, D.K., 2017. Prediction of Resistivity Index by Use of Neural Networks With Different Combinations of Wireline Logs and Minimal Core Data (see associated supplementary discussion). SPE Reserv. Eval. Eng. 20, 240–250. https://doi.org/10.2118/181751-PA

Shahin, M.A., Jaksa, M.B., Maier, H.R., 2009. Recent Advances and Future Challenges for

Artificial Neural Systems in Geotechnical Engineering Applications. Adv. Artif. Neural Syst. 2009, 1–9. https://doi.org/10.1155/2009/308239

TAO, G., KING, M.S., 1993. POROSITY AND PORE STRUCTURE FROM ACOUSTIC WELL LOGGING DATA. Geophys. Prospect. 41, 435–451. https://doi.org/10.1111/j.1365-2478.1993.tb00578.x

Ukaonu, C., Odubanjo, T., Lawal, K.A., Eyitayo, S.I., Ovuru, M.I., Anyadike, E., Matemilola, S., 2017. Use of Petro-Elastic Analysis to Evaluate Potential for Sand Production in Petroleum Reservoirs, in: Nigeria Annual International Conference and Exhibition. https://doi.org/10.2118/189177-MS

Van der Aalst, W.M.P., Rubin, V., Verbeek, H.M.W., van Dongen, B.F., Kindler, E., Günther, C.W., 2010. Process mining: a two-step approach to balance between underfitting and overfitting. Softw. Syst. Model. 9, 87.

Verma, A., Cheadle, B., … A.R., 2012. Porosity and permeability estimation using neural network approach from well log data, in: SPE Annual Technical Conference and Exhibition. pp. 1–6.

Wagener, T., Gupta, H. V., 2005. Model identification for hydrological forecasting under uncertainty. Stoch. Environ. Res. Risk Assess. 19, 378–387. https://doi.org/10.1007/s00477-005-0006-5

Waszczyszyn, Z., Słoński, M., 2010. Selected Problems of Artificial Neural Networks Development. Springer, Vienna, pp. 237–316. https://doi.org/10.1007/978-3-211-99768-0_5

Wilamowski, B.M., Yu, H., 2010. Improved computation for Levenberg–Marquardt training. IEEE Trans. neural networks 21, 930–937.

William R. Moore, Y.Z.M.J.U.T.B., 2011. Uncertainty Analysis in Well-Log and Petrophysical Interpretations 17–28. https://doi.org/10.1306/13301405M963478

Williams, D.M., 1990. The Acoustic Log Hydrocarbon Indicator. Soc. Petrophysicists Well-Log Anal.

Yashrakshita, 2013. Estimating Uncertainty in Well Log Analysis by Monte Carlo Simulation, in: SPG, 10th Biennial International Conference & Exposition.

Yu, Y., Seyler, D.J., McCormack, M.D., 2008. Method for estimating missing well log data. US12250983.

Zendehboudi, S., Ahmadi, M.A., James, L., Chatzis, I., 2012. Prediction of condensate-to-gas ratio for retrograde gas condensate reservoirs using artificial neural network with particle swarm optimization. Energy and Fuels 26, 3432–3447. https://doi.org/10.1021/ef300443j

Zendehboudi, S., Shafiei, A., Bahadori, A., James, L.A., Elkamel, A., Lohi, A., 2014. Asphaltene precipitation and deposition in oil reservoirs – Technical aspects, experimental and hybrid neural network predictive tools. Chem. Eng. Res. Des. 92, 857–875. https://doi.org/10.1016/J.CHERD.2013.08.001

Zoveidavianpoor, M., 2014. A comparative study of artificial neural network and adaptive neurofuzzy inference system for prediction of compressional wave velocity. Neural Comput. Appl. 25, 1169–1176. https://doi.org/10.1007/s00521-014-1604-2

Zoveidavianpoor, M., Samsuri, A., Shadizadeh, S.R., 2013. Prediction of compressional wave velocity by an artificial neural network using some conventional well logs in a carbonate reservoir. J. Geophys. Eng. 10, 045014. https://doi.org/10.1088/1742-2132/10/4/045014

Chapter 9 Summary, Conclusions and Recommendations

9.1 Summary

This work has investigated the use intelligent systems such as artificial neural networks, recurrent neural networks, and Gaussian process regression to provide the input parameters for dynamic geomechanical properties of reservoir formation. The investigations led to the development of data driven models. The dataset includes laboratory data and well logs from real reservoir formations. The developed models have been developed to integrate and address the knowledge gap and incorporate the dynamic nature of real-life sequential data.

The thesis presents innovative data-driven models to evaluate geomechanical formation properties such as bulk modulus, Young's modulus, Poisson's ratio, porosity, shear modulus, and sanding potential dynamically. This provides safer, inexpensive and continuous measurements of the formation properties along the wellbore of the reservoir formation. These models serve as effective tools to facilitate formation evaluation for strategic decisions, analysis and development of potential reservoir formations.

9.2 Conclusions

9.2.1 A new static Young's modulus prediction model for formation evaluation

This study has developed a model for predicting a critical geomechanical property – Young's modulus. Static Young's modulus represents the actual characteristic deformation property of the formation better than the dynamically estimated Young's modulus. The reasons for this have been established in this study. However, static Young's modulus is destructive and costly; core samples are not always readily accessible. Dynamic static Young's modulus, on the other hand, is less expensive, non-destructive, and continuous along a wellbore of the formation. A novel model is

developed to estimate static Young's modulus from the more easily obtainable dynamic Young's modulus by using multilinear analytical regression.

The study outperforms all previously established analytical models by including a lithology dependent parameter to account for the discrepancy observed in the values of static versus dynamic Young's modulus. A sensitivity analysis of the model is conducted using Monte Carlo simulation.

9.2.2 **A new data-driven sonic well log prediction model for sanding potential evaluation**

This study has developed a model to instantaneously predict compressional and shear wave transit time logs. The model assists field engineers in the initial assessment for the likelihood of a formation to sanding during reservoir formation exploration and evaluation. The model is developed using a new configuration of the artificial neural network. Artificial neural networks are complex intelligent systems capable of deciphering and mimicking non-linear complex pattern among the network variables; therefore, ANN is able to bridge the non-linear relationship observed in the well logs.

The study integrates multilayer perceptron network using a backpropagation algorithm to define the relationship between the well logs. The relationship defines by the model is used to predict the compressional and shear sonic well logs. Gamma-ray and formation bulk density are sufficient well logs inputs for the successful deployment of the model. The model is applied to assess sanding potential determination model to ascertain the probability of the formation to produce sand during exploration and development. This is a step forward due to the ability of the model to provide real-time data for immediate assessment of formation to sanding thereby eliminating the need to send data offsite for complex geophysical compilations.

9.2.3 **A new data-driven model shear transit time prediction model for field development**

This study developed a shear wave transit time prediction model using Gaussian process regression. Gaussian processes are intelligent systems based on Gaussian distribution that are capable of establishing non-linear patterns and relationships between variables of interest. In this study, exponential Gaussian process regression is used because of its high accuracy and precision in estimating the shear wave necessary for better formation evaluation in offset wells that lack shear wave measurements. The model is data-driven with real well log data from a sandstone formation in the Niger Delta.

In this study, five predictors are used to improve the accuracy and efficiency needed as input in formation property estimations like Poisson's ratio. Poisson's ratio is very sensitive and delicate to input dynamic measurements, hence the need for such a robust model. Poisson's ratio is used as a calibration and quality check tool in formations with questions data due to this sensitive. Values of Poisson's ratio are strictly between 0 and 0.5 except for cases where anisotropy is established, then negative values are observed.

9.2.4 **A new dynamic data-driven model for sonic well log prediction for formation evaluation**

This study has developed a dynamic sonic well log prediction model for formation evaluation using a recurrent neural network. The study is an improvement to the previously developed sonic log model using the artificial neural network. Recurrent neural networks are networks with the capability of ANN and the added capability to storage memory. This allows such networks store values of previously established relationships for forward prediction and determination of nonlinear complex relationships between variables, in this case, reservoir formation well logs. The

model is data-driven and uses data from the Norwegian continental shelf and the Niger Delta. Both formations are sandstone formations

In this study, a special type of recurrent neural network is considered known as non-linear autoregressive with exogenous input recurrent neural network. The architecture provides a highly accurate and robust model to predict the sonic well logs by using past predictions with exogenous input to predict current and future sonic logs. Different combination of gamma-ray and neutron logs are used as exogenous inputs for the model. The model estimations are subsequently used to evaluate real reservoir formation by estimating some sonic dynamic formation evaluation properties namely, sonic ratio, sonic difference, sonic porosity, and Poisson's ratio. The model presents a unique tool for the assessment of reservoir formations from exploration and development which is safe and inexpensive.

9.2.5 **An assessment of ANN as a reliable sonic well logging tool.**

The study provides an assessment of the suitability and reliability of ANN for producing well logs. Although ANN is gaining a lot of attention and is quite a popular technique to estimate well logs where data is missing, it has its inherent shortcomings, which are not often discussed in the literature.

In this study, the methodology for developing a base case ANN model is presented with a case study. The challenges often encountered in the development of such ANN models are then discussed and evaluated as seen in the developed model. The shortcomings and pitfalls are exposed by demonstrating the weakness of the base model and subsequent models derived from the base model. The study suggests that though ANN is a robust and reliable tool for predicting sonic logs, there are many pitfalls to which inexperienced developers are likely to encounter. The study also

alludes to the fact that there are no hard and fast rules to determining the best model for sonic well logging. The best ANN models for a particular formation are often arrived at through iterations, best practices and past experiences. Th study provides some guidance and suggestion as to how to overcome some of the challenges and shortcoming of ANN models as a sonic well logging tool.

9.3 Recommendations

This research has endeavored to introduce novel and innovative concepts to provide safe, reliable and inexpensive techniques of providing tools for formation evaluation. However, several knowledge gaps and scope of work that could be further addressed include, but are not limited to:

- Models to establish relationships between dynamically estimated formation properties and static formation properties should be investigated to provide more reliable formation properties that are more descriptive of the characteristics of the formation.

- Intelligent systems present a unique opportunity to advance the estimation and prediction of many complex processes in the petroleum industry. Further study should be conducted to investigate the applicability of these intelligent systems to previously established analytical methods such as genetic algorithms.

- The performance and error functions of these models should be investigated and compared to other data-driven models and analytical techniques.

- Modeling the universal applicability of model in different geographical location and setting could be further investigated. The formation considered in this research has mainly focused on sandstone formation, but carbonate formations should also be considered.

- Modeling of uncertainty should be investigated more closely. The range of the input data varies depending on the data being considered. The extremities within the range should be considered to ensure that the models are robust and efficient, hence, capable of handling large data sets.

- Selection of input arguments should be considered independently for selected formations different geological settings. The selection of input data that provides the best prediction may vary depending on the formation being considered.

- Generalization of these models should be investigated to ensure the suitability of the models as predictive validation and quality check tools in reservoir formation evolution for field development and management.

- The models proposed here are reliable and robust; however, they inherit both aleatory and epistemic uncertainty. It is important to understand and consider these uncertainties as part of the formation properties evaluation.

- Validation of developed models should be conducted with real-life data to enhance generalization, suitability and reliability of data-driven models.

Appendixes

During the course of the research, we collaborated with other researchers and co-authored the publications presented in this appendix.

A.1 Modeling Investigation of Low Salinity Water Injection in Sandstones and Carbonates: Effect of Na^+ and SO_4^{2-}

Preface

A version of this chapter has been published in the Fuel Journal 2018. Cleverson Esene is the primary author and performed the simulation. Co-author David Onalo conducted the literature review and wrote the introduction section of the paper. Co-author Dr. Sohrab Zendehboudi reviewed and prepared the final draft of the paper. He provided valuable insights on necessary sections to include to make the work publishable. Co-author Dr. Lesley James as a subject matter expert of enhanced oil recovery provided technical guidance on key areas to investigate in the simulation study. Co-author Dr. Stephen Butt provided technical assistance and review of the paper. Cleverson Esene and I carried out most of the analysis. The first draft of the manuscript was prepared by Cleverson Esene and I, and subsequently revised the manuscript, based on the feedback from the co-authors and also a peer review process by Cleverson Esene.

Abstract

Low salinity water injection (LSWI) has gained great attention as a promising enhanced oil recovery (EOR) method with numerous advantages (e.g., economic and environmental aspects), compared to other conventional chemical EOR methods. For the past two decades, a number of laboratory studies have been performed by researchers to understand the main pore-scale mechanisms of oil displacement during LSWI; however, further experimental and modeling research works are required to comprehend the LSWI governing mechanisms. The focus of this paper is to investigate important aspects such as oil recovery mechanisms, oil-water wettability alterations, changes in pH of formation water, and mineral reaction (dissolution/precipitation) which occur during LSWI in sandstones and carbonates. To explore the effect of ion-exchange, a compositional model is developed with the aid of laboratory data by Computer Modelling Group (CMG) where Na^+ and SO_4^{2-} are used as interpolants to model LSWI in sandstones and carbonates cores respectively.

***Keywords**:* Low Salinity Water Injection (LSWI), Precipitation and Dissolution, Ionic-Exchange, Sandstones, Carbonates, Oil Recovery Factor.

A.1.1. Introduction

Post-primary oil production drive may leave behind up to 85% of the proven reserves in a petroleum formation. Water flooding can reduce the amount of oil saturation to nearly 60% and low salinity water injection (LSSWI) may produce an extra 15% so that about 40% of the residual oil can be recovered [1,2]. It appears that LSSWI is becoming one of the most popular enhanced oil recovery (EOR) technique, based on the literature [3–9]. This is probably due to the low cost associated with its implementation when compared to other EOR techniques. Low salinity water is referred to smart water, ion-engineered water, and advanced ion management water in various research studies by many researchers; however, the methodology and mechanisms behind the increase in oil recovery remain the same [9,10]. The mechanisms responsible for the increased oil recovery have been identified to be wettability alteration, double layer expansion, multicomponent ionic exchange, fines migration, and mineral dissolution [3,6,8–19]. However, the dominant mechanisms for the oil recovery increase still remain a subject of debate among researchers. The above mechanisms alter the rock-brine-oil equilibrium from its inherent state so that they might modify important properties such as permeability and wettability to improve the oil recovery. Wettability alteration appears to be the most widely accepted dominant mechanism for low salinity water injection [4,7,13,18–24].

These are a few mathematical modeling on LSWI in the open sources where contradictions and vital limitations are found in them. For instance, Altahir et al. [25] studied the LSWI strategy in carbonates in core-flood experiments by considering the improved oil recovery and pH increase; however, they did not take into consideration the changes in the composition of the rock [25]. Vajihi et al. [26] also investigated LSWI oil recovery and residual oil saturation in core-flood where ions exchange and effect of the flowrate were not discussed in their work [26]. Didier et al.

[27] suggested that pH is the key factor in wettability alteration in Fontainebleau and Ottawa sandstones. The results show that oil adhesion occurs at pH values of higher than 6 – 8. Other research works concluded that the oil adhesion experiences at pH values lower than 6 – 8 (for instance, a pH of 4) [27]. In another work, Al-Shalabi and Sepehrnoori [9] suggest that more modeling research works need to be conducted in carbonates than sandstones because it is assumed that the mechanisms that controls the wettability alteration in sandstone is known – clay, but the mechanism is not known in carbonates.

The composition and salinity of the low salinity water are not constant and universal in all formations across the world. Hence, systematic studies need to be carried out to determine the optimum salinity and concentration of the selected low salinity water. During laboratory investigation of sandstone and carbonate cores, as the salinity of the LSWI is reduced, there is an increase in the oil recovery; however, after a certain threshold value, there is no significant increase in the oil recovery upon further reduction of salinity in the LSWI process. This suggests that there is an optimum salinity and concentration for the various formations under LSWI. It was observed that the optimum salinity can range for sandstones, a reduction in LSWI salinity of up to 100% to give salinities as low 100 to 2000 ppm is possible [28,29], but for carbonates, 50% reduction in LSWI salinity yields LSWI of 1000 to 5000 ppm [6,8,12,15,30,31] for effective low salinity water injection schemes.

A balance of adsorption capacity, cation exchange capacity, and pH window for clay is necessary to evaluate the effectiveness of LSWI in sandstones [17]. In core flood experiments conducted by Zhang and Morrow [2], up to 33% increase was observed in Berea sandstone which contained clay, while no significant increase was observed in clay-free Berea sandstone when the brine with 1% salinity was injected. In sandstones with kaolinite clay, fines migration due to the desorption

of kaolinite clay from the mixed-wet sandstone surface is suggested as the mechanism responsible for the increased oil recovery by LSWI [32]. An increase in the injection pressure and a reduction in permeability are often accompanied with the increased oil recovery in core flood experiments [33,34]. There are a limited number of research investigations on the formation damage during LSWI in the open sources [35]. Typical pH values of 4-6 are attainable in sandstone reservoirs; the pH in the formation increases as the low salinity water is injected in formations due to cation exchange of the effluent and clay anion surfaces; however, a pH value greater than 10 is seldom encountered due to the inherent CO_2 in the hydrocarbon-bearing formations, which acts as a pH buffer [32]. During laboratory investigation of LSWI, the concentration of divalent ions such as Ca^{2+} and Mg^{2+} in the effluent were lowered, leading to an increase in oil recovery; however, when the cores were pre-flushed with NaCl to remove the divalent ions, there was no significant oil recovery [32]. The ions contribute to the electric surface charge and an electric double layer is formed. The expansion of the electric double layer has also been suggested as the dominant mechanism that considerably affects the oil recovery over the LSWI process [30,36]. This can be measured by the zeta potential of the surface.

More than half of the proven oil reserves are found in carbonates. Efficient exploitation and recovery of these reserves are challenging due to the low permeability and porosity of the porous system, particularly the matrix blocks [6]. The dominant mechanism in carbonates may be attributed to the wettability alteration of the mixed to oil-wet formations to more water-wet formations, leading to a higher oil production. Monovalent and divalent ions that alter the rock-brine equilibrium are referred to potential determining ions and the mechanism behind their alteration in the formation is known as a multicomponent ionic exchange. Austad et al. [16] investigated the effect of seawater salinity on oil recovery in the Ekofisk field as a highly fractured

carbonate reservoir. The surface charge is positive with Ca^{2+} in equilibrium with the formation brine at a pH value of 7-8. Ekofisk seawater has a Ca^{2+} ion concentration less than half of the formation brine concentration. When the seawater is injected into the formation, Ca^{2+} is desorbed from the surface into the injected water to balance the rock-brine equilibrium; but the desorption alters the rock-oil equilibrium. The negatively charged carboxylic components ($R\text{-}COO^-$) attached to the Ca^{2+} are desorbed, leading to an increase in the crude oil mobility and eventually an increase in the amount of oil recoverable. SO_4^{2-} ions can also promote the desorption of carboxylic oil components from the carbonate surface by adsorbing Ca^{2+} to produce $CaSO_4$ [13,20,37–39]. Enhanced oil recovery is also attributed to the rock dissolution [40,25,41], though Austad et al. [42] suggested that the rock dissolution is not necessary for increased oil recovery based on a series of experimental runs. The initial wettability, salinity, ions present, and wetting phase are the critical parameters that influence wettability alteration, production mechanism, and oil recovery. In the laboratory scale in the absence of Ca^{2+} and Mg^{2+}, an increase in SO_4^{2-} concentration of the injected fluid fails to improve the oil recovery, implying that divalent potential determining cations are needed to improve oil recovery through SO_4^{2-} adsorption [16,43–45]. Based on the literature, there are no numerical studies to discuss about the production behavior/trend of LSWI in carbonates and sandstones. To the best of our knowledge, the effects of mineral dissolution and precipitation have not been numerically investigated in the previous related research works. Wettability alteration appears to be the dominant mechanism for LSWI; however, there has not been a sufficient number of numerical compositional studies in the literature to validate this claim because of the difficulty to entirely capture ion exchange by most commercial simulators. Other phenomena, which occur during LSWI, such as the change in the local pH in the formation water, ionic-exchange, and mineral reactions (in carbonates) have not been studied adequately.

In this paper, a compositional simulation model was built employing the CMG-GEM module to study the effect of concentration of sodium ion (Na+) and sulfate (SO_4^{2-}) in sandstones and carbonates, respectively. The first step is to build a fluid model with CMG-Winprop such that the fluid properties such as saturation pressure, gas/oil ratio, formation volume factor, relative oil volume, and oil density are tuned to match the available experimental data for the reservoir fluids. Then, the matched fluid model is imported into a 1-D generic reservoir and the initial ionic compositions of the brine are provided from the laboratory analysis. The simulation model uses Na+ and SO_4^{2-} ions for ion exchange in sandstone reservoir and carbonate reservoir, respectively. Na^+ and SO_4^{2-} concentrations in the sandstone and carbonate are altered to find the impact of the ion concentration on pH, mineral precipitation and dissolution, and oil recovery.

A.1.2. Theoretical analysis: ion exchange in lswi

There is a chemical equilibrium between the ionic concentration of the connate water or the initial formation water and the ions which are adsorbed onto the clay surface in the reservoir [47].

Figure A1. 1 shows a typical representation of clay mineral, ionic bridge, oil and typical ions to describe the important interaction mechanisms in LSWI

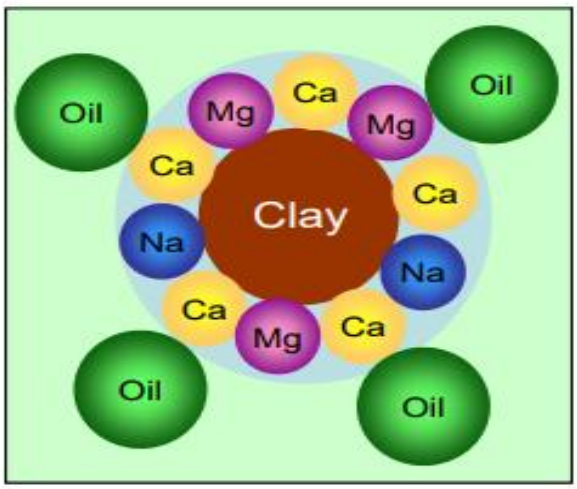

Figure A1. 1. Schematic representation of clay mineral, ionic bridge, oil and typical ions to describe the important interaction mechanisms in LSWI (Modified after Lager et al. [32]

The polar oil components are bound to the clay surface in the presence of an ionic bridge which lies between the actual clay and oil. This makes the rock preferentially oil wet as shown in

Figure A1. 1in a molecular level. Once the low salinity water is injected, it causes the ion exchange between the monovalent ions and divalent ions (e.g., Na exchanging with Ca). During this ionic exchange, the oil is released from the divalent ions and becomes producible. This reduces the overall residual oil saturation and causes a shift in wettability to more water wet rock.

Injecting water with an ionic concentration, which is different from the original formation water, causes a chemical reaction and an ionic exchange. There are two typical ionic exchange reactions which can occur during LSWI. The reactions involve the alkali and alkali earth metals particularly sodium, calcium, and magnesium as given below [47].

$$Na^+ + \frac{1}{2}(Ca - X_2) \rightleftharpoons (Na - X) + \frac{1}{2}Ca^{2+} \quad \text{(A1 1)}$$

$$Na^+ + \frac{1}{2}(Mg - X_2) \rightleftharpoons (Na - X) + \frac{1}{2}Mg^{2+} \quad \text{(A1 2)}$$

where X represents the clay mineral in the reservoir rocks. The above reactions are reversible, implying that the monovalent ions are exchanged with divalent ions during LSWI. For instance, Na^+ is taken by the exchanger and Ca^{2+}/Mg^{2+} are freed to represent the forward reactions (see Equations (A1 1) and (A1 2). In this case, the oil initially bounded on Ca and Mg (as shown in

Figure A1. 1) is released, causing the rock surface to become more water wet. Similar to the chemical reactions, ion-exchange reactions can be defined by the equilibrium constant as represented by the following expression:

$$K\ Na/Ca = \frac{\left[a\left(Ca^{2+}\right)\right]^{0.5} a(Na-X)}{a(Na^+)[a(Ca-X_2)]^{0.5}} \quad \text{(A1 3)}$$

$$K\ Na/Mg = \frac{\left[a\left(Mg^{2+}\right)\right]^{0.5} a(Na-X)}{a(Na^+)[a(Mg-X_2)]^{0.5}} \quad \text{(A1 4)}$$

in which, *a* stands for the activity. The activity of i^{th} component (a_i) is related to the activity coefficient (γ_i) through the following equation:

$$a_i = \gamma_i m_i \qquad \text{(A1 5)}$$

where m_i refers to the molality of component *i*.

Substituting Equation (A1 5) into Equations (A1 3) and (A1 4) results in Equations (A1 6) and (A1 7) to determine the equilibrium constant, as shown below:

$$K_{Na/Mg} = \frac{\left[m\left(Mg^{2+}\right)\right]^{0.5} m(Na-X)}{m(Na^{+})\,[m(Mg-X_2)]^{0.5}} \quad x \quad \frac{\left[\left(\gamma\, Mg^{2+}\right)\right]^{0.5} \gamma(Na-X)}{\gamma(Na^{+})\,[\gamma(Mg-X_2)]^{0.5}} \qquad \text{(A1 6)}$$

$$K_{Na/Ca} = \frac{\left[m\left(Ca^{2+}\right)\right]^{0.5} m(Na-X)}{m(Na^{+})\,[m(Ca-X_2)]^{0.5}} \quad x \quad \frac{\left[\left(\gamma\, Ca^{2+}\right)\right]^{0.5} \gamma(Na-X)}{\gamma(Na^{+})\,[\gamma(Ca-X_2)]^{0.5}} \qquad \text{(A1 7)}$$

The activity coefficient of sodium and calcium ions in the aqueous phase can be calculated by the Debye-Huckel model or by the B-dot model; however, the evaluation of the activity coefficient of Na-X, Ca-X_2 and Mg-X_2, which correspond to Na^+, Ca^{2+} and Mg^{2+} on the exchanger surface, is not an easy task. Therefore, the selectivity coefficient is used by CMG instead of the equilibrium constant, as introduced by Equations (A1 8) and (A1. 9):

$$K'_{Na/Mg} = \frac{\left[m\left(Mg^{2+}\right)\right]^{0.5} \zeta(Na-X)}{m(Na^{+})\,[\zeta(Mg-X_2)]^{0.5}} \quad x \quad \frac{\left[\left(\gamma\, Mg^{2+}\right)\right]^{0.5}}{\gamma(Na^{+})} \qquad \text{(A1 8)}$$

$$K'_{Na/Ca} = \frac{\left[m\left(Ca^{2+}\right)\right]^{0.5} \zeta(Na-X)}{m(Na^{+})\,[\zeta(Ca-X_2)]^{0.5}} \quad x \quad \frac{\left[\left(\gamma\, Ca^{2+}\right)\right]^{0.5}}{\gamma(Na^{+})} \qquad \text{(A1. 9)}$$

ζ(Na-X), ζ(Ca-X_2), and ζ(Mg-X_2) stand for the equivalent fraction of $Na^+/Ca^{2+}$and Na^+/Mg^{2+} on the exchanger, respectively. The selectivity coefficient, which is a function of operational

conditions, is used, since they can be measured unlike equilibrium constants which are thermodynamic variables. Hence, $K'_{Na/Ca}$ and $K'_{Na/Mg}$ are estimated using the experimental measurements. Appelo, et al. [48] reported the selectivity coefficient between Na^+ and many ions which are used in the CMG simulation package.

In CMG-GEM, all component moles are represented as moles per grid block volume. The total moles of Na-X, Ca-X_2, and Mg-X_2 in a grid block are $VN_{Na\text{-}X}$, $VN_{ca\text{-}X2}$, and $VN_{Mg\text{-}X2}$, respectively; where V is the grid block volume. For any value of cation exchange capacity in the grid block, the following equation needs to be satisfied

$$VN_{Na\text{-}X} + VN_{ca\text{-}X2} + VN_{Mg\text{-}X2} = V\phi(CEC) \qquad \text{(A1 10)}$$

In a control volume (see Figure A1. 2), the material balance equation for the ion of charge i^+ that includes ion exchange with an exchanger X in the aqueous phase is expressed by Equation (A1 11);

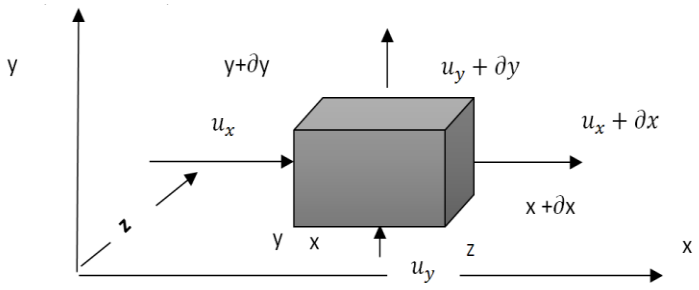

Figure A1. 2 A control volume/element of a 3-D flow in directions x, y, and z

$$\Delta T_{aq}^{u} y_{iw}^{u} \left(\Delta P^{n+1} + -\rho_{aq}^{u} g \Delta h\right) + \Sigma \Delta D_{iaq}^{u} \Delta y_{iaq}^{u} + VR_{i,aq}^{n+1} + VR_{i,mn}^{n+1} + q_{i}^{n+1} \quad \text{(A1 11)}$$

$$-\frac{V}{\Delta t}\left(\left(N_{i,aq}^{n+1} - N_{i-x}^{n+1}\right) - \left(N_{i,aq}^{n} - N_{i-x}^{n}\right) = 0,\right.$$

Where T = Transmissibility; y = mole fraction, P = pressure, g = acceleration due to gravity, h = height, D= Diffusivity, V = grid block volume, R = reaction rate, q = injection, $VR_{j,aq}^{n+1}$ = Intra aqueous reaction rate, $VR_{j,mn}^{n+1}$ = Mineral dissolution/precipitation, n + 1 = implicit time step for grid block, u = explicit time step for grid block, N = Number of moles of mineral and *i =1 …n*th represents the number of components.

Running CMG, the governing equations are solved simultaneously along with the phase, chemical, and ion-exchange equations through using Newton's method.

A.1.3. Model development

This section illustrates the main steps to obtain the fluid and rock properties and to conduct the modeling simulations using CMG

A.1.3.1. Fluid Behavior Modeling

To create a fluid model used for the simulation of LSWI, various steps should be taken (see Figure A1. 3). Fluid composition given in Table A1. 1 1 and Table A1. 2 is first used to build an EOS model using Peng Robinson equation of state to represent the original reservoir fluid. The EOS model is then tuned against the experimental data of Constant composition expansion (CCE), Constant volume depletion (CVD), and Differential liberation (DL) after which a flash process of the reservoir fluid at standard condition of 60^{o}F and 14.7psia is simulated. A good match is obtained between the experimental and modeled fluid properties. Figure A1. 3 depicts the flow chart to illustrate how the fluid model is built for this simulation.

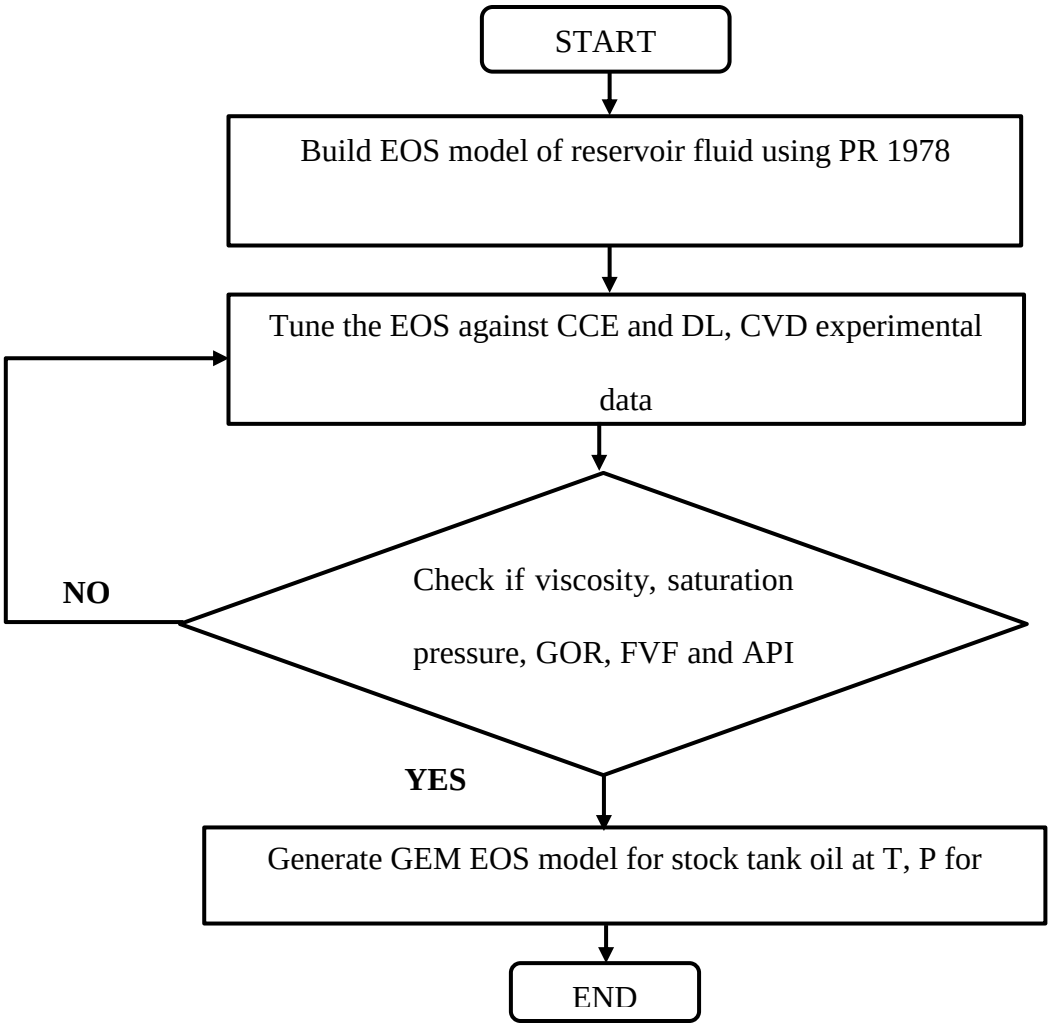

Figure A1. 3 Flowchart to prepare the EOS fluid model

PVT Data. Laboratory experiments were conducted for Saturation Pressure, Constant Composition Expansion test and Differential Liberation test. From the laboratory experiments, the total Gas Oil Ratio (GOR), Saturation Pressure, Formation Volume Factor (FVF) and API Gravity are 247 scf/stb, 740 Psi, 1.18, 40.0 respectively. The oil viscosity used for this study is 0.65 cP measured at bubble point. These experiments were added to the CMG - Winprop model to obtain an idea of how close the current EoS is to modeling the observed fluid behavior. The supplied data for reservoir oil fluid compositions/heavy fractions, separator test results, constant composition

test results, differential liberation test results are all used for tuning the EoS to match the fluid behavior. The fluid compositions and the laboratory heavy fraction analysis utilized in this study are provided in Table A1. 1 and Table A1. 2 which are available in Computer modeling Group, 2017 [46].

Table A1. 1 Black oil composition [46]

Component	Mole %
CO_2	0.1183
N_2	0.0016098
C_1	0.1154103
C_2	0.060058
C_3	0.0647635
i-C_4	0.0221657
n-C_4	0.047551
i-C_5	0.0328152
n-C_5	0.0370254
C_6	0.065135

Table A1. 2. Laboratory heavy fraction analysis for C7 – C30+ [46]

Components	Mole,%	Molecular weight, g/gmol	Specific gravity
C7	0.084205	91.931365	0.7400
C8	0.098941	103.11563	0.74659
C9	0.078385	113.43017	0.8129
C10	0.051514	132.0084	0.7937
C11	0.031329	147	0.7930
C12	0.021299	161	0.8040

C13	0.019318	175	0.8150
C14	0.014488	190	0.8260
C15	0.013374	206	0.8360
C16	0.010649	222	0.8430
C17	0.00904	237	0.8510
C18	0.009659	251	0.8560
C19	0.008173	263	0.8610
C20	0.005325	275	0.8660
C21	0.003963	291	0.8710
C22	0.00322	300	0.8760
C23	0.002353	312	0.8810
C24	0.001981	324	0.8850
C25	0.001857	337	0.8880
C26	0.001857	349	0.8920
C27	0.001981	360	0.8960
C28	0.002105	372	0.8990
C29	0.002105	382	0.9020
C30+	0.064516	400	0.9700

Peng Robinson equation of state is employed to construct the fluid model through using the fluid compositions where the regression procedure on experimental constant composition expansion, constant volume depletion, differential liberation, and separator test is carried out. Figure A1. 4 shows the phase envelope to characterize the fluid used in this modeling/simulation work.

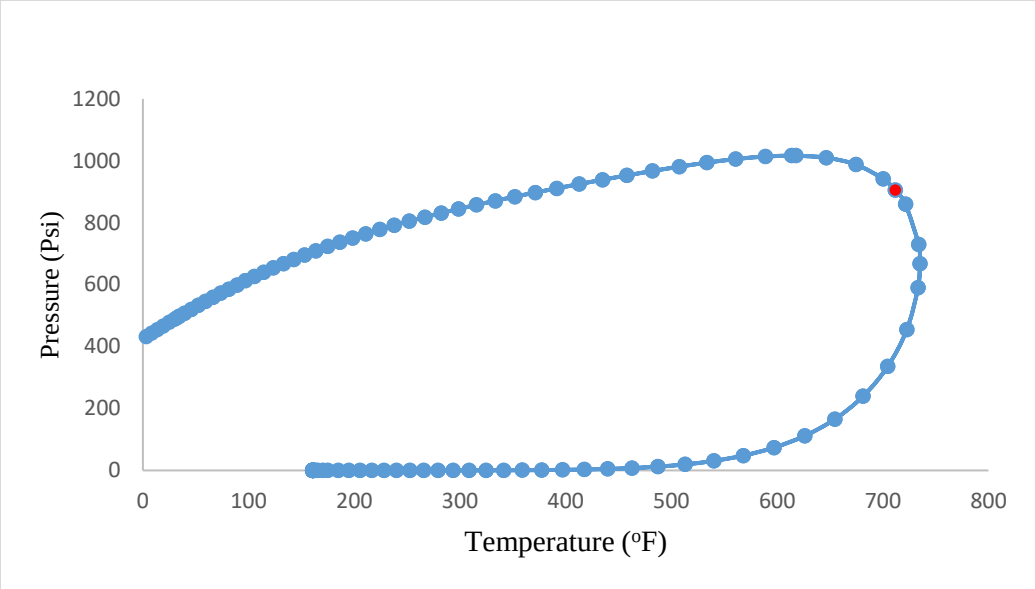

Figure A1. 4. Pressure-temperature (P-T) diagram of the modeled reservoir fluid.

The comparison between the initial GOR, final GOR and the experimental data is shown in Figure A1. 5 (after regression).

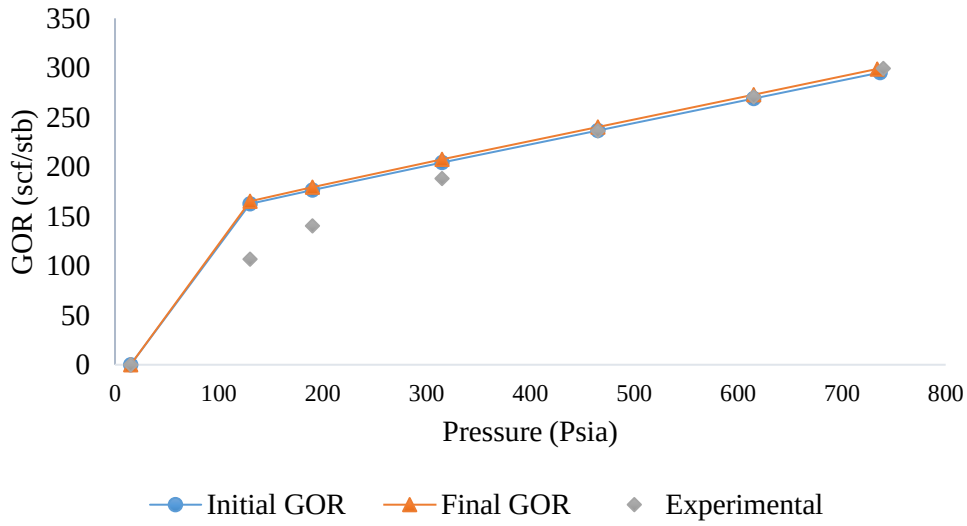

Figure A1. 5. Comparison of measured gas oil ratio (GOR), initial GOR (before tuning), and final GOR (after tuning)

As can be seen in Figure A1. 5, an improvement is achieved to match the experimental GOR by tuning the Pc and Tc of the heavier components during regression procedure. The similar

comparisons between the experimental and the final parameter for the fluid are shown in Figure A1. 6 for the relative oil volume and Figure A1. 7 for the saturation pressure. Based on the comparison (showing relatively small error), it can be concluded that the modeled fluid behaves the same as the real reservoir fluid.

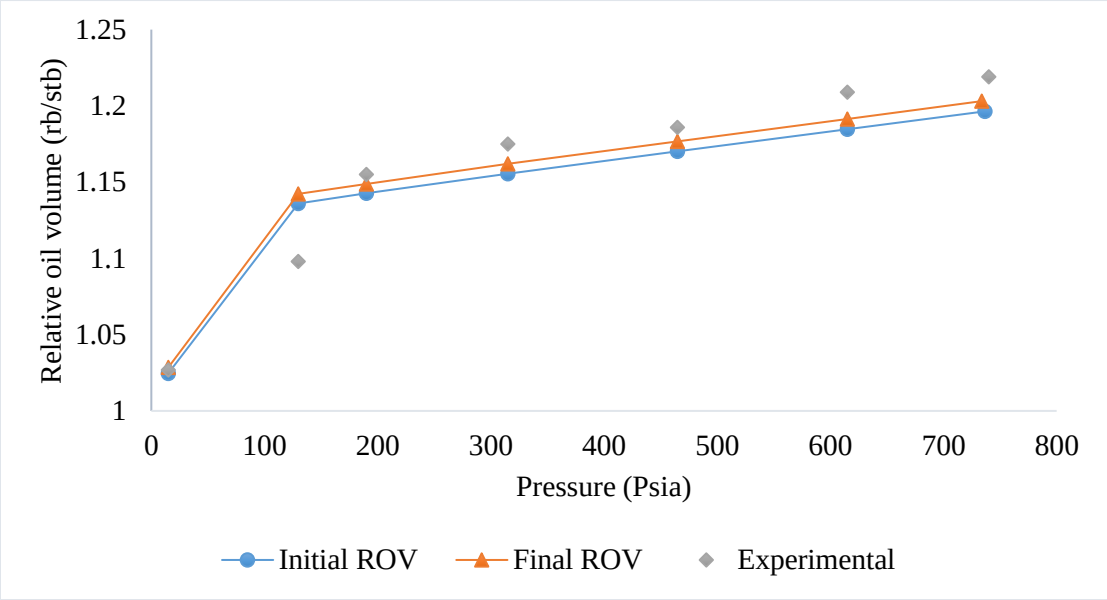

Figure A1. 6. Comparison of measured relative oil volume (ROV), initial ROV (before tuning) and final ROV (after tuning)

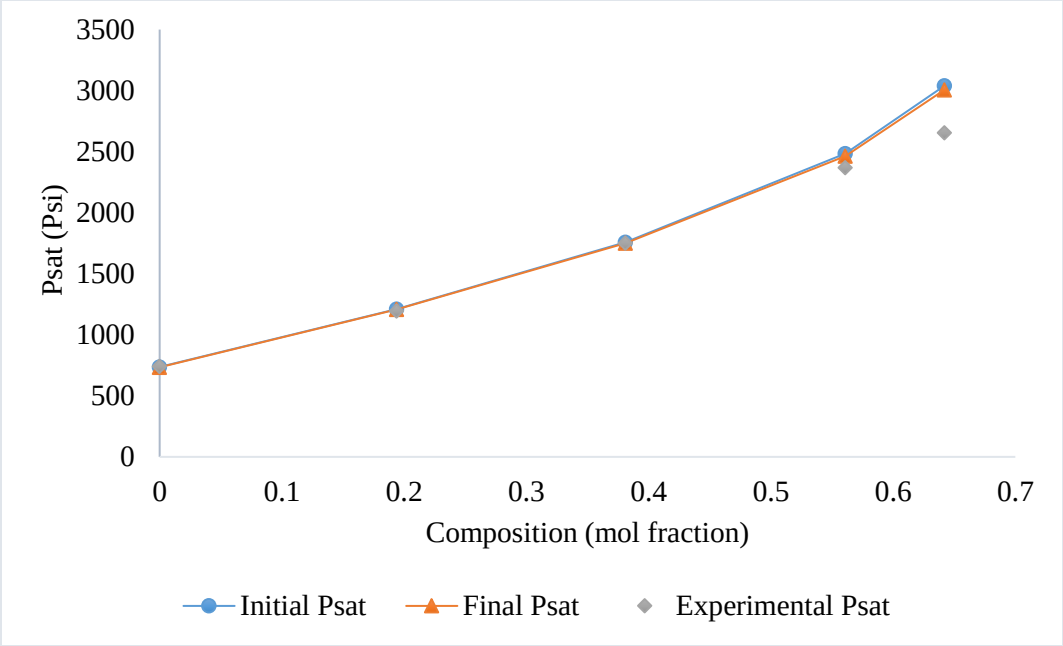

Figure A1. 7. Comparison of measured Psat, initial Psat (before tuning) and final Psat (after tuning)

Tuning the EOS model to attain a good matching between the modeling results and available experimental data, Table A1. 3 shows the reduction in error percentage (through comparing the values before and after tuning) for a part of important fluid properties used in this research work. This final error reduction percentage between the before and after tuning results shows that a valid match has been obtained through the regression analysis carried out using the Winprop EoS module in CMG.

Table A1. 3. Experimental and modeled fluid properties

Property/Data	Experimental	Before tuning	After tuning	Error reduction
Psat, psi	740.0000	740.040	736.70	0.4 %
GOR, scf/stb	247.000	247.000	248.881	0.4 %
FVF, bbl/stb	1.180	1.140	1.159	1.3 %
API	40.000	41.000	40.009	0.25

The main source of error is through Plus fraction splitting of the grouped/lumped heavy carbon fractions. Through the lumping of the carbon fractions, technique such as Kays mixing rule is employed to determine the resultant properties such as critical temperature, critical pressure, acentric factor, and mole fraction. This process is accompanied with a degree of error which is unassociated with pure and single carbon number.

A.1.3.2. Reservoir Modeling

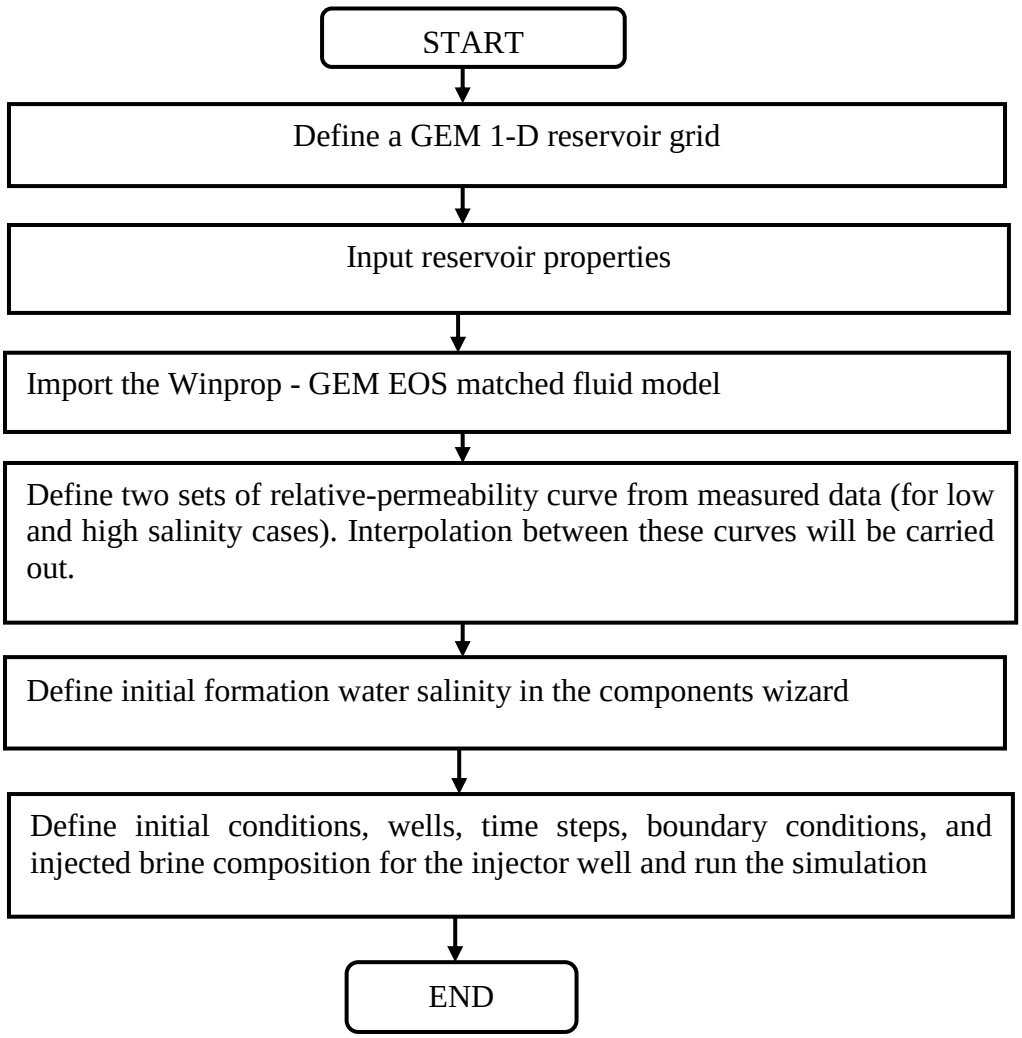

Figure A1. 8. A simple approach to develop GEM reservoir compositional model for LSWI

We consider a 1-D model to simulate a core flood displacement test with CMG-GEM compositional simulator. The steps taken to build the compositional generic reservoir model for LSWI simulation are represented in a flowchart as demonstrated in Figure A1. 8.

A core of length 2.87 ft and a diameter of 0.1228 ft is considered to replicate the core dimensions used for a water flood experiment conducted by CMG [46]. The total grid of 50 is used in the I-direction and 1grid in J and K directions. The reservoir porosity is 0.24. The matrix permeability (k_m) and fracture permeability (k_f) are 11.43 mD and 1000 mD, respectively. Figure A1. 9 shows a schematic representation of the 1-D compositional generic model which is built in CMG-GEM to study important aspects of LSWI.

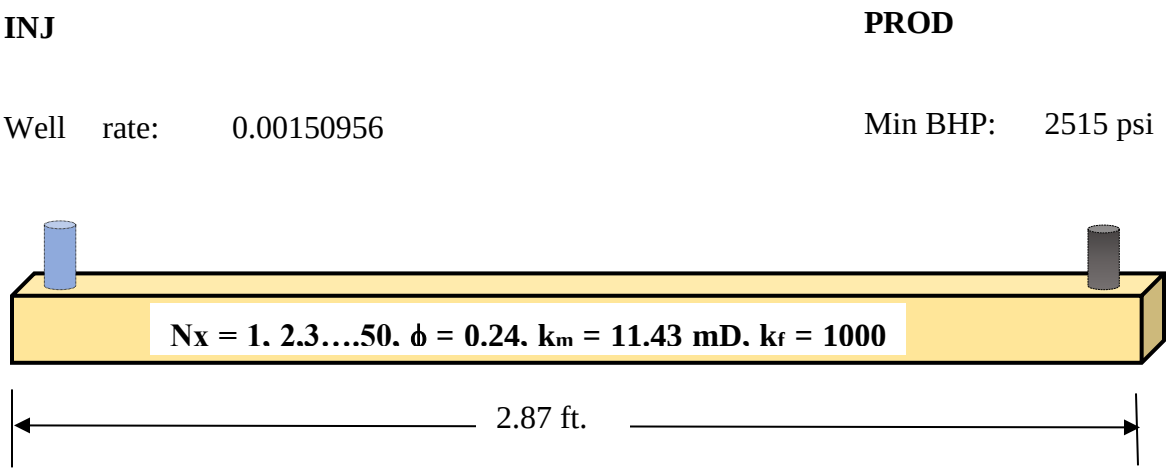

Figure A1. 9. Schematic of the 1-D model structure

The injector well is constrained by an injection flow rate of 0.00150956 bbl/day and by a maximum bottom hole flowing pressure (BHP) of 4000 psi. A minimum BHP of 2515 psi is considered for the producer well. The finite difference method is used (as a mathematical strategy) by CMG to discretize the conservation mass or/and momentum equations of the oil and water/brine phases during the LSWI process. The mass balance equations are written for the fracture and matrix domains which are discretized in an adaptive-implicit manner for each grid block. The equations

are then solved interactively by CMG where the primary constraints are used for the convergence purpose.

Input Data. To construct a 1-D numerical reservoir model, the model properties, which were used by Computer modeling Group for their experimental investigation of 1-D laboratory core flood, were employed in the current simulation work. Reservoir properties (for sandstone and carbonate) and the laboratory end-point relative permeability data are tabulated in Table A1. 4 and Table A1. 5, respectively. Also, the plot of the resultant relative permeability versus water saturation used for this study is shown in Figure A1. 10.

Table A1. 4 Model properties [46]

Parameter	Field unit	SI unit
Initial Reservoir pressure	2515 psi	17.23 x 10-6 N/m2
Permeability	11.43 mD (Matrix) 1000 mD (Fracture)	1.12 x 10-14 m2 9.86 x 10-13m2
Matrix Porosity	0.24	0.24
Fracture porosity	1.00	1.00
Initial oil saturation	0.80	0.80
Connate Water saturation	0.20	0.20
Cross sectional area	0.01185ft2	0.00110m2
Grid thickness	0.10888 ft	0.01011m

Table A1. 5. Laboratory end-point relative permeability data [46]

Description/Parameter	Value
Property	Damage
Endpoint saturation: Connate water	0.20
Endpoint saturation : Residual oil	0.29
Endpoint saturation: Irreducible oil for gas	0.37

Endpoint saturation : critical gas	0.03
Relative permeability at connate water	0.30
Relative permeability at irreducible oil	0.20
Exponent for calculating Krow	3.00

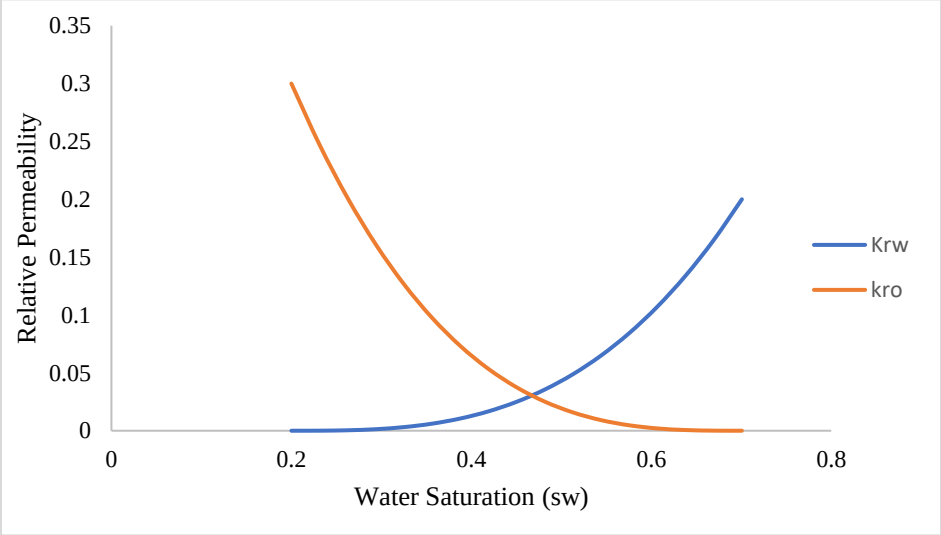

Figure A1. 10. Relative Permeability curve

Brine Water Analysis. This section presents the laboratory water analysis of the formation water with total dissolved salt of 245980 ppm as listed in Table A1. 6 (as a part of the input date in the simulator). The total Na^+ and SO_4^{2-} ions originally present in the formation water are 68520 ppm and 612 ppm, respectively. Figure A1. 11 illustrates the simulation runs to study the effect of Na^+ and SO_4^{2-} on the oil recovery in the sandstone and carbonate.

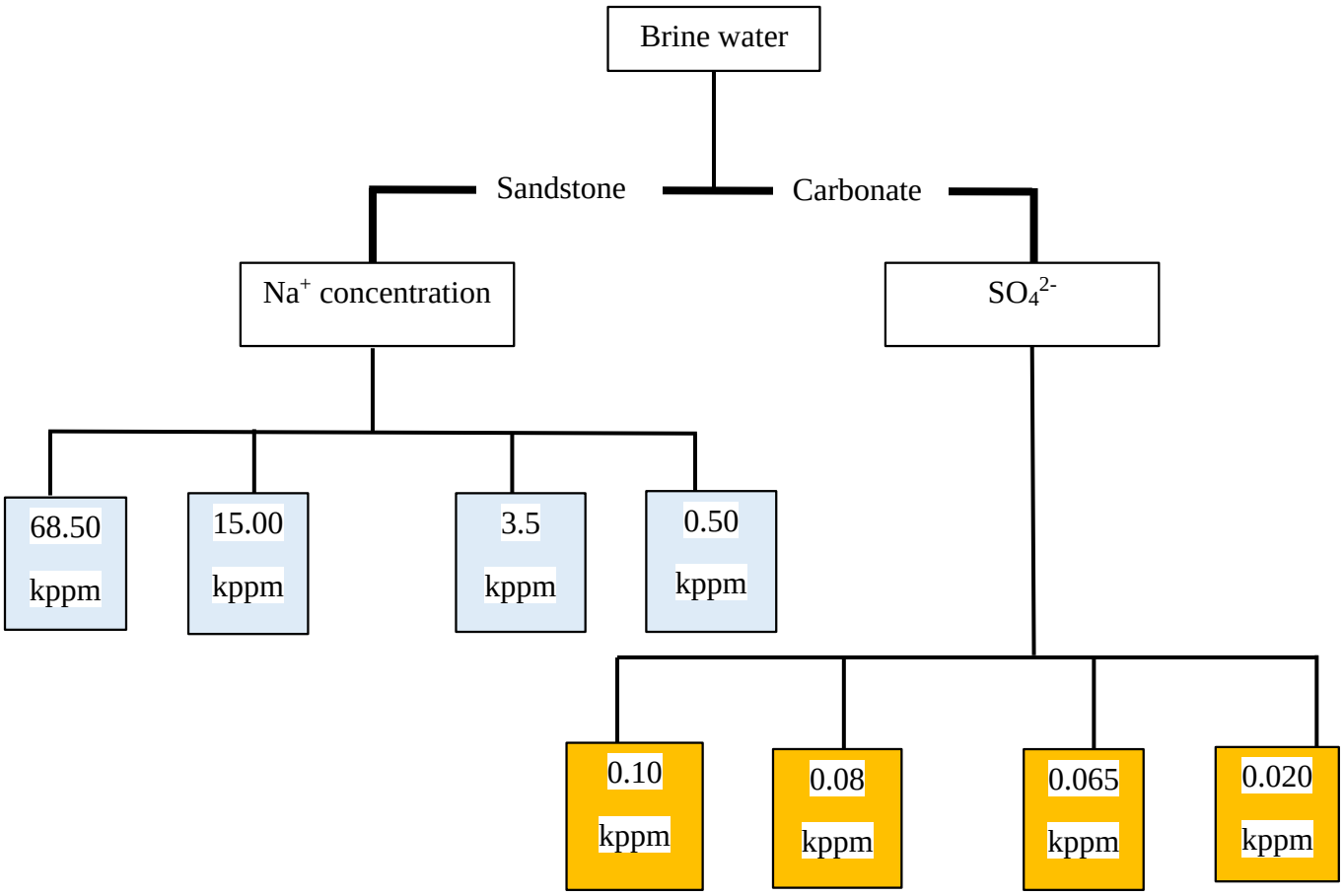

Figure A1. 11. Design of simulation runs to understand the impact of Na^+ and SO_4^{2-} in the LSWI process

Table A1. 6. Initial laboratory formation water compositions/mineral volume fractions [46]

Component/ion		Formation water
Calcium	Ca^{2+}	18492 ppm
Magnesium	Mg^{2+}	2320 ppm
Strntium	Sr^{2+}	1880 ppm
Sodium	Na^+	68520 ppm
Potassium	K^+	4050 ppm
Barium	Ba_2^+	2.5 ppm
Bicarbonate	HCO_3^-	0

Carbonates	CO_3^{2-}	0
Chloride	Cl^-	150060 ppm
Sulphate	SO_4^{2-}	612 ppm
Hydroxide	H^+	0
Boron	Br_2^+	43.7 ppm
Total dissolved salts (TDS)		245980 ppm
pH		5.22
Volume fraction of calcite		0.5
Volume fraction of dolomite		0.5

Boundary and Initial Conditions. There are two types of boundary condition implemented by CMG for the solution of PDE's; namely, Newman and Dirchelet (or fixed pressure) boundary conditions. These boundary conditions are the set of constraints (primary and secondary) which are defined as the input into the simulator in terms of BHP and well flow rates. The initial brine compositions and the measured relative permeability for the high and low salinity conditions are defined as a set into CMG and the interpolation will be carried out for the salinity values between the limits.

Although CMG model has been validated with the experimental data and the results have been also compared with other commercial simulators such as PHREEQC, concluding the model is suitable or applicable as a tool for the study of LSWI, it is only capable of modeling low salinity water injection in sandstones by using Na^+ as an interpolant between the low salinity relative permeability curve and high salinity relative permeability curve. Only Ca^{2+} or SO_4^{2-} can be used as an interpolant for modeling in carbonates. Hence, the complexities of ion exchange during this process cannot be effectively captured.

Modeling Wettability Alteration

The effect of wettability alteration during low salinity water injection is modeled by the shifting of relative permeability curves. Typically, two sets of relative permeability curves are defined in this study as input to represent high salinity (625000 Kppm) and low salinity conditions (1 Kppm) as shown in Figure A1. 12. Interpolation between these two curves is usually carried out by the interpolant. The interpolant is the equivalent ionic fraction on the rock surface and these relative permeability curves are usually measured from the laboratory experiments [46] which serve as input during numerical modeling.

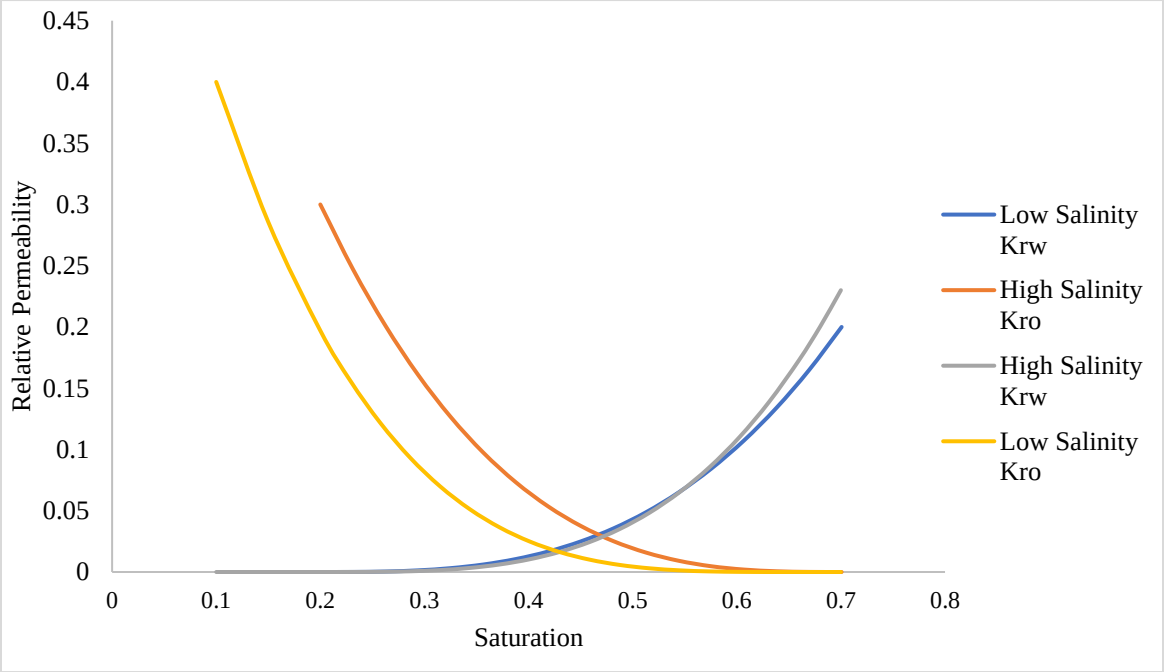

Figure A1. 12. Experimental high and low Salinity relative permeability curves [46].

A.1.4. Results and discussion

This section presents the main results obtained from LSWI simulation runs, with focus on the important mechanisms/phenomena during the recovery process.

A.1.4.1. Effect of LSWI on Oil Recovery in Sandstone and Carbonate.

Figure A1. 13 shows the effect of pore volume of LSWI on recovery factor for the sandstone reservoir at various concentrations of Na^+ ions where the Na^+ concentrations of 68.52 kppm,15.00 kppm, 3.50 kppm, and 0.50 kppm are examined.

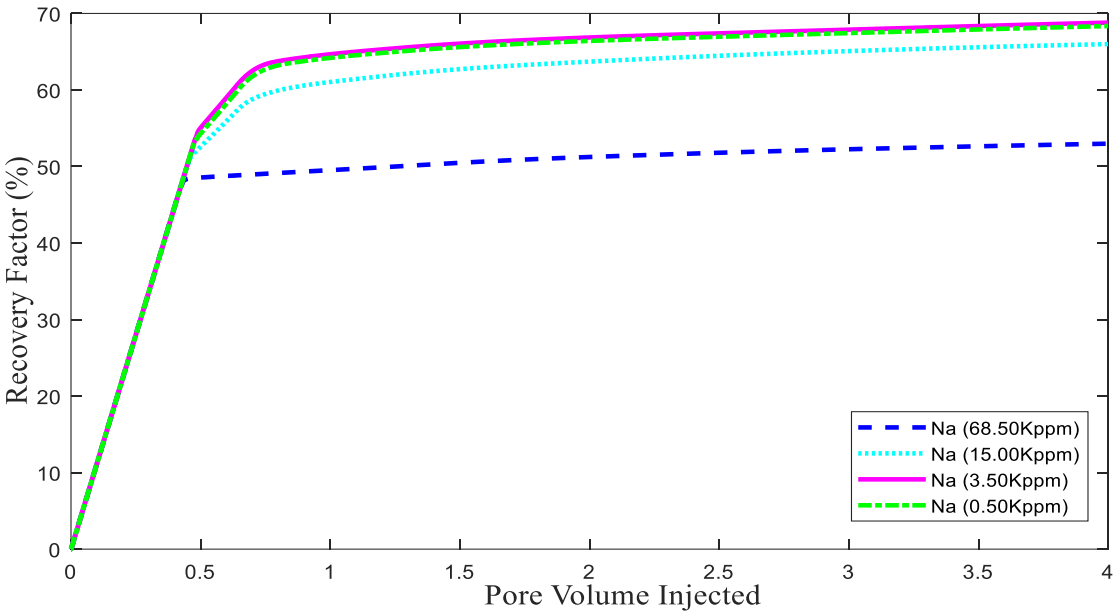

Figure A1. 13. Oil recovery versus injected pore volume and Na+ concentration

It is observed that the ultimate oil recovery factor increases from 51 % to 68 % by decreasing Na^+ concentration in the injected brine from 68.52 kppm to 0.5 kppm after injecting 4.0 pore volumes of brine into the reservoir. Indeed, the highest recovery factor is attained with a concentration of 3.5 kppm for Na^+.

Further decrease of Na^+ concentration below 3.5 Kppm provides no improvement in the oil recovery as illustrated in Figure A1. 14 which shows the ultimate recovery factor after 4.0 injected PV. Further reduction in the Na^+ concentration does not lead to further increment in the ultimate oil recovery due to the subsequent reductions of Na^+ ions in the injected brine. As the Na^+ concentration in the injected brine is reduced, the brine-rock equilibrium is altered and Na^+ on the surface of the formation must be desorbed thereby releasing the formation Na^+ to balance the equilibrium state. This desorption of Na^+ from the sandstone surface leads to a replacement by a divalent ion to attain a new ionic bridge equilibrium state. This phenomenon causes the polar oil components attached to divalent ion to be released. At a certain point in the reduction Na^+ in the injection brine, there will be no more free ions on the formation surface to balance the reduction of Na^+ in the effluent. At this point, a further reduction in Na^+ will not lead to higher oil recovery. In our simulations, this occurred at 3.5 Kppm.

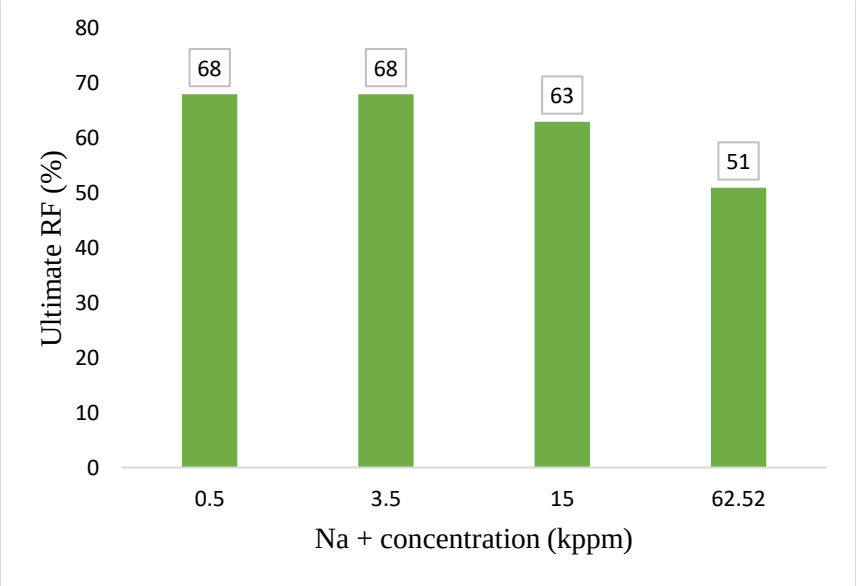

Figure A1. 14. Final oil recovery for different Na+ concentration in the sandstone case

The impact of concentration of SO_4^{2-} ions on the oil recovery in the carbonate is investigated where the SO_4^{2-} concentration varies from 0.02 kppm to 0.10 kppm, as demonstrated in Figure A1. 15. It is observed that the ultimate recovery increases from 53.4% to 66 % if the concentration of SO_4^{2-} in the injected brine lowers from 0.1 kppm to 0.02 kppm where 4 pore volumes of injected brine are used in the LSWI.

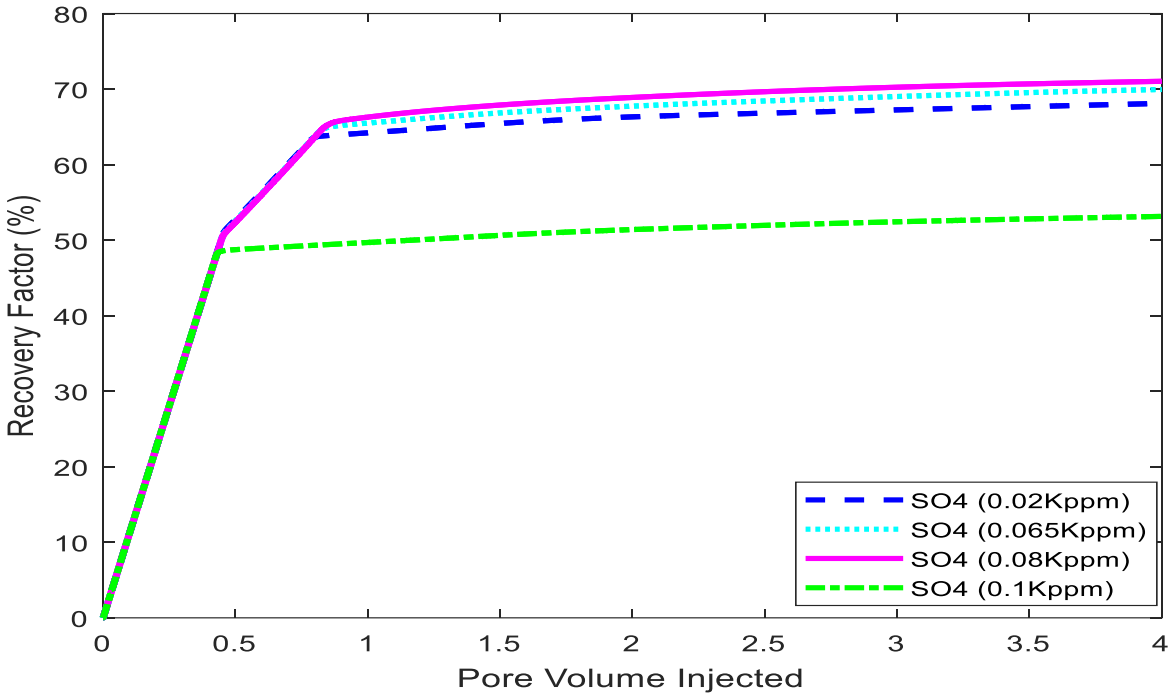

Figure A1. 15. Oil recovery factor by altering S042- concentration

As clear from Figure A1. 16 which shows the ultimate recovery factor, the variation of RF with SO_4^{2-} concentration does not follow a similar trend as observed in sandstone. As depicted in Figure A1. 15, RF increases when SO_4^{2-} concentration decreases from 0.1 kppm to 0.08 kppm; however, the recovery factor decreases if the SO_4^{2-} concentration lowers further after 0.08 kppm. This observation has been debatable by many researchers. According to the experimental investigation

conducted by (Chinedu , 2008) on the effect of rock wettability on oil recovery for secondary and tertiary oil recovery process, it was reported that there is a critical low salinity at which injecting SO_4^{2-} gives the highest increase in contact angle. Hence, there is a critical salinity that yields the optimum oil recovery. The critical salinity in this study is 0.08kppm.

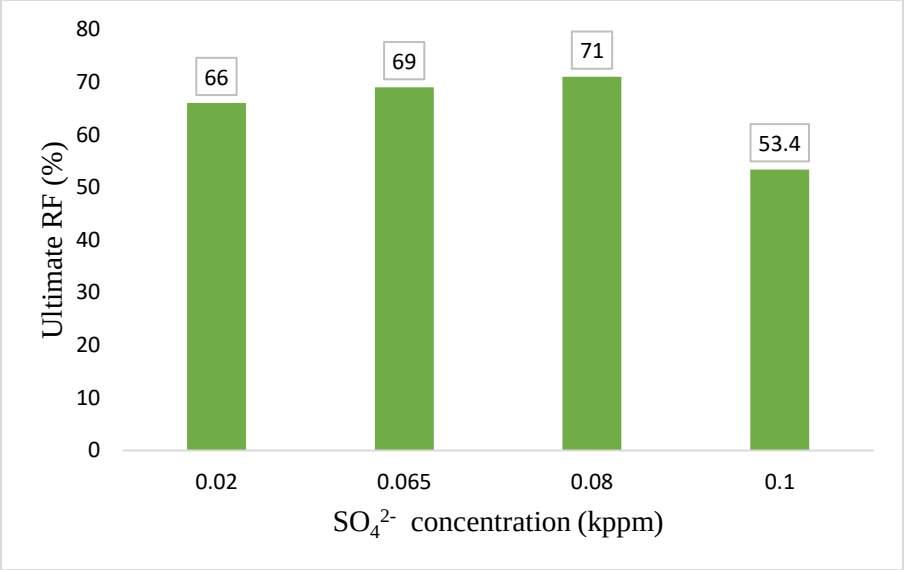

Figure A1. 16. Ultimate oil recovery versus the magnitude of SO42- concentration

According to Figure A1. 15, a sensitivity analysis is required to determine the optimum concentration of SO_4^{2}- that offers the highest ultimate oil recovery in the carbonate. In this research work, the optimum SO_4^{2-} concentration is 0.08 Kppm, as the highest ultimate oil recovery of 72% is attained at this particular concentration after 4.0 pore volumes of injected brine. Further reduction in the concentration yields lower recovery factor as depicted in Figure A1. 15.

Effect of LSWI on pH. For sandstone, the initial pH of formation water increases after 2.5 days under LSWI operation. The increase in the local pH is because more proton ions are released during the exchange of monovalent ion of Na^+ and Ca-X_2, leading to the release of Ca^{2+} ions in the formation water. In this study, the local pH during LSWI for sandstone varies from 5 to 9, 5 to 8,

and 5 to 7.13 for 3.5 kppm, 15 kppm, and 62.52 kppm of Na^+ concentration respectively, as shown in Figure 17.

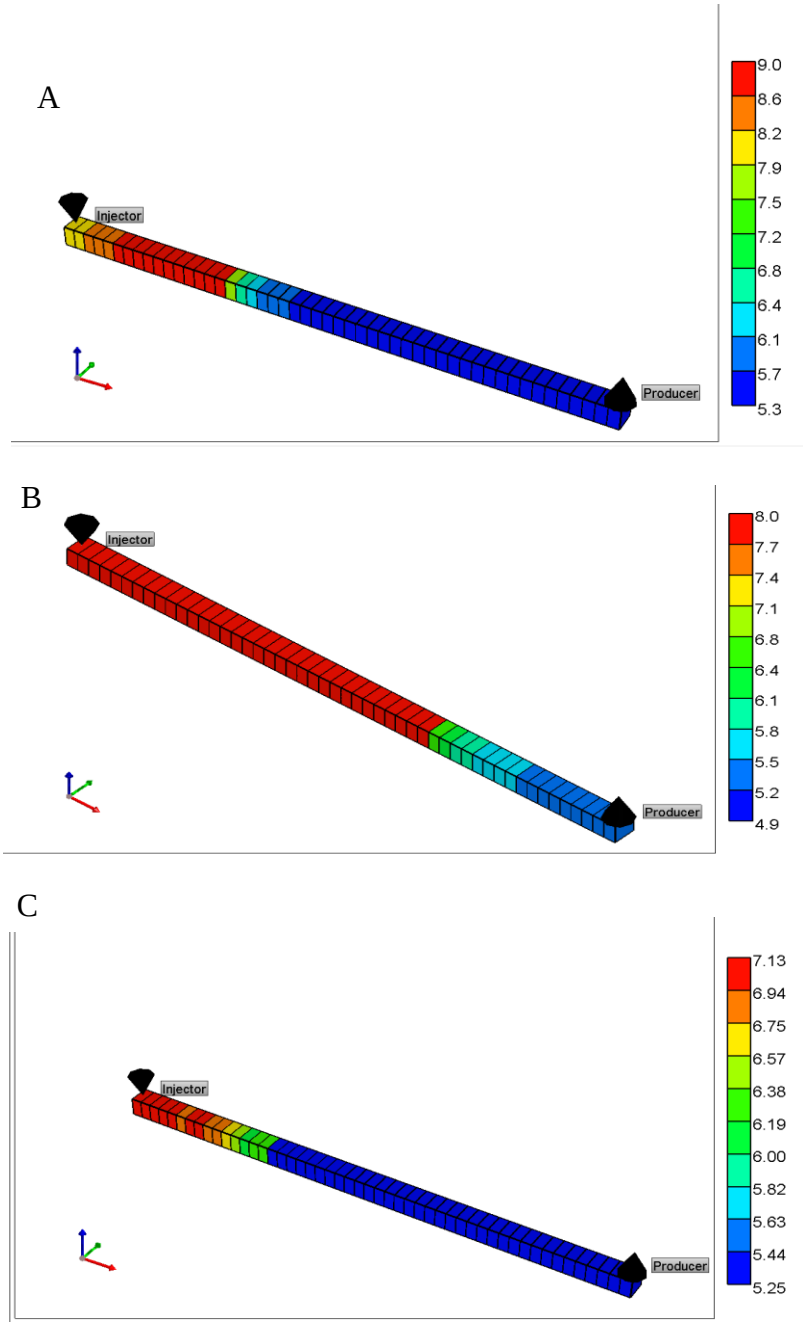

Figure A1. 17. 3D representation of pH change in sandstone for A(3.5 kppm), B(15 kppm), and C (62.52 kppm).

Figure A1. 17 and Figure A1. 18 show the variation of pH with Na^+ concentration for the sandstone case. It is observed that there is a gradual increase in the pH while decreasing the salinity. As the Na^+ concentration in the injected brine is reduced, there is an ionic exchange between a monovalent ion and a divalent ion which are mainly between Na^+ and $Ca\text{-}X_2$ or Na^+ and $Mg\text{-}X_2$ respectively. This phenomenon will cause a release of Na^+ into the injected brine and formation water in other to attain a new ionic equilibrium. The release of Na^+ with protons ions will cause an increase in the local pH of the formation. In this study, the local pH during LSWI for sandstone varies from (5 to 9), (5 to 8), and (5 to 7.13) for 3.5 Kppm, 15 Kppm and 62.52 Kppm of Na^+ concentration respectively as shown in Figure A1. 18. It can also be observed that the lower the salinity of Na^+ concentration in the injected brine, the higher the increase in the local pH because more Na^+ will be released from formation water to remedy this deficiency and this will, in turn, increase the pH.

This increase in pH during LSWI contributes to the overall effective mechanism of increasing the recovery factor in sandstone, because the injected water behaves like an alkaline solution which is capable of decreasing the interfacial tension between oil and water phases.

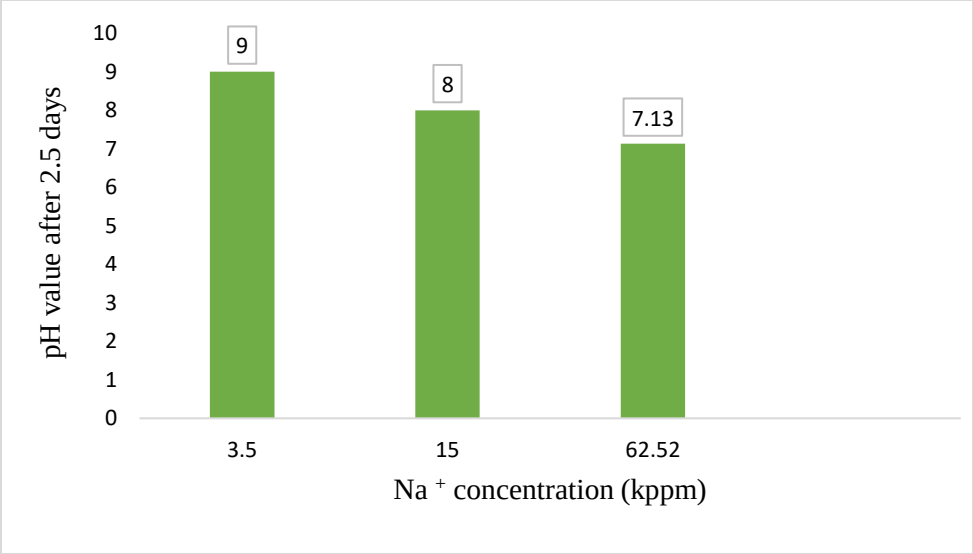

Figure A1. 18. pH change in sandstone versus Na+ concentration

For the carbonate case as shown in Figure A1. 19 and Figure A1. 20, there is no increase in the pH even though there is also a release of proton ions during ion exchange. This is due to the fact that an increased solubility of CO_2 (liberated from $CaCO_3$) in the aqueous phase is experienced with decreasing the salinity which results in the formation of a weak acid and bicarbonates of HCO_3^{2-} . This will cancel the proton effect according to the following reaction as shown in Equation (A1. 12), where the bicarbonates act as a buffer.

A

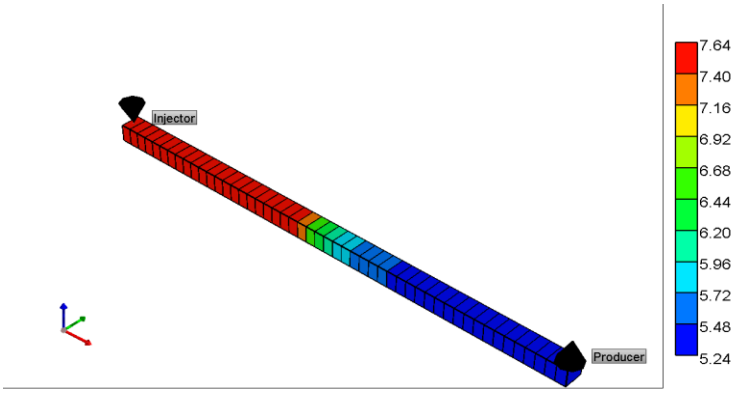

B

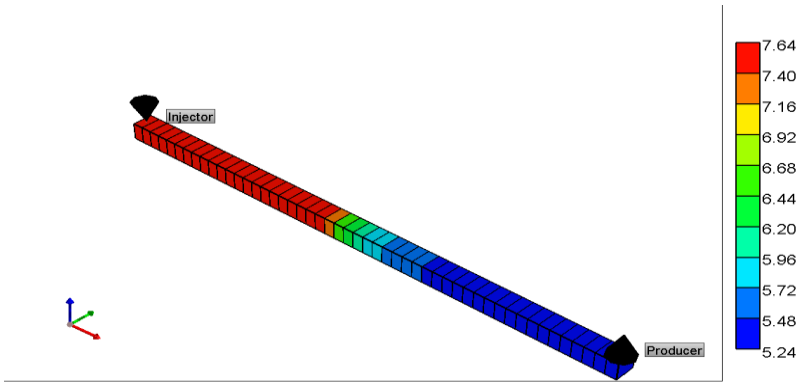

C

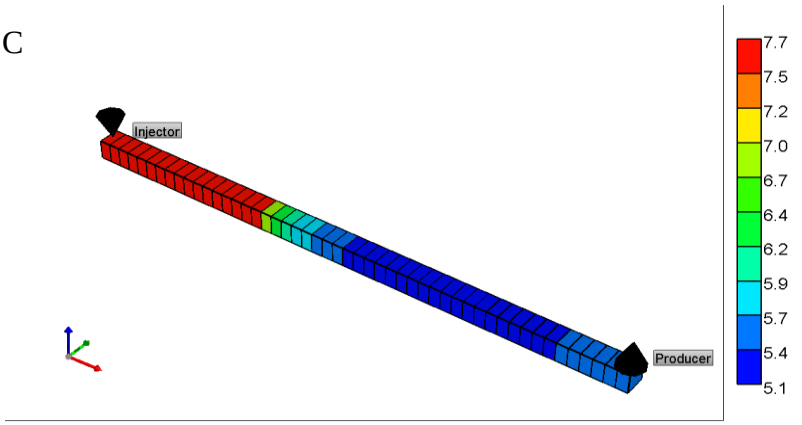

Figure A1. 19. 3D representation of pH change in carbonate for A (0.1 kppm), B (0.08 kppm), and C (0.065 kppm)

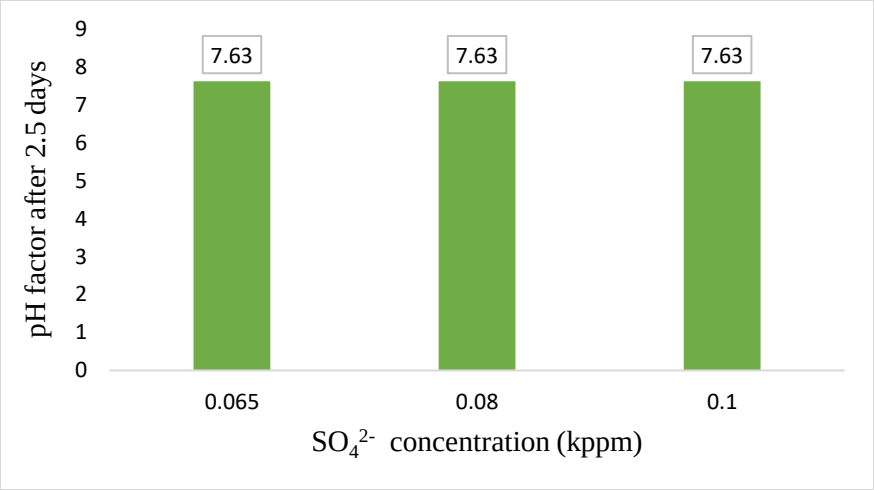

Figure A1. 20. pH change in carbonates in terms of SO42-

$$H_2O_{aq} + CaCO_{3_s} \leftrightarrow H^+_{aq} + HCO^{2-}_{3\ aq} + Ca^{2+}_{aq} \quad \text{(A1. 12)}$$

Hence the resultant increase in pH during LSWI for carbonates is only about ±1 units for every ±10000ppm increase or reduction of salinity. Thus, pH has no predominant effect on altering interfacial tension in carbonate reservoirs so that it does not appreciably contribute to change in the total oil recovery.

A.1.4.2. Effect of LSWI on Mineral Dissolution and Precipitation.

Figure A1. 21 and Figure A1. 22 depict property distance plots to demonstrate the calcite precipitation and dolomite dissolution, respectively, during LSWI through a cross-section of (1, 1, 1 – 25, 1, 1) along I- direction. It should be noted that the sign convention, used by CMG, is -ve for precipitation and +ve for dissolution. Low salinity favors more precipitation as seen in Figure A1. 21. This behavior/mechanism is further explained by the following equation:

$$Calcite + H^+ \leftrightarrow Ca^{++} + HCO^{2-}_3 \quad \text{(A1. 13)}$$

During the low salinity injection and in the presence of CO_2, the gas will be favorably dissolved into water and HCO^{2-}_3 is formed when Ca^{2+} ions are surplus. It shifts Equation (A1. 13) to the left

side, causing precipitation of calcite. According to Figure A1. 21 the amount of precipitated calcite is very small. Even though the equilibrium rate cannot be measured by CMG during the simulation run, there was evidence of precipitation in the property distance plot. This phenomenon should not be overlooked as the precipitation of calcites in some cases might occur faster in the presence of catalytic ions in the formation water, resulting in considerable influence on porosity, permeability, and total oil recovery.

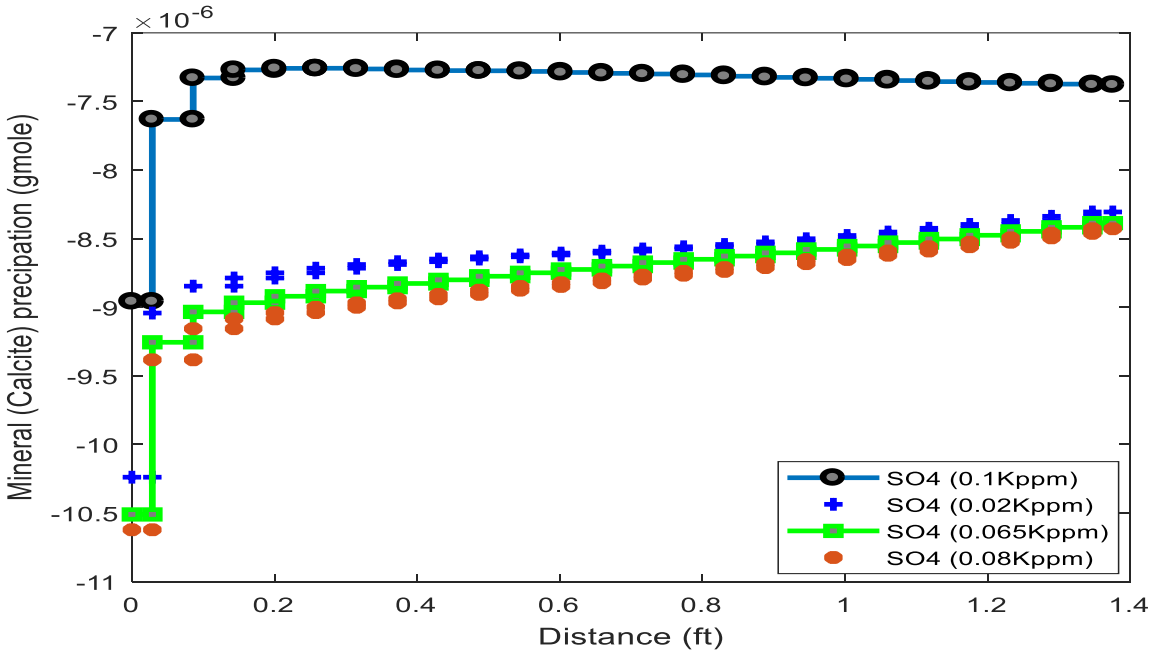

Figure A1. 21. Effect of LSWI on mineral (calcite) precipitation in carbonates.

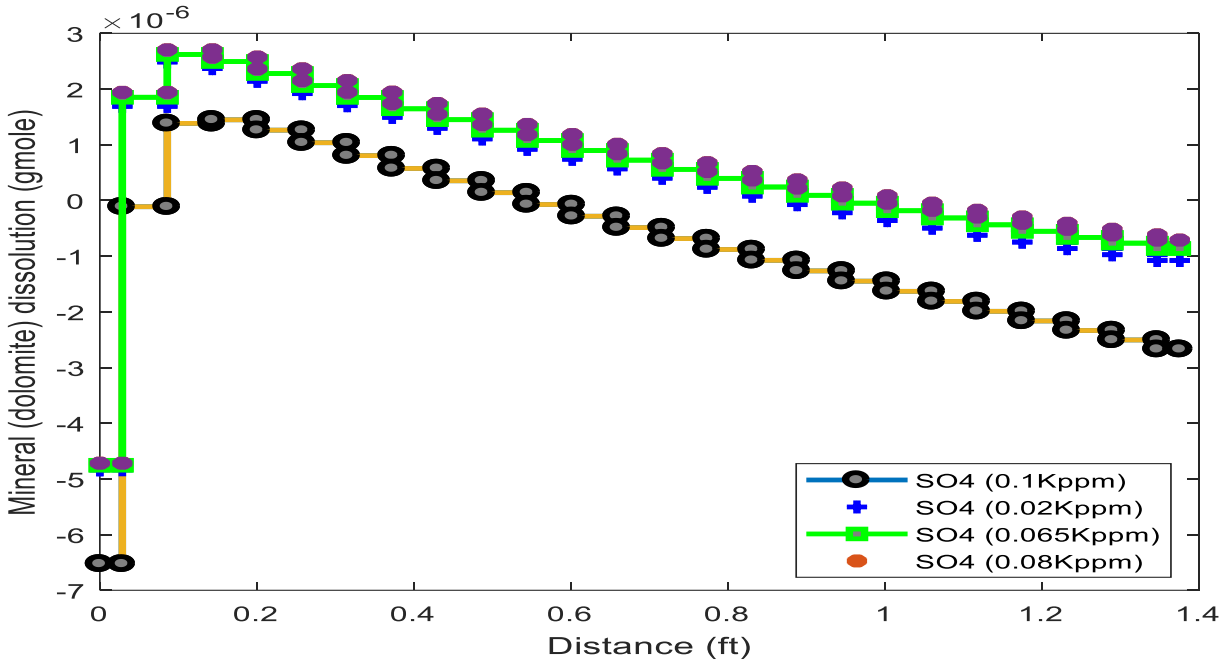

Figure A1. 22. Influence of LSWI on mineral (dolomite) dissolution in carbonates

Similarly, Figure A1. 22 demonstrates the dolomite dissolution in the carbonate system as low salinity favors dissolution of dolomite. This behavior is illustrated by the following reaction:

$$\text{Dolomite} + 2H^{+} \leftrightarrow Ca^{++} + 2HCO_3^{2-} + Mg^{++} \quad \text{(A1. 14)}$$

Based on Equation (A1. 14), there is surplus of H^{+} ions, but there is deficiency of HCO_3^{2-} and Ca^{++}. The deficiency and surplus cause that the reaction moves to the right side to dissolve more dolomite. The equilibrium rate of this reaction is not known as this parameter cannot be measured with CMG. However, Figure A1. 22 reveals the occurrence of the dissolution process in carbonate cases.

LSWI is identified as a prominent EOR technique where microscale investigation of this process is needed to capture the important recovery mechanisms that result in considerable changes in oil

saturation distribution and oil and rock properties. To further understand the detailed physics at both micro and micro scales, the systematic experimental and modeling works seem necessary.

This study provides further insight of the LSWI process through conducting numerical simulation of LSWI as an EOR method. CMG-GEM is only capable of modeling low salinity water injection in sandstones by using Na^+ as an interpolant between the low salinity relative permeability curve and high salinity relative permeability curve. Only Ca^{2+} or SO_4^{2-} can be used as an interpolant for modeling in carbonates. Therefore, during this study, the main challenge was to capture LSWI using a different ion aside Na^+, Ca^{2+} or SO_4^{2-} as an interpolant. However, to a large extent, it gives considerably good results when compared to experimental and other numerical commercial simulators such as PHREEQC.

In this study, we confirm that wettability alteration is one of the dominant mechanisms for additional recovery during LSWI process. Furthermore, we conclude that an increase in pH represents another important mechanism for additional oil recovery in sandstone reservoirs. Most importantly, it was found that there are two vital phenomena including mineral dissolution and precipitation occurring in sandstone and carbonates over LSWI, respectively which are capable of changing the reservoir properties and causing flow assurance problems (pore throat plugging), consequently leading to further operating expenditures during production operations.

A.1.5. Conclusions

LSWI as an EOR technique leads to an improvement in conventional water flooding processes. Moreover, it exhibits more advantages, compared to other chemical EOR Process in terms of its relatively low capital cost, environmental impact, and relative ease of field implementation. This research work presents modeling simulation of LSWI for sandstones and carbonates to investigate variation of pH, calcite precipitation, dolomite dissolution, recovery mechanisms, and oil recovery factor over the production process. The following conclusions are drawn based on the results:

- A decrease in salinity content for a sandstone reservoir offers a considerable increase in the oil recovery factor until a critical salinity below which no significant change occurs in the recovery factor.
- Analyzing the recovery data of carbonate reservoirs, there is an optimum salinity which gives the maximum oil recovery; further decrease behind this particular salinity lowers the recovery factor.
- The impact of the local pH (while increasing this parameter) is more noticeable in sandstone reservoirs, compared to carbonates. This factor coupled with wettability alteration provides effective/higher driving force for LSWI operation in sandstones. It is known that an increase in pH reduces the oil-water interfacial tension and consequently the residual oil saturation (S_{or}), leading to a greater oil recovery.
- No considerable improvement in oil recovery from carbonates is noticed with increasing local pH, due to the formation of bicarbonates HCO_3^{2-} which neutralizes the proton H^+. Hence, the main driving force causing higher oil recovery with low salinity injection in carbonates is the wettability alteration. This occurs due to the release of divalent ions which

cause a shift in the oil-water relative permeability curve towards more water wet porous system.

- The effect of mineral reactions including both precipitation of calcite and dissolution of dolomite is important during LSWI even though the reaction rate is low. Nevertheless, under favorable conditions in the presence of catalytic ions, the mineral dissolution and precipitation can occur at a much faster rate which can appreciably change reservoir properties and hence affect oil recovery.
- Further modeling and experimental investigations are recommended to systematically study the influence of mineral reactions as this may be a dominant factor affecting oil recovery in the presence of bicarbonates and other catalytic ions in the formation water.

Nomenclatures

Acronyms

CEC	Cation Exchange Capacity
LSWI	Low Salinity Water Injection
EOR	Enhanced Oil Recovery
CMG	Computer Modelling Group
TDS	Total Dissolved Salt
R.F	Recovery Factor
Na	Sodium
Ca	Calcium
Kppm	Kilo parts per million
mD	milli Darcy
SO_4^{2-}	Sulphate ion
Na^+	Sodium ion
Ca^{2+}	Calcium ion
Mg^{2+}	Magnesium ion
$R\text{-}COO^-$	Carboxylic components

CO_2	Carbon dioxide
N_2	Nitrogen gas
C_1 - C30+	Hydrocarbon chain compounds
Psat	Saturation Pressure
GOR	Gas Oil Ratio
EoS	Equation of State
FVF	Formation Volume Factor
API	American Petroleum Institute
BHP	Bottom Hole Pressure
CCE	Constant Composition Expansion
CVD	Constant Volume Depletion
DL	Differential Liberation
ROV	Relative Oil Volume

Variables and parameters

V	Grid block volume (m^3)
u	Darcy velocity (ft/day)
P	Pressure ($Psia$)
T	Transmissibility
R	Reaction rate ($moles/m^3$)

a Activity

D Diffusivity

M Molality

N Number of moles of mineral

K’ Selectivity coefficient

h height

K_{row} Oil water relative permeability

q_i Injection and production rate of component i (m^3/s)

g Acceleration due to gravity

K Equilibrium constant

f fugacity (-)

X exchanger

na Aqueous component

y mole fraction

$VR_{j,aq}^{n+1}$ Intra aqueous reaction rate

$VR_{j,mn}^{n+1}$ Mineral dissolution/precipitation

Greek letters

ρ Mass density $(\frac{Kg}{m^3})$

μ Viscosity (centipoise)

ϕ Porosity (-)

γ_i Activity coefficient

Δ Difference operator

Subscripts

aq Aqueous

w Water

mn Mineral component

Superscripts

u =n Explicit time step for grid block

n+1 Implicit time step for grid block

References

[1] Al-Shalabi EW, Sepehrnoori K, Delshad M. Does the double layer expansion mechanism contribute to the LSWI effect on hydrocarbon recovery from carbonate rocks? SPE Reserv Characterisation Simul Conf Exhib New Approaches Characterisation Model Complex Reserv RCSC 2013 2013;1:319–35. doi:10.2118/165974-MS.

[2] Zhang Y, Morrow NR. Comparison of Secondary and Tertiary Recovery with Change in Injection Brine Composition for Crude Oil/ Sandstone Combinations. SPE/DOE Symp Improv Oil Recover 2006:1–15. doi:10.2523/99757-MS.

[3] Sheng JJ. Critical review of low-salinity waterflooding. J Pet Sci Eng 2014;120:216–24. doi:10.1016/j.petrol.2014.05.026.

[4] Koleini MM, Mehraban MF, Ayatollahi S. Effects of low salinity water on calcite/brine interface: A molecular dynamics simulation study. Colloids Surfaces A Physicochem Eng Asp 2018;537:61–8. doi:10.1016/J.COLSURFA.2017.10.024.

[5] Xie Q, Brady P V., Pooryousefy E, Zhou D, Liu Y, Saeedi A. The low salinity effect at high temperatures. Fuel 2017;200:419–26. doi:10.1016/J.FUEL.2017.03.088.

[6] Shalabi EW Al, Sepehrnoori K, Delshad M. Mechanisms behind low salinity water injection in carbonate reservoirs. Fuel 2014;121:11–9. doi:10.1016/J.FUEL.2013.12.045.

[7] Dang C, Nghiem L, Nguyen N, Chen Z, Nguyen Q. Mechanistic modeling of low salinity water flooding. J Pet Sci Eng 2016;146:191–209. doi:10.1016/J.PETROL.2016.04.024.

[8] Sharma H, Mohanty KK. An experimental and modeling study to investigate brine-rock interactions during low salinity water flooding in carbonates. J Pet Sci Eng 2017. doi:10.1016/J.PETROL.2017.11.052.

[9] Al-Shalabi EW, Sepehrnoori K. A comprehensive review of low salinity/engineered water injections and their applications in sandstone and carbonate rocks. J Pet Sci Eng 2016;139:137–61. doi:10.1016/J.PETROL.2015.11.027.

[10] Kilybay A, Ghosh B, Chacko Thomas N. A Review on the Progress of Ion-Engineered Water Flooding. J Pet Eng 2017;2017:1–9. doi:10.1155/2017/7171957.

[11] Zhang Y, Xie X, Morrow NR. Waterflood Performance By Injection Of Brine With Different Salinity For Reservoir Cores. SPE Annu. Tech. Conf. Exhib., Society of Petroleum Engineers; 2007. doi:10.2118/109849-MS.

[12] Al-Attar HH, Mahmoud MY, Zekri AY, Almehaideb RA, Ghannam MT. Low Salinity Flooding in a Selected Carbonate Reservoir: Experimental Approach. EAGE Annu. Conf. Exhib. Inc. SPE Eur., Society of Petroleum Engineers; 2013. doi:10.2118/164788-MS.

[13] Peimao Zhang *, Medad T. Tweheyo and, Austad T. Wettability Alteration and Improved Oil Recovery in Chalk: The Effect of Calcium in the Presence of Sulfate 2006. doi:10.1021/EF0600816.

[14] Nasralla RA, Nasr-El-Din HA. Double-Layer Expansion: Is It A Primary Mechanism of Improved Oil Recovery by Low-Salinity Waterflooding? SPE Improv. Oil Recover. Symp., Society of Petroleum Engineers; 2012. doi:10.2118/154334-MS.

[15] Yousef AA, Al-Saleh S, Al-Jawfi MS, Al-Salehsalah SH, Al-Jawfi MS. New recovery method for carbonate reservoirs through tuning the injection water salinity: Smart WaterFlooding. 73rd Eur Assoc Geosci Eng Conf Exhib 2011 Unconv Resour Role Technol Inc SPE Eur 2011 2011;4:2814–30. doi:10.2118/143550-MS.

[16] Austad T, Strand S, Høgnesen EJ, Zhang P. Seawater as IOR Fluid in Fractured Chalk. 2005 SPE Int Symp Oilf Chem 2005:1–10. doi:10.2118/93000-MS.

[17] Austad T, Rezaeidoust A, Puntervold T. Chemical Mechanism of Low Salinity Water Flooding in Sandstone Reservoirs. SPE Improv. Oil Recover. Symp., 2010. doi:10.2118/129767-MS.

[18] Fathi SJ, Austad T, Strand S. "Smart Water" as a Wettability Modifier in Chalk: The Effect of Salinity and Ionic Composition. Energy & Fuels 2010;24:2514–9. doi:10.1021/ef901304m.

[19] Experimental and theoretical study of wettability alteration during low salinity water flooding-an state of the art review. Colloids Surfaces A Physicochem Eng Asp 2017;520:622–39. doi:10.1016/J.COLSURFA.2017.02.006.

[20] Strand S, Austad T, Puntervold T, Høgnesen EEJ, Olsen M, Barstad SMF. "Smart water" for oil recovery from fractured limestone: a preliminary study. Energy & 2008;21:3126–33. doi:10.1021/ef800062n.

[21] Austad T. Enhanced Oil Recovery Field Case Studies. Gulf Professional Publishing; 2013. doi:10.1016/B978-0-12-386545-8.00013-0.

[22] Standnes DC, Austad T. Wettability alteration in chalk. J Pet Sci Eng 2000;28:111–21. doi:10.1016/S0920-4105(00)00083-8.

[23] Fathi SJ, Austad T, Strand S. Effect of Water-Extractable Carboxylic Acids in Crude Oil on Wettability in Carbonates 2011. doi:10.1021/ef200302d.

[24] Hassenkam T, Mitchell AC, Pedersen CS, Skovbjerg LL, Bovet N, Stipp SLSS, et al. Low Salinity Effect at Pore Scale: Probing Wettability Changes in Middle East Limestone. Energy & Fuels 2016;30:3768–75. doi:10.1021/acs.energyfuels.5b02562.

[25] Altahir M, Yu M, Hussain F. LOW SALINITY WATER FLOODING IN CARBONATE ROCKS – DISSOLUTION EFFECT 2017:1–8.

[26] Vajihi F, Diaz P, Sagbana I, Zabihi H, Farhadi A, Sherhani S. Effect of Low Salinity Water Injection on Capillary Pressure and Wettability in Carbonates 2017:1–9.

[27] Didier M, Chaumont A, Joubert T, Bondino I, Hamon G. Contradictory Trends for Smart Water Injection Method : Role of Ph and Salinity From Sand / Oil / Brine Adhesion Maps. Sca 2015:1–12.

[28] Hassenkam T, Mitchell AC, Pedersen CS, Skovbjerg LL, Bovet N, Stipp SLS. The low salinity effect observed on sandstone model surfaces. Colloids Surfaces A Physicochem Eng Asp 2012;403:79–86. doi:10.1016/j.colsurfa.2012.03.058.

[29] Tong Z, Xie X, Morrow NR. Crude Oil Composition and the Stability of Mixed Wettability in Sandstones 2003;44:233–42.

[30] Mahani H, Keya AL, Berg S, Bartels W-BW-B, Nasralla R, Rossen W. Driving mechanism of low salinity flooding in carbonate rocks. Eur 2015 2015:210–36. doi:10.2118/174300-MS.

[31] Yousef AA, Al-Saleh SH, Al-Kaabi A, Al-Jawfi MS. Laboratory investigation of the impact of injection-water salinity and ionic content on oil recovery from carbonate reservoirs. SPE Reserv Eval Eng 2011;14:578–93. doi:10.2118/137634-PA.

[32] Lager A, Webb KJ, Black CJJ, Singleton M, Sorbie KS. Low Salinity Oil Recovery - An Experimental Investigation 2008:0–12.

[33] Zhang Y, Xie X, Morrow NR. Waterflood performance by injection of brine with different salinity for reservoir cores. Proc - SPE Annu Tech Conf Exhib 2007;2:1217–28. doi:10.2523/109849-MS.

[34] Bennion DB, Bennion DW, Thomas FB, Bietz RF. Injection Water Quality-A Key Factor to Successful Waterflooding. J Can Pet Technol 1998;37. doi:10.2118/98-06-06.

[35] Sheng JJ. Formation damage in chemical enhanced oil recovery processes. Asia-Pacific J Chem Eng 2016;11:826–35. doi:10.1002/apj.2035.

[36] Nasralla R a, Nasr-el-din H a. Double-Layer Expansion: Is It A Primary Mechanism of Improved Oil Recovery by Low-Salinity Waterflooding? Eighteenth SPE Improv Oil Recover Symp 2012:1–17. doi:10.2118/154334-MS.

[37] Yu L, Standnes DC, Skjaeveland SM. Wettability Alteration of Chalk by Sulphate Containing Water, Monitored by Contact Angle Measurement. Int Symp Soc Core Anal 2007:1–12.

[38] Ahmadi P, Riazi M, Malayeri MR. Investigation of wettability alteration of carbonate rock in presence of sulfate, calcium 2017:1–9.

[39] Alhammadi M, Mahzari P, Sohrabi M. NEW EXPERIMENTAL EVIDENCE ON THE DOMINANT MECHANISM OF OIL RECOVERY BY LOW SALINITY 2017:1–12.

[40] Hiorth A, Cathles LM, Kolnes J, Vikane O, Lohne A, Korsnes RI, et al. A Chemical Model for the Seawater-CO2 - Carbonate System – Aqueous and Surface Chemistry. Soc Core Anal 2008:1–12.

[41] Gachuz-muro H, Sohrabi M. Prediction , Control and Validation of Rock Dissolution During Smart Water Injection and Its Impact on Waterflood Performance 2017:1–12.

[42] Austad T, Strand S, Puntervold T. Is Wettability Alteration of Carbonates By Seawater

Caused By Rock Dissolution ? Changes 2009;3:1–6.

[43] Fathi SJ, Austad T, Strand S. “smart water” as a wettability modifier in chalk: The effect of salinity and ionic composition. Energy and Fuels 2010;24:2514–9. doi:10.1021/ef901304m.

[44] Austad, T., Strand, S., & Puntervold T. Is wettability alteration of carbonates by seawater caused by rock dissolution. . Proc. SCA Int. Symp. Noordwijk, Netherlands, 2009, p. 2009–43.

[45] Zhang P, Tweheyo MT, Austad T. Wettability alteration and improved oil recovery by spontaneous imbibition of seawater into chalk: Impact of the potential determining ions Ca2+, Mg2+, and SO42-. Colloids Surfaces A Physicochem Eng Asp 2007;301:199–208. doi:10.1016/j.colsurfa.2006.12.058.

[46] Computer Modelling Group 2017

[47] Dang, C., et al., Modeling and Optimization of Low Salinity Waterflood. Vol. 1. 2015. 55-73.

[48] Appelo, C.A.J., and D. Postma. 2005. Geochemistry, groundwater and pollution,.2nd ed. Amsterdam, the Netherlands.

A.2 A New Shear Wave Velocity Prediction Technique for Clastic Rocks

Preface

A version of this chapter has been submitted to the journal of petroleum science and engineering 2018. The concept was developed by Olalere Oloruntobi and David Onalo. Olalere Oloruntobi is the primary author. Co-author David Onalo conducted part of the literature review and helped in the initial analysis, development of the model and draft of the paper. Co-author Dr. Sunday Adedigba reviewed and provided technical advice for the concept of paper. Co-author Dr. Raghu Chunduru reviewed and provided technical advice for the concept of paper. Co-author Dr. Lesley James provided technical assistance and review for the paper. Co-author Dr. Stephen Butt provided technical assistance, review and development of the concept of the paper. The manuscript was prepared by Olalere Oloruntobi, and subsequently revised the manuscript, based on the feedback from the co-authors and also a peer review process.

Abstract

Theoretical and experimental investigations of elastic wave propagation in sedimentary rocks have shown that shear wave velocity is strongly correlated to compressional wave velocity because most of the factors that affect the shear wave velocity also affect the compressional wave velocity. In areas where shear wave velocity logs are not available, empirical relations based on regression analyses are often used to estimate the shear wave velocity from the compressional wave velocity. However, most of the existing empirical relationships were developed mainly for consolidated rocks and they are lithology specific. When applied over a long lithological column that consists of several stratigraphic units, the existing empirical relations may produce inaccurate estimates. In this paper, a new shear wave velocity prediction technique that can be applied to a wide range of lithologies (clean and non-clean/mixed-lithology formations) and formation strengths (loose, unconsolidated and consolidated formations) in clastic environments is being proposed. Model's development is based on the combination of laboratory and in situ measurements obtained from different depositional environments. The model is validated using wireline log data acquired from three wells in the Tertiary Deltaic System of the Niger Delta basin. The well data covers a wide range of fields, formations, pressure regimes and depths. In the new model, the shear wave velocity is expressed as a function of compressional wave velocity and formation bulk density. The accuracy of the new shear wave velocity prediction model is quantified using statistical analysis. An excellent agreement is observed between the predicted shear wave velocity and the actual shear wave velocity measurements.

Keywords: Shear velocity, Compressional velocity, Empirical relation, Well logs, Formations.

A.2.1. Introduction

The advent of advanced dipole sonic logging tools allows the measurements of shear and compressional wave velocities in soft and hard formations. This greatly extends the application of acoustic measurements to rock/reservoir modeling. For a given lithology, the ratio of compressional velocity (V_p) to shear velocity (V_s) can be used to identify the formation fluid type (Hicks and Berry 1956; Kuster and Toksöz 1974; Gregory 1976; Tatham and Stoffa 1976; Robertson and Pritchett 1984; Ensley 1985**;** Williams 1990**;** Brie et al. 1995; Hamada 2004; Kozlowski et al. 2017). Since the ratio of compressional to shear velocity varies significantly with formation fluid type and differential pressure, this parameter can be very useful in seismic monitoring of producing reservoirs (Khazanehdari and McCann, 2005). The ratio of compressional to shear velocity has also been used to identify and predict the onset of abnormally high formation pressure (Dvorkin et al. 1999; Li et al. 2000; Walls et al. 2000; Ebrom et al. 2006; Saleh et al. 2013). Moreover, Information about rock compressional and shear wave velocities can be used for lithology identifications (Pickett 1963; Nations 1974; Kithas, 1976; Tatham 1982; Eastwood and Castagna 1983; Domenico 1984**;** Rafavich et al. 1984; Miller and Stewart 1990**;** Johnston and Christensen 1993**;** Potter et al. 1996). Fabricius et al. (2007) used the combination of compressional and shear wave velocities to estimate the formation permeability in carbonate rocks. Attempts have also been made to improve the prediction of formation bulk density from the combination of compressional and shear wave velocities (Miller and Stewart 1991; Ursenbach 2001; Ursenbach, 2002). Compressional and shear wave velocities are perhaps the most important input parameters required to estimate the rock mechanical properties (Tixier et al. 1975; Coates and Denoo 1980; Potter and Foltinek 1997; Ohen 2003; Chang et al. 2006; Ameen et al., 2009; Najibi et al., 2015). These properties are required for wellbore stability analyses, compaction and

subsidence, hydraulic fracturing, perforation strategy and sand production prediction. Other applications of compressional and shear wave velocities data include porosity determination, seismic interpretation, bright spot analyses, amplitude variation with offset (AVO) analyses and prospect evaluation.

From the acoustic logging perspective, most of the offset well data were acquired with a borehole compensated sonic log which could largely measure the compressional wave velocity. Moreover, in the present-day wells, acquisition of shear velocity logs in drilled wells is not so common possibly due to economic reasons. The lack of shear wave velocity log data in the majority of the offset and present-day wells imposes severe limitations on the applications of acoustic measurements to rock physics. In areas where shear wave velocity log data are not available, they are often estimated from the compressional wave velocity using empirical relations. Even if the shear wave velocity log is run in a well, comparison with its prediction from other well log data can be used as a quality control tool. In this paper, shear and compressional velocities are expressed in kilometers per second (km/s), and formation density is expressed in grams per cubic centimeter (g/cm^3) unless otherwise stated.

The relationship between the shear wave velocity and compressional wave velocity has long been established. Carroll (1969) established a power relationship between the shear and compressional wave velocities for volcanic and granitic rocks based on laboratory acoustic experiments conducted on 62 core samples (Equation (A2. 1). In Carrol's model, the shear and compressional wave velocities are expressed in kilofeet per second (kft/sec). Lee (2010) suggested that at low effective stress, the relationship between the shear and compressional wave velocities for unconsolidated sediments can also be described by a power law.

$$V_s = 0.937562V_p^{0.81846} \quad \text{(A2. 1)}$$

Castagna et al. (1985) developed an empirical relation based on in-situ sonic and field seismic measurements in mudrocks (Equation (A2. 2). The mudrock model is one of the most widely used empirical relations for clay formations (Jørstad et al. 1999).

$$V_s = 0.862V_p - 1.172 \quad \text{(A2. 2)}$$

Han et al. (1986) proposed another popular linear empirical relation for brine saturated well-consolidated sandstone and shaly sandstone formations based on several laboratory ultrasonic experiments conducted on cores taken from Gulf of Mexico wells and quarries at differential pressures between 5 to 40 MPa (Equation (A2. 3). The rock porosities vary from 3% to 30% and the volume of clay vary between 0% to 55%.

$$V_s = 0.79V_p - 0.85 \quad \text{(A2. 3)}$$

Based on Hamilton et al. (1970) and Hamilton (1971) data set, Krishna et al. (1989) proposed a linear relationship between shear and compressional velocities for brine-saturated shallow marine sediments based on in-situ measurements in offshore San Diego, California (Equation (A2. 4), where shear and compressional velocities are expressed as meters per second (m/s).

$$V_s = 2.924V_p - 4170.9 \quad \text{(A2. 4)}$$

Williams (1990) expressed the ratio of compressional velocity to shear wave velocity as a function of shear wave travel time for water-bearing sandstone and shale formations (Equation (A2. 5). For sandstone formations, the regression coefficients C and D are 1.182 and 0.00422 respectively. For shale formations, the regression coefficients C and D are 1.276 and 0.00374 respectively. However, mathematical manipulation of Williams's model will give a linear relationship. The

velocities and the sonic travel time in Williams's model are in feet per micro-second and micro-seconds per foot respectively.

$$\frac{V_p}{V_s} = C + D\Delta t_s \tag{A2. 5}$$

Krief et al. (1990) observed a quasi-linear relationship between the square of shear wave velocity and square of compressional wave velocity in consolidated clean sandstone and shaly sandstone formations (Equation (A2. 6), where Q and R are regression coefficients.

$$V_s^2 = QV_p^2 - R \tag{A2. 6}$$

Jørstad et al. (1999) also proposed a best-fit least-squares linear regression model for shaly sands in a Tertiary turbidite system (Equation (A2. 7). In the model of Jørstad et al. (1999), shear and compressional wave velocities are expressed in meters per second (m/s).

$$V_s = 0.89662V_p - 1166.5 \tag{A2. 7}$$

Vernik et al. (2002) proposed nonlinear empirical relations for partially consolidated and consolidated water bearing sandstone and shale formations (Equation (A2. 8). For sandstone formations, the values of M, N and H are 1.267, 0.372 and 0.00284 respectively and for shale formations, the values of M, N and H are 0.79, 0.287 and 0.00284 respectively).

$$V_s = \sqrt{-M + N{V_p}^2 + H{V_p}^4} \tag{A2. 8}$$

Brocher (2005) developed a nonlinear (polynomial fit) relation for a wide variety of common lithologies using ultrasonic laboratory, well logs, vertical seismic profiling (VSP) and field tomography data for rocks with velocities in the range of $1.5 < V_p < 7.5$ km/s (Equation (A2. 9).

$$V_s = 0.7858 - 1.2344V_p + 0.7949{V_p}^2 - 0.1238{V_p}^3 + 0.0064{V_p}^4 \quad \text{(A2. 9)}$$

Ojha and Sain (2014) established a second order polynomial fits for shallow marine sediments found at depth of 277 feet to 899 feet below the sea floor in Kerala-Konkan basin on the west cost of India (Equation (A2. 10), where P, Q and R are constant parameters.

$$V_s^2 = PV_p^4 - QV_p^2 + R \quad \text{(A2. 10)}$$

There are other empirical relationships that have been developed for various formations in clastic environments. Majority of these empirical relationships are linear and Table A2. 1 provides the summary. Shear wave velocity can also be estimated from other petrophysical data (Tosaya 1982; Castagna et al. 1985; Han et al. 1986; Eberhart-Phillips et al. 1989; Miller and Stewart 1990). During the last few decades, several researchers have also attempted to predict the shear wave velocity from well log data using artificial intelligent methods (Rezaee et al. 2007; Rajabi et al., 2010; Asoodeh and Bagheripour 2012; Maleki et al. 2014; Bagheripour et al. 2015; Nourafkan and Kadkhodaie-Ilkhchi 2015; Al-Dousari et al. 2016; Anemangely et al. 2017). However, shear wave velocity predictions from compressional wave velocity data are the most reliable because most factors that affect compressional velocity also affect shear velocity (Xu and White, 1995).

Table A2. 1. Other empirical relationships

S/N	Model	Equation	Remarks
1	Miller and Stewart (1991)	$V_s = 0.8V_p - 861$ (A2. 11) (V_s and V_p are in m/s)	Developed from consolidated brine-saturated clean sandstones and shaly-sandstones based on cores taken from Gulf of Mexico wells and quarries.

2	Greenberg and Castagna (1992)	$V_s = 0.80416V_p - 0.85588$ (A2. 12)	Developed for consolidated clean sands
		$V_s = 0.76969\,V_p - 0.86735$ (A2. 13)	Developed for consolidated clean shales
3	Mabrouk and Pennington (2009)	$V_s = V_p\sqrt{\frac{\nu-0.5}{\nu-1}}$ (A2. 14)	Developed for consolidated clean sands. The Poisson's ratio ν is obtained from Anderson et al. (1973).
4	Hossain et al. (2012)	$V_s = 0.95V_p - 1.27$ (A2. 15)	Derived for glauconitic greensand in the North Sea using isoframe model.
		$V_s = 0.76V_p - 0.76$ (A2. 16)	Derived for glauconitic greensand in the North Sea using core data.
		$V_s = 0.86V_p - 0.96$ (A2. 17)	Derived for glauconitic greensand in the North Sea using well log data.
5	Bailey and Dutton (2012)	$V_s = 0.75V_p - 562.5$ (A2. 18) (V_s and V_p are in m/s)	Developed for consolidated Kimmeridge Clay formation in the North Sea.
6	Lee (2013)	$V_s = 0.59V_p - 0.6$ (A2. 19)	Developed for unconsolidated Shallow Sediments in the Gulf of Mexico.

The majority of the existing empirical relations between shear and compressional wave velocities were developed mainly for a specific lithology. When applied over a long lithological column that consists of several stratigraphic units, the existing empirical relations may produce inaccurate results due to the high degree of variability in the relationships between shear and compressional wave velocities for different lithologies. Empirical relations that work very well for brine saturated clean sandstone or shaly-sandstone formations may perform poorly in shale formations and vise versa. Moreover, most of the available empirical relations in the open literature were developed

for consolidated rocks and their applications to unconsolidated formations (compressional velocity less than 2.3 km/s) may produce inaccurate estimates (Ramcharitar and Hosein 2016). In this paper, attempt is made to develop a simple new shear wave prediction model that can be applied to a wide range of lithologies, rock strengths and depths in clastic environments. The new model can be applicable to shallow marine sediments, unconsolidated and consolidated formations.

A.2.2. Model Development

Laboratory investigations on brine saturated porous rocks have shown that shear wave velocity is directly proportional to the compressional wave velocity (Castagna et al. 1985; Han et al. 1986). From the elastic theory, shear wave velocity is also related to the square root of the formation bulk density (Hamada 2004). There are several ways to combine the above two conditions. One of the possible ways is to expressed shear wave velocity as a function of $\frac{V_p}{\sqrt{\rho}}$. In general, shear wave velocity increases with the function $\frac{V_p}{\sqrt{\rho}}$. To be applicable to any type of formation strengths (loose sediments, unconsolidated and consolidated formations), a power law relationship is proposed between the shear wave velocity and the function $\frac{V_p}{\sqrt{\rho}}$ (Equation (A2. 20). The assumption of a power law relationship follows a reasoning that the majority of empirical relations between rock strength and rock petrophysical properties in clastic rock environments follow either a power law or exponential relationship (Chang et al. 2006). When applied over consolidated rocks at short intervals or rocks in the deeper sections of a sedimentary basin where the formation density is relatively constant, Equation (A2. 20) will reduce to Carroll's model (Equation 1).

$$V_s = A\left[\frac{V_p}{\sqrt{\rho}}\right]^m \qquad \text{(A2. 20)}$$

When the shear wave velocity is zero (as it is in fluids: oil, water or gas), the formation bulk density and compressional wave velocity will have non-zero positive values. Hence, Equation (A2. 20) is not adequate to describe the above physical condition. Therefore, a modified power law relationship is proposed (Equation (A2. 21) which considers the above condition.

$$V_s = A\left[\frac{V_p}{\sqrt{\rho}}\right]^m - B \qquad \text{(A2. 21)}$$

To determine the values of the constant parameters A, B and m, Equation ((A2. 21) is calibrated to laboratory and in situ measurements obtained from different geographical locations. The calibration data covers a wide range of lithologies, formation strengths and effective stresses. This allows the new model to cover a wide range of conditions usually found at shallower and deeper depths of a sedimentary basin. Table A2. 2 provides the source of the data used in calibrating Equation ((A2. 21).

Table A2. 2. Type and source of the data used for calibration.

S/N	Type	Formations	Source
1	Laboratory (5 and 30 MPa DP)	Consolidated brine saturated clean and shaly sandstone formations obtained from Gulf of Mexico (GOM) wells and quarries in USA.	Han et al. (1986)
2	Laboratory (3 and 7 MPa CP)	Consolidated and unconsolidated brine saturated glauconic greensand formations obtained from the Nini oil field in the North Sea.	Hossain et al. (2012)
3	Laboratory (1 and 20 MPa DP)	Water saturated loose clean beach sand.	Prasad (2002)
4	Borehole seismic	Water saturated shallow loose sediments at 50 to 70 ft in the Niger Delta.	Ajayi et al. (2014)

By fitting Equation ((A2. 21) to the data set presented in Table A2. 2, the values of the parameters A, B and m are determined to be 2.41, 2.35 and 0.70 respectively (Equation (A2. 22).

$$V_s = 2.41\left[\frac{V_p}{\sqrt{\rho}}\right]^{0.70} - 2.35 \qquad \text{(A2. 22)}$$

Figure A2. 1 shows the plot of the predicted shear velocity derived from Equation ((A2. 22) versus the measured shear wave velocity obtained from the data set presented in Table A2. 2 along with the histogram of the residual. There is an excellent agreement between the predicted and measured shear wave velocities with a remarkable narrow trend despite the data were obtained from various regions with different lithologies. The inclusion of the formation bulk density normalizes the lithology effect and perturbs the estimates closer to the measured values. The maximum deviation is ± 0.20 km/s with root-mean-square error (RMSE) of 9.2% and coefficient of determination (R^2) value of 0.98.

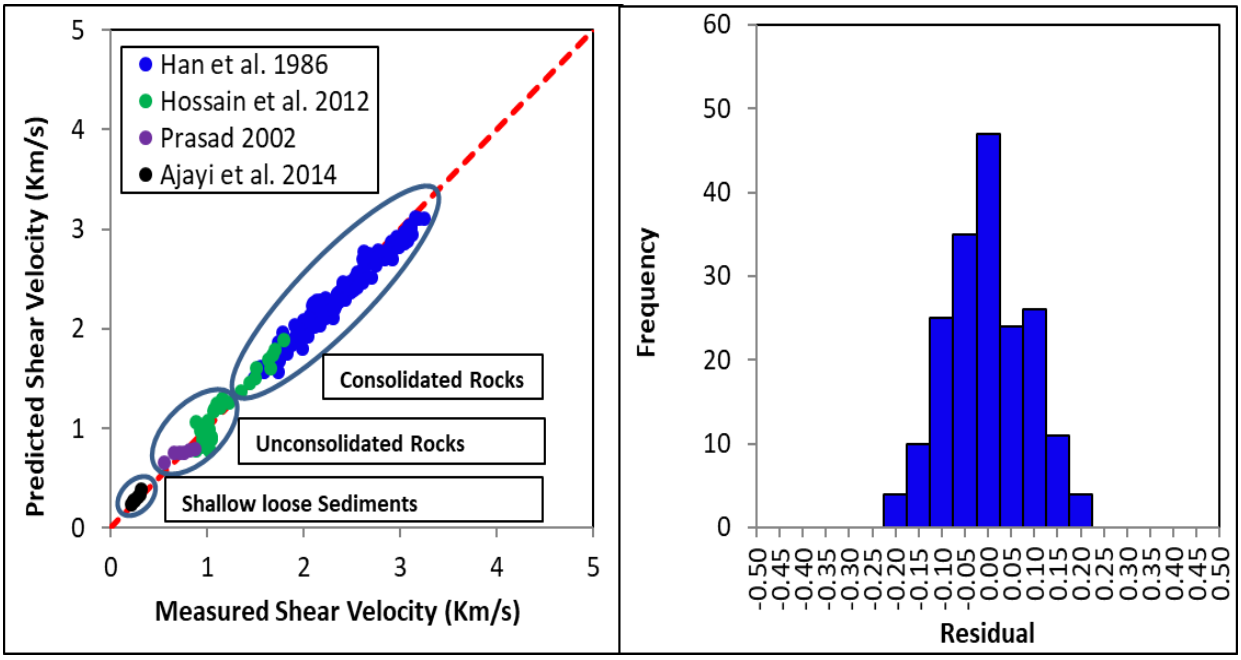

Figure A2. 1 Comparison of predicted and measured shear wave velocities.

A.2.3. Field Examples

To further demonstrate the applicability of the new shear wave velocity prediction model, three wells from the tertiary deltaic system in the Niger Delta Basin are considered as the case studies. The Niger Delta Basin is an extensional rift basin that consists of Tertiary clastic sediments with thickness up to 12 km (Doust and Omatsola 1990; Oloruntobi et al. 2018). It is located in the Niger Delta and the Gulf of Guinea along the west of central Africa, covering an area of about 75,000 km^2 (Evamy et al. 1978). The sequence stratigraphy of the basin consists of Benin formations, Agbada formations and Akata formations in descending order (Short and Stauble 1967; Avbovbo 1978b; Adewole et al. 2016). The Benin formations consist of mainly top medium to coarse-grained continental sands. The Agbada formations consist of an alternating sequence of sands and shales. All commercial productions of oil and gas in the basin are from deltaic sandstones of Agbada formations. The Akata formations consist of mainly under-compacted marine shales. The wells presented in this paper only penetrate the Benin and Agbada formations. The geothermal gradient varies across the Niger Delta basin. Based on the average surface temperature of 74°F, the geothermal gradient varies between 1.2 – 3.0^oF per 100 feet (Avbovbo, 1978b). The basin's structural trapping mechanisms are growth faults associated with rollover anticlines (Daukoru 1975). The Niger Delta sands have good porosity and permeability (sands with porosity higher than 25% and permeability in the Darcy range are not uncommon). In this paper, all depths are with respect to true vertical depth (TVD) below the mean sea level (MSL). Figure A2. 2 shows the location map of the three wells. Well A is an exploratory gas well, located about 70 km northwest of Port Harcourt in the onshore region of the basin. The well was drilled to a total depth of 11,894 ft in the 6'' hole section. However, the required wireline log data were only acquired in the 8 ½'' hole section of the well. The well penetrated both the normally pressured and overpressure

intervals with the onset of overpressure at 8,220 ft. Well B is an exploratory oil well, located about 94 km southeast of Port Harcourt in the offshore depo-belt of the basin. The well was drilled to a total depth of 11,554 ft in the 12 ¼'' hole section. The required wireline log data were acquired in the 12 ¼'' hole section of the well. The subsurface pressure regime of well B is normal over the entire intervals being penetrated. Well C is an appraisal oil well, located about 65 km southwest of Bomadi in the offshore region of the basin. The well was drilled to a total depth of 8,115 ft in the 8 ½'' hole section. The required wireline log data were acquired over the entire sections of the well (8 ½'' pilot hole, 12 ¼'' hole and 8 ½'' main hole). The subsurface pressure regime of well C is normal from below the seabed to the well total depth.

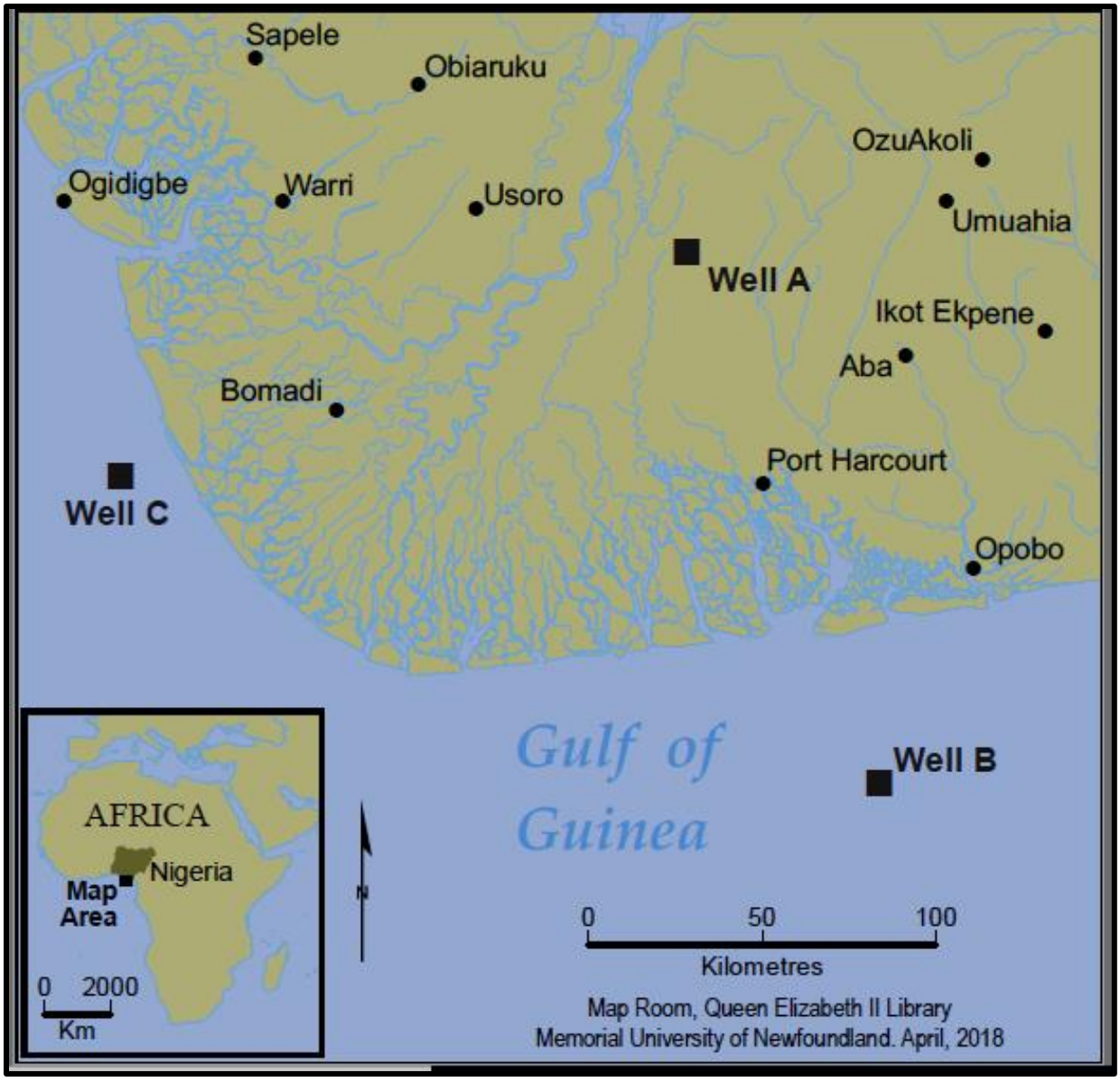

Figure A2. 2. Location map for well A, B and C

Table A2. 3 provides the summary of the well data. The well data covers a wide range of fields (onshore and offshore), formations (sand, shaly-sand, shale, consolidated and unconsolidated), depths (1,024 – 11,499 ft) and pressure regimes (normal and overpressure). Figure A2. 3 to Figure A2. 5 display the suite of wireline log data that were acquired in the three wells. The measured data consist of gamma-ray, shear and compressional slowness, formation bulk density, caliper, neutron porosity, formation deep resistivity and formation pore pressure. The log data frequency

is between 0.25 – 0.5 ft. Although all the necessary environmental corrections (effects of hole size, borehole rugosity, tool stand-off, mud type, filter cake thickness, etc.) have been applied to the log data, the inclusion of the caliper logs will help to identify the likely regions of poor wellbore conditions which may result in poor data acquisition/measurements. Further quality checks on the input data were performed using the possible Poisson's ratio values (0 – 0.5), compression velocity of seawater (1.61 km/s) and compressional velocity of sandstone matrix (5.49 km/s). Well C contains the shear wave velocity, compressional wave velocity and formation bulk density data in the shallowest unconsolidated formations where there is a general lack of acoustic and nuclear (Compton scattering) measurements across the industry due to the difficulty of acquiring such logs in large diameter boreholes. The log data in the topmost sections of Well C were acquired in the 8 ½'' pilot hole that was drilled for shallow gas investigations prior to opening up the well to a bigger hole size for normal drilling operations.

Table A2. 3. The well data summary

Name	Log Interval	Location	Well Type	Lithology	Available log data
Well A	7,975 – 10,392 ft	Onshore	Gas well	Shale - Sand	Gamma-ray, V_s, V_p, RHOB, Neutron, Caliper, & ILD
Well B	8,300 – 11,499 ft	Offshore	Oil well	Shale - Sand	Gamma-ray, V_s, V_p, RHOB, Neutron, Caliper, & ILD
Well C	1,024 – 8,094 ft	Offshore	Oil well	Shale - Sand	Gamma-ray, V_s, V_p, RHOB, Neutron, Caliper, & ILD

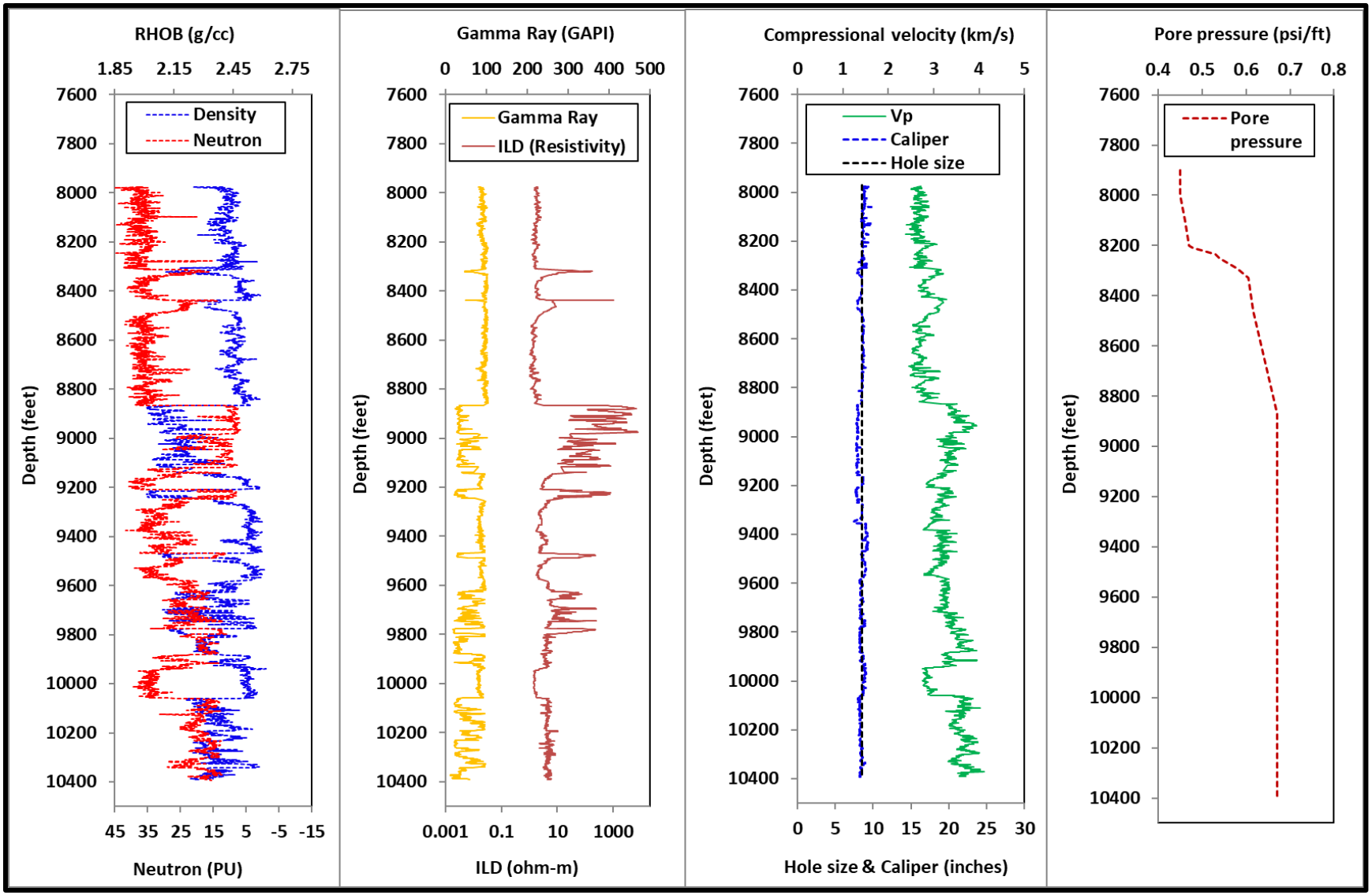

Figure A2. 3. Measured petrophysical data for well A.

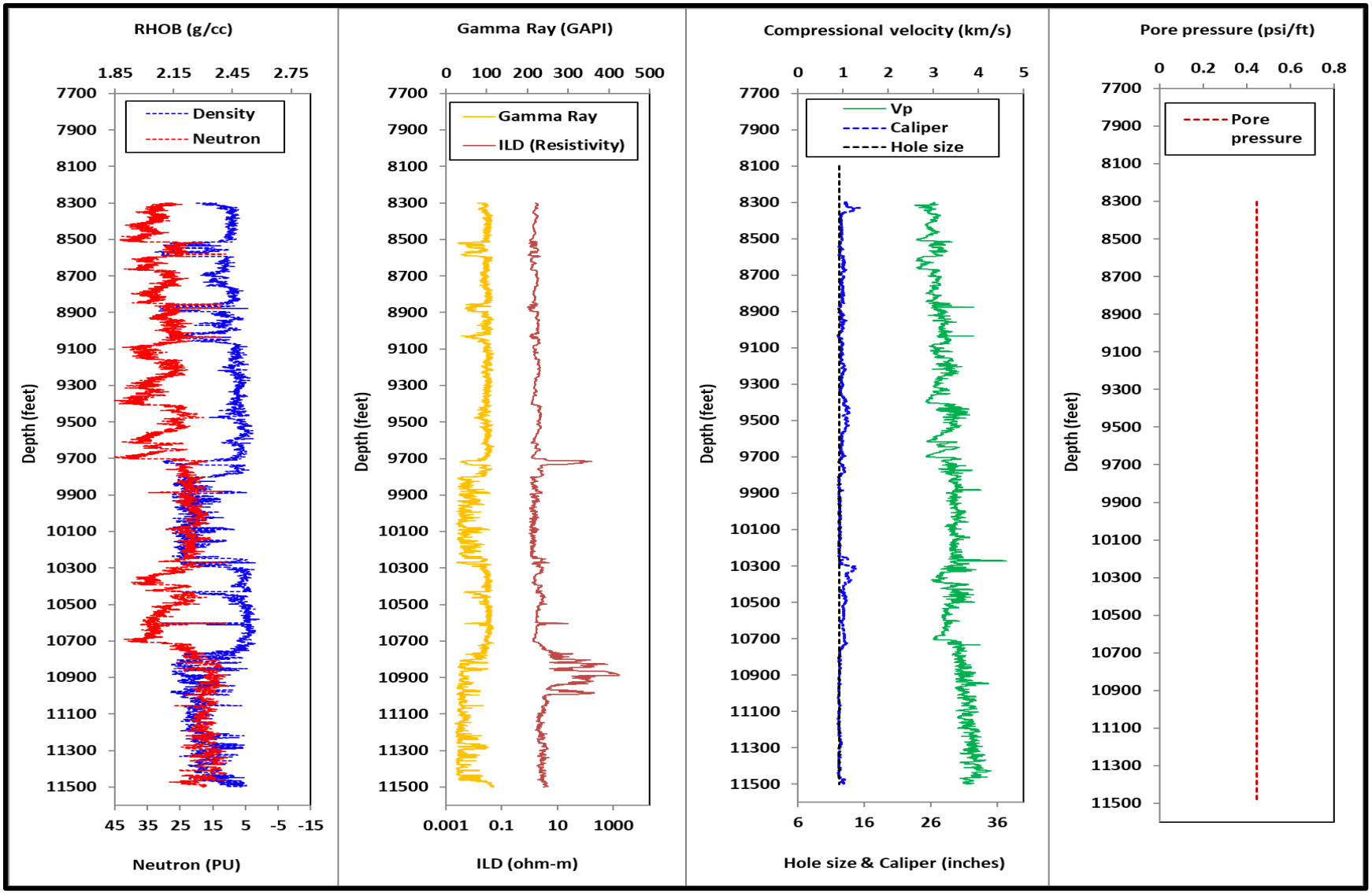

Figure A2. 4. Measured petrophysical data for well B.

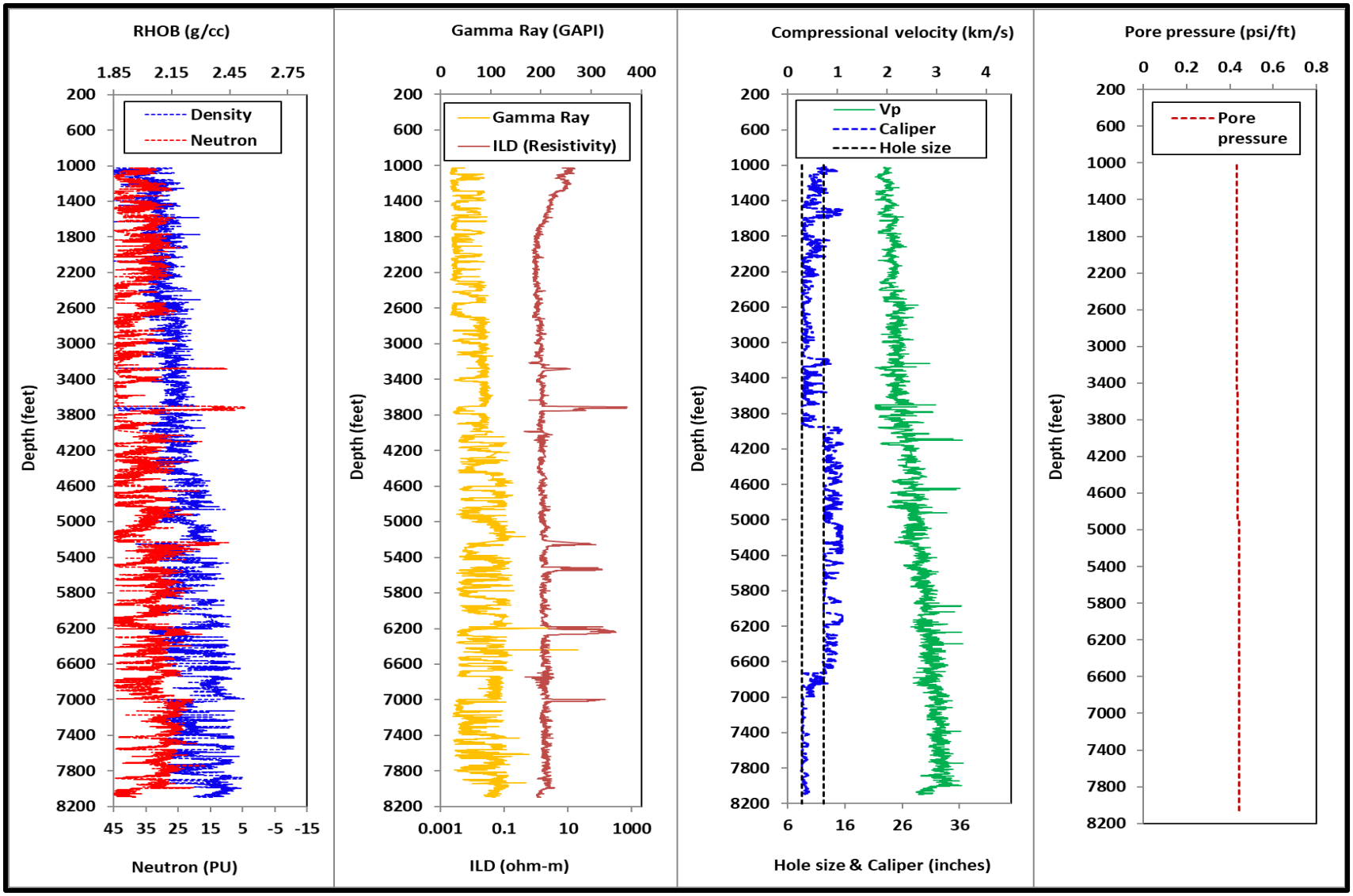

Figure A2. 5. Measured petrophysical data for well C

A.2.4. Discussion

Figure A2. 6 shows the comparison of predicted and measured shear wave velocity against depth for the three wells. The shear wave velocity is computed using Equation ((A2. 22). An excellent agreement is observed between the shear wave velocity estimates and the actual shear wave velocity measurements (log). The new model is able to predict the shear wave velocity across different stratigraphic units (clean and non-clean/mixed-lithology formations) with good accuracy due to the inclusion of lithology-dependent parameter. Accurate shear wave velocity predictions are also observed in the consolidated (well A, B and deeper sections of well C) and unconsolidated formations (shallowest sections of well C) due to the nature of the model and inclusion of additional compaction-dependent parameter. The new model appears to work well in gas, oil and water-saturated rocks. In gas/light hydrocarbon saturated rocks as compared to brine filled rocks, the compressional velocity and formation bulk density will decrease while the shear velocity will slightly increase (Toksöz et al. 1976). Since the new shear wave velocity prediction model contains both compressional velocity and formation bulk density terms, and the fact that the formations are consolidated (well A), it is possible that these two properties counteract such that the predicted shear wave velocity slightly increases in gas filled rocks when compared to brine filled rocks. The new model also produces good estimates in normally pressured and overpressured intervals (well A) since the model is developed from data that covers a wide range of effective stresses. Even for rocks that contain microcracks, Equation ((A2. 22) can still be applicable. For consolidated rocks that contain microcracks, changes in effective stress will cause significant changes in compressional wave velocity with negligible changes in formation bulk density. Under this condition, shear wave velocity in the new model will respond only to compressional wave velocity until the effective stress is high enough to close all the microcracks.

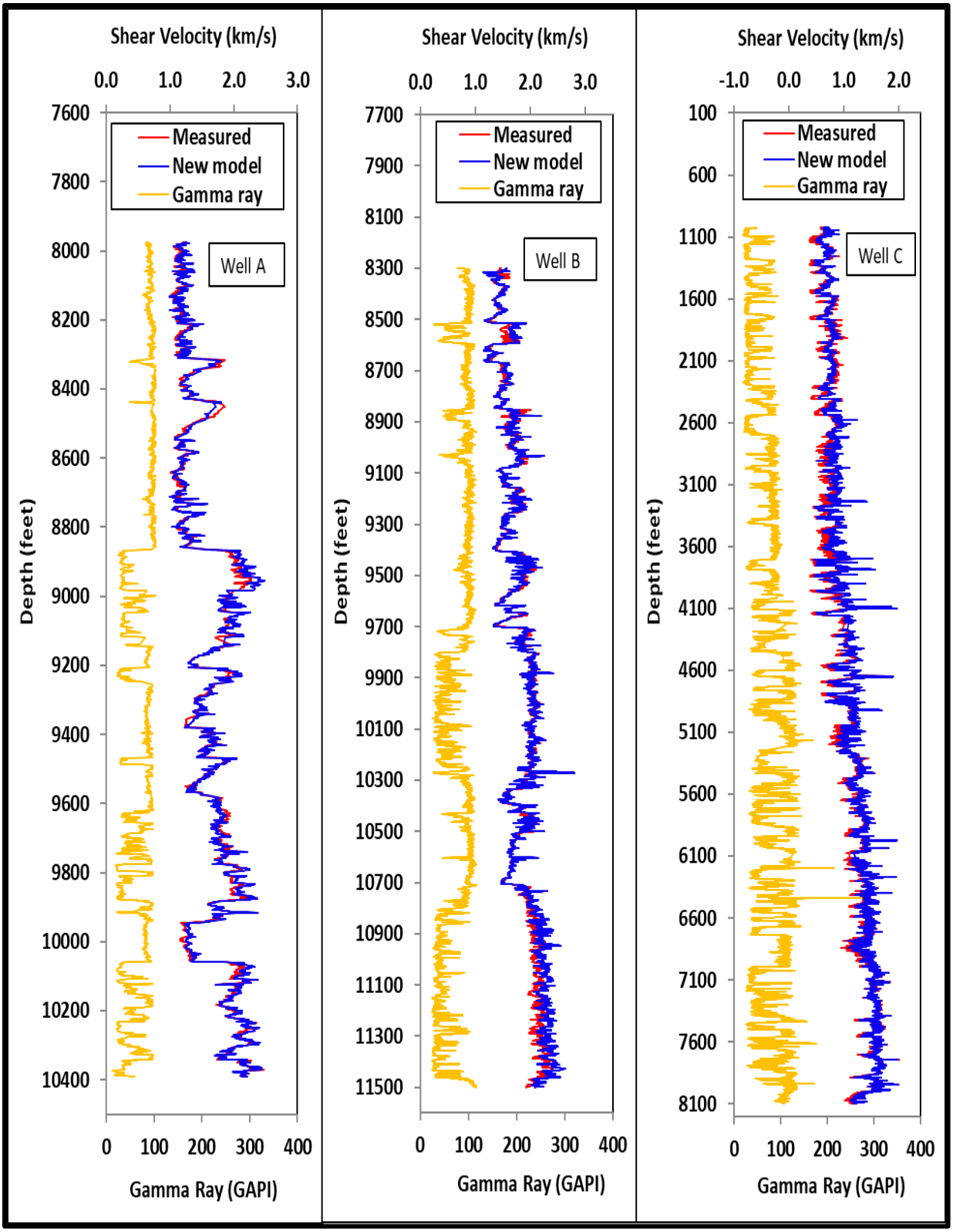

Figure A2. 6. Comparison of predicted and measured (log) shear wave velocities profile.

Figure A2. 7 to Figure A2. 9 show the cross-plots of the predicted shear wave velocity versus the measured (log) shear wave velocity using Equation (A2. 20) (new model), Equation (A2. 2) (Castagna et al. 1985), and Equation (A2. 3) (Han et al. 1986). The error distribution charts are also provided along with the cross-plots. The models of Castagna and Han have been selected for comparison because they are the most widely used empirical relations. More so, large number of the experimental data used to calibrate the new model in this paper were obtained from Han. For the new model, the plots again show an excellent agreement between the measured (log) and predicted shear wave velocities with remarkable non-scattered trends and normal error distributions. The new model produces lower RMS errors (Table A2. 4), lower maximum deviations (MD) and better distributions than the most widely used empirical relations. In general, the new model outperforms the most widely used empirical relations.

Table A2. 4. Comparison of RMSE and maximum deviation for different models.

Name	New Model		Han et al. 1986		Castagna et al. 1985	
	RMSE	MD	RMSE	MD	RMSE	MD
Well A	7%	±0.20 km/s	12%	±0.30 km/s	12%	±0.50 km/s
Well B	9%	±0.20 km/s	9%	±0.30 km/s	12%	±0.45 km/s
Well C	7%	±0.15 km/s	12%	±0.20 km/s	11%	±0.35 km/s

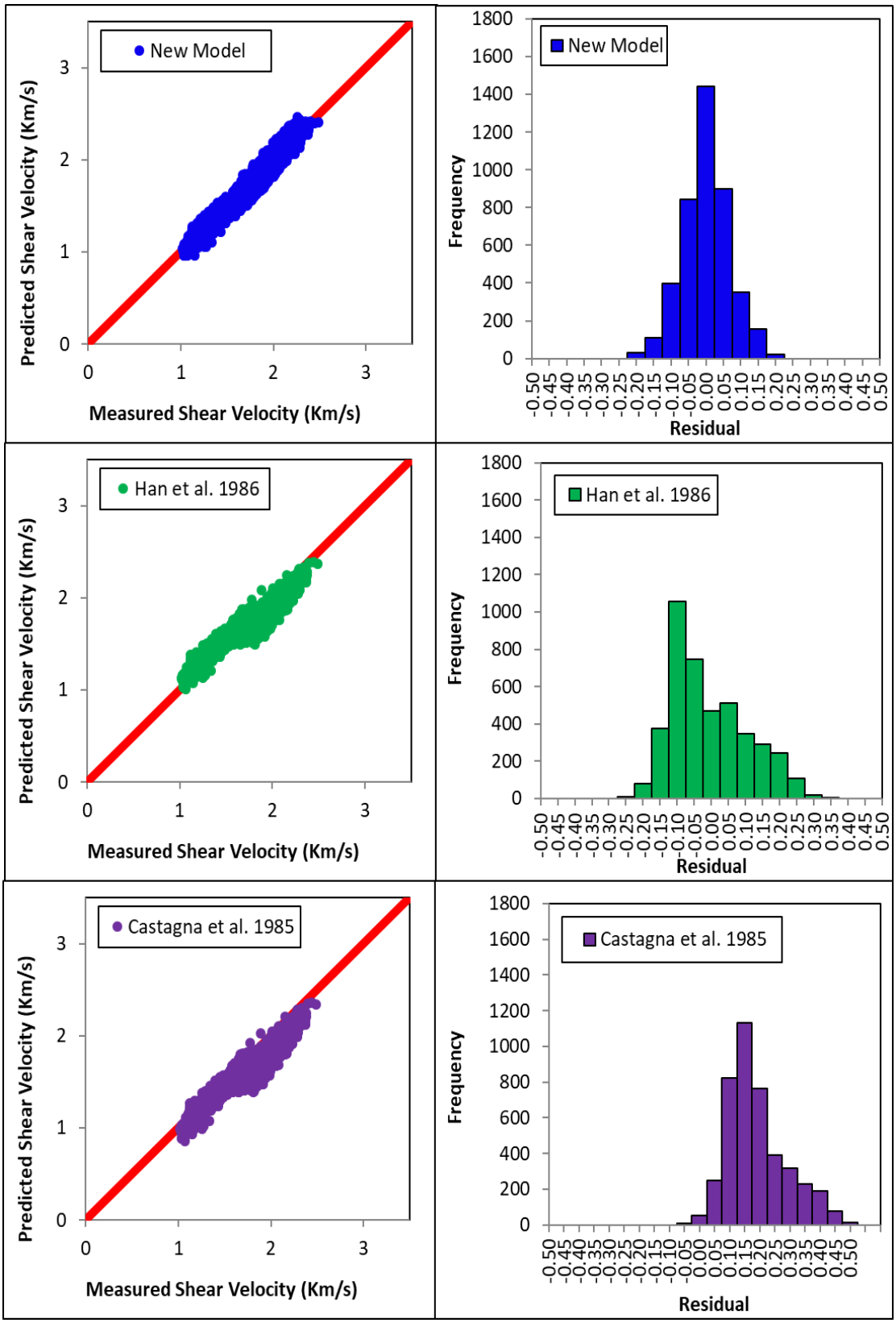

Figure A2. 7Comparison of predicted and measured (log) shear wave velocities for well A

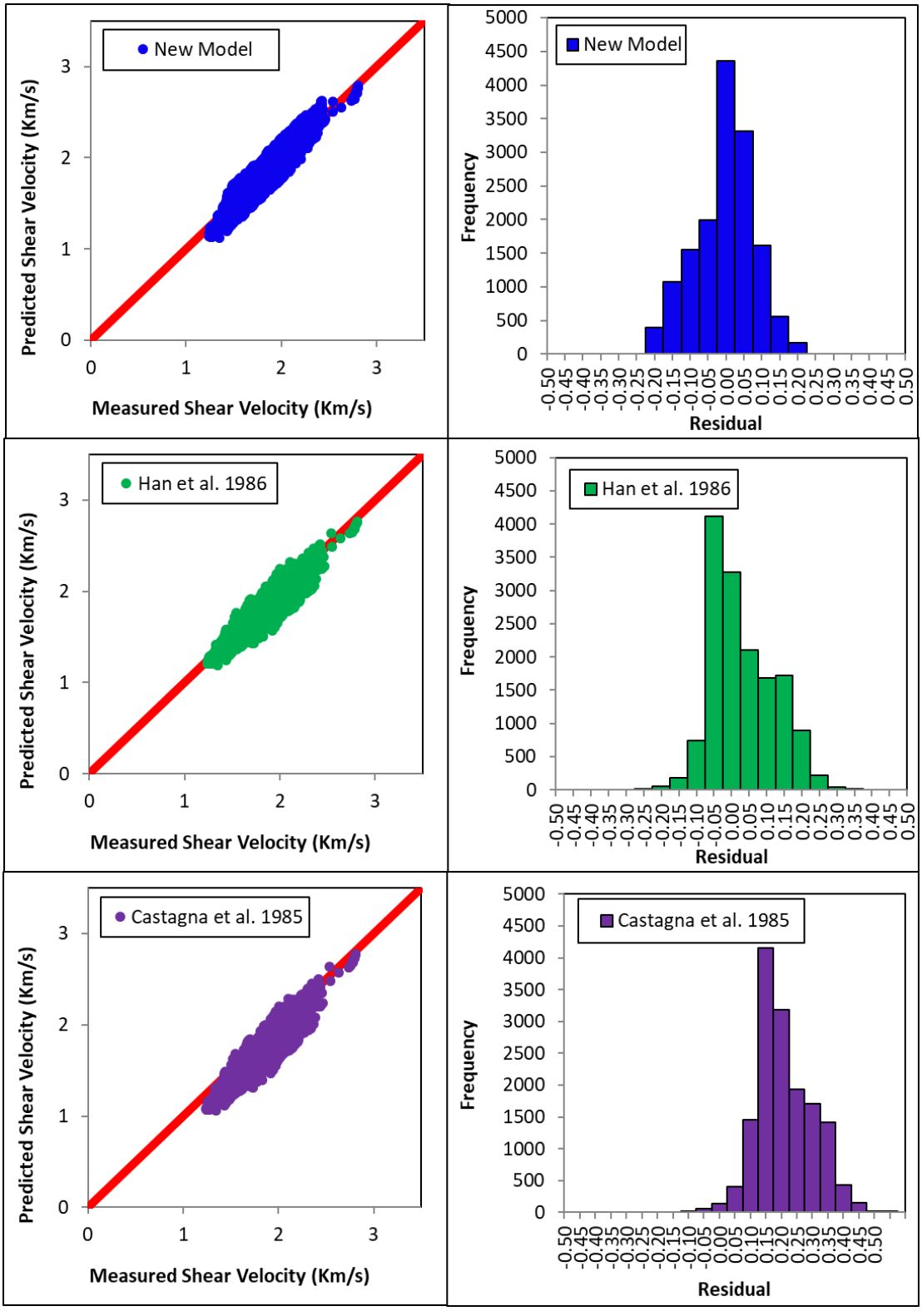

Figure A2. 8. Comparison of predicted and measured (log) shear wave velocities for well B

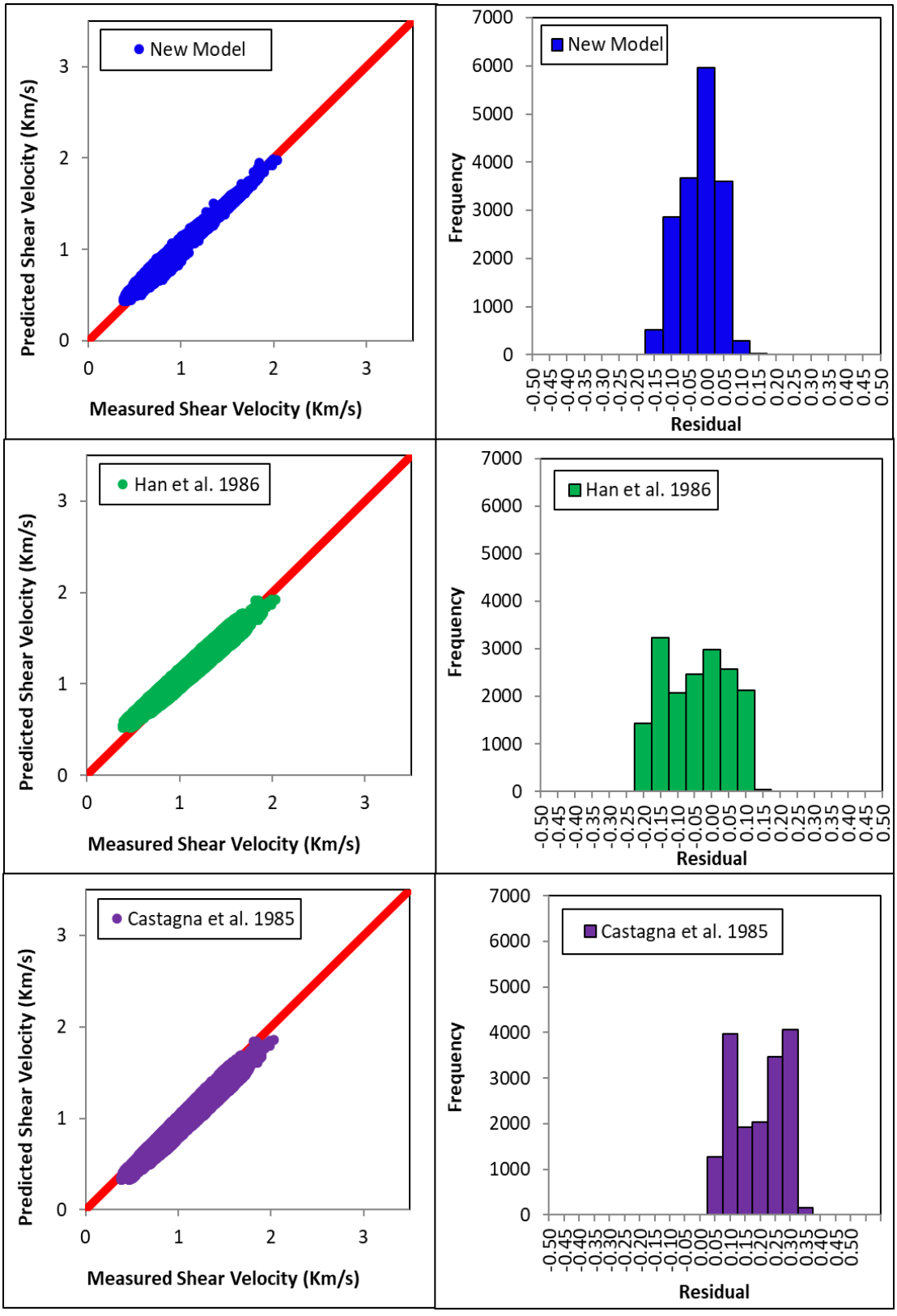

Figure A2. 9. Comparison of predicted and measured (log) shear wave velocities for well C

A.2.5. Conclusion

Data obtained from different geographical locations have been used to develop and validate the new shear wave velocity prediction model. The model is developed primarily for clastic formations. The new model incorporates an additional lithology-compaction dependent parameter, making it suitable for consolidated and unconsolidated rocks. The model appears to work well for multiple stratigraphic units (clean sands, clean shales and non-clean/mixed-lithology formations) in clastic environments. In the case study wells, the new model also appears to predict the shear wave velocity fairly accurately in gas, oil and water saturated rocks. The statistical analysis shows that the accuracy of the new shear wave velocity prediction model is quite high with low root-mean-square errors, low maximum deviations and normal error distribution curves. In general, there is an excellent agreement between the measured and predicted shear velocities. The nature of the new model (modified power law) and the inclusion of the density term improve the accuracy of the shear wave prediction. The new shear wave velocity prediction model does not cover carbonate and evaporite environments. Separate models may need to be developed for these environments.

Acknowledgments

The authors thankfully acknowledge the support provided by the Advanced Drilling Technology Laboratory Group, Memorial University of Newfoundland, Canada. Special thanks to Richard Ebisike of Shell for reviewing the manuscript.

Nomenclature

RHOB	Bulk density log (g/cm3)
K	Bulk modulus (MPa)
V_p	Compressional wave velocity (km/s)
CP	Confining pressure
ILD	Deep resistivity (ohms.m)
^oF	Degree Fahrenheit
DP	Differential pressure
ft	feet
ρ_b	Formation bulk density (g/cc)
MD	Maximum deviation
PU	Porosity unit
G	Shear modulus (MPa)
Δt_s	Shear transit time in microseconds per foot ($\mu second/ft$)
V_s	Shear wave velocity (km/s)

Reference

Adewole, E.O., Macdonald, D.I.M., Healy, D., 2016. Estimating density and vertical stress magnitudes using hydrocarbon exploration data in the onshore Northern Niger Delta Basin, Nigeria: Implication for overpressure prediction. J. African Earth Sci. 123, 294–308. https://doi.org/10.1016/j.jafrearsci.2016.07.009

Ajayi, J.., Adepelumi, A.., Agih, C., 2014. Determination of rock elastic parameters using VP/VS relation-ship for escravos area, Niger delta, Nigeria. Int. J. Adv. Geosci. 2, 140–149.

Al-Dousari, M., Garrouch, A.A., Al-Omair, O., 2016. Investigating the dependence of shear wave velocity on petrophysical parameters. J. Pet. Sci. Eng. 146, 286–296.

Ameen, M.S., Smart, B.G.D., Somerville, J.M., Hammilton, S., Naji, N.A., 2009. Predicting rock mechanical properties of carbonates from wireline logs (A case study: Arab-D reservoir, Ghawar field, Saudi Arabia). Mar. Pet. Geol. 26, 430–444.

Anderson, R.A., Ingram, D.S., Zanier, A.M., 1973. Determining Fracture Pressure Gradients From Well Logs. J. Pet. Technol. 25, 1259–1268. https://doi.org/10.2118/4135-PA

Anemangely, M., Ramezanzadeh, A., Tokhmechi, B., 2017. Shear wave travel time estimation from petrophysical logs using ANFIS-PSO algorithm: A case study from Ab-Teymour Oilfield. J. Nat. Gas Sci. Eng. 38, 373–387.

Asoodeh, M., Bagheripour, P., 2012. Prediction of compressional, shear, and stoneley wave velocities from conventional well log data using a committee machine with intelligent systems. Rock Mech. rock Eng. 45, 45–63.

Avbovbo, A.A., 1978a. Tertiary lithostratigraphy of the Niger Delta. Am. Assoc. Pet. Geol. Bull. 62, 295–306.

Avbovbo, A.A., 1978b. Geothermal gradients in the southern Nigeria basin. Bull. Can. Pet. Geol. 26, 268–274.

Bagheripour, P., Gholami, A., Asoodeh, M., Vaezzadeh-Asadi, M., 2015. Support vector regression based determination of shear wave velocity. J. Pet. Sci. Eng. 125, 95–99.

Bailey, T., Dutton, D., 2012. An Empirical Vp/Vs Shale Trend for the Kimmeridge Clay of the Central North Sea, in: 74th EAGE Conference and Exhibition Incorporating EUROPEC 2012.

Brie, A., Pampuri, F., Marsala, A.F., Meazza, O., 1995. Shear sonic interpretation in gas-bearing sands, in: SPE Annual Technical Conference and Exhibition. Society of Petroleum Engineers.

Brocher, T.M., 2005. Empirical Relations between Elastic Wavespeeds and Density in the Earth's Crust. Bull. Seismol. Soc. Am. 95, 2081–2092. https://doi.org/10.1785/0120050077

Carroll, R.D., 1969. The determination of the acoustic parameters of volcanic rocks from compressional velocity measurements, in: International Journal of Rock Mechanics and Mining Sciences & Geomechanics Abstracts. Elsevier, pp. 557–579.

Castagna, J.P., Batzle, M.L., Eastwood, R.L., 1985. Relationships between compressional-wave and shear-wave velocities in clastic silicate rocks. Geophysics 50, 571–581. https://doi.org/10.1190/1.1441933

Chang, C., Zoback, M.D., Khaksar, A., 2006. Empirical relations between rock strength and physical properties in sedimentary rocks. J. Pet. Sci. Eng. 51, 223–237.

Coates, G.R., Denoo, S.A., 1980. Log derived mechanical properties and rock stress, in: SPWLA 21st Annual Logging Symposium. Society of Petrophysicists and Well-Log Analysts.

Daukoru, J.W., 1975. PD 4(1) Petroleum Geology of the Niger Delta. World Pet. Congr.

Domenico, S.N., 1984. Rock lithology and porosity determination from shear and compressional wave velocity. Geophysics 49, 1188–1195.

Doust, H., Omatsola, E., 1990. Niger Delta, in: Divergent / Passive Margin Basins. pp. 201–238.

Dvorkin, J., Mavko, G., Nur, A., 1999. Overpressure detection from compressional-and shear-wave data. Geophys. Res. Lett. 26, 3417–3420.

Eastwood, R.L., Castagna, J.P., 1983. Basis for interpretation of Vp/Vs ratios in complex lithologies, in: SPWLA 24th Annual Logging Symposium. Society of Petrophysicists and Well-Log Analysts.

Eberhart-Phillips, D., Han, D., Zoback, M.D., 1989. Empirical relationships among seismic velocity, effective pressure, porosity, and clay content in sandstone. Geophysics. https://doi.org/10.1190/1.1442580

Ebrom, D., Heppard, P., Albertin, M., 2006. OTC 18399 Travel-Time Methods of Vp / Vs Determination for Pore Pressure Prediction Using Lookahead VSPs. Offshore Technol. Conf. (OTC 18399).

Ensley, R.A., 1985. Evaluation of direct hydrocarbon indicators through comparison of compressional-wave and shear-wave seismic data - a case study of the Myrnam gas field Alberta. Geophysics 50, 37–48. https://doi.org/10.1190/1.1441834

Evamy, B.D., Haremboure, J., Kamerling, P., Knaap, W.A., Molloy, F.A., Rowlands, P.H., 1978. Hydrocarbon habitat of Tertiary Niger delta. Am. Assoc. Pet. Geol. Bull. 62, 1–39.

Fabricius, I.L., Baechle, G., Eberli, G.P., Weger, R., 2007. Estimating permeability of carbonate rocks from porosity and vp ⁄ vs. GEOPHYSICS 72, E185–E191. https://doi.org/10.1190/1.2756081

Greenberg, M.L., Castagna, J.P., 1992. Shear-Wave Velocity Estimation in Porous Rocks: Theoretical Formulation, Preliminary Verification and Applications1. Geophys. Prospect. 40, 195–209. https://doi.org/10.1111/j.1365-2478.1992.tb00371.x

Gregory, A.R., 1976. Fluid saturation effects on dynamic elastic properties of sedimentary rocks. Geophysics 41, 895–921.

Hamada, G.M., 2004. Reservoir Fluids Identification Using Vp/Vs Ratio. Oil Gas Sci. Technol. – Rev. IFP 59, 649–654.

Hamilton, E.L., 1971. Elastic properties of marine sediments. J. Geophys. Res. 76, 579–604.

Hamilton, E.L., Bucker, H.P., Keir, D.L., Whitney, J.A., 1970. Velocities of compressional and shear waves in marine sediments determined in situ from a research submersible. J. Geophys. Res. 75, 4039–4049.

Han, D., Nur, A., Morgan, D., 1986. Effects of porosity and clay content on wave velocities in

sandstones. Geophysics 51, 2093–2107. https://doi.org/10.1190/1.1442062

Hicks, W.G., Berry, J.E., 1956. Application of continuous velocity logs to determination of fluid saturation of reservoir rocks. Geophysics 21, 739–754.

Hossain, Z., Mukerji, T., Fabricius, I.L., 2012. V p-V s relationship and amplitude variation with offset modelling of glauconitic greensand. Geophys. Prospect. 60, 117–137. https://doi.org/10.1111/j.1365-2478.2011.00968.x

Johnston, J.E., Christensen, N.I., 1993. Compressional to shear velocity ratios in sedimentary rocks, in: International Journal of Rock Mechanics and Mining Sciences & Geomechanics Abstracts. Elsevier, pp. 751–754.

Jørstad, A., Mukerji, T., Mavko, G., 1999. Model-based shear-wave velocity estimation versus empirical regressions. Geophys. Prospect. 47, 785–797. https://doi.org/10.1046/j.1365-2478.1999.00154.x

Khazanehdari, J., McCann, C., 2005. Acoustic and petrophysical relationships in low-shale sandstone reservoir rocks. Geophys. Prospect. 53, 447–461.

Kithas, B.A., 1976. Lithology, gas detection, and rock properties from acoustic logging systems, in: SPWLA 17th Annual Logging Symposium. Society of Petrophysicists and Well-Log Analysts.

Kozlowski, M., Quirein, J., Engelman, B., Wolanski, K., Ochalik, S., 2017. Quantitative Interpretation of Sonic Compressional and Shear Logs for Gas Saturation in Medium Porosity Sandstone, in: SPWLA 58th Annual Logging Symposium. Society of Petrophysicists and Well-Log Analysts.

Krief, M., Garat, J., Stellingwerf, J., Ventre, J., 1990. A Petrophysical Interpretation Using The Velocities Of P And S Waves (full-waveform Sonic). Log Anal. 31, 355–369.

Krishna, K.S., Rao, D.G., Murty, G.P.S., Ramana, Y. V, 1989. Sound velocity, density, and related properties along a transect across the Bay of Bengal. Geo-marine Lett. 9, 95–102.

Kuster, G.T., Toksöz, M.N., 1974. Velocity and attenuation of seismic waves in two-phase media:

Part I. Theoretical formulations. Geophysics 39, 587–606.

Lee, M.W., 2013. Comparison of Methods for Predicting Shear-Wave Velocities of Unconsolidated Shallow Sediments in the Gulf of Mexico. US Dep. Inter. US Geol. Surv.

Lee, M.W., 2010. Predicting S-wave velocities for unconsolidated sediments at low effective pressure. U. S. Geol. Surv.

Li, Q., Heliot, D., Zhao, L., Chen, Y., 2000. Abnormal pressure detection and wellbore stability evaluation in carbonate formations of east Sichuan, China, in: IADC/SPE Drilling Conference (IADC / SPE 59125). Society of Petroleum Engineers.

Mabrouk, W.M., Pennington, W.D., 2009. Compressional and shear wave velocity in terms of petrophysical parameters in clean formations. J. Pet. Sci. Eng. 65, 62–66.

Maleki, S., Moradzadeh, A., Riabi, R.G., Gholami, R., Sadeghzadeh, F., 2014. Prediction of shear wave velocity using empirical correlations and artificial intelligence methods. NRIAG J. Astron. Geophys. 3, 70–81.

Miller, S.L.M., Stewart, R.R., 1991. The relationship between elastic-wave velocities and density in sedimentary rocks: A proposal. Crewes Res. Rep. 260–273.

Miller, S.L.M., Stewart, R.R., 1990. Effects of lithology, porosity and shaliness on P-and S-wave velocities from sonic logs. Can. J. Explor. Geophys. 26, 94–103.

Najibi, A.R., Ghafoori, M., Lashkaripour, G.R., Asef, M.R., 2015. Empirical relations between strength and static and dynamic elastic properties of Asmari and Sarvak limestones, two main oil reservoirs in Iran. J. Pet. Sci. Eng. 126, 78–82.

Nations, J.F., 1974. Lithology and porosity from acoustic shear and compressional wave transit time relationships, in: SPWLA 15th Annual Logging Symposium. Society of Petrophysicists and Well-Log Analysts.

Nourafkan, A., Kadkhodaie-Ilkhchi, A., 2015. Shear wave velocity estimation from conventional well log data by using a hybrid ant colony–fuzzy inference system: A case study from Cheshmeh–Khosh oilfield. J. Pet. Sci. Eng. 127, 459–468.

https://doi.org/https://doi.org/10.1016/j.petrol.2015.02.001

Ohen, H.A., 2003. Calibrated Wireline Mechanical Rock Properties Model for Predicting and Preventing Wellbore Collapse and Sanding., in: SPE European Formation Damage Conference. Society of Petroleum Engineers.

Ojha, M., Sain, K., 2014. Velocity-porosity and velocity-density relationship for shallow sediments in the Kerala-Konkan basin of western Indian margin. J. Geol. Soc. India 84, 187–191.

Oloruntobi, O., Adedigba, S., Khan, F., Chunduru, R., Butt, S., 2018. Overpressure prediction using the hydro-rotary specific energy concept. J. Nat. Gas Sci. Eng. 55, 243–253.

Pickett, G.R., 1963. Acoustic Character Logs and Their Applications in Formation Evaluation. J. Pet. Technol. (SPE 452) 15, 659–667. https://doi.org/10.2118/452-PA

Potter, C.C., Foltinek, D.S., 1997. Formation elastic parameters by deriving S-wave velocity logs. Consort. Res. Elastic Wave Explor. Seismol. Res. Rep. 9, 1–13.

Potter, C.C., Miller, S.L.M., Margrave, G.F., 1996. Formation elastic parameters and synthetic P-P and P-S seismograms for the Blackfoot field. CREWES Res. Rep. 8, 37-1-37–18.

Prasad, M., 2002. Acoustic measurements in unconsolidated sands at low effective pressure and overpressure detection. Geophysics 67, 405–412.

Rafavich, F., Kendall, C.H.S.C., Todd, T.P., 1984. The relationship between acoustic properties and the petrographic character of carbonate rocks. Geophysics 49, 1622–1636.

Rajabi, M., Bohloli, B., Ahangar, E.G., 2010. Intelligent approaches for prediction of compressional, shear and Stoneley wave velocities from conventional well log data: A case study from the Sarvak carbonate reservoir in the Abadan Plain (Southwestern Iran). Comput. Geosci. 36, 647–664.

Ramcharitar, K., Hosein, R., 2016. Rock Mechanical Properties of Shallow Unconsolidated Sandstone Formations, in: SPE Trinidad and Tobago Section Energy Resources Conference (SPE 180803). Society of Petroleum Engineers.

Rezaee, M.R., Ilkhchi, A.K., Barabadi, A., 2007. Prediction of shear wave velocity from petrophysical data utilizing intelligent systems: An example from a sandstone reservoir of Carnarvon Basin, Australia. J. Pet. Sci. Eng. 55, 201–212.

Robertson, J.D., Pritchett, W.C., 1984. Direct hydrocarbon detection using comparative P-wave and S-wave seismic sections. Geophysics 50, 383–393. https://doi.org/doi: 10.1190/1.1441918

Saleh, S., Williams, K., Rizvi, A., 2013. Predicting Subsalt Pore Pressure with Vp/Vs. Offshore Technol. Conf. (OTC 24157).

Short, K.., Stauble, A.., 1967. Outline of Geology of Niger Delta. Am. Assoc. Pet. Geol. Bull. 51, 761–779.

Tatham, R.H., 1982. Vp/Vs and lithology. Geophysics 47, 336–344. https://doi.org/10.1190/1.1441339

Tatham, R.H., Stoffa, P.L., 1976. V p/V s—A potential hydrocarbon indicator. Geophysics 41, 837–849.

Tixier, M.P., Loveless, G.W., Anderson, R.A., 1975. Estimation of Formation Strength From the Mechanical-Properties Log (incudes associated paper 6400). J. Pet. Technol. 27, 283–293.

Toksöz, M.N., Cheng, C.H., Timur, A., 1976. Velocities of seismic waves in porous rocks. Geophysics 41, 621–645.

Tosaya, C., Nur, A., 1982. Effects of diagenesis and clays on compressional velocities in rocks. Geophys. Res. Lett. 9, 5–8. https://doi.org/10.1029/GL009i001p00005

Tosaya, C.A., 1982. Acoustical Properties of Clay-Bearing Rocks. PhD Thesis, Stanford Univ.

Ursenbach, C.P., 2002. Generalized Gardner relation for gas-saturated rocks. CREWES 2002 Res. Rep. 14, 1–6.

Ursenbach, C.P., 2001. A generalized Gardner relation. CREWES 2001 Res. Rep. 13, 77–82.

Vernik, L., Fisher, D., Bahret, S., 2002. Estimation of net-to-gross from P and S impedance in

deepwater turbidites. Lead. Edge 21, 380. https://doi.org/10.1190/1.1471602

Walls, J., Dvorkin, J., Mavko, G., Nur, A., 2000. Use of Compressional and Shear Wave Velocity for Overpressure Detection, in: Offshore Technology Conference (OTC 11912). Offshore Technology Conference.

Williams, D.M., 1990. The acoustic log hydrocarbon indicator, in: SPWLA 31st Annual Logging Symposium. Society of Petrophysicists and Well-Log Analysts.

Xu, S., White, R.E., 1995. A new velocity model for clay-sand mixtu res1. Geophys. Prospect. 43, 91–118. https://doi.org/10.1111/j.1365-2478.1995.tb00126.x